Microscopic and mesoscopic descriptions of the Nonlinear Noisy Leaky Integrate-and-Fire model: long-time behavior and numerical simulations

Alejandro Ramos Lora

Programa de doctorado en Física y Matemáticas (FisyMat)

UNIVERSIDAD DE GRANADA

Universidad de Granada

Marzo, 2024

Directores:
María José Cáceres Granados & José Alfredo Cañizo Rincón

Editor: Universidad de Granada. Tesis Doctorales
Autor: Alejandro Ramos Lora
ISBN: 978-84-1195-925-4
URI: https://hdl.handle.net/10481/108796

Microscopic and mesoscopic descriptions of the Nonlinear Noisy Leaky Integrate-and-Fire model: long-time behavior and numerical simulations

Alejandro Ramos Lora

Abstract

This doctoral thesis focuses on the analytical and numerical study of the "Nonlinear Noisy Leaky Integrate-and-Fire" (NNLIF) neural network model, a well-known model coming from kinetic theory, i.e., built from a microscopic description of individual neurons interacting with each other, by means of a mesoscopic statistical description of the network. In our research we have made use of both the microscopic and mesoscopic descriptions of the model in order to understand it as completely as possible.

In chapter 1 we present an extensive introduction, with an exhaustive development of the NNLIF model with a single population of neurons, i.e., instead of considering excitatory and inhibitory neurons separately, an average population of them is considered. In addition, we present a section dedicated to the synthesis of the main results ordered by chapters, which serves as a summary of the thesis results.

The numerical study of the microscopic description of the model is found in chapter 2, where a multitude of numerical simulations are shown, giving a general picture of the model behavior. Through these results we try to answer the question: What happens after the blow-up? By implementing new solution definitions to the microscopic system, as well as experimenting with different values of the synaptic delay, we arrive at relevant conclusions, such as the tendency towards a "plateau" state instead of blow-up, in highly excitatory networks with delay.

With respect to the mesoscopic system, modeled by a nonlinear Fokker-Planck partial differential equation, our investigation is separated into two lines of research: In chapter 3 we provide new theoretical results on the stability of the equation equilibria, improving and complementing previous knowledge on its local behavior. The way to arrive at these results is through an extensive study on the existence and regularity properties of the linear version of the Fokker-Planck equation. The joint application of this study and spectral methods on linear operators, allow us to extend previous results on the stability of equilibria for this equation, in a vector space that includes part of the nonlinear term. Finally, the linearization of the nonlinear equation around its equilibria, its association with a Volterra type integral equation, and the adaptation of known results for the latter, allow us to establish clear and easily verifiable criteria on the stability or instability of the nonlinear Fokker-Planck equation equilibria. The second line of research deals with the

global behavior of the mesoscopic system, for this purpose in chapter 4 we define a discrete sequence called "sequence of pseudo-equilibria" and perform an analytical study of its monotonicity, for each range of values of the nonlinear Fokker-Planck equation parameters. Following the intuition acquired during the numerical simulation of the microscopic system, we think that this discrete sequence must describe the long-term behavior of the nonlinear equation for high values of the synaptic delay. To test the veracity of this claim, we perform a rigorous demonstration in the case of low excitatory neuron populations, improving on previous results, and provide a comprehensive numerical study to support our idea. In particular, it is worth mentioning the emergence of periodic solutions for strongly inhibitory networks when we consider high values for the delay.

After performing our analytical and numerical study of the NNLIF model, in chapter 5 we have considered the model that takes into account the refractory state of neurons after synapses, considering two distinct populations between active and inactive neurons. Here we apply the techniques developed in chapters 2 and 4 to this model, to provide a global picture of its long-time behavior, together with new phenomena observed in the microscopic system, such as periodic solutions in the excitatory case without the need for delay.

Apart from the research on the NNLIF model, in chapter 6 we have carried out a literature review and report on numerical results, about other microscopic models of interest in physics and biology. In particular, we have studied models of interaction between particles through attractive-repulsive potentials of the power-law type. This type of potentials have been widely studied in the scientific literature and are related, depending on the value of their parameters, to important problems such as crystallization or collective behavior phenomena. To complement the review, we have implemented a powerful computational tool to calculate minima of the interaction energy of these models, and we show several results obtained with it.

Finally, the conclusions of the thesis are presented in chapter 7, where we show a synthesis of the main results of our research, as well as a discussion of these results, their possible extensions and open problems.

Microscopic and mesoscopic descriptions of the Nonlinear Noisy Leaky Integrate-and-Fire model: long-time behavior and numerical simulations

Alejandro Ramos Lora

Resumen

Esta tesis doctoral se centra en el estudio analítico y numérico del modelo de redes neuronales "Nonlinear Noisy Leaky Integrate-and-Fire" (NNLIF), un conocido modelo proveniente de teoría cinética, es decir, construido a partir de una descripción microscópica de neuronas individuales que interactúan entre ellas, por medio de una descripción estadística mesoscópica de la red. En nuestra investigación hemos hecho uso tanto de la descripción microscópica como mesocópica del modelo, con la finalidad de entenderlo de la forma más completa posible.

En el capítulo 1 presentamos una amplia introducción, con un desarrollo exhaustivo del modelo NNLIF con una única población de neuronas, es decir, donde en vez de considerar neuronas excitadoras e inhibidoras por separado, se considera una población promedio de ellas. Además presentamos una sección dedicada a la sintetización de los resultados principales ordenados por capítulos, que sirve a modo de sumario de resultados de la tesis.

El estudio numérico de la descripción microscópica del modelo se encuentra en el capítulo 2, donde se muestran multitud de simulaciones numéricas, dando una imagen general del comportamiento del modelo. A través de estos resultados tratamos de responder a la pregunta ¿Qué ocurre después del blow-up? Implementando nuevas definiciones de solución al sistema microscópico, así como experimentando con distintos valores del retardo sináptico, llegamos a conlusiones relevantes, como la tendencia hacia un estado "meseta" en vez de blow-up, en redes muy excitadoras con retardo.

Con respecto al sistema mesoscópico, modelado por una ecuación en derivadas particales de Fokker-Planck no lineal, nuestra investigación se separa en dos vías: En el capítulo 3 ofrecemos nuevos resultados teóricos sobre la estabilidad de los equilibrios de esta ecuación, mejorando y complementando el conocimiento previo sobre su comportamiento local. La forma de llegar a estos resultados es a través de un extensivo estudio sobre las propiedades de existencia y regularidad de la versión lineal de la ecuación de Fokker-Planck. La aplicación conjunta de este estudio y métodos espectrales sobre operadores lineales, nos permiten ampliar resultados anteriores sobre la estabilidad de los equilibrios de esta ecuación, en un espacio vectorial que incluye parte del término no lineal. Por último la linealización de la ecuación no lineal alrededor de sus equilibrios, su asociación con una ecuación integral de tipo Volterra, y la adaptación de resultados conocidos

para esta última, nos permiten establecer criterios claros y fácilmente comprobables sobre la estabilidad o inestabilidad de los equilibrios de la ecuación de Fokker-Planck no lineal. La segunda vía trata sobre el comportamiento global del sistema mesoscópico. Para ello en el capítulo 4 definimos una sucesión discreta llamada "sucesión de pseudo-equilibrios" y realizamos un estudio analítico de su monotonía, para cada rango de valores de los parámetros de la ecuación de Fokker-Planck no lineal. Siguiendo la intuición adquirida durante la simulación numérica del sistema microscópico, pensamos que esta sucesión discreta debe describir el comportamiento a largo plazo de la ecuación no lineal para valores altos del retardo sináptico. Para comprobar la veracidad de esta afirmación, realizamos una demostración rigurosa en el caso de poblaciones de neuronas poco excitadoras, mejorando resultados anteriores, y ofrecemos un exhaustivo estudio numérico. En concreto merece la pena mencionar la aparición de soluciones periódicas para redes fuertemente inhibidoras cuando consideramos valores altos para el retardo.

Tras elaborar nuestro estudio analítico y numérico del modelo NNLIF, en el capítulo 5 hemos considerado el modelo que tiene en cuenta el estado refractario de las neuronas después de realizar sinapsis, considerando dos poblaciones distintas entre neuronas activas e inactivas. Aquí se aplican las técnicas desarrolladas en los capítulos 2 y 4 a este modelo, para ofrecer una imagen global de su comportamiento a largo plazo, junto con nuevos fenómenos observados en el sistema microscópico, como soluciones periódicas en el caso excitador sin necesidad de retardo.

Aparte de la investigación sobre el modelo NNLIF, en el capítulo 6 hemos realizado una revisión bibliográfica sobre otros modelos microscópicos de interés en física y biología. En concreto hemos estudiado modelos de interacción entre partículas a través de potenciales atractivo-repulsivos del tipo leyes de potencias. Este tipo de potenciales han sido estudiados ampliamente en la literatura científica y guardan relación, dependiendo del valor de sus parámetros, con problemas importantes como la cristalización o fenómenos de comportamiento colectivo. Para complementar la revisión bibliográfica, hemos implementado una potente herramienta computacional para calcular mínimos de la energía de interacción de estos modelos, y mostramos diversos resultados obtenidos con ella.

Por último, las conclusiones de la tesis se presentan en el capítulo 7, donde mostramos una síntesis de los resultados principales de nuestra investigación, así como una discusión de los mismos, planteamiento de sus posibles extensiones y problemas abiertos.

Agradecimientos

En primer lugar, quiero agradecer a mis directores, María José y Jose, por el voto de confianza que me dieron para realizar esta tesis, por haber estado durante estos años dedicando gran parte de su tiempo a nuestro trabajo conjunto y por su inestimable ayuda durante mi período de maduración como investigador.

También quiero agradecer a José Antonio Carrillo su amabilidad por invitarme a pasar un mes de estancia en la Universidad de Cambridge, así como sus consejos. Agradezco a David J. Wales y Jose Miguel Mantas su amabilidad al proveerme de herramientas computacionales con las que desarrollar parte de mi investigación.

Me gustaría agradecer a Delphine Salort, Antoni Guillamon, Juan Calvo, Stéphane Mischler, Claudia García y Sara Merino por formar parte del tribunal para la defensa de esta tesis. También agradezco a Havva Yoldas y Pierre Roux por realizar los informes necesarios para obtener la mención internacional en la tesis.

Agradezco a la Universidad de Granada, al Departamento de Matemática Aplicada y al Instituto de Matemáticas de Granada por poner a mi disposición todos los medios, materiales y humanos, que he necesitado para llevar a cabo mis objetivos durante este período.

Mi mayor agradecimiento a Ana, sin quien no habría conseguido completar esta etapa. Has estado siempre junto a mí, en cada momento de este proceso, ayudándome en todo lo que he necesitado, y por eso te estaré siempre agradecido.

Quiero agradecer a mis padres, Jose y Estrella, junto a mi hermano Dani, su apoyo durante todos estos años. Nunca dudaron en animarme a seguir estudiando, ni dudaron de que pudiera conseguir aquello que me propusiera, y siempre me ayudaron en el camino.

Por último, agradezco a los demás jóvenes investigadores que he conocido durante mi período predoctoral, en especial a Nicolás y Elena, por su ayuda, inspiración e influencia.

Financiación

Esta tesis ha sido posible gracias a la financiación obtenida a través de la beca PRE2018-086776 asociada al proyecto "Ecuaciones en derivadas parciales en modelos de física y biología: análisis y simulación numérica" (MTM2017-85067-P), por parte del Ministerio de Ciencia e Innovación de España, con soporte económico del Fondo Social Europeo.

Contents

List of Figures

Chapter 1

Introduction

The challenge posed by complex systems, featuring numerous particles or agents engaged in nonlinear interactions leading to emergent behaviors, stands as a fundamental subject in the fields of physics and biology. Within the domain of applied mathematics, several models addressing such complexities have been explored, offering dual perspectives encompassing both microscopic and mesoscopic descriptions. Among the complex systems, the brain emerges as one of the most captivating subjects, serving as the focal point for the majority of our endeavors in this study.

Groundbreaking scientific advances in biology and chemistry have allowed scientists a much deeper and more precise understanding of the functioning of the brain and thus of neurons. However, there are still many open questions in the field of neuroscience. Thus, a more profound understanding of the brain could be a crucial tool in medicine to cure or even eradicate a multitude of mental illnesses such as Alzheimer's or Parkinson's disease. Furthermore, a holistic understanding of the brain could help to take psychological treatments to a much more sophisticated level, to tackle depression, anxiety and other psychological problems, as well as to improve our understanding of human beings and the way they think and act.

Several mathematical models of the brain and networks of neurons have emerged over the last decades, that predict and deepen our understanding of the structure of the nervous system. In the recent years, the enhancement of computational power has allowed researchers, by performing numerical simulations and experiments, to go beyond the theoretical study of neural network models. This thesis aims to contribute to this task and apply the state-of-the-art knowledge in partial differential equations and numerical simulations to improve existing techniques and develop new ones that will extend our knowledge of neural networks, using both the study of these models from the microscopic point of view (individual neurons interacting with each other in large numbers) and from the mesoscopic point of view (statistical study of ensembles of neurons). Besides this topic, we will also discuss other models of particle interaction, in which we will review the existing scientific literature and implement computational tools that can enhance the existing results.

1.1 Neuron structure and activity

Neurons are the fundamental cells of the nervous system, responsible for carrying out the functions of processing and transmitting chemical and electrical signals in the brain. They are the basic unit of structure and function in the nervous system, and play a crucial role in everything from muscle movement to cognitive functions such as thought and memory. Let us give a schematic description of the structure of a typical neuron, as well as how the signal transmission process they perform works [88, 89].

Structure of a neuron (see figure 1.1):

- **Dendrites:** These tree-like extensions at the beginning of the neuron are designed to receive signals from other neurons. Each dendrite is covered in synapses, the points of contact where neurotransmitters from other neurons are received.
- **Soma (Cell Body):** Contains the nucleus and most cellular organelles. It integrates the signals received from dendrites and decides whether to pass the signal along the neuron.
- **Axon:** This long, thin projection conducts electrical impulses away from the cell body. Axons can be very long (over a meter in some human neurons).
- **Myelin Sheath:** This is a layer of fatty tissue encasing the axon, made by glial cells. Myelin segments are separated by nodes of Ranvier, where action potentials are regenerated.
- **Axon Terminals (Synaptic Buttons):** These small swellings at the end of the axon are where neurotransmitters are released into the synaptic cleft, the space between neurons.

Signal transmission process:

The **membrane potential** or **membrane voltage** (V) of a neuron is the difference of electrical potential between the inside of the cell and the medium. At rest, neurons maintain a stable electric charge, known as the **resting potential**, V_L, around -70 millivolts (mV). This is achieved through the activity of ion pumps and channels. The sodium-potassium pump plays a crucial role by expelling 3 sodium ions (Na^+) for every 2 potassium ions (K^+) it brings in, creating a concentration gradient and charge difference across the cell membrane. Additionally, leak channels allow small amounts of Na^+ and K^+ ions to move in and out, contributing to the resting potential.

When a neuron receives sufficient stimulating signals, a localized change in electric charge occurs at a specific point called the axon hillock. This change, known as local potential changes, can depolarize the membrane. If the depolarization reaches a threshold level, we will usually call **firing potential** V_F, typically around -55 mV, it triggers the initiation of an action potential.

The action potential progresses through distinct phases. Initially, during depolarization, voltage-activated Na^+ channels open, permitting Na^+ ions to flow into the cell, making the interior more positively charged. After reaching a peak charge (around +40 mV), these Na^+ channels close, and voltage-activated K^+ channels open. This allows K^+ ions to exit the cell, restoring a negative charge, a process known as repolarization. Subsequently, K^+ channels slowly close, which can lead to hyperpolarization, briefly making the cell more negative than its resting potential (**reset potential** V_R). After an action potential, there are refractory periods; the absolute **refractory period** τ, i.e. a time during which the neuron does not interact fully or partially with the other neurons and remains at rest, preventing the initiation of another action potential due to inactive Na^+ channels.

At the end of the axon, synaptic transmission takes place. Here, the action potential causes calcium ions ($Ca2^+$) to enter the neuron. This influx of $Ca2^+$ triggers the release of neurotransmitters from the neuron's terminal into the synapse. These neurotransmitters then cross the synaptic cleft and bind to receptors on the receiving neuron, affecting its electrical charge.

The receiving neuron integrates all incoming signals, both **excitatory** and **inhibitory**, depending on whether they increase or decrease its membrane potential, through a process called signal summation. This summation can occur spatially (combining signals from various sources) or temporally (accumulating signals over time), and it ultimately determines whether the receiving neuron generates its own action potential.

So basically, in summary, a neuron receives signals through the dendrites from other neurons, which may be **excitatory** or **inhibitory**, with a **synaptic delay** between the time of emission of the signals and reception by the particular neuron under consideration. When the **membrane potential** of the neuron reaches a **threshold**, the neuron **spikes**, **reset** to a lower membrane voltage value, and sends an electrical impulse to the other neurons, depending on whether it is excitatory or inhibitory. This spiking process generates a lethargy in the neuron called a **refractory state**.

To mathematically model this process [50, 75, 91, 124], the neuron's membrane is considered as a circuit in which the time evolution of the membrane potential $V(t)$ multiplied by the capacitance C_m is given by an input current $\tilde{I}(t)$.

$$C_m \frac{dV}{dt}(t) = \tilde{I}(t).$$

The input current can be split in different terms, if we consider the effect of the ionic channels mentioned above (Na and K) and the aggregated effect of any other channels (let us call it leak channels L), leading us to rewrite the above equation as

$$C_m \frac{dV}{dt}(t) = -g_{Na}\left(V(t) - V_{Na}\right) - g_K\left(V(t) - V_K\right) - g_L\left(V(t) - V_L\right) + I(t), \qquad (1.1.1)$$

where g_{Na}, g_k and g_L are the conductances, and V_{Na}, V_k and V_L are the reversal potentials corresponding to each channel, and I is the remainder of the input current, once the effects of the ion channels Na, K and L are considered separately.

The basic difference between the mathematical models that describe the behavior of neurons in this way lies in the complexity of the current and simplification of the different ionic channel. For instance in the **Hodgkin-Huxley (HH)** model [83, 84] they use equation (1.1.1) together with a system of ordinary differential equations (ODEs) to determine the state of sodium and potassium channels. However, in this thesis we will focus on the **Integrate and Fire (IF)** model, derived from the model proposed by Lapicque's in 1907 [73, 91], where the ionic currents of potassium and sodium are include in the leak current.

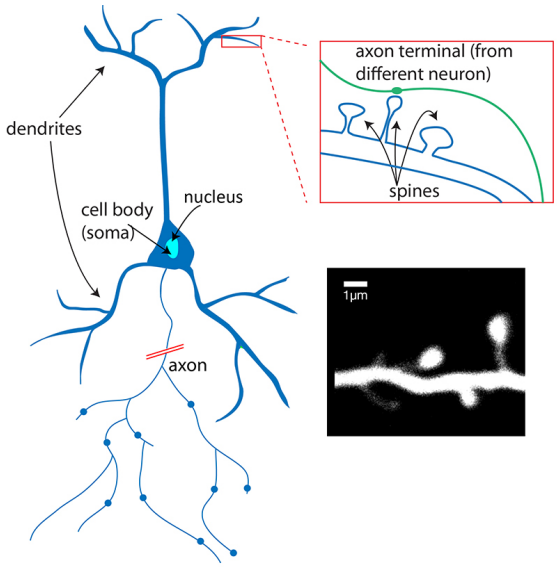

Figure 1.1: **Neuron structure.** Reference: Alan Woodruff ; De Roo et al / CC BY-SA 3.0 via Commons. https://qbi.uq.edu.au/files/7701/Neuron-dendrites-axon-cell_brain-physiology_QBIc.jpg.

1.2 Nonlinear Noisy Leaky Integrate and Fire: from microscopic to mesoscopic

Nonlinear Noisy Leaky Integrate and Fire (NNLIF) neuronal models stand as some of the most basic representations employed to explain the functioning of neuronal networks [9–11, 91, 102, 120]. Over the last decades, there has been a thorough exploration of NNLIF models from a mathematical standpoint, encompassing both numerical and analytical perspectives. This examination has occurred at the microscopic level, involving Stochastic Differential Equations (SDE) [52, 53, 93], and at the mesoscopic/macroscopic level, employing mean field limits characterized by Fokker-Planck type equations (FPE) [14, 16, 18–20, 29, 86, 115]. The substantial volume of publications and lingering inquiries surrounding these models underscores their mathematical intricacy, despite their apparent simplicity. In this section we present the different systems associated with the NNLIF model that will be studied during the thesis.

1.2.1 Microscopic system

Let us consider a large set of $\mathcal{N}$ identical neurons which are connected to each other in a network and described by the NNLIF model, which represents the network activity in relation to the membrane potential, that is, the potential difference on both sides of the neuronal membrane, also called neuron potential or membrane/neuron voltage. The membrane potential $V_i(t)$ of a single neuron i is given by [10, 11, 44, 114]:

$$C_m \dot{V}_i(t) = -g_L(V_i(t) - V_L) + I_i(t), \quad i = 1, \dots, \mathcal{N}, \tag{1.2.1}$$

where C_m is the capacitance of the membrane, g_L is the leak conductance, V_L is the resting potential and $I_i(t)$ are the synaptic currents. These currents are produced by the local and external synapses, i.e. they are the sum of spikes received from C neurons, inside and outside the neuron network:

$$I_i(t) = \sum_j \sum_k J_{ij} \delta(t - t_k^j - d), \quad i = 1, \dots, \mathcal{N}.$$

The Dirac delta $\delta(t - t_k^j - d)$ models the input contribution of each spike; t_k^j is the time when the k-th spike of the j-th neuron took place, J_{ij} is the synaptic strength (positive value for excitatory neurons and negative value for inhibitory ones), and $d \geq 0$ in the argument is the synaptic delay, that is, the time elapsed between neuron j spiking and neuron i perceiving the spike.

A neuron spikes when its membrane voltage reaches the firing threshold value V_F. Then, the neuron discharges itself by sending a spike perturbation over the network, and its membrane potential is set to the reset value V_R. The values of the resting, reset and fire potentials should fulfill $V_L < V_R < V_F$.

We consider networks in which pair correlations can be neglected, as a consequence of the network sparse random connectivity, i.e., $C/\mathcal{N} \ll 1$. We also consider each input as a small contribution compared to the firing threshold ($|J_{ij}| \ll V_F$). Under these conditions (see [10]), if we assume every neuron in the network to spike according to Poisson processes with a common instantaneous probability of emitting a spike per unit time ν, and we consider the mean-field limit when the number of neurons tends to infinity, $\mathcal{N} \to \infty$, given in [10, 11], we can describe the synaptic current of a typical neuron as

$$I_i(t) \simeq \mu_c(t) + \sigma_c(t)\eta_i(t), \quad i = 1, \ldots, \mathcal{N},$$

where $\mu_c(t)$ represents the average value of the current (aggregating the excitatory and inhibitory neurons in the network), $\sigma_c^2(t)$ its variance, and $\eta_i(t)$ is a Gaussian white noise. The average value of the current is split according to external, ν_{ext}, and internal, $N(t)$, activities: $\mu_c(t) = b\nu_{ext} + bN(t)$, where ν_{ext} is a constant and $N(t)$ is the firing rate of the network, that is the number of spikes per unit time. Also $\sigma_c(t) = \sqrt{2a(N(t))}$, with diffusion parameter $a(N) = a_0 + a_1 N$ $(0 \leq a_0, a_1)$, which will be usually considered $a = a_0 = 1$ throughout the thesis. The parameter b will be called the *connectivity parameter* and its value describes how excitatory or inhibitory the network is. If $b > 0$ the network is average-excitatory; a high value of b means that neurons are highly connected, on the other hand $b < 0$ describes a network which is average-inhibitory. The limiting case $b = 0$ means that neurons are not connected with each other and the system becomes linear.

Without loss of generality, usually we shall consider $C_m = g_L = 1$ and the translation of V by a factor $V_L + b\nu_{ext}$ so that the equation (1.2.1), describing the time evolution of the membrane potential of a single neuron in the network, becomes

$$\frac{d}{dt}V_i(t) = -V_i(t) + bN(t-d) + \sqrt{2a_0}\eta_i(t), \quad i = 1, \ldots, \mathcal{N}, \tag{1.2.2}$$

or, in the case without transmission delay ($d = 0$)

$$\frac{d}{dt}V_i(t) = -V_i(t) + bN(t) + \sqrt{2a_0}\eta_i(t), \quad i = 1, \ldots, \mathcal{N}. \tag{1.2.3}$$

As we mentioned above, the system of stochastic differential equations (SDE) is completed with the following boundary condition: $V_i(t_s^-) = V_F$ and $V_i(t_s^+) = V_R$, with t_s any firing time.

Through the analysis of the mean-field limit to the microscopic NNLIF model carried out in [52, 53, 93] we can write the system of SDE describing the evolution in time of the potential $V_i(t)$ for a typical neuron in the network in terms of the *theoretical expectation* $e(t) := \mathbb{E}(M_t)$, where $(M_t)_{t\geq 0}$ counts the number of times that $V_i(t)$ reaches the firing threshold V_F before t. Then $e(t)$ is the theoretical expected number of times that value V_F has been reached, by any neuron of the network before time t. Assuming that the neurons become asymptotically independent, $e(t)$ can be found as the limit of the integral form of the interaction term:

$$e(t) = \lim_{\mathcal{N}\to\infty} \frac{1}{\mathcal{N}} \int_0^t \sum_j \sum_k \delta\left(s - \tau_k^j\right) ds = \lim_{\mathcal{N}\to\infty} \frac{1}{\mathcal{N}} \sum_j^N \sum_k \mathbb{1}_{\{\tau_k^j \leq t\}}, \tag{1.2.4}$$

where $\left(\tau_k^j\right)_{k\geq 1}$ denotes the sequence of spike times of the j neuron of the network. In [52,53] it was proved that the mean firing rate $N(t)$ is the time derivative of the expectation $N(t) = e'(t)$. In this way, we can write equation (1.2.2) as

$$\frac{d}{dt}V_i(t) = -V_i(t) + be'(t-d) + \sqrt{2a_0}\eta_i(t), \quad i = 1, \ldots, \mathcal{N}, \tag{1.2.5}$$

and equation (1.2.3), without delay, becomes

$$\frac{d}{dt}V_i(t) = -V_i(t) + be'(t) + \sqrt{2a_0}\eta_i(t), \quad i = 1, \ldots, \mathcal{N}. \tag{1.2.6}$$

1.2.2 Mesoscopic system

The microscopic stochastic description developed above has a related nonlinear Fokker-Planck equation, which arises as the mean-field limit of a large set of $\mathcal{N}$ identical neurons which are connected to each other in a network [10, 93], as $\mathcal{N} \to \infty$. It is given by the following nonlinear Fokker-Planck equation:

$$\partial_t p(v,t) + \partial_v \left[(-v + bN_p(t-d))\, p(v,t)\right] - \partial_v^2 p(v,t) = \delta_{V_R} N(t), \tag{1.2.7a}$$

where we always denote $\delta_{V_R}(v) \equiv \delta(v - v_R)$, the delta function at the point $v = V_R$. The unknown $p(v,t) \geq 0$ is the probability density of finding neurons at voltage $v \in (-\infty, V_F]$ and time $t \geq 0$, so we are mainly interested in nonnegative solutions for this equation. Each neuron spikes when its membrane voltage reaches the firing threshold value V_F, discharges immediately afterwards, and its membrane potential is restored to the reset value $V_R < V_F$. This resetting effect is described by the right hand side of (1.2.7a), the boundary condition

$$p(V_F, t) = 0, \qquad \text{for } t > 0, \tag{1.2.7b}$$

and the definition of the firing rate $N_p(t)$ as the flux at V_F,

$$N_p(t) := -\partial_v p(V_F, t) \geq 0. \tag{1.2.7c}$$

Moreover, there is a delay $d \geq 0$ in the synaptic transmission, which is included in the drift coefficient $-v + bN(t-d)$. Its effect is sometimes also included in a factor multiplying the diffusion term [10, 14], but we assume the diffusion coefficient to be 1 for simplicity. Our techniques can easily be applied to a constant diffusion coefficient $a = a_0$, but we always consider a coefficient $a = 1$. In order to have unique solutions, the system must include an initial condition of the form

$$p(v, t) = p_0(v, t) \qquad \text{for } v \in (-\infty, V_F] \text{ and } t \in [-d, 0], \tag{1.2.7d}$$

where p_0 is a given function, which will usually be taken throughout the thesis as a constant function in $-d \leq t \leq 0$. The system (1.2.7a) is nonlinear since the firing rate $N_p(t)$ is computed by (1.2.7c). We recall that key parameter of system (1.2.7) is the *connectivity parameter* b, which gives us information on whether the network is on average excitatory or inhibitory: if $b > 0$ the network is average-excitatory; if $b < 0$ the network is average-inhibitory; if $b = 0$ the system is linear and neurons are not connected to each other.

Given any nonnegative, integrable initial condition $p(v, 0) = p_0(v) \geq 0$, the system (1.2.7) satisfies the conservation law $\int_{-\infty}^{V_F} p(v, t)\, \mathrm{d}v = \int_{-\infty}^{V_F} p_0(v)\, \mathrm{d}v$ at any time t for which the solution is defined [18, 29, 115] (we always assume $\lim_{v \to -\infty} p(v, t) = 0$, or other reasonable conditions which ensure appropriate decay of solutions as $v \to -\infty$). For simplicity, and since this does not entail any qualitative changes to the system, we will always consider $\int_{-\infty}^{V_F} p_0(v)\, \mathrm{d}v = 1$.

The number of stationary solutions of equation (1.2.7) and their profiles are well understood [14]. The *probability steady states* (or simply steady states) of the system (1.2.7) are integrable, nonnegative solutions to the following equation:

$$\begin{cases} \partial_v \left[(-v + bN_\infty)\, p_\infty(v) \right] - \partial_v^2 p_\infty(v) = \delta_{V_R} N_\infty, \\ N_\infty := -\partial_v p_\infty(V_F), \qquad p_\infty(V_F) = 0, \\ \text{and} \quad \int_{-\infty}^{V_F} p_\infty(v)\, \mathrm{d}v = 1. \end{cases} \tag{1.2.8}$$

Interchangeably, they are also called *equilibria* in the literature, and we will use either of them as synonyms. These profiles are continuous in $(-\infty, V_F]$, differentiable in $(-\infty, V_R) \cup (V_R, V_F]$, and they are given by

$$p_\infty(v) = N_\infty e^{-\frac{(v - bN_\infty)^2}{2}} \int_{\max(v, V_R)}^{V_F} e^{\frac{(w - bN_\infty)^2}{2}}\, \mathrm{d}w, \tag{1.2.9}$$

where the *stationary firing rate* N_∞ is a solution of the implicit equation

$$N_\infty I(N_\infty) = 1 \tag{1.2.10}$$

with $I(N)$ defined as

$$I(N) := \int_{-\infty}^{V_F} e^{-\frac{(v-bN)^2}{2}} \int_{\max(v,V_R)}^{V_F} e^{\frac{(w-bN)^2}{2}} \,\mathrm{d}w \,\mathrm{d}v. \tag{1.2.11}$$

This implicit equation is obtained as a consequence of the conservation of mass, i.e., the condition $\int_{-\infty}^{V_F} p_\infty(v)\,\mathrm{d}v = 1$.

1.2.3 System with refractory state

A more realistic model than the one presented above, which we will study in chapter 5, is the one that considers a refractory period for neurons that have just fired, i.e. a period of post-firing inactivity.

For the microscopic system, as we have an SDE for each neuron, representing the value of its membrane voltage, we simply define a refractory time τ and keep the potential of each neuron without evolving during this time after a spike. However, in the mesoscopic system we must use a mechanism that allows us to consider two distinct populations of neurons: the active population that has not fired or fired before time $t-\tau$, which we represent by the probability density $p(v,t)$, and the proportion of population which fired between time $t-\tau$ and t, which we will call $R(t)$. To do this, we could use the formulation found in [10], where the refractory population is defined as

$$R(t) = \int_{t-\tau}^{t} N_p(s)ds,$$

being N_p the firing rate associated to p. Nevertheless, we will use the formulation set out in [16], which will be explained below.

The model which describes this phenomenon can be written by adding an ordinary differential equation to (1.2.7), ir order to describe the evolution in time of the refractory state R, in addition to changing the Dirac's delta multiplying term in the Fokker-Planck equation:

$$\begin{cases} \partial_t p(v,t) + \partial_v \left[(-v + bN_p(t-d))\, p(v,t)\right] + \partial_v^2 p(v,t) = \frac{R(t)}{\tau}\delta_{V_R}, \quad v \le V_F, \\ \frac{dR(t)}{dt} = N_p(t) - \frac{R(t)}{\tau}, \quad t \ge 0, \\ N_p(t) := -\frac{\partial p}{\partial v}(V_F, t) \ge 0, \end{cases} \tag{1.2.12}$$

together with the boundary condition $p(V_F, t) = 0$ and such conditions as are necessary to ensure the proper decay of the function in $v = -\infty$. The initial condition to this system of equations is given by

$$\begin{aligned} p(v,t) &= p_0(v,t), \qquad \text{for } v \in (-\infty, V_F] \text{ and } t \in [-d, 0], \\ R(t) &= R_0(t) \geq 0, \qquad \text{for } t \in [-d, 0]. \end{aligned}$$

As in the model without refractory state, $N_p(t)$ represents the flux of neurons in the threshold V_F (firing potential), V_R represents the reset potential and b is the connectivity parameter. The drift and diffusion coefficients are given by $-v + bN_p(t-d)$ and $a = 1$, where parameter $d \geq 0$ inserted in the drift is the transmission delay. Lastly, τ represents the refractory time, i.e. the duration of the refractory period, during which neurons in this state do not interacts with the rest of the network.

By integrating the equation (1.2.12) we derive the following mass conservation law:

$$\int_{-\infty}^{V_F} p_0(v,0)dv + R_0(0) = \int_{-\infty}^{V_F} p(v,t)dv + R(t), \tag{1.2.13}$$

which means that the sum of the active neurons and those in a refractory state is preserved at all times. We set this quantity to 1 without loss of generality.

The time stationary solutions to equation (1.2.12) are given by

$$(v - bN_\infty)p_\infty(v) + \partial_v p_\infty(v) + \frac{R_\infty}{\tau} H(v - V_R) = 0, \quad R_\infty = \tau N_\infty, \tag{1.2.14}$$

where $H(x)$ is the Heaviside function, which means $H(x) = 0$ for $x < 0$ and $H(x) = 1$ for $x \geq 0$.

The solution to this equation can be directly computed as

$$p_\infty(v) = N_\infty e^{-\frac{(v-bN_\infty)^2}{2}} \int_{\max(v,V_R)}^{V_F} e^{\frac{(w-bN_\infty)^2}{2}} dw, \quad R_\infty = \tau N_\infty. \tag{1.2.15}$$

By imposing the conservation law (1.2.13) we get the implicit equation whose solution determines the number of stationary states to system (1.2.12):

$$1 = N_\infty(I(N_\infty) + \tau), \tag{1.2.16}$$

where $I(N)$ is defined in equation (1.2.11).

1.3 State of the art

To the best of our knowledge, this section summarizes the state-of-the-art mathematical results on the NNLIF model. The results can be divided into those related to the global in time existence of solution versus blow-up phenomenon, and those about steady states and long time behavior of the solutions. All of these questions have been addressed for the Fokker-Planck equation (1.2.7), as well as for microscopic models [46,47,66] similar to the one given by the SDE (1.2.6).

Existence theory for the Fokker-Planck equation (1.2.7) was developed in [14, 18, 29, 115]. In [29] an existence criterion for the nonlinear system (1.2.7) without delay ($d = 0$) was given: the solution exists as long as the firing rate $N(t)$ remains finite. The authors proved that for $d = 0$ and $b < 0$ (average-inhibitory case) solutions are global in time, while for $b > 0$ a blow-up phenomenon may appear if the initial condition is concentrated near the threshold potential V_F [14], or if a large connectivity parameter b is considered [115]. In that case, solutions are not globally defined for all times. The blow-up phenomenon disappears if some transmission delay is taken into account, i.e. if $d > 0$, leading to global existence as proved in [18]. Blow-up may also be avoided by considering a stochastic discharge potential [16].

At the microscopic scale analogous criteria for existence and blow-up phenomena were studied in [53]. For the corresponding SDE the notion of solution was extended to the notion of physical solutions in [52]. Physical solutions continue after system synchronization, this is after the blow-up phenomenon, and therefore, they are global in time.

Along with the existence of solutions, the other main line of research from the mathematical point of view for this model is the existence of equilibria and their asymptotic behavior. The study on the number of steady states of the Fokker-Planck equation was carried out in [14] and it can be summarized as follows:

- **Strongly excitatory:** ($b > b_e$) there is no steady state.
- **Highly excitatory:** ($b_e > b > V_F - V_R$) there are at least two steady states.
- **Excitatory:** ($0 < b < V_F - V_R$) there is at least one steady state.
- **Inhibitory, unconnected and low excitatory:** for $b \leq 0$ or $b > 0$ small enough, there is only one steady state.

In the linear case ($b = 0$) [14] proved that solutions converge exponentially fast to the unique steady state. In the quasi-linear case ($|b|$ small), the same is proved in [25] if the initial condition is close enough to the equilibrium.

These results were proved by means of the entropy dissipation method, considering the relative entropy functional between the solution p and the stationary solution p_∞, given by

$$H(p|p_\infty) := \int_{-\infty}^{V_F} \frac{(p(v,t) - p_\infty(v))^2}{p_\infty(v)} \, \mathrm{d}v = \|p - p_\infty\|_{L^2(p_\infty^{-1})}.$$

Recently, approaches based on Doeblin & Harris's theorems in probability have been used in the study of the asymptotic behavior of various equations related to neural networks, for both elapsed time [23] and integrate-and-fire models [59,117]. Both strategies (entropy method and Harris-type theorems), seem to be suitable only for systems that are nearly linear.

It has also been proved that there are no periodic solutions, if $b > 0$ is large enough, $V_F \leq 0$ and a transmission delay is considered [18,115]. Recently in [87] it was shown that periodic solutions can appear in the average-inhibitory case if a large delay is considered for an approximation of the integrate-and-fire model.

The extension of previous analysis on equilibria and asymptotic behavior in the case of the model wit refractory period was done in [16,20]. We summarize here these results:

1. **Number of equilibria:**
   (a) **Excitatory:** ($b > 0$) there is an odd number of steady states (considering multiplicity).
   (b) **Inhibitory:** ($b < 0$) there is only one steady state.
2. **Asymptotic Behavior:** In the linear case ($b = 0$) and the quasi-linear case (b small) it was proved that that solutions converge exponentially fast to the unique steady state.

For the model with refractory periods, the results in [86,136] numerically show periodic solutions.

Parallel to the analytical study, numerical solvers are also developed to better understand the complex dynamics of the Fokker-Planck models [14,19,20,58,86]. However, there is a major difficulty in showing what happens after the blow-up phenomenon, because the firing rate diverges.

The are more realistic NNLIF model than the ones considered in this thesis, which include different populations of excitatory and inhibitory neurons instead of an average population. For those who want to consult the mathematical formulation of the model with separate excitatory and inhibitory populations, its full derivation can be found in [118]. Extensions of the results reported here for the one-population model to the two-population model can also be found in [19,20].

In addition to the studies on the NNLIF models, others have been developed for different PDE families, and their related SDE, which also describe the activity of a neural network, based on the integrate and fire approach: population density models of integrate and fire neurons with jumps [59–61, 102]; Fokker-Planck equations for uncoupled neurons [98, 99]; and Fokker-Planck equations including conductance variables [15, 106, 107, 112] There are also closely related models, not strictly of NNLIF type, such as time elapsed models [103–105] which are derived as mean-field limits of Hawkes processes [39, 40]; McKean-Vlasov equations [1, 97], which are the mean-field equations associated with a large number of Fitzhugh-Nagumo neurons [69]; Nonlinear Fokker-Planck systems which describe networks of grid cells [32,33] and are rigorously achieved by mean-field limits [27]; or cortical models [7, 45] based on the Hodgkin-Huxley description.

1.4 Main results

To conclude this introduction, we will present the main results of our research, arranged by chapter, trying to make them as self-contained as possible. The definitions and results stated and referenced in this section will be repeated with a different numbering in their respective chapters. Thus this section can be omitted if the thesis is to be read in its entirety, or it can be read together with the conclusions (chapter 7) for a summarized view of the thesis.

In chapter 2 we will make a general numerical study of the NNLIF model with an average population and no refractory state, through the microscopic point of view given by the SDEs system. We will propose an Euler-Maruyama type numerical scheme and we will also implement the so-called *cascade mechanism* to better approximate the definition of *physical solution* given by Delarue et al. in [52, 53]. In the numerical results we will find first known behaviors of the model, validating our scheme by finding a multitude of phenomena that have already been seen with the scheme for the Fokker-Planck equation. Additionally, we will find new behaviors that were not known until now, such as the *plateau state*, being the existence of transmission delay one of the fundamental ingredients for the appearance of this.

Our work with the microscopic system and the importance of delay for the emergence of new behaviors motivates us to make a change in the usual approach used to study the asymptotic behavior of NNLIF models, based on entropy methods [14, 25]. Thus, in chapter 3, we will carry out an intensive study of the linear NNLIF model, with the aim of studying the local behavior of the nonlinear equation (1.2.7). Alongside the study of the linear model, we will use techniques similar to those developed in [38, 74, 96]. By working on the spectrum of the operator associated to the linear equation, we will be able to linearize the equation around its equilibria, give an easily testable criterion for its stability and relate the stability of the linearized equation to the nonlinear equation.

Continuing with the idea of the importance of delay as a possible determinant of the stability or instability of solutions to equation (1.2.7), in chapter 4 we define the *sequence of pseudo equilibria* together with its associated *sequence of firing rates*. The idea behind these sequences is that the nonlinear equation with delay is piecewise linear in the delay intervals. Therefore if the delay is large enough, the equation will tend exponentially towards the corresponding equilibrium in each delay interval. Then, for fixed values of the parameters defining the behavior of the nonlinear system (b and $N(0)$), we can construct the sequence of pseudo-equilibria whose elements will be those intermediate equilibria if we consider the system to be piecewise linear.

These mathematical tools will allow us, through the study of a discrete sequence given by a difference equation, to perform a global characterization of the long-time behavior of the non-linear Fokker-Planck equation (1.2.7) with large delay. The prediction that this discrete sequence determines the asymptotic behavior of the nonlinear PDE is justified in several ways: we give extensive numerical evidence where this always occurs; we provide an analytical proof in the case of weak connections (b small); and we provide a connection between the sequence of pseudo-equilibria and the stability criterion in chapter 3 for the linearized equation. The joint use of the sequence of pseudo-equilibria and simulations on the mesoscopic model has also allowed to find periodic states in the strongly inhibitory case, as shown in [87] for an approximation to the system (1.2.7).

In chapter 5, we apply the techniques developed in chapters 2 and 4 to the NNLIF model with refractory state. To do so, we study the model numerically both from the microscopic (SDEs system) and mesoscopic (Fokker-Planck equation) points of view, and we also carry out an analytical study of the sequence of pseudo equilibria for this model, with several objectives in mind. The study of the microscopic model will allow us to extend the definition of physical solution provided in [52,53] to the refractory state case, and will also allow us to find periodic solutions in the no-delay excitatory case, something that has not been found before. The analysis of the sequence of pseudo equilibria, together with the numerical simulations of the mesoscopic system, will serve to characterize the global asymptotic behavior of the NNLIF model with refractory state and large delay.

Finally, in chapter 6 we provide a scientific review of other models from kinetic theory. Specifically, models of interaction between particles through attractive-repulsive potentials of the power law type, which are used to describe mathematically phenomena such as the collective behavior of populations or crystallization. In addition to the review, we show several numerical simulations in which local or global minima of the interaction energy of these particles have been calculated.

1.4.1 Chapter 2

This chapter deals with a thorough numerical exploration of the NNLIF model from the perspective of the microscopic system explained in section 1.2.1. Apart from corroborating results obtained in other papers for the mesoscopic system, this allows us to investigate situations where the numerical schemes used in simulations of the Fokker-Planck equation present problems. In this sense, the original results shown in this chapter, which were not previously found for a mesoscopic description of the NNLIF model, are those related to blow-up situations in the different regimes of the connectivity parameter b. As our interest is mainly based on the study of the blow-up from the microscopic point of view, and this occurs only when we are in the excitatory regime [14], i.e. when $b > 0$, we will only consider these cases. Before showing the main results of the chapter, we will briefly define and explain the concepts necessary for a correct understanding of the results.

Blow-up: The concept of blow-up or blow-up in finite time, from the point of view of the Fokker-Planck equation (1.2.7), refers to the absence of a global existence of solution to the equation as stated in [14]. According to existence theory carried out in [29], there exists a solution to (1.2.7) as long as the value of the firing rate does not explode, that is to say, as long as $N_p(t) < \infty$ for $t \in [0, T]$ being $T > 0$ the maximum time of existence. Therefore, we will say that there is a blow-up when there is a time $T > 0$ where N diverges. From a microscopic point of view, this translates into a synchronization of the system where neurons fire at the same time.

Classical and physical solutions to the SDE (1.2.6)*:* In [52], the authors offer a new notion of solution to the usual one for this system of stochastic equations. With this solution they try to avoid the blow-up and to study the long term behavior of this system. For this reason we will implement it in our simulations to see what happens in blow-up situations. The basic differences between the two notions of solution are the existence of discontinuities in expectation and the establishment of a fixed or dynamic firing threshold and restart potential. Furthermore, in the physical solution, in order to guarantee uniqueness given the possibility of jumps in expectation, the cascade mechanism is used. For the physical solution to make sense, we need $b < V_F - V_R$, in order to avoid neurons to spike twice at time time.

Definition 1.4.1 (*Classical solution*)**.** A classical solution $V(t)$ to equation (1.2.6), with $0 < t < T$, is a strong solution in this interval, which satisfies:

1. The sequence of spiking times is given by

$$\tau_0 = 0, \ \tau_k = \inf\{t > \tau_{k-1} : V(t^-) \geq V_F\}, \quad k \geq 1.$$

And the membrane potential is reset to V_R immediately after: $V(t) = V_R$.

2. The firing rate $N(t) = e'(t)$ is a bounded continuous function in $0 < t < T$.

Definition 1.4.2 (*Physical solution*)**.** A physical solution $V(t)$ to equation (1.2.6), with $0 < t < T$, is a weak solution which satisfies:

1. The sequence of spiking times is given as follows

$$\tau_0 = 0,\ \tau_k = \inf\{t > \tau_{k-1} : V(t^-) + b\Delta e(t) \geq V_F\}, \quad k \geq 1.$$

It is strictly increasing and cannot accumulate in finite time. The membrane potential is reset to: $V(t) = V(t^-) - (V_F - V_R) + b\Delta e(t)$.

2. The discontinuity points of the function e satisfy:

$$\Delta e(t) = \inf\left\{\alpha \geq 0 : \mathbb{P}\left(V(t^-) + b\alpha \geq V_F\right) < \alpha\right\}, \tag{1.4.1}$$

where $\mathbb{P}$ is the probability function of the associated probability space and $\Delta e(t)$ is the variation of the expectation, $\Delta e(t) := e(t) - e(t^-)$.

Cascade mechanism: The rough definition of this mechanism is given in section 2.2.1, however this is fundamentally a firing criterion established for neurons that have reached the threshold or are so close to reaching it that the instantaneous influence of those that have arrived will cause them to fire immediately. Also a dynamic restart potential is set, taking into account the value of the neuron's potential before firing and the size of the "impulse" produced by the others neurons concurrently firing (for a detailed explanation of both the meaning of classical and physical solutions and the cascade mechanism, see [52, 53]).

Trivial solution: We use this name for the situation after blow-up (without delay) with $b > V_F - V_R$ and therefore in the classical solution approach. All neurons are continuously spiking so we represents graphically that as a approximated Dirac's delta at $v = V_R$.

Plateau state or plateau distribution: In this chapter we found that presence of delay in situations where there would otherwise be blow-up, causes the system to tend to the state in which the histogram of voltages shows a uniform distribution between V_R and V_F. It can also occur for $b = V_F - V_R$ without delay.

Equilibrium or steady state: For the mesoscopic system we already established this is a profile p_∞ given by formula (1.2.9), being the stationary firing rate N_∞ a solution to the implicit equation (1.2.10). In the microscopic system we refer to the distribution of voltages V_i, for $i = 1, .., \mathcal{N}$, whose histogram approaches p_∞.

Having explained these concepts, we can now summarize the main results shown in the chapter:

1. Blow-up situation with $b < V_F - V_R$. Physical solution with and without cascade mechanism: We observe that the microscopic system is able to overcome the blow-up, i.e. to continue after full synchronization of the system and converge to the corresponding steady state. This occurs by applying the physical solution concept, and therefore when $b < V_F - V_R$ and there is a unique equilibrium.

2. Bi-stability between low equilibrium and plateau state for $V_F - V_R < b < b_e$ for the delayed system: As explained in section 1.3, there are two equilibria in the range $V_F - V_R < b < b_e$. In this case, we observe a decisive influence of the delay on the behavior of the system is observed. For the case with delay, there is bistability between the low equilibrium and the plateau distribution, depending only on the initial condition of the system. If there is no delay, depending also on the initial condition, the system may tend to the low equilibrium or to the trivial solution.

3. Plateau state or trivial solution for $b > b_e$ depending on the delay: In this range of values of b there is no equilibrium of the system, so that any initial condition will inexorably lead to blow-up, and hence to the trivial solution. In case of non-zero delay, the membrane voltages of the neurons will be distributed according to a plateau distribution, avoiding blow-up.

4. Limit case $b = V_F - V_R$. No need for delay: If we start with an initial condition conducive to blow-up, we find that the system tends to the plateau state. For this specific value of b, which serves as a boundary between the case with a single equilibrium and two equilibria, the limit $N_\infty \to \infty$ is exactly an stationary firing rate of equation (1.2.7). It therefore makes sense that the system tends to the plateau, because the plateau is the limit of profiles given by (1.2.9) when $N_\infty \to \infty$.

1.4.2 Chapter 3

To study the long-time behavior of the NNLIF model, applications of entropy methods have only given results for weakly connected networks (small b) so far, i.e. almost linear systems. Building on these results, we give further properties of the linear operator and extend some of them to the linearization of the PDE (1.2.7). We can thus obtain results about its long term behavior using a different approach that does not require the connectivity parameter b to be small. Here is a summary of the results for solutions to (1.2.7):

1. We give a new proof that, for small $|b|$, the (unique) equilibrium is stable. Our proof works for a given small $|b|$, and any delay $d \geq 0$; this should be compared to [18], where a condition on d was needed. See Section 3.4.1 for a precise statement. The proof we present here is also different from the one, mentioned above, that we proved in chapter 4 by pseudo equilibria sequence.

2. With a similar proof, in Section 3.4.2 we show that linearized stability of an equilibrium implies its nonlinear stability without delay, which is a new result as far as we know. We expect the same to be true also for any positive delay, but the proof runs into technical difficulties that we have not been able to overcome.

3. More importantly, we give explicit criteria to study whether a given equilibrium is linearly stable or not. These criteria are intimately related to the slope at which the curve $N \mapsto (I(N))^{-1}$ crosses the diagonal in Figure 1.2, which also determines the behavior of the firing rate sequence, which provides the pseudo equilibria sequence (see chapter 4 for more details).

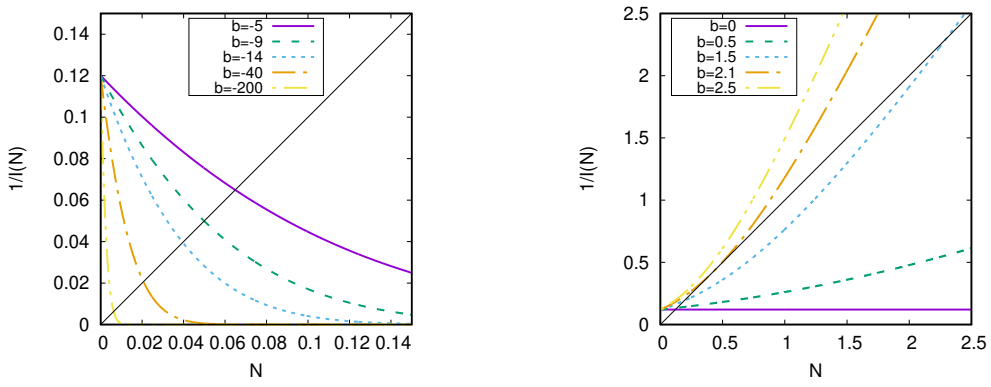

Figure 1.2: **Function $\frac{1}{I(N)}$ (see (1.2.11)) for different values of the connectivity parameter b.** Each crossing with the diagonal corresponds to an equilibrium of equation (1.2.7). Firing and reset potentials set to $V_F = 2$ and $V_R = 1$ respectively.

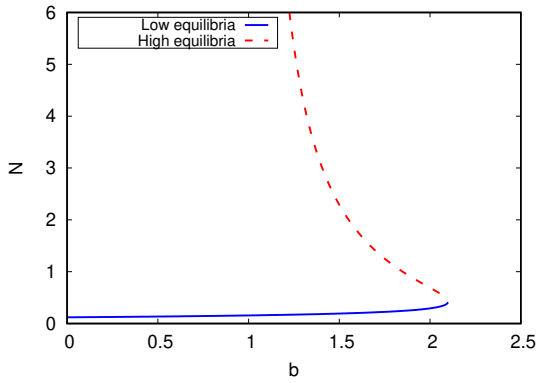

Figure 1.3: **Values of N solving $NI(N) = 1$, for each b.** Point $b = 1$ corresponds to $b = V_F - V_R$ for the selected parameter values. Therefore, there is only one equilibrium for $b < 1$ and two equilibria for $b > 1$, when equilibria exist. The dashed line has a vertical asymptote at $b = 1$. Firing and reset potentials set to $V_F = 2$ and $V_R = 1$ respectively.

Point 3 is in our opinion the most surprising one, since it gives a rather complete picture of the asymptotic behavior of the PDE (1.2.7). In order to state more precisely our theorem regarding point 3 we need to introduce a few definitions. First, given a fixed $N \geq 0$ and $b \in \mathbb{R}$ we define the linear operator L_N, acting on functions $u = u(v)$, by

$$L_N u := \partial_v^2 u + \partial_v((v - bN)u) + \delta_{V_R} N_u. \tag{1.4.2}$$

This operator is formally obtained by replacing N_p on the nonlinear term in the right hand side of (1.2.7a) by N. The associated linear PDE,

$$\partial_t p = L_N p, \tag{1.4.3}$$

with the same Dirichlet boundary condition as before and $N_u(t) := -\partial_v u(V_F, t)$, models a situation where neurons evolve with a fixed background firing rate. A central part of our strategy is based on a careful study of the linear operator L_N. The PDE (1.4.3) has a unique (probability) stationary state p_∞, explicitly given by a very similar expression to (1.2.9):

$$p_\infty^N(v) = \overline{N} e^{-\frac{(v-bN)^2}{2}} \int_{\max(v,V_R)}^{V_F} e^{\frac{(w-bN)^2}{2}} \, \mathrm{d}w, \tag{1.4.4}$$

where $\overline{N}$ is a normalizing factor to ensure that p_∞^N is a probability distribution. It is also known that solutions to this linear equation converge exponentially to equilibrium in the weighted norm $L^2(1/p_\infty)$, which is a natural norm when considering a quadratic entropy [14,25]. By studying some well-posedness and regularization bounds for the linear equation, we are able to show that this exponential decay is also true in the smaller space

X given by

$$X := \{u \in \mathcal{C}(-\infty, V_F] \cap \mathcal{C}^1(-\infty, V_R] \cap \mathcal{C}^1[V_R, V_F] \mid u(V_F) = 0 \text{ and } \|u\|_X < \infty\}, \quad (1.4.5)$$

where

$$\|u\|_X := \|u\|_\infty + \|\partial_v u\|_\infty + \|u\|_{L^2(\varphi)} + \|\partial_v u\|_{L^2(\varphi)} \quad (1.4.6)$$

and

$$\varphi(v) := \exp\left(\frac{(v - bN)^2}{2}\right), \qquad v \in (-\infty, V_F].$$

It is understood that the $L^2(\varphi)$ norms are taken on $(-\infty, V_F]$. The linear space X is a Banach space with the above norm. We observe that $X \subseteq L^2((p_\infty^N)^{-1})$ since for some constant $C > 0$

$$\frac{1}{p_\infty^N(v)} = C\varphi(v) \qquad \text{for all } v \le V_R, \quad (1.4.7)$$

and for any $u \in X$ we have

$$\begin{aligned}\int_{V_R}^{V_F} u(t,v)^2 p_\infty^N(v)^{-1}\,\mathrm{d}v &\lesssim \int_{V_R}^{V_F} u(t,v)^2 \frac{1}{V_F - v}\,\mathrm{d}v \\ &\le \|\partial_v u(\cdot,t)\|_\infty^2 \int_{V_R}^{V_F} (V_F - v)\,\mathrm{d}v \lesssim \|u\|_X^2, \quad (1.4.8)\end{aligned}$$

where we have used the estimate

$$|u(t,v)| \le \|\partial_v u(t,\cdot)\|_\infty (V_F - v) \qquad \text{for } v \le V_F,$$

easily obtained via the mean value theorem and the fact that $u(V_F) = 0$. Inequalities (1.4.7) and (1.4.8) show that $\|u\|_{L^2(p_\infty^{-1})} \lesssim \|u\|_X$, so $X \subseteq L^2(p_\infty^{-1})$.

The property that the linear PDE decays exponentially to equilibrium in a certain space is often stated by saying that it has a *spectral gap* in that space. The technique we use to "shrink" the space where a given linear PDE has a spectral gap was used in [38] in relation to a coagulation-fragmentation PDE, and is linked to operator techniques described in [74] and [96]. A spectral gap in the space X allows us to carry out stability arguments in a more natural way, since now the firing rate N_p, considered as an operator $-\partial_v p(V_F)$ acting on p, is a *bounded* linear operator on X. This allows us to relate the linearized and the nonlinear equations, and to give more precise estimates on the range of parameters where stability or instability take place.

Given $b \in \mathbb{R}$ and a probability equilibrium p_∞ of the PDE (1.2.7), we call $N_\infty := -\partial_v p_\infty(V_F)$ the equilibrium firing rate, and we define the *linearized* equation at p_∞ by

$$\begin{aligned}\partial_t u =&\partial_v^2 u + \partial_v((v - bN_\infty)u) + \delta_{V_R} N_u - bN_u(t-d)\partial_v p_\infty \\ =&L_\infty u - bN_u(t-d)\partial_v p_\infty,\end{aligned} \tag{1.4.9}$$

where $L_\infty \equiv L_{N_\infty}$ is the linear operator from (1.4.2), with $N = N_\infty$. We notice that this equation has a delay d in the last term. We add the same boundary condition as before, that is,

$$u(V_F, t) = 0, \qquad \text{for } t > 0. \tag{1.4.10}$$

Definition 1.4.3. Take $b \in \mathbb{R}$ and $d \geq 0$. We say that a probability equilibrium p_∞ of system (1.2.7) is *linearly stable* if there exist $C \geq 1$ and $\lambda > 0$ such that all solutions u to the linearized equation (1.4.9)–(1.4.10) with an initial condition $u_0 \in \mathcal{C}([-d, 0]; X)$ such that

$$\int_{-\infty}^{0} u_0(v, t)\, \mathrm{d}v = 0 \qquad \text{for all } t \in [-d, 0] \tag{1.4.11}$$

satisfy

$$\|u(\cdot, t)\|_X \leq Ce^{-\lambda t} \sup_{\tau \in [-d,0]} \|u_0(\cdot, \tau)\|_X \qquad \text{for all } t \geq 0. \tag{1.4.12}$$

We say that p_∞ is *linearly unstable* if this is not true for $\lambda = 0$ and any $C \geq 1$; that is, if for any $C \geq 1$ there exists u_0 satisfying (1.4.11) and $t > 0$ such that

$$\|u(\cdot, t)\|_X \geq C \sup_{\tau \in [-d,0]} \|u_0(\cdot, \tau)\|_X.$$

In Chapter 3 whenever p_∞ is an equilibrium of the nonlinear problem, we define

$$q(v, t) := e^{tL_\infty} \partial_v p_\infty, \tag{1.4.13}$$

where e^{tL_∞} denotes the flow of the linear problem (1.4.2) (that is: $e^{tL_\infty} u_0$ is the solution to problem (1.4.2) with initial condition u_0). In agreement with our previous notation we set

$$N_q(t) := -\partial_v q(V_F, t), \qquad \text{for } t > 0 \tag{1.4.14}$$

and call $\hat{N}_q$ the Laplace transform of N_q,

$$\hat{N}_q(\xi) := \int_0^\infty e^{-\xi t} N_q(t)\, \mathrm{d}t. \tag{1.4.15}$$

We prove in Section 3.2 that $|N_q(t)| \leq Ce^{-\lambda t}$ for some $C, \lambda > 0$, and hence $\hat{N}_q(\xi)$ is well defined for $\Re(\xi) > -\lambda$. Here is the final theorem that we are able to prove in Section 3.5:

Theorem 1.4.4. *Take $b \in \mathbb{R}$ and $d \geq 0$, and let p_∞ be a (probability) stationary state of system (1.2.7), and define $\hat{N}_q$ by (1.4.13)–(1.4.15). The steady state p_∞ is linearly stable if and only if all zeros of the analytic function*

$$\Phi_d(\xi) := 1 + b\hat{N}_q(\xi)\exp(-\xi d)$$

(defined for $\Re(\xi) > -\lambda$) are located on the real negative half-plane $\{\xi \in \mathbb{C} \mid \Re(\xi) < 0\}$.

This result simplifies the numerical study of the stability of equilibria, and gives some theoretical consequences. For example, we have:

Corollary 1.4.5. *Take $b \in \mathbb{R}$. If a probability stationary state p_∞ of system (1.2.7) is linearly stable for $d = 0$, then it is linearly stable also for small enough $d > 0$.*

There is a specific value of $\hat{N}_q$ which is linked to the function $I(N)$: in Lemma 3.5.5 we show that

$$b\hat{N}_q(0) = \frac{\mathrm{d}}{\mathrm{d}N}\Big|_{N=N_\infty}\left(\frac{1}{I(N)}\right).$$

As a consequence, analyzing the zeros of $\Phi_d(\xi)$ gives us the following criterion of stability/instability, often easier to check:

Theorem 1.4.6. *Let us set $V_R < V_F \in \mathbb{R}$, $b \in \mathbb{R}$, and let p_∞ be a probability distribution, which is an equilibrium of the nonlinear equation (1.2.7).*

1. *If*
$$\frac{\mathrm{d}}{\mathrm{d}N}\Big|_{N=N_\infty}\left(\frac{1}{I(N)}\right) > 1$$
then p_∞ is a linearly unstable equilibrium, for any delay $d \geq 0$.

2. *If*
$$|b|\int_0^\infty |N_q(t)|\,\mathrm{d}t < 1$$
then the equilibrium p_∞ is linearly stable, for any delay $d \geq 0$.

3. *If*
$$\frac{\mathrm{d}}{\mathrm{d}N}\Big|_{N=N_\infty}\left(\frac{1}{I(N)}\right) < -1 \tag{1.4.16}$$
then the equilibrium p_∞ is linearly unstable when the delay d is large enough.

This criterion is also in agreement with the prediction of the pseudo equilibria sequence given in chapter 4 for networks with large transmission delay. It strikes us that the criterion is given in terms of the slope of $\frac{1}{I(N)}$ (see (1.2.11) for an explicit expression of I), which determines the behavior of the discrete sequence of firing rates studied in chapter 4.

The function $1/I(N)$ can be studied analytically (see chapter 4) to obtain the following consequences of Theorem 1.4.6:

- Case 1 in Theorem 1.4.6 can be proved to hold in the excitatory case $b > 0$, assuming there are two equilibria. The higher equilibrium satisfies $\frac{\mathrm{d}}{\mathrm{d}N}\Big|_{N=N_\infty}\left(\frac{1}{I(N)}\right) > 1$ (with N_∞ the highest stationary firing rate). Hence assuming there are two equilibria, the higher equilibrium is unstable.

- We are not able to check case 2 in Theorem 1.4.6 analytically in any case (though numerical checks are straightforward). This case takes place for the lower equilibrium if there are two of them, and for the single equilibrium when there is only one.

- Case 3 in Theorem 1.4.6 can be rigorously proved to hold when $b < 0$ is sufficiently negative. Hence there is some $b_p < 0$ such that for $b < b_p$ and large enough $d > 0$, the unique equilibrium p_∞ is linearly unstable.

We note that Theorem 1.4.6 may not be fully exhaustive (even ignoring the critical cases where $\frac{\mathrm{d}}{\mathrm{d}N}\Big|_{N=N_\infty}(1/I(N)) = \pm 1$), since it may happen that none of its three possibilities are satisfied. However, from our simulations we suspect that the criterion is in fact exhaustive (excepting the critical cases where $\frac{\mathrm{d}}{\mathrm{d}N}\Big|_{N=N_\infty}(1/I(N)) = \pm 1$), since we expect $N_q(t)$ to have a fixed sign for all $t > 0$, and then

$$|b| \int_0^\infty |N_q(t)|\,\mathrm{d}t = \left|\frac{\mathrm{d}}{\mathrm{d}N}\Big|_{N=N_\infty}\left(\frac{1}{I(N)}\right)\right|.$$

On the other hand, point 3 of Theorem 1.4.6 does not give information on the case of strongly inhibitory systems with small delay. For those cases we must study the zeros of Φ_d, as indicated by Theorem 1.4.4, and the best we can say is Corollary 1.4.5.

The stability criteria in Theorem 1.4.4 and 1.4.6 can be checked numerically and allow us to give a rather complete picture of the stability of equilibria, including the threshold delay for which the equilibrium becomes unstable, as shown in Figure 1.4. Though it is not contained in Theorem 1.4.6, we point out that the expected behavior of the nonlinear system (1.2.7) when (b, d) is in the unstable region with $b < 0$ should be periodic, as shown consistently in simulations (see chapter 4). That is, we expect solutions to converge to a unique (up to time translations) periodic solution with period approximately equal to $2d$. Since the analysis leading to Theorem 1.4.6 is based on the linearized equation, we are not able to show a global behavior such as periodic solutions, but the mechanism for their appearance seems to be given by the presence of delayed negative feedback: in the literature on delay equations there are many instances of periodic behavior, arising due to a delayed system in which the driving force works against the displacement that the system has seen in the previous delay period. See for example the books [54] (especially chapter XV) or [65] for an exposition of this topic.

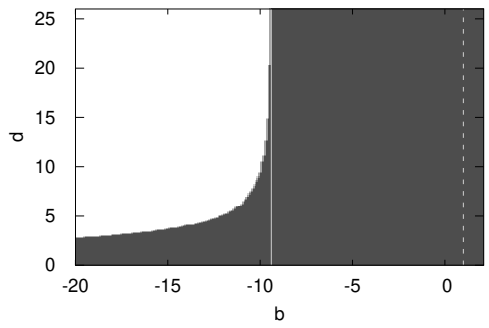

Figure 1.4: **Stability map of the linearized equation.** For each pair of values of the connectivity parameter and transmission delay (b, d), this color map shows the stability (red) or instability (blue) for the solutions of the linearized equation (1.4.9). The vertical black solid line placed at $b^* \approx -9.4$ separates the region of unconditional stability (for any delay d), from that where stability depends on the value of d. The vertical dashed line at $b = 1$ separates the region with a unique steady state (left) from the one with two steady states (right). For cases with two steady states we consider the lower one. The stability condition considered to make the map is based on the statement in Theorems 1.4.4, 1.4.6 (see proof to Theorem 3.5.4 in Section 3.5 for a better understanding of the stability criterion): for each b we find its related equilibrium p_∞, in case of two equilibria we choose the lowest one, which is the only one stable for $d = 0$; we derive p_∞ and use it as initial condition for the linear system given by equation (1.2.7a), being N_∞ the stationary firing rate associated to p_∞; then for each $d > 0$, we compute $Q(k) := -be^{-ikd} \int_0^\infty N_q(t) e^{ikt} dt$, with $k \in \mathbb{R}$ and $q(v, t) = e^{tL_\infty} \partial_v p_\infty$; finally we count the number of times that $Q(k)$ crosses the line $(1, \infty)$ taking into account its orientation. If the net balance of crossings is different from 0, the equilibrium p_∞ related to (b, d) is unstable, otherwise stable. For cases with net 0 crossings we have also computed zeros of function $\Phi_d(\xi) := 1 + b\hat{N}_q(\xi) \exp(-\xi d)$, given in Theorem 1.4.4, to be sure about stability, confirming the results obtained in the previous form.

1.4.3 Chapter 4

We numerically show the relationship between a discrete sequence of *pseudo-equilibria* (defined below) and the long term behavior of the nonlinear system (1.2.7) with large delay. For the case with small connectivity parameter b, we give analytical results on the exponential convergence to equilibrium of the nonlinear system, based on the sequence of pseudo-equilibria and the techniques developed in chapter 3. Our results gives additional evidence for the expected behaviors described in chapter 3, considering large delay d.

Definition 1.4.7 (Firing rates sequence)**.** Given I the function (1.2.11), a firing rates sequence $\{N_{k,\infty}\}_{k\geq 0}$ is a solution of the recursive equation

$$N_{k+1,\infty} := \frac{1}{I(N_{k,\infty})} \quad k = 0, 1, 2, \ldots, \text{ with a provided initial datum } N_{0,\infty}. \tag{1.4.17}$$

We remark that this sequence is well defined since $I(N) > 0$. Associated to a firing rates sequence $\{N_{k,\infty}\}_{k\geq 0}$ we define a pseudo-equilibria sequence:

Definition 1.4.8 (Pseudo-equilibria sequence)**.** Given a firing rates sequence $\{N_{k,\infty}\}_{k\geq 0}$ its associated pseudo equilibria sequence is given by

$$p_{k,\infty}(v) = N_{k,\infty} e^{-\frac{\left(v-bN_{k-1,\infty}\right)^2}{2}} \int_{\max(v,V_R)}^{V_F} e^{\frac{\left(w-bN_{k-1,\infty}\right)^2}{2}} dw, \quad k = 1, 2, \ldots \tag{1.4.18}$$

The behaviors of the sequence of firing rates and sequence of pseudo-equilibria are determined by the values of the connectivity parameter b, the reset potential V_R and the threshold potential V_F, completely detached from the characteristics of the nonlinear system (1.2.7).

The number of equilibria to the firing rate sequence is given by the number of solutions to the following equation:

$$NI(N) = 1, \text{ with } 0 \leq N. \tag{1.4.19}$$

We have denoted the unknown in the equation with N and hope that it will not confuse the reader with the firing rate of the nonlinear system (1.2.7). Since the equation is the same as in the case of system (1.2.7), for fixed parameter b there will be the same number of equilibria to the pseudo-equilibria sequence and the nonlinear system, with identical firing rate values (see figure 1.3).

In the following results we will indistinctly use convergence of the sequence of firing rates or pseudo-equilibria to an equilibrium, because in section 4.3 we showed that if the sequence of firing rates converges to a value, the sequence of pseudo-equilibria will converge pointwise to the equilibrium of the nonlinear system associated to that firing rate.

Analytical results:

1. In the case without equilibria, the firing rate sequence diverges.

2. If there is one equilibrium N^*, the firing rate sequence converges to that equilibrium regardless of the initial condition.

3. If there are two equilibria to the firing rate sequence, N_1^* and N_2^*, the lowest is stable and the highest is unstable. Furthermore: if $N_{0,\infty} < N_2^*$, the sequence $\{N_{k,\infty}\}_{k\geq 0}$ will converge to N_1^*; if $N_{0,\infty} > N_2^*$, the sequence $\{N_{k,\infty}\}_{k\geq 0}$ will diverge.

4. For the nonlinear system (1.2.7) with small connectivity parameter b and large delay d, the equilibrium is stable in terms of the behavior of the sequence of pseudo-equilibria. While a similar result was previously established through the use of the entropy method [25], we present here an entirely distinct strategy, based on the techniques developed in chapter 3. Our result establishes improvements in the range of b and d that can be considered to achieve convergence.

Our numerical results show the global behavior of the NNLIF system with large delay, though its connection with the sequence of pseudo-equilibria. The excitatory cases ($b > 0$) with no equilibrium or one equilibrium were simulated in chapter 2 (particle system SDE) with and without delay, so we have focused on the case with two equilibria, where we can observe both convergence to equilibrium and plateau state phenomena, depending on the initial condition. We have also simulated the inhibitory case $b < 0$, where the sequence of pseudo-equilibria gives meaning to the periodic solutions that had been observed numerically [87]. The sequence of pseudo-equilibria gives us the behavior that the nonlinear system with large delay must exhibit, and this is exactly what happens in the simulations.

Numerical results:

1. In the excitatory case ($b = 1.5$ and $d = 10$) with two equilibria whose firing rates are $N_1^* < N_2^*$: the nonlinear system converges to the lowest equilibrium if the firing rate associated to the initial condition is $N_0 < N_2^*$; the system tends to the plateau state (defined above in results of chapter 2). In both cases the system follows the steps given by the firing rate and pseudo-equilibria sequences for each delay interval.

2. In the inhibitory case ($b < 0$ and different delay values), which has a unique equilibrium: the nonlinear system converges to the steady state if $b > b^* \approx -9.4$ regardless of the delay value; the system converges to the steady state for any $b < 0$ if the delay is low enough (or zero); the system converges to a 2-cycle $\{p^-, p^+\}$ where p^-, p^+ are elements of the pseudo-equilibria sequence, if $b < b^*$ and d is large enough.

To have a precise idea of the values of (b, d) for which the equilibrium is stable or unstable (and therefore tends to 2-cycle), see figure 1.4. Thus in this chapter we give more evidence on the correct application of the theory developed in chapter 3 for the linearized equation, numerically testing how the local behaviors studied in chapter 3 can also be global.

1.4.4 Chapter 5

In this chapter we apply the techniques developed in chapters 2 and 4 to the NNLIF model with refractory period described in section 1.2.3. This variant of the NNLIF model is characterized by considering that after synapsis, neurons remain for a certain time ($\tau > 0$) without interacting with the rest of the network. From the analytical point of view, we will define a succession of pseudo-equilibria equivalent to the one defined in chapter 4 for the model without refractory state, and we will study its monotonicity. After which, we will perform two types of numerical experiments:

- Simulations of the microscopic system associated with this model, through the numerical scheme designed in section 2.3, to observe what happens after the blow-up.
- Simulations of the mesoscopic system, using the numerical scheme developed in [118], in order to study the global long-time behavior of the system and its suitability to the behavior of the pseudo-equilibrium sequence.

Regarding the numerical simulation, we have considered a fixed value of the refractory period $\tau = 0.06$, in the same order of magnitude as that used in other papers in the scientific literature on this model [16, 20, 86]. As explained in the chapter, the number of equilibria in the NNLIF model with refractory period must be odd [16], except for particular values of b where there are equilibria with multiplicity 2. Specifically, 1 or 3 equilibria are observed numerically depending on the value of b, as shown in Figure 1.5. Therefore a fixed value of τ allows us to choose representative values of b with which there are 1 or 3 equilibria. In our case we have done simulations with $b = 2$ and $b = 2.3$.

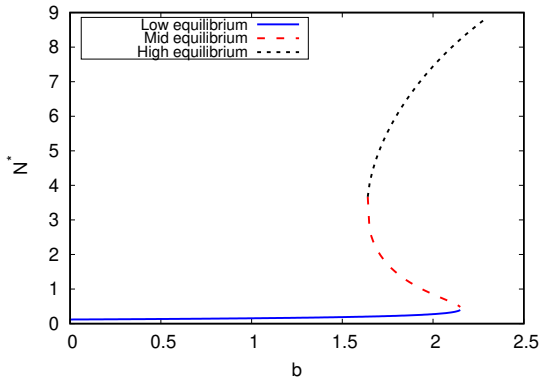

Figure 1.5: **Values N solving $N(I(N) + \tau) = 1$, for each b.** The refractory time is set to $\tau = 0.06$. There is one solution in $(-\infty, 1.64)$ and $(2.15, +\infty)$. There are three solutions in $(1.64, 2.15)$. Firing and reset potentials set to $V_F = 2$ and $V_R = 1$ respectively.

We can divide the summary of the main results of the chapter between analytical results, performed for the pseudo-equilibrium sequence, and numerical results, given by the simulations performed for the non-linear system with large delay.

Analytical results regarding the firing rate sequence:

1. For the excitatory regime ($b > 0$), in the case of one equilibrium, it should be stable regardless of the initial condition.

2. In the case of three equilibria, there is bi-stability between the low and high equilibria, depending on the value of the firing rate of the initial condition.

3. For the inhibitory case ($b < 0$), where there is always a unique equilibrium, which is unstable. The firing rate sequence tends towards a 2-cycle.

Numerical results for the nonlinear system with large delay:

1. **Mesoscopic system:**

   (a) For the inhibitory case, the equilibrium is stable without delay, for any b, and it becomes unstable for large delay, and $b < b^* \approx -9.5$, as the system tends towards a 2-cycle. We have observed a linear inverse dependence between the value of the refractory period and the value of the connectivity at which periodic solutions appear.

   (b) In the case with three equilibria, convergence to low equilibrium is guaranteed if the initial condition is below the intermediate equilibrium in terms of firing rate. In cases where the initial condition is between intermediate and high equilibrium, convergence to high is also observed. Nevertheless, in the cases with initial condition higher than the high equilibrium, we observed a oscillatory phenomena between delay intervals.

   (c) In the case with a high unique equilibrium, its stability presents some problems. At the end of each delay interval the system is close to its pseudo-equilibrium. However, oscillations appear between delay intervals.

2. **Microscopic system:** In the excitatory cases, considering initial conditions that force a blow-up situation, we observe oscillatory solutions. This was found before in [20, 86] for small delay. However, this is the first time that this is observed for zero delay. This leads us to think in the extension of the notion of physical solution, established by Delarue et al. in [52], to the microscopic system with refractory state.

1.4.5 Chapter 6

We consider minimizers of the N-particle interaction potential energy and briefly review numerical methods used to calculate them. We consider simple pair potentials which are attractive at short distances and repulsive at long distances, focusing on examples which are sums of two powers. The range of powers we look at includes the well-known case of the Lennard-Jones potential, but we are also interested in less singular potentials which are relevant in collective behavior models. We report on results using the software GMIN [130] developed by Wales and collaborators for problems in chemistry. For all cases, this algorithm gives good candidates for the minimizers for relatively low values of the particle number N. This is well-known for potentials similar to Lennard-Jones, but not for the range which is of interest in collective behavior. Standard minimization procedures have been used in the literature in this range, but they are likely to yield stationary states which are not minimizers. We illustrate numerically some properties of the minimizers in 2D, such as lattice structure, Wulff shapes, and the continuous large-N limit for locally integrable (that is, less singular) potentials.

Chapter 2

Microscopic description of the Non-linear Noisy Leaky Integrate and Fire neuron model. Physical solution and blow-up

2.1 Introduction

The aim of this chapter[1] is to perform a numerical study on the microscopic description of the NNLIF model, with a triple intention: To compare the two families of models, Fokker-Planck equations (1.2.7) and Stochastic Differential Equations (SDEs) (1.2.5), better understand the notion of physical solution proposed in [52] for the SDEs, study what happens after blow-up for the physical solutions, and understand how it translates to the Fokker-Planck equation. Although the complete derivation of the microscopic description used in this chapter was previously made in section 1.2.1, we will recall the main elements to be used for a better reading and understanding of the chapter.

Let us consider a large set of $\mathcal{N}$ identical neurons which are connected to each other in a network and described by the Nonlinear Noisy Leaky Integrate and Fire (NNLIF) model. The membrane potential $V_i(t)$ of a single neuron i is given by:

$$\frac{d}{dt}V_i(t) = -V_i(t) + be'(t-d) + \sqrt{2a_0}\eta_i(t), \quad i = 1, \dots, \mathcal{N}, \tag{2.1.1}$$

where $d \geq 0$ is the transmission delay, $\eta_i(t)$ are Gaussian white noises, the connectivity parameter b shows how excited or inhibited the network is (if $b > 0$ average-excitatory, $b < 0$ average-inhibitory and $b = 0$ neurons are not connected with each other) and $e'(t)$ is

[1] This chapter compiles the work published in [17].

the derivative of the theoretical expectation, defined as the theoretical expected number of times that value V_F has been reached, by any typical neuron of the network before time t (see section 1.2.1 for a deeper explanation). The system is completed with the boundary condition: $V(t_s^-) = V_F$ (with V_F firing threshold) and $V(t_s^+) = V_R$ (with V_R reset potential), where t_s is the firing time. The mean firing rate $N(t)$ coincides with the time derivative of the expectation, $N(t) = e'(t)$, so we will use them interchangeably to mean the same thing.

This microscopic stochastic description has a related nonlinear Fokker-Planck equation (the full details of which can be found in the section 1.2.2):

$$\partial_t p(v,t) + \partial_v \left[(-v + bN_p(t-d))\, p(v,t)\right] - \partial_v^2 p(v,t) = \delta_{V_R} N(t), \tag{2.1.2}$$

This Partial Differential Equation (PDE) provides the evolution in time $t \geq 0$ of the probability density $p(v,t) > 0$ of finding neurons at voltage $v \in (-\infty, V_F]$. The right hand side represents the fact that neurons return to the reset potential V_R, just after they reach the threshold potential V_F . This means that $p(V_F, t) = 0$. Moreover, $p(-\infty, t) = 0$ is assumed.

We point out the system is nonlinear, for $b \neq 0$, because the firing rate is computed as follows: $N(t) := -a_0 \frac{\partial p}{\partial v}(V_F, t) \geq 0$, which guarantees that the solution of the related Cauchy problem satisfies the conservation law:

$$\int_{-\infty}^{V_F} p(v,t)dv = \int_{-\infty}^{V_F} p^0(v)dv, \quad \text{for } t \in [0,T),$$

for a given initial datum $p(v,0) = p^0(v) \geq 0$ and $T > 0$ the maximal time of existence [18, 29, 115]. Without loss of generality we will take $\int_{-\infty}^{V_F} p^0(v)dv = 1$.

The chapter is structured as follows: Section 2.2 summarizes the notions of solution to the Stochastic Differential Equation (2.1.1), which were analyzed in [52, 53]; in section 2.3, we explain the numerical schemes developed to obtain our numerical results, which are described in section 2.4; and finally in section 2.5, we collect the conclusions and perspectives about the topic.

2.2 Classical and physical solutions to the SDE

In this section we summarize the notions of solution to the Stochastic Differential Equation (2.1.1), which were analyzed in [52, 53]. The main difference between *classical* and *physical* solutions lies in the regularity of the expectation $e(t)$. For classical solutions $e(t)$ is continuous, while for physical ones, $e(t)$ can present certain positive jump discontinuities. In excitatory networks ($b > 0$), there is no global existence for classical solutions when the transmission delay is zero and blow-up situations occur [53]. However, for physical solutions, there is global existence even after the blow-up occurs [52]. From a neurophysiological point of view, the classical notion implies that neurons only fire when they reach the threshold potential. With the physical definition, they can fire if their membrane potentials are close to the threshold value.

Here we present both notions of solution, which are required to understand our study. (See [52, 53] for more precise definitions and an extensive explanation).

Definition 2.2.1 (*Classical solution*)**.** A classical solution $V(t)$ to equation (2.1.1), with $0 < t < T$, is a strong solution in this interval, which satisfies:

1. The sequence of spiking times is given by

$$\tau_0 = 0, \ \tau_k = \inf\{t > \tau_{k-1} : V(t^-) \geq V_F\}, \quad k \geq 1.$$

   And the membrane potential is reset to V_R immediately after: $V(t) = V_R$.

2. The firing rate $N(t) = e'(t)$ is a bounded continuous function in $0 < t < T$.

Definition 2.2.2 (*Physical solution*)**.** A physical solution $V(t)$ to equation (2.1.1), with $0 < t < T$, is a weak solution which satisfies:

1. The sequence of spiking times is given as follows

$$\tau_0 = 0, \ \tau_k = \inf\{t > \tau_{k-1} : V(t^-) + b\Delta e(t) \geq V_F\}, \quad k \geq 1.$$

   It is strictly increasing and cannot accumulate in finite time. The membrane potential is reset to: $V(t) = V(t^-) - (V_F - V_R) + b\Delta e(t)$.

2. The discontinuity points of the function e satisfy:

$$\Delta e(t) = \inf\left\{\alpha \geq 0 : \mathbb{P}\left(V(t^-) + b\alpha \geq V_F\right) < \alpha\right\}, \tag{2.2.1}$$

   where $\mathbb{P}$ is the probability function of the associated probability space and $\Delta e(t)$ is the variation of the expectation, $\Delta e(t) := e(t) - e(t^-)$.

In view of these two definitions, we can realize that a classical solution is also a physical solution without jumps, i.e. $\Delta e(t) = 0$, since $e \in C^1([0,T)]$. Moreover, the membrane potential is reset to $V(t) = V(t^-) - (V_F - V_R) + b\Delta e(t)$, which is V_R since $\Delta e(t) = 0$ and $V(t^-) = V_F$. However, physical solutions may have some jumps with size $\Delta e(t)$, and neurons may spike before they strictly reach the firing voltage V_F. After that, they are reset to $V(t^-) - (V_F - V_R) + b\Delta e(t)$, which is bigger than V_R.

Remark 2.2.3. The notion of physical solution requires that neurons cannot fire more than one spike at the same time. This fact holds if the connectivity parameter b is less than $V_F - V_R$, as we will show in section 2.2.1. We recall that in this case there is a unique steady state to the nonlinear Fokker-Planck equation 2.1.2 modeling the system in the mesoscopic scale [14].

Condition (2.2.1), which might appear very technical, is actually a way of measuring the jumps allowed, so that neurons cannot fire more than once at the same time. For physical solutions, the sequence of spike times, $(\tau_k)_{k\geq 0}$, indicates that a neuron fires if $V(t^-) \geq V_F - b\Delta e(t)$, Proposition 2.1 of [52] proves that for any time t the jump $\Delta e(t)$ satisfies

$$\Delta e(t) = \mathbb{P}\left(V(t^-) + b\Delta e(t) \geq V_F\right).$$

But this size of $\Delta e(t)$ does not guarantee a physical solution. Therefore $\Delta e(t)$ must be the jump α such that

$$\alpha = \mathbb{P}\left(V(t^-) + b\alpha \geq V_F\right)$$

and provides a physical solution. As proposed in [52], the latter happens if α is large enough to 'absorb' the neuron from $V_F - b\alpha$ to V_F. This suggests that $\Delta e(t)$ must be the largest α for which 'absorption' can occur and then

$$\begin{aligned}\Delta e(t) &= \sup\left\{\alpha \geq 0 : \forall \alpha' \leq \alpha, \mathbb{P}\left(V(t^-) + b\alpha' \geq V_F\right) \geq \alpha'\right\} \\ &= \inf\left\{\alpha \geq 0 : \mathbb{P}\left(V(t^-) + b\alpha \geq V_F\right) < \alpha\right\}.\end{aligned}$$

We will see numerically how classical solutions are not able to avoid blow-up situations, which was proved in [14] for the Fokker-Planck equation and for the SDE in [53]. However, for $b < V_F - V_R$ solutions with jumps, i.e. physical solutions, will be able to avoid blow-up phenomena, as it was shown in [52]. In the case of the delayed equation (2.1.1), physical solutions are actually classical. The delay itself guarantees global existence of a classical solution (therefore physical) without jumps, i.e. $\Delta e(t-d)$=0, because $e(t-d)$ is always continuous in this case (see [18, 52]).

The proof of the existence of physical solutions was given in [52] following two different strategies: considering the limit of a particle system when the size of the network tends to infinite and, approximating (2.1.1) by delayed equation (2.1.1) with transmission delay tending to zero, $d \to 0$.

2.2.1 Spikes cascade mechanism for an $\mathcal{N}$ particle system

As we already explained, the SDE (2.1.1) arises as mean field limit of networks composed by $\mathcal{N}$ neurons, with $\mathcal{N} \to \infty$. Therefore, in our simulations, we consider a particle system with $\mathcal{N}$ neurons, that approximates the SDE (2.1.1). Before explaining our numerical schemes we describe the cascade mechanism introduced in [52], which will be implemented in our algorithm. The cascade mechanism establishes how to determine the number of neurons in the network that fire at time t, so that the uniqueness of the physical solution is guaranteed (see [52] for details).

Let us define the set $\Gamma_0 := \{i \in \{1, ..., \mathcal{N}\} : V_i(t^-) = V_F\}$. If that set is not empty, t is a spike time, and neurons in Γ_0 spike at same time t. Then, we consider a second time dimension, the "cascade time axis". We order the spikes that the rest of neurons in the network emits, as a consequence of receiving a kick of size $b\,|\Gamma_0|\,/\mathcal{N}$:

$$\Gamma_1 := \left\{ i \in \{1, ..., \mathcal{N}\} \setminus \Gamma_0 : V_i(t^-) + b\frac{|\Gamma_0|}{\mathcal{N}} \geq V_F \right\}.$$

Iteratively, for $k \in \mathbb{N}_0$

$$\Gamma_{k+1} := \left\{ i \in \{1, ..., \mathcal{N}\} \setminus \Gamma_0 \cup ... \cup \Gamma_k : V_i(t^-) + b\frac{|\Gamma_0 \cup ... \cup \Gamma_k|}{\mathcal{N}} \geq V_F \right\}.$$

The cascade continues until $\Gamma_l = \emptyset$ for some $l \in \{1, ..., \mathcal{N}\}$. Along the cascade time axis, a 'virtual' time axis located at t, neurons in Γ_{k+1} spike after neurons in $\Gamma_0 \cup ... \cup \Gamma_k$, with $k + 1 < l$. We can then define

$$\Gamma := \bigcup_{0 \leq k \leq \mathcal{N}-1} \Gamma_k,$$

which is the set of all neurons that spike at time t, according to the natural order of the cascade. Finally, we update the membrane potential of each neuron in the network by setting:

$$V_i(t) = V_i(t^-) + \frac{b\,|\Gamma|}{\mathcal{N}} \text{ if } i \notin \Gamma, \quad V_i(t) = V_i(t^-) + \frac{b\,|\Gamma|}{\mathcal{N}} - (V_F - V_R) \text{ if } i \in \Gamma.$$

At the end of the cascade process $V_i(t) \leq V_F$ for all $i \in \{1, ..., \mathcal{N}\}$. If $i \notin \Gamma$, it is clear that $V_i(t) < V_F$. And if $i \in \Gamma$, then $V_i(t) = V_i(t^-) + \frac{b|\Gamma|}{\mathcal{N}} - (V_F - V_R)$. Therefore, since $|\Gamma| < \mathcal{N}$ and $b < V_F - V_R$ (see Remark 2.2.3), we obtain

$$V_i(t) = V_i(t^-) + \frac{b\,|\Gamma|}{\mathcal{N}} - (V_F - V_R) \leq V_i(t^-) + b - (V_F - V_R) < V_i(t^-) \leq V_F.$$

We note that all the neurons feel the spikes from the cascade, a kick of size $\frac{b|\Gamma|}{\mathcal{N}}$.

Remark 2.2.4. We note that the relationship between $\Delta e(t)$ and the cascade mechanism for an $\mathcal{N}$ particle system is $\Delta e(t) = \frac{\Gamma}{\mathcal{N}}$. Moreover, Proposition 3.4 of [52] proves the discrete version of (2.2.1) in Definition 2.2.2

$$\Delta e(t) = \frac{\inf\left\{k \in \{0,\dots,\mathcal{N}\} : \sum_{i=1}^{\mathcal{N}} \mathbb{1}_{\left\{V_i(t^-) \geq V_F - b\frac{k}{\mathcal{N}}\right\}} \leq k\right\}}{\mathcal{N}},$$

which motivates the notion of physical solutions to the SDE (2.1.1).

2.3 Numerical scheme

We consider the general equation (2.1.1) with a transmission delay $d \geq 0$.

Let us consider a system of $\mathcal{N}$ identical neurons, and a uniform mesh in the time interval $[0, T]$, with $n+1$ nodes and time step $\Delta t = \frac{T}{n}$:

$$t_0 = 0,\ \dots,\ t_j = t_0 + j\Delta t,\ \dots\ t_n = T.$$

If $d \neq 0$, the value of Δt is chosen as a multiple of it.

The membrane potential of each neuron $i \in \{1, ..., \mathcal{N}\}$ evolves over time following equation (2.1.1). Thus, we integrate this equation over each interval $[t_j, t_{j+1}]$ to obtain:

$$V_i(t_{j+1}) = V_i(t_j) - \int_{t_j}^{t_{j+1}} V_i(s)\ ds + \int_{t_j}^{t_{j+1}} be'(s-d)\ ds + \int_{t_j}^{t_{j+1}} \sqrt{2a_0}\eta(s)\ ds. \quad (2.3.1)$$

After that, using the Euler-Maruyama method for stochastic differential equations, we approximate equation (2.3.1) by

$$V_i(t_{j+1}) = V_i(t_j) - V_i(t_j)\Delta t + be'(t_j - d)\Delta t + \sqrt{2a_0\Delta t}B_i \quad \text{for } i \in \{1, ..., \mathcal{N}\}, \quad (2.3.2)$$

where $V_i(t_j)$ is the approximate value of the membrane potential of the ith neuron at time t_j, and B_i is a Brownian motion with main value and variance given by $\nu_0 = 0$ and $\sigma^2 = \Delta t$. Moreover, we approximate the time derivative of the expectation in terms of the variation of the expectation: $e'(t_j - d) \approx \frac{\Delta e(t_j - d)}{\Delta t}$. Taking into account that the system is nonlinear, the variation of the expectation is computed in two different ways, according to classical and physical solutions. In the first case, we count the number n_d^j of particles having spiked in the interval $[t_{j-1} - d, t_j - d]$. For the physical solution, we consider the number of neurons which reach the firing threshold, following the spikes cascade mechanism described in section 2.2.1 at time t_j, since in this case $d = 0$. In both cases the calculated quantity is divided by the total number of particles $\mathcal{N}$.

Considering the initial condition, as well as the firing and reset conditions, we write our algorithms as follows:

$$\begin{cases} V_i^{j+1} = V_i^j - V_i^j \Delta t + b\frac{n_d^j}{\mathcal{N}} + \sqrt{2a_0\Delta t}B_i, \quad \text{for } i \in \{1, ..., \mathcal{N}\},\ j \in \{0, ..., n\} \\ V_i^0 \text{ initial condition} \\ \text{If } V_i^{j+1} \approx \tilde{V}_F \Rightarrow V_i^{j+1} \leftarrow \tilde{V}_R, \end{cases} \tag{2.3.3}$$

where $n_d^j/\mathcal{N}$ represents the variation of the expectation, and V_i^j the approximate value of the membrane potential of the ith neuron at time t_j. The firing and reset conditions will be different for each type of solution, as explained in section 2.2. There is, however, a common element; we say that a neuron spikes when its voltage reaches a firing threshold $\tilde{V}_F$, and immediately afterwards it returns to the reset potential $\tilde{V}_R$.

Classical solution. In this case, $\tilde{V}_F = V_F$ and $\tilde{V}_R = V_R$, and the numerical scheme (2.3.3) is rewritten as follows:

$$\begin{cases} V_i^{j+1} = V_i^j - V_i^j \Delta t + b\frac{n_d^j}{\mathcal{N}} + \sqrt{2a_0\Delta t}B_i, \quad \text{for } i \in \{1, ..., \mathcal{N}\},\ j \in \{0, ..., n\} \\ V_i^0 \text{ initial condition} \\ \text{If } V_i^{j+1} \approx V_F \Rightarrow V_i^{j+1} \leftarrow V_R. \end{cases} \tag{2.3.4}$$

The number of neurons which reached the firing threshold in the interval $[t_{j-1} - d, t_j - d]$ is recorded in n_d^j, and their membrane voltages are set to V_R. If $d \neq 0$, then, $\Delta e(t_j) = \Delta e(0)$, for $t_j \leq d$.

Physical solution. We do not consider delayed systems for this case. The variation of the expectation, and the firing and reset conditions follow the cascade mechanism explained in section 2.2.1. Thus, the numerical scheme (2.3.3) becomes:

$$\begin{cases} V_i^{j+1} = V_i^j - V_i^j \Delta t + b\frac{n^j}{\mathcal{N}} + \sqrt{2a_0\Delta t}B_i, \quad \text{for } i \in \{1, ..., \mathcal{N}\},\ j \in \{0, ..., n\} \\ V_i^0 \text{ initial condition} \\ \text{If } V_i^{j+1} \geq V_F - b\frac{n^j}{\mathcal{N}} \Rightarrow V_i^{j+1} \to V_i^{j+1} + b\frac{n^j}{\mathcal{N}} - (V_F - V_R), \end{cases} \tag{2.3.5}$$

where n^j is the record value that counts the number of neurons which reach the firing threshold at time t_j, according to the cascade mechanism. The condition $V_i^{j+1} \geq V_F - b\frac{n^j}{\mathcal{N}}$ means that neurons fire before reaching the threshold value V_F. If $\frac{n^j}{\mathcal{N}}$ is a considerable amount, this creates a crucial difference with the process considered in the classic description. To compare the results obtained by the particle system with those known for the Fokker-Planck equation, we need a sufficiently large number of particles and a time step small enough. After some tests, we find those values which guarantee that: $\mathcal{N} = 80000$ for the number of neurons and $\Delta t = 10^{-6}$ or $\Delta t = 10^{-8}$ for the time step, depending on the nature of the problem. The comparison between the approximate values of the solution of the Fokker-Planck equation (2.1.2) and our numerical results is made using histograms of the voltages from our simulations.

2.4 Numerical results

The behavior of solutions of the NNLIF models depends strongly on the value of the connectivity parameter b. Depending on that value, there is a different number of steady states. That number is found solving equation (1.2.10), which is an implicit equation for the firing rate N:

$$NI(N) = 1, \quad \text{with } I(N) = \int_{-\infty}^{V_F} e^{-\frac{(v-bN)^2}{2}} \int_{\max(v,V_R)}^{V_F} e^{\frac{(w-bN)^2}{2}} \, \mathrm{d}w \, \mathrm{d}v,$$

(see [14] for details). Figure 2.1 shows the intersections between $I(N)N$ and the straight line 1, which provide the stationary firing rates of the Fokker-Planck equation (2.1.2).

We structure our results taking into account the restriction in the connectivity parameter so that the notion of physical solution makes sense. First, we analyze the case $b < V_F - V_R$, where there is a unique stationary state (see figure 2.1) and the notion of physical solution makes sense. In the case $b \geq V_F - V_R$, where physical solutions do not make sense, we address the study in two different subsections: First, we describe the case $b > V_F - V_R$, and secondly, we analyze the limiting case ($b = V_F - V_R$), right at the value where the notion of physical solution ceases to make sense. Through the particle system, we replicate the results obtained in [14] for the Fokker-Planck and we study the behavior of the system beyond blow-up phenomenon. For connectivity values $b \geq V_F - V_R$, we observe the formation of certain distributions, which we call "plateau". To our knowledge, these types of distributions had not been shown before for the NNLIF models. We end this section with a justification for their formation, section 2.4.4.

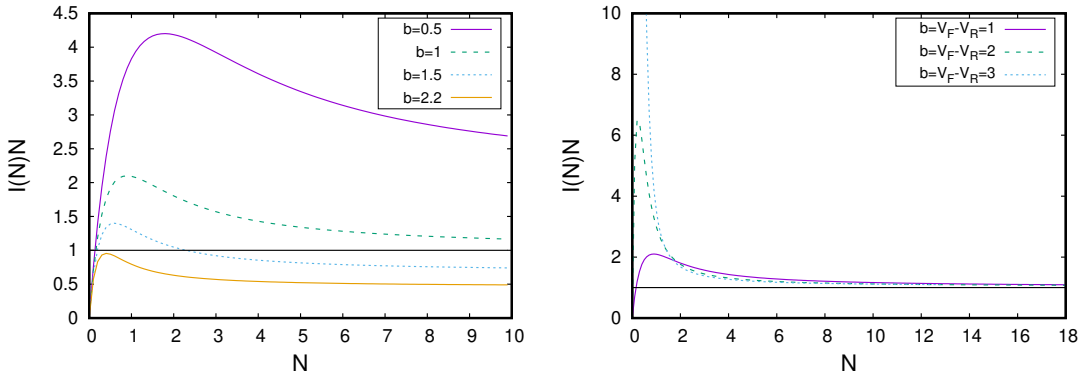

Figure 2.1: **Number of steady states depending on the connectivity parameter b**. Intersections between function $I(N)N$ and the straight line one provide the stationary firing rates of the Fokker-Planck equation (2.1.2). *Left*: Function $I(N)N$ for fixed values: $V_F = 2$, $V_R = 1$ and $a = 1$ and different values of the connectivity parameter b. *Right*: Function $I(N)N$ for values of connectivity parameter exactly the distance between V_F and V_R. $V_R = 1$ and V_F takes the values $\{2, 3, 4\}$.

For every value of b, simulations have been performed with and without delay, as well as using the cascade mechanism when the physical solution makes sense. In the simulations, unless otherwise indicated, we consider the following fixed values: 80000 neurons, i.e., $\mathcal{N} = 80000$, $a = 1$, $V_R = 1$ and $V_F = 2$. The number of neurons considered has been numerically tested, proving its validity for each experiment performed. Figure 2.2 shows two experiments with different values of $\mathcal{N}$. We can observe that for values $\mathcal{N} = 80000$ and $\mathcal{N} = 800000$ the distributions shapes are very similar, even taking into account the stochastic behavior of the system. However, for low values of $\mathcal{N}$ the voltage distribution is very sharp and differs from those calculated for higher values of $\mathcal{N}$.

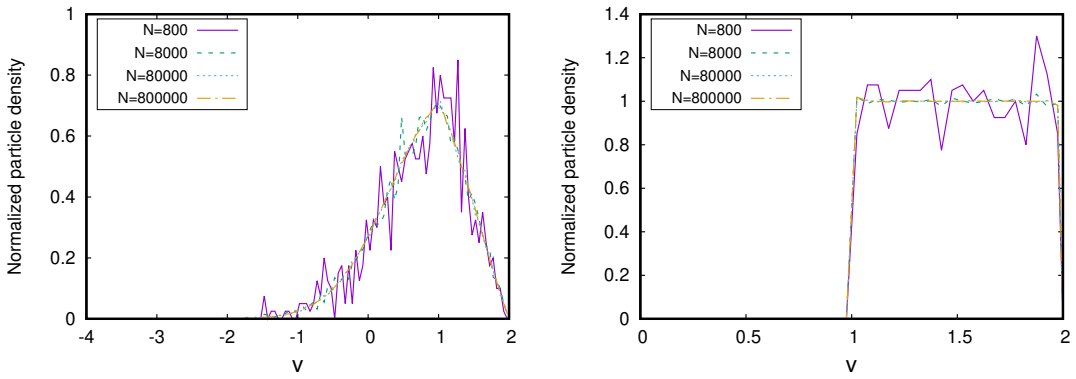

Figure 2.2: **Numerical tests to set the number of neurons $\mathcal{N}$ that approximate the system with $\mathcal{N} \to \infty$.** *Left*: $b = 1.5$. The system starts with a Gaussian initial condition and evolves towards a steady state. Distribution at time $t = 0.5$. *Right*: $b = 1$. A very singular situation where neurons are evenly distributed between V_R and V_F. Distribution at time $t = 0.005$.

2.4.1 Physical solutions: $b < V_F - V_R$

In this section we describe the behavior of the physical solutions of the model. We also compare the results with those obtained for the delayed system and for the Fokker-Planck description. We recall that in this case there is a unique stationary solution (see figure 2.1) and the solutions can explode in a finite time, if the initial data is highly concentrated around the threshold potential [14]. We numerically study these two properties of the model for the particle system.

We consider $b = 0.5$ in our simulations (the behavior for different values of b is qualitatively equivalent), and two different kind of initial data, whose histograms are described in figure 2.3. These histograms show the initial distribution through which we order the 80000 neurons that compose the particle system, depending on the value of their membrane potential. In the left plot we consider a normal distribution with $\nu_0 = 0$ and $\sigma^2 = 0.25$. We consider this initial condition for simulations which describe global existence situations. While in the right plot, we consider a normal distribution with $\nu_0 = 1.83$ and $\sigma = 0.003$, placed very close to the threshold potential ($V_F = 2$). This initial condition is used to study the blow-up phenomenon.

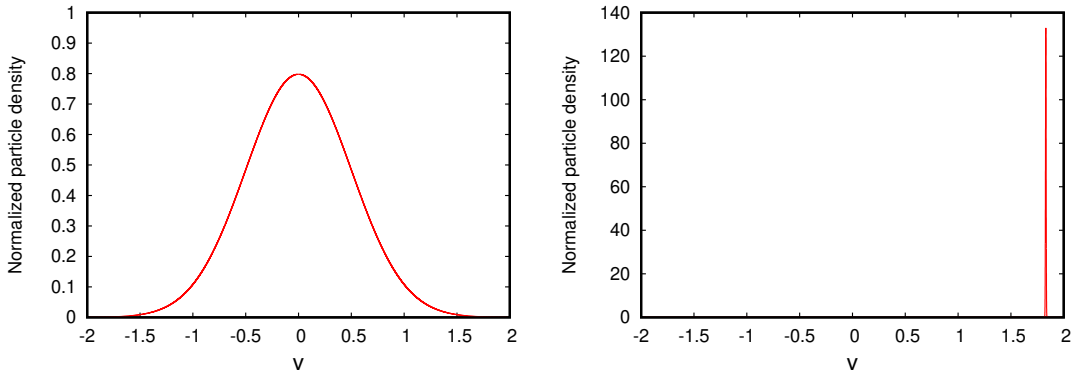

Figure 2.3: **Two initial distributions of the particle system**. *Left*: normal distribution with $\nu_0 = 0$ and $\sigma^2 = 0.25$. *Right*: normal distribution with $\nu_0 = 1.83$ and $\sigma = 0.003$.

Convergence to the stationary solution

We consider an initial datum which is far from V_F (left plot of figure 2.3), and the algorithm for classical solutions described in section 2.3. Figure 2.4 shows the evolution in time of the solution until it reaches the steady state.

We observe a very sparse firing rate value, figure 2.4a, whose arithmetic mean is around the value 0.14, in accordance with the value found for the Fokker-Planck equation [14]. Figure 2.4b shows the evolution of the expectation along the simulation. At the beginning the expectation remains almost zero, because the initial condition guarantees that there are not neurons spiking. After that the expectation increases due to the effect of the diffusion. The distribution of the voltage values at the end of the simulation is shown in figure 2.4c compared to the the stationary solution of Fokker-Planck equation given in [14].

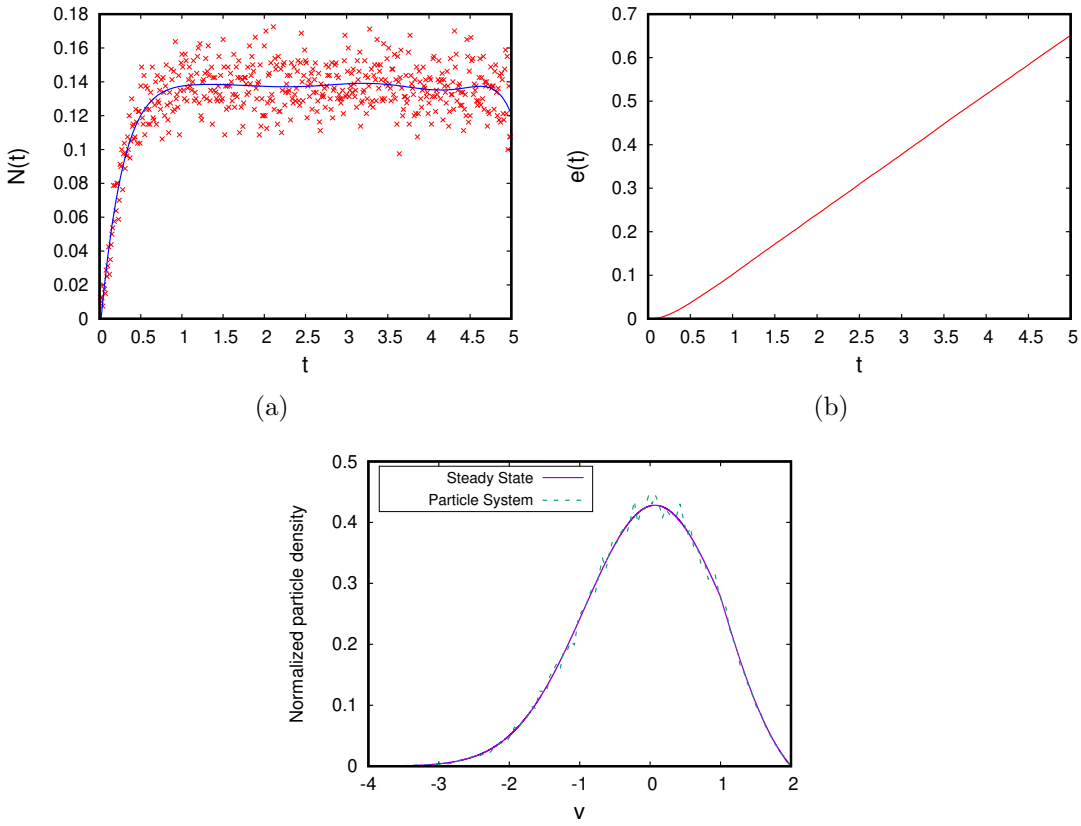

Figure 2.4: **Convergence to the steady state. $\mathbf{b = 0.5}$.** The initial condition is a normal distribution with $\nu_0 = 0$ and $\sigma^2 = 0.25$. *(a)* Time evolution of the firing rate. *(b)* Time evolution of the expectation. *(c)* Particle voltage distribution at final time 5 in comparison with the stationary solution of Fokker-Planck equation.

Blow-up phenomenon

To describe the blow-up phenomenon we consider the initial datum given in figure 2.3 Right, and, as first step, the algorithm for classical solutions (see section 2.3). The evolution in time of the solution is described in figure 2.5. Figures 2.5a and 2.5b show that blow-up occurs at the beginning of the simulation, the firing rate increases very fast. We observe that the expectation is set to 1, which means the total number of spikes is already $\mathcal{N}$. Since the initial distribution of neurons is an approximation of a Dirac delta centered near the threshold value V_F, the value $\Delta e = 1$ indicates that the blow-up has occurred, because all neurons have fired in this short time frame. Our numerical code verified this by tracking the activity of each neuron individually and showing that each neuron fired once in this period. After that the increasing rate of the expectation decreases.

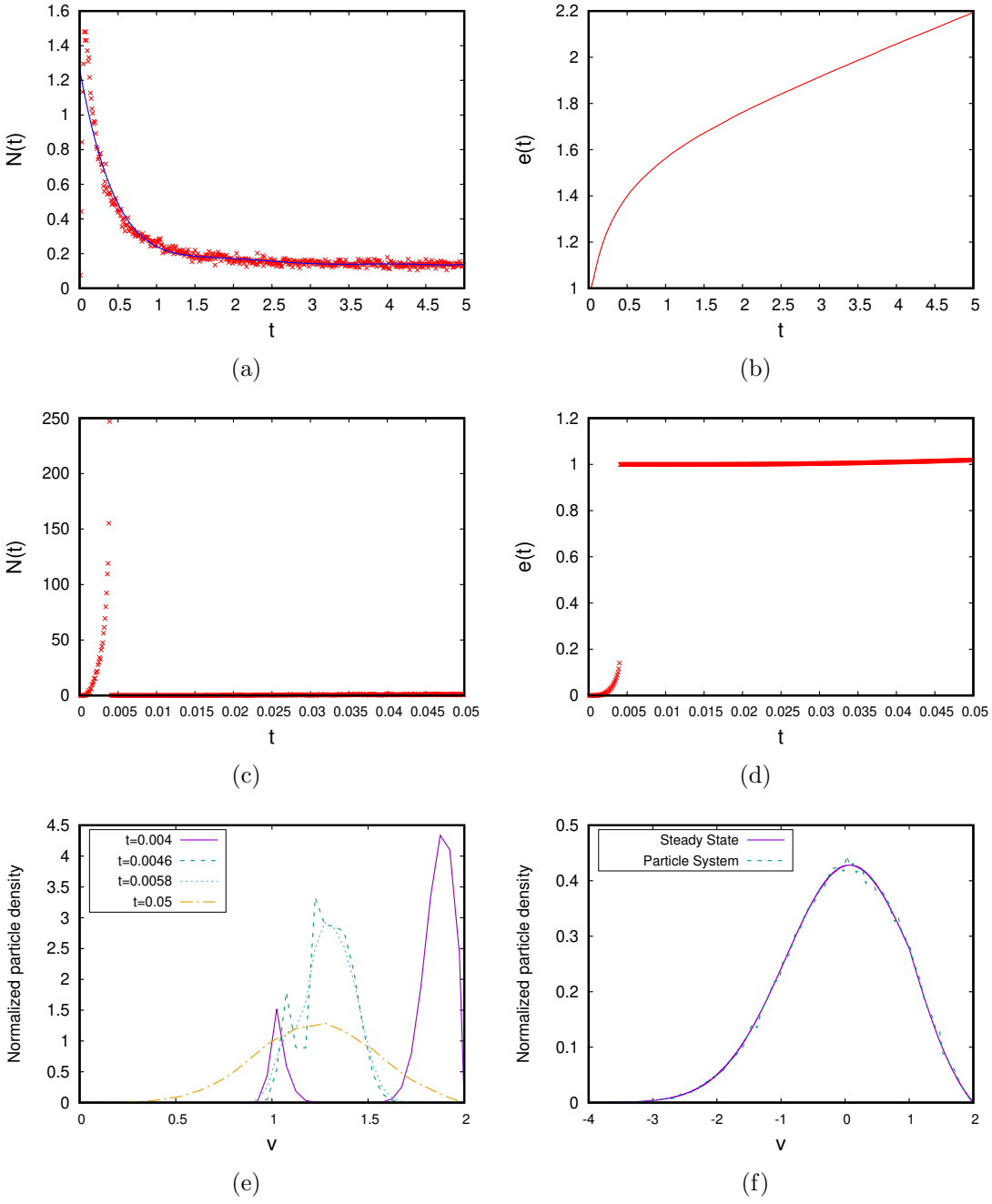

Figure 2.5: **Blow-up phenomenon with classical approach**. $\mathbf{b = 0.5}$. The initial condition is a normal distribution with $\nu_0 = 1.83$ and $\sigma = 0.003$. *(a)* Time evolution of the firing rate. *(b)* Time evolution of the expectation. *(c)* Time evolution of the firing rate before and after the blow-up. *(d)* Time evolution of the expectation before and after the blow-up. *(e)* Time evolution of the particle voltage distribution before and after the blow-up. *(f)* Particle voltage distribution at time 5 in comparison with the stationary solution of Fokker-Planck equation.

In figure 2.5a we see how the firing rate increases very fast to its maximum value, and then decreases to the stationary value. Figures 2.5c and 2.5d show the singularity that occurs during the blow-up time, when the derivative of the expectation, i.e., the firing rate, becomes infinity for the mean field limit. After that, the expectation shows that every neuron has spiked and then it grows slowly. In the figure 2.5e, we observe the value of the voltages distribution before and after the blow-up phenomenon. The distribution at $t = 0.004$ is obtained before almost all the neurons spike at once. After that, the distribution shows a very singular shape ($t = 0.0046$), to subsequently becomes more regular and evolves to the steady state.

Therefore, figure 2.5 shows that the particle system continues after the blow-up and converges to the unique stationary distribution (see figure 2.5f). In this process, the notion of a classical solution is lost, since the expectation has a jump and therefore, the solution really becomes physical. After the synchronization of the system (explosion time), the expectation becomes continuous again and the system evolves towards the steady state, in a classical way.

Cascade mechanism

To better understand the notion of physical solution, we repeat the previous experiment considering the cascade mechanism (see section 2.3). We observe that the behaviour of the particle system is very similar with both approaches. In figures 2.6a and 2.6b the firing rate and the expectation perform a similar behavior to the blow-up one described with the algorithm without cascade mechanism. The voltages distribution before and after the blow-up, figure 2.6c, are also similar to the one showed before. After that, the system stabilizes to the unique steady state (see figure 2.6d).

The main differences between both approaches are observed in figure 2.6e, which describes the values of the voltages distributions in the blow-up time. The distribution with cascade mechanism is shifted to the right, since the reset value is $\tilde{V}_R = V(t^-) - (V_F - V_R) + b\Delta e(t)$, which is different from V_R because $\Delta e(t) \neq 0$. Moreover, we appreciate a group of neurons that has not yet fired, in the "cascade off" picture, while the "cascade on" distribution has completely overtaken the firing threshold. This happens because the cascade mechanism allows neurons to fire at $\tilde{V}_F = V_F - b\Delta e(t)$. Also the expectation variation is different to the computed in the classical case, since it counts spikes which occur beyond Γ_0 (see section 2.2.1). In particular, the variation of the expectation computed without cascade mechanism was $\Delta e(t) = 0.303075$, lower than that calculated in the cascade model, whose value is $\Delta e(t) = 0.574662$.

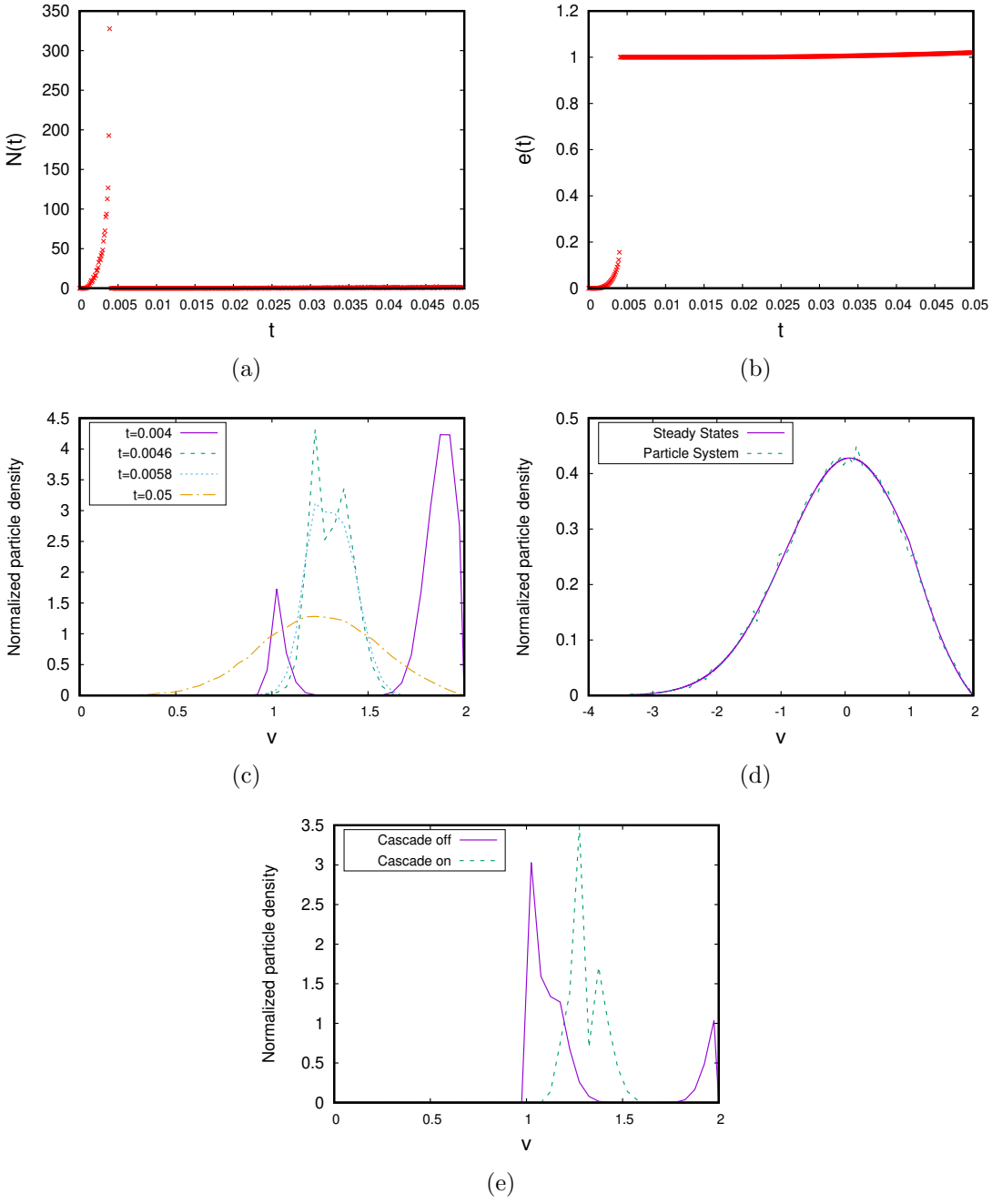

Figure 2.6: **Blow-up phenomenon with cascade mechanism**. $\mathbf{b = 0.5}$. The initial condition is a normal distribution with $\nu_0 = 1.83$ and $\sigma = 0.003$. *(a)* Time evolution of the firing rate before and after the blow-up. *(b)* Time evolution of the expectation before and after the blow-up. *(c)* Time evolution of the particle voltage distribution before and after the blow-up. *(d)* Particle voltage distribution at time 5 in comparison with the stationary solution of Fokker-Planck equation. *(e)* Comparison of the voltage distributions in the blow-up moment with both approaches: with and without cascade mechanism.

Transmission delay

Finally, we analyze how the transmission delay avoids the blow-up phenomenon. With this aim we consider: a normal distribution with mean $\nu_0 = 1.83$ and standard deviation $\sigma = 0.003$, as initial distribution; and three different transmission delays: $d = 0.1$, $d = 0.01$ and $d = 0.001$. Figure 2.7 shows that neurons achieve managing to dodge the blow-up phenomenon, because the firing rate and the expectation prevent the singularities with the transmission delay.

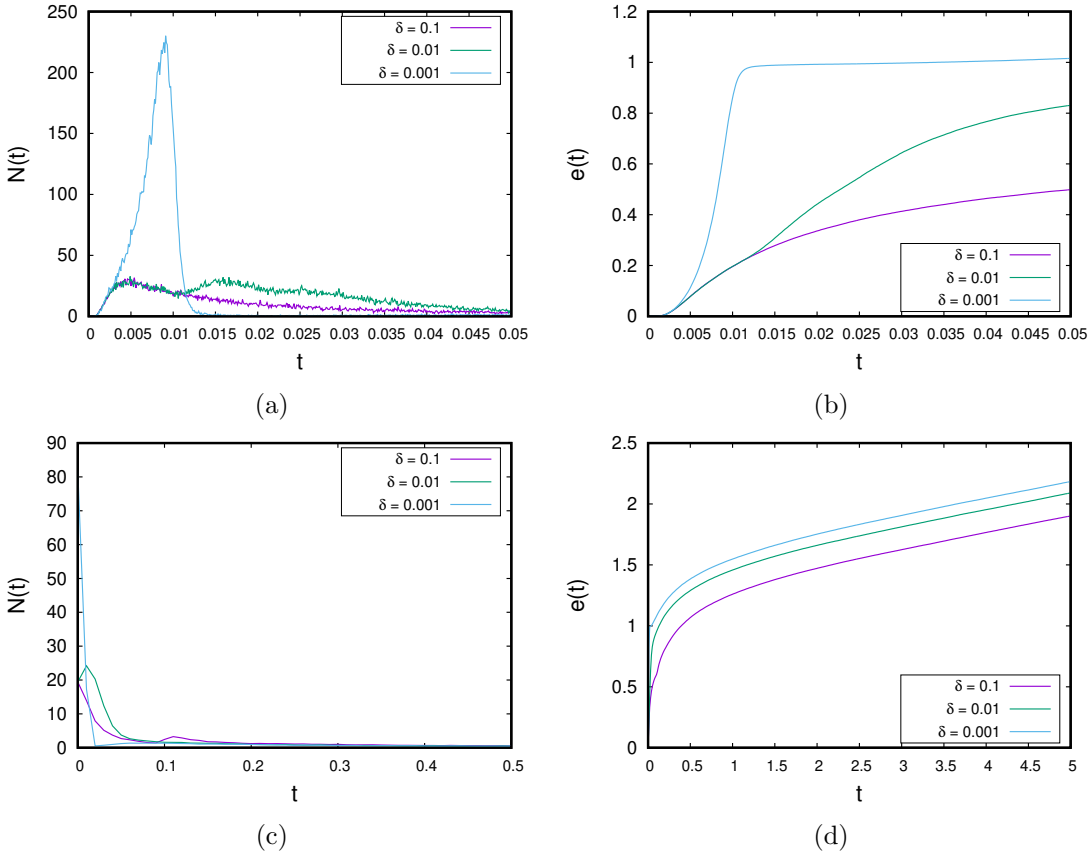

Figure 2.7: **Blow-up situation with delay**. $\mathbf{b = 0.5}$. The initial condition is a normal distribution with $\nu_0 = 1.83$ and $\sigma = 0.003$. We considered different values for the delay. *(a)* Time evolution of the firing rate until 0.05. *(b)* Time evolution of the expectation until 0.05. *(c)* Time evolution of the firing rate until time 0.5. *(d)* Time evolution of the expectation until time 5.

In figure 2.7a we observe how the firing rate increases until it reaches its maximum value and then decreases. Therefore, the expectation does not present any singularity, see figure 2.7b, and the solution is classical. However, if $d \to 0$ the firing rate diverges in finite time, because its maximum value is higher when the value of the transmission delay is

reduced, and the solution will be physical, instead of classical. In the long time behavior, the firing rates converge to the stationary value, see figure 2.7c, since the growth rates of the expectation are the same, figure 2.7d. As a consequence, the system converges to the unique steady state.

2.4.2 Non-physical solutions $b > V_F - V_R$

In this section we focus on the case $b > V_F - V_R$, where the notion of physical solutions does not make sense, since the neuronal network is strongly excitatory and neurons could fire more than one spike at the same time (see Remark 2.2.3). We remember that for this range of values of b, the system has two steady states or none (see figure 2.1). We describe both situations with $b = 1.5$ (two steady states) and $b = 2.2$ (no steady states).

Case with two steady states. Connectivity parameter b = 1.5

For $b = 1.5$, the long time behavior for Fokker Planck Equation solutions was numerically studied in [14]: the steady state with lowest firing rate is stable, while the higher one is unstable, and the network explodes at finite time for certain initial conditions. Here we reproduce these phenomena at the level of the particle system. We discover that the particle system, in cases where blow-up occurs, tends to a "plateau distribution" if we consider a transmission delay.

Convergence to the stationary solution with the lowest firing rate.- Let us consider two different initial conditions for the particle system voltages, which are far from the threshold V_F, (see figure 2.8a): a normal distribution with $\nu_0 = 0$ and $\sigma^2 = 0.25$, and the profile given by

$$p(v) = \frac{N}{a} e^{-\frac{(v-N)^2}{2a}} \int_{max(v,V_R)}^{V_F} e^{\frac{(w-bN)^2}{2a}} dw \tag{2.4.1}$$

with $N = 2.31901$, which approximates the highest stationary firing rate. The profile (2.4.1) is an approximation of the steady state for the Fokker-Planck equation with the highest firing rate (see [14] for details).

In the first case, where the initial condition is a normal distribution, the particle system tends to the steady state with lowest firing rate value, see figure 2.8b. The evolution over time is described in terms of the firing rate in figure 2.8c, and also through the expectation in figure 2.8d. The firing rate evolves towards the lowest stationary value, and therefore, the expectation presents a linear growth at the end of the simulation.

To describe the unstability of the steady state with the highest firing rate value, we consider the second initial datum, profile (2.4.1). In figure 2.8b, we see that the distribution of voltages ends up in the same steady state as in the previous case. Simulations starting with the profile (2.4.1) and a little increase of the value N produce the explosion in finite time, as in [14]. Therefore, based on our results, and results in [14], the steady state with the highest firing rate appears to be a "limit state" between situations of convergence towards the lowest steady state and those of blow-up.

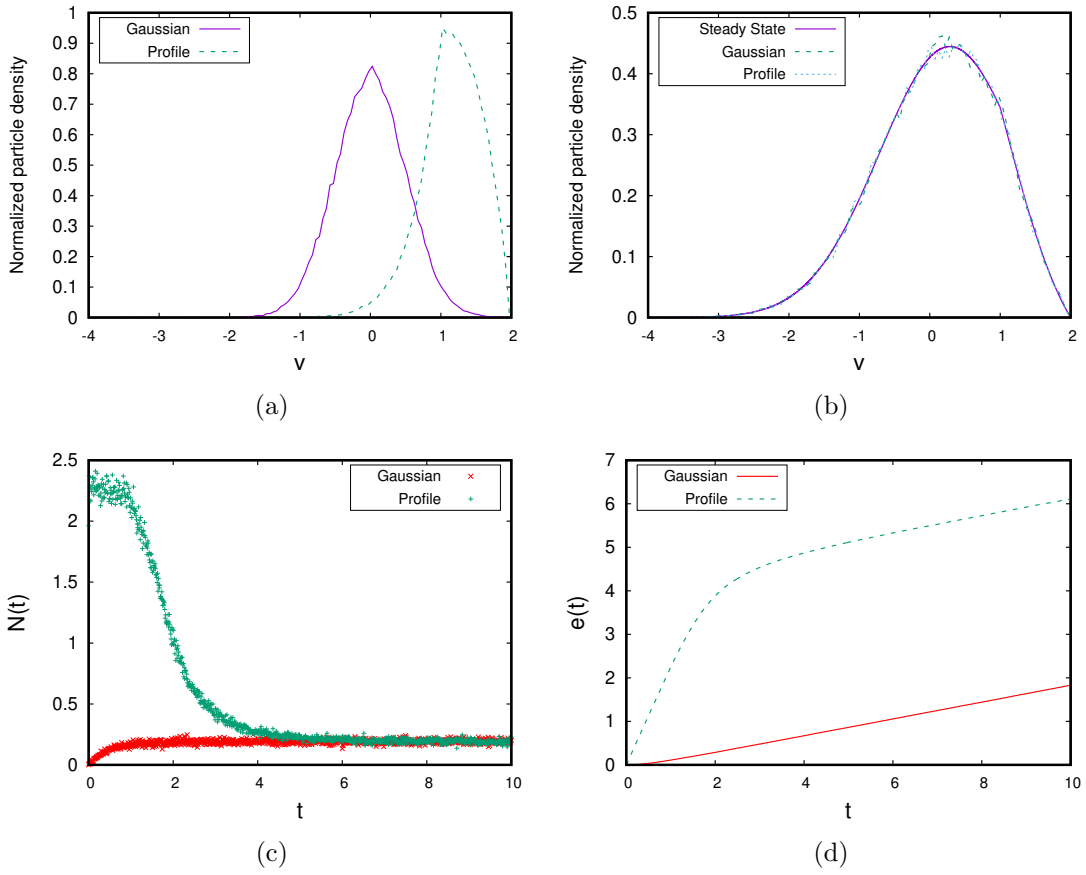

Figure 2.8: **Convergence to the lowest steady state. b = 1.5**. The initial condition is a normal distribution with $\nu_0 = 0$ and $\sigma^2 = 0.25$ in the "Gaussian" case and a profile distribution given by equation (2.4.1) in the "Profile" one. *(a)* Initial conditions used in the simulations. *(b)* Particle voltage distributions at time 5 in comparison with the lowest steady state of Fokker-Planck equation. *(c)* Time evolution of the firing rate. *(d)* Time evolution of the expectation.

Blow-up phenomenon.- We consider an initial condition given by a normal distribution with $\nu_0 = 1.83$ and $\sigma = 0.003$ (right plot of figure 2.3), and we show the data obtained during the simulation in figure 2.9. After a short period of time, almost all neurons spike simultaneously (blow-up phenomenon). Then neurons reset their voltages to the value V_R.

However, the variation of the expectation computed in the blow-up time is so large that the whole network can spike again in the next step. This means that, if blow-up occurs at time t_{j-1}, then $b\frac{n^j}{N} > V_F - V_R$, due to the high value of the connectivity parameter b. This phenomenon causes the system to be in a constant state of blow-up and reset, which we call "trivial solution". In figure 2.9a we observe the voltages distributions obtained before and after the blow-up. The final value of the voltage distribution shows that all neurons are located in V_R. So that "trivial solution" appears to be a Dirac delta at V_R, because neurons reset to V_R at blow-up time. Consequently, in figure 2.9b we see that the final value of the expectation is near to $T/\Delta t = 5 \times 10^6$, which is the value that expectation would reaches if all neurons spike in each step from beginning to end of the simulation. In figure 2.9c we see clearly the moment when the firing rate diverges for the first time. We observe that immediately after blow-up time, the firing rate is zero because the potentials of the neurons are reset to V_R.

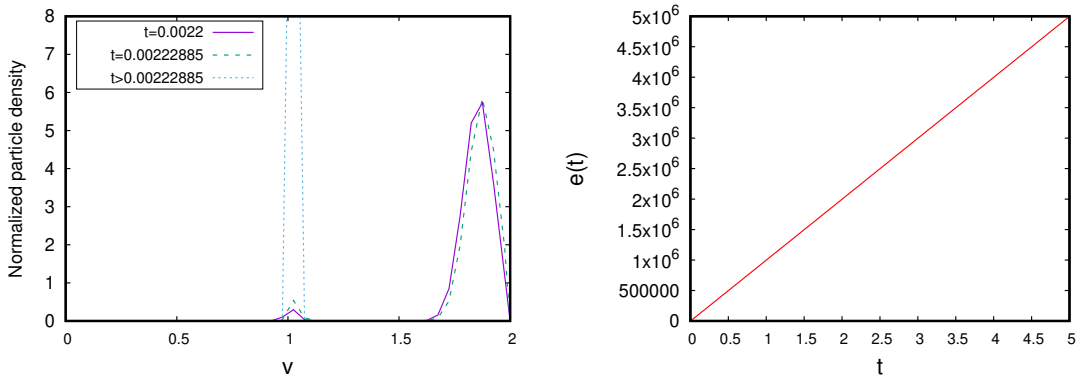

Figure 2.9: **Blow-up phenomenon**. $\mathbf{b = 1.5}$. The initial condition is a normal distribution with $\nu_0 = 1.83$ and $\sigma = 0.003$. *(a)* Time evolution of the particle voltage distribution before and after the blow-up. *(b)* Time evolution of the expectation. *(c)* Time evolution of the firing rate.

Transmission delay.- We analyze here what happens in the blow-up situation, when transmission delays are taken into account and the system avoids the explosion. We consider the initial datum given in the right plot of figure 2.3 and develop several simulations with different transmission delay values: $d = 0.1$ and $d = 0.01$. In figure 2.10 we show both simulations. With a transmission delay the voltage distribution avoids blow-up and it converges to a new state. We have called to this state "plateau distribution", see figures 2.10c and 2.10d. In this new distribution almost all neurons voltages are located between V_R and V_F. Moreover, the probability to find any voltage in $v \in [1, 2)$ is almost the same.

In both simulations, see figures 2.10a and 2.10b, the firing rates tend to increase. This behavior is in full agreement with the formation of the "plateau" distributions observed in figures 2.10c and 2.10d. On the other hand, the comparison between figures 2.10a and 2.10b shows the influence of the delay size. As the delay gets smaller and smaller, the firing rate tends to diverge in a finite time. We checked it for $d = 0.00001$, with which the system does not avoid the blow-up. All neurons spike at once and the distribution converges to the "trivial solution". Finally, we remark that the time needed to get close to the "plateau" state is directly proportional to the value of the delay, see figures 2.10c and 2.10d.

Case without steady states. Connectivity parameter b = 2.2

We also study the case with $b = 2.2$, which represents highly excited neural networks that do not exhibit stationary states (see figure 2.1). In figure 2.11 we can observe that the blow-up is guaranteed regardless of the initial conditions, without transmission delay (see [115]). In that simulation the initial distribution is far from the firing threshold and the firing rate diverges in finite time. On the right side of the figure we see the last output for the distribution, before all the neurons fire at once.

When a transmission delay is considered, the system avoids blow-up and converges to a "plateau" state. Figure 2.12 shows time evolution of the particle system, with an initial distribution close to V_F and with a transmission delay value $d = 0.1$. In this situation, the firing rate increases, but does not diverge in finite time, as we can see in figure 2.12a. The firing rate also represents the growth rate of expectation, as shown in figure 2.12b. As in the case $b = 1.5$, that behavior is reflected in the evolution of the potentials distribution. At the beginning of the simulation, figure 2.12c , we see how the system oscillates between a shape similar to that which occurs without delay and a "plateau" distribution. Some time later, the system approaches the "plateau" distribution, i.e., a uniform distribution in (V_R, V_F), as shown in figure 2.12d. This behavior was observed for Fokker-Planck equation solutions in figure 2 of [20], and although the evolution of the solutions was not shown in said article, the construction of the "plateau" distribution was already observed.

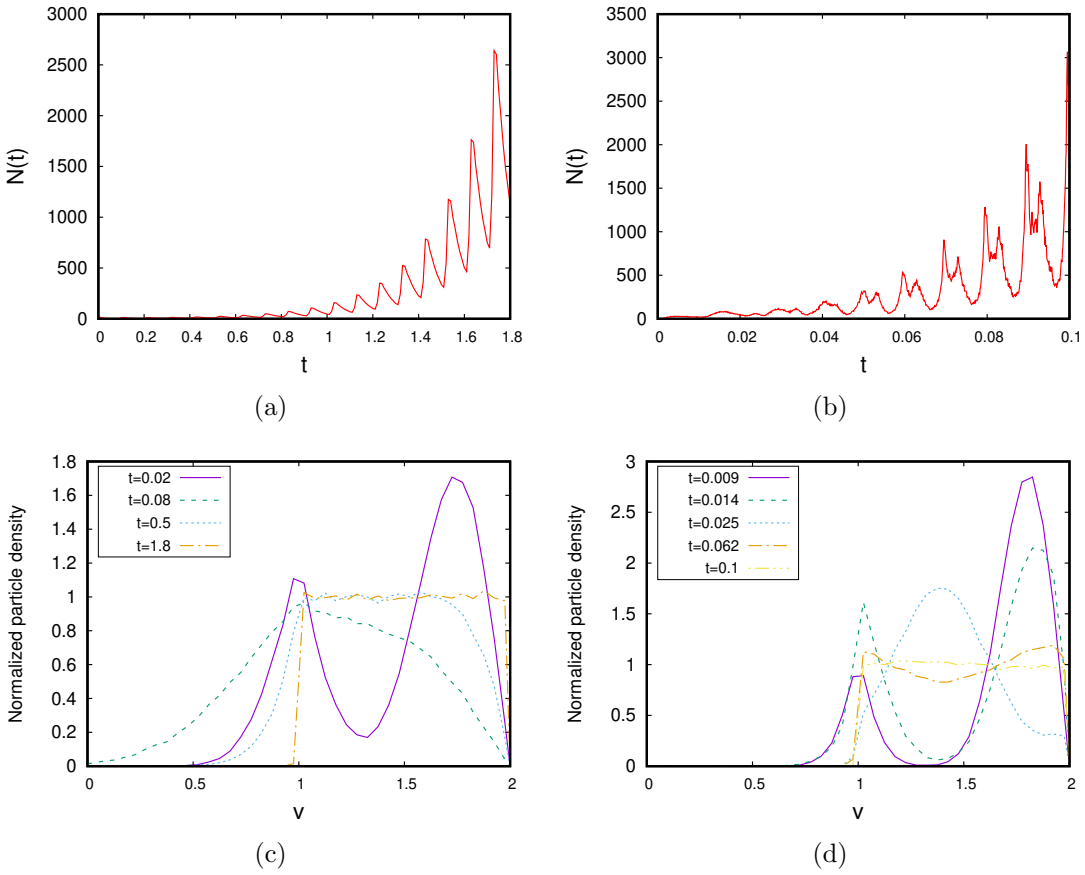

Figure 2.10: **Blow-up situation with delay**. $\mathbf{b = 1.5}$. The initial condition is a normal distribution with $\nu_0 = 1.83$ and $\sigma = 0.003$. On the left $d = 0.1$. On the right $d = 0.01$. *(a)* and *(b)* Time evolution of the firing rate. *(c)* and *(d)* Time evolution of the particle voltage distribution.

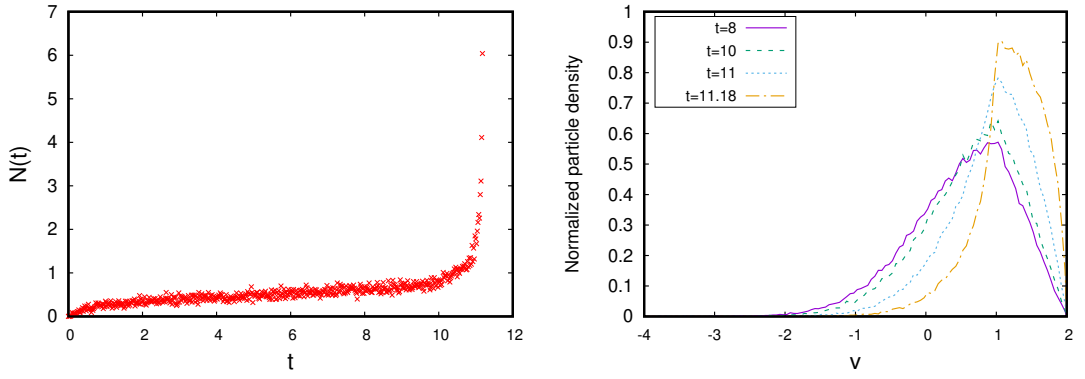

Figure 2.11: **Blow-up phenomenon without delay. $\mathbf{b = 2.2}$**. The initial condition is a normal distribution with $\nu_0 = 0$ and $\sigma^2 = 0.25$. *Left*: Time evolution of the firing rate. *Right*: Time evolution of the particle voltage distribution before the blow-up.

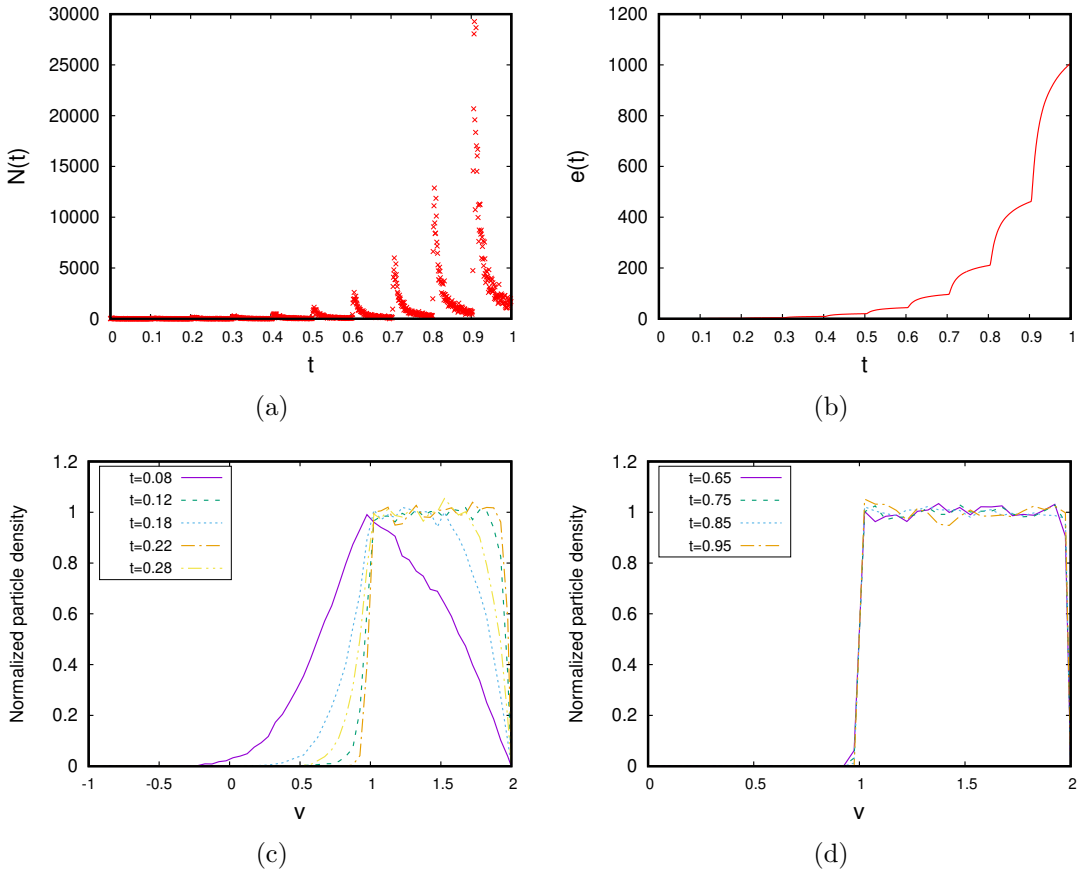

Figure 2.12: **Blow-up situation with delay**. $\mathbf{b = 2.2}$. The initial condition is a normal distribution with $\nu_0 = 1.83$ and $\sigma = 0.003$, and the delay value $d = 0.1$. *(a)* Time evolution of the firing rate. *(b)* Time evolution of the expectation. *(c)* and *(d)* Time evolution of the particle voltage distribution during the formation of the "plateau" state.

2.4.3 Limiting case $b = V_F - V_R$

In this section we analyze the limiting case for which the notion of physical solution no longer makes sense (see section 2.2.1). This case is in between of two regimes: for values $b < V_F - V_R$, there is only one steady state (see figure 2.1) and simulations show that all neurons in the system can fire at the same time, and then converge towards the steady state (see section 2.4.1). However, if $b > V_F - V_R$, the system needs the transmission delay to avoid the explosion, because the physical solutions do not make sense (see section 2.4.2). For $V_F = 2$ and $V_R = 1$, the limiting value of the connectivity parameter is $b = 1$. For this value of b, neurons can spike twice if their membrane potentials are close to V_F. Therefore, we focus on studying this case through the delayed and non-delayed algorithms, without cascade mechanism. As first test, we checked the convergence to the unique stationary state, starting with a distribution of neurons with membrane potentials

far from the threshold value. We skip these figures here, and concentrate on the results found for possible explosion situations. Throughout this section, the initial condition will be always a normal distribution with mean $\nu_0 = 1.83$ and variance $\sigma = 0.003$ (see figure 2.3).

The delayed system approximates the solution of the particle system as the transmission delay d tends to zero. With this purpose, we have made the comparison of the non-delayed system with the sufficiently low delayed one ($d = 0.0001$) in figure 2.14.

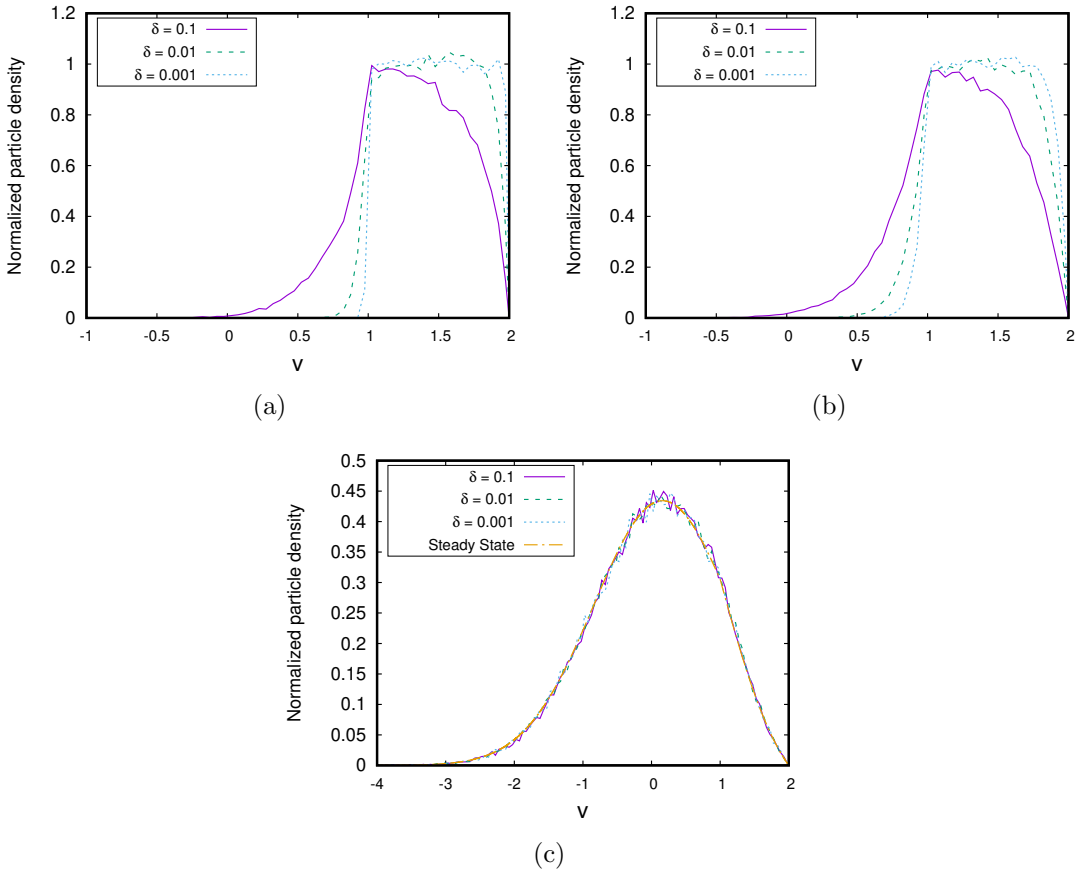

Figure 2.13: **Time evolution of a particle system with high transmission delays**. $\mathbf{b = 1}$. The initial condition is a normal distribution with $\nu_0 = 1.83$ and $\sigma = 0.003$ in all simulations for different delays. *(a)* Particle voltage distribution at time $t = 0.0012$ with different delay values. *(b)* Particle voltage distribution at time $t = 0.0025$ with different delay values. *(c)* Particle voltage distribution at time $t = 5$ with different delay values compared to the steady state of the Fokker-Planck equation.

For the non-delayed case, we observe in figure 2.14a how the voltages distribution approaches the firing threshold and the system achieves the "plateau" state, which appears to be a stable state, as shown in figure 2.14c. The transition between all neurons firing at once and the "plateau" distribution occurs extremely quickly. However, the delayed system oscillates further until it approaches the "plateau" distribution (see figure 2.14b). This "plateau" state seems to be also stable as shown in figure 2.14d. The dynamics of the firing rates can be seen in the bottom of figure 2.14. In the non-delayed case, the firing rate remains constant from almost the beginning in a very high value (see figure 2.14e). This means that the system has converged towards the "plateau" distribution, and that value is an approximation of an infinite firing rate. In the case with delay the firing rate undergoes oscillations prior to the formation of the "plateau" (see figure 2.14f). Later, once the "plateau" is formed, its value tends to grow. In the long term it should reach the value of the non-delayed case, which would give a more defined form to the "plateau".

We have also studied the effect of higher values of delay for blow-up situations. As the delay value increases, the "plateau" state becomes unstable and the system tends to the unique steady state, as shown in figure 2.13. For the lower values $d = 0.001$ and $d = 0.01$ the system remains close to the "plateau" distribution for a while. However, for $d = 0.1$, the system does not even come close to the "plateau" state, see figures 2.13a and 2.13b. Finally, figure 2.13c shows how the system tends to the steady state for the three delay values considered, even for the lowest ones, for which the system was close to the "plateau" state.

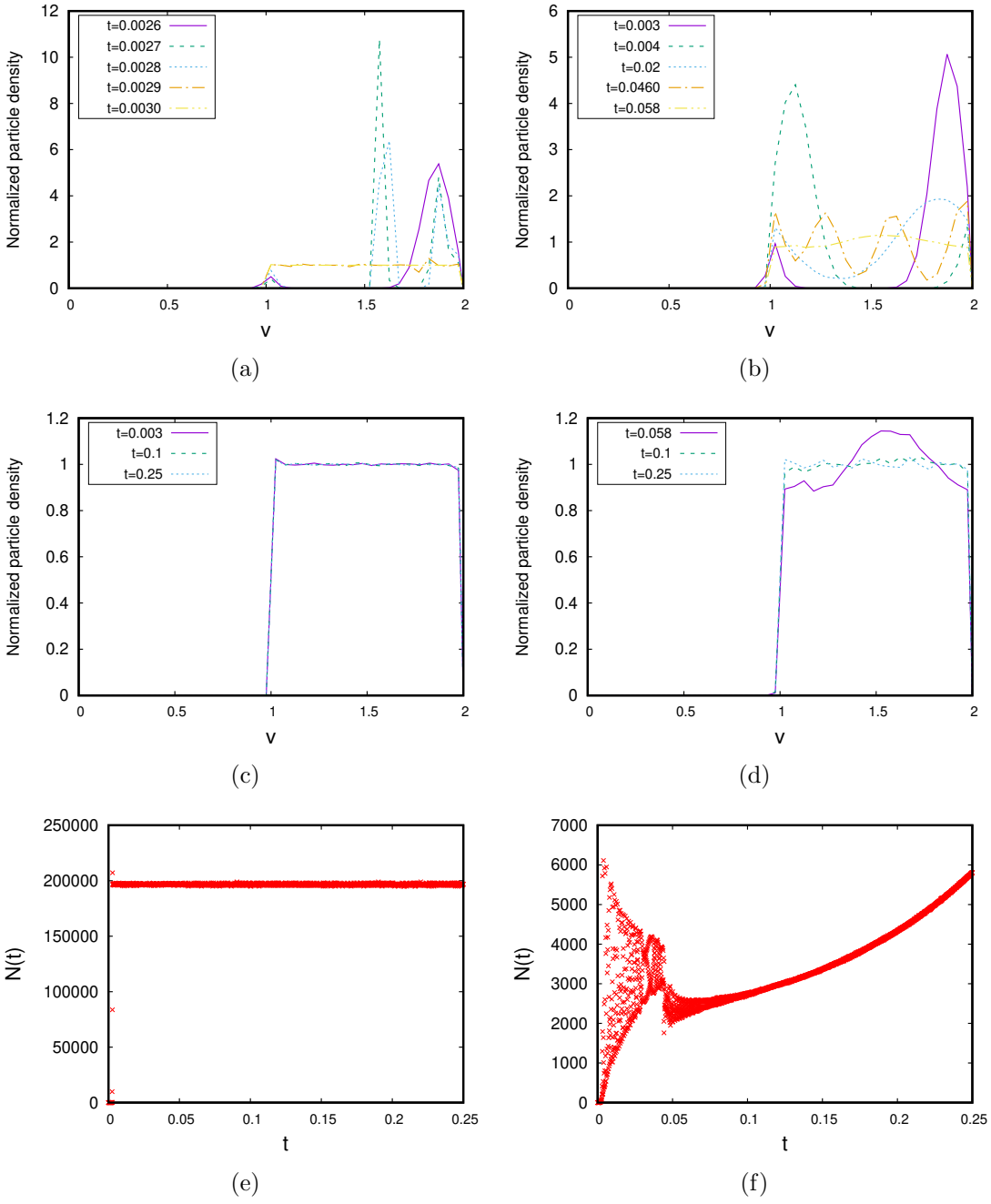

Figure 2.14: **Time evolution of a particle system without transmission delay and with a very small delay $\mathbf{d = 0.0001}$. $\mathbf{b = 1}$.** The initial condition is a normal distribution with $\nu_0 = 1.83$ and $\sigma = 0.003$ in both simulations. *(a)* Time evolution of the particle voltage distribution without delay. *(b)* Time evolution of the particle voltage distribution with delay. *(c)* Time evolution of the particle voltage distribution without delay. *(d)* Time evolution of the particle voltage distribution with delay. *(e)* Time evolution of the firing rate without delay. *(f)* Time evolution of the firing rate with delay.

2.4.4 Plateau formation

In this section we try to understand the formation of the observed "plateau" distributions. Additionally, we propose a possible explanation of that behavior.

Figure 2.15 shows the comparison of the "plateau" distributions found for $b = 1.5$ and $b = 2.2$, and the following profiles:

$$p(v) = \frac{\tilde{N}}{a} e^{-\frac{(v-bN)}{2a}} \int_{max(v,V_R)}^{V_F} e^{\frac{(w-bN)^2}{2a}} dw, \quad N \in \mathbb{R}^+, \tag{2.4.2}$$

where $\tilde{N} = a \left(\int_{-\infty}^{V_F} e^{-\frac{(v-bN)}{2a}} \int_{max(v,V_R)}^{V_F} e^{\frac{(w-bN)^2}{2a}} dw dv \right)^{-1}$, which guarantees the conservation law: $\int_{-\infty}^{V_F} p(v) dv = 1$. There is a high coincidence between the "plateau" distributions and the profiles (2.4.2) as N increases. Furthermore, the dynamics of the particle system appears to go through states with the form (2.4.2) with increasing N, during the formation of its "plateau" states (for instance, see figure 2.12c).

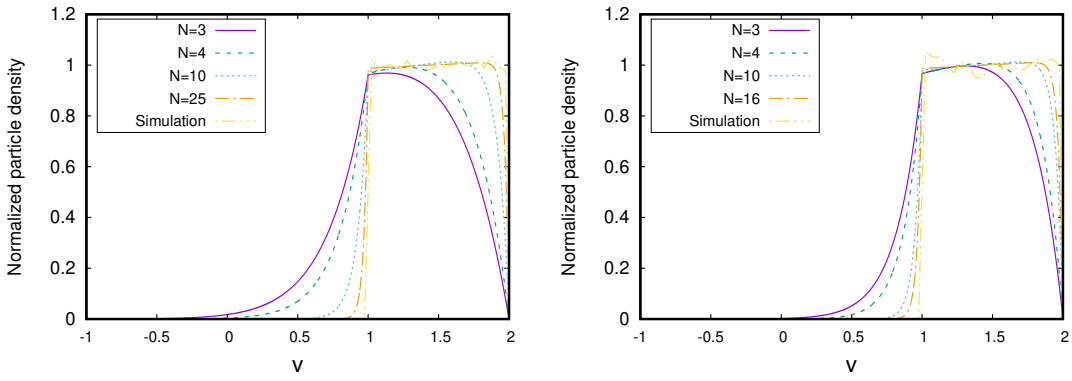

Figure 2.15: **Comparison of "plateau" distributions with profiles** (2.4.2)**.** *L*eft: $b = 1.5$. *R*ight: $b = 2.2$.

On the other hand, we know that steady states of the Fokker-Planck equation are profiles (2.4.2) as long as $\tilde{N} = N$, which is exactly the equation (3.6) in [14]. That is, the implicit equation $NI(N) = 1$, with $I(N) = a^{-1} \int_{-\infty}^{V_F} e^{-\frac{(v-bN)}{2a}} \int_{max(v,V_R)}^{V_F} e^{\frac{(w-bN)^2}{2a}} dw dv$. Therefore, for any N that is not a solution of that implicit equation, the profile (2.4.2) is not a stationary distribution of the system. As a consequence, the profiles shown in figure 2.15 are not stationary states. For $b = 1.5$ (left plot) there are two steady states, but neither corresponds to the values shown in that figure, and for $b = 2.2$ (right plot) there are no stationary solutions.

Therefore, the question is: does the system evolve towards profiles (2.4.2) with N tending to infinity? Based on our results, we think the answer could be affirmative, because:

- For the delayed systems, figures 2.10 and 2.12 show that the particle system appears to tend to different profiles (2.4.2), during the time intervals $J_m = (m\,d, (m+1)\,d)$, with $m \in \mathbb{N}$. In these intervals, the system seems to evolve towards "pseudo-stationary" states that verify the equation

$$\frac{\partial}{\partial v}\left[(v - bN_d^m)p_m + a\frac{\partial}{\partial v}p_m(v) + \tilde{N}_d^m H(v - V_R)\right] = 0,$$

  for certain values N_d^m and $\tilde{N}_d^m$. Thus,

$$(v - bN_d^m)p_m + a\frac{\partial}{\partial v}p_m(v) + \tilde{N}_d^m H(v - V_R) = C,$$

  and taking into account the boundary condition $p_m(V_F) = 0$ and $a\frac{\partial}{\partial v}p_m(V_F) = -\tilde{N_d}^m$ we find $C = 0$. Then, we can integrate the equation and find that

$$p_m(v) = \frac{\tilde{N}_d^m}{a} e^{-\frac{(v-bN_d^m)^2}{2a}} \int_{\max(v,V_R)}^{V_F} e^{\frac{(w-bN_d^m)^2}{2a}}\, dw, \tag{2.4.3}$$

  with $\tilde{N}_d^m = a\left(\int_{-\infty}^{V_F} e^{-\frac{(v-bN_d^m)}{2a}} \int_{max(v,V_R)}^{V_F} e^{\frac{(w-bN_d^m)^2}{2a}} dwdv\right)^{-1}$, which guarantees the conservation law: $\int_{-\infty}^{V_F} p_m(v)dv = 1$. The profile (2.4.3) corresponds to (2.4.2).

  In certain sense, we can understand N_d^m as an approximation of a "pseudo-stationary" firing rate in the delay time.

- Moreover, Figure 2.10(a) and figure 2.12(a) show how the firing rates increase over time. This also causes the sequences of N_d^m and $\tilde{N}_d^m$ values to increase. As a result, profiles (2.4.3) look more and more like a "plateau" distribution, since $\lim_{N_d^m \to \infty} p_m(v) = \frac{1}{V_F - V_R} H(v - V_R)$, for $v < V_F$.

- In the case $b = 1$ we also find a "plateau" distribution in the blow-up situations (see figure 2.14), even without the presence of transmission delay. In this case, there is only one steady state with finite firing rate. However, $b = 1$ is the only connectivity value with which $\lim_{N\to\infty} NI(N) = 1$ (see left plot of figure 2.1 and [14]). The last statement leads us to think that profile (2.4.2) with $N \to \infty$, i.e. $\tilde{p}(v) := \frac{1}{V_F - V_R} H(v - V_R)$ for $v < V_F$ and $\tilde{p}(V_F) := 0$, is also a stationary solution. Although it would not be in the classical sense, since $\tilde{p}(V_R^-) \neq \tilde{p}(V_R^+)$.

2.5 Conclusions

In this chapter we have made progress on the path towards a better understanding of the NNLIF models. We have numerically analyzed the particle system that originates these models. First, we have validated our numerical scheme by comparing our results with those obtained for the Fokker-Planck equation in [14, 18, 20]. After which, we have discovered new properties of the solutions. Specifically, we have shown what happens to the particle system when the blow-up phenomenon occurs in a finite time. We have discovered that system behavior after the blow-up depends on the connectivity parameter b:

- For weakly connected systems, that is, $b < V_F - V_R$, the system overcomes the explosion and tends to its unique steady state. This fact is in agreement with the global existence theory and with the notion of physical solution, instead of classical one [52]. At the instant of the explosion, the firing rate diverges, but in such a way that the singularity of the expectation is controlled. Then the neurons tend to the equilibrium distribution of the system.

- For highly connected systems, understood as $b \geq V_F - V_R$, the concept of physical solution no longer makes sense, because neurons can fire twice at the same time. For this range of values, the system presents a wealth of properties, since it can have one, two or none steady state. Our numerical results show that:

  - In situations where the blow-up would occur in a finite time, the system tends to a "plateau" distribution when synaptic delays are taken into account. That happens even with an initial distribution far from the threshold potential, in cases where there are no steady states.
  - When the system exhibits two steady states, only the one with the lowest firing rate is stable, as shown in [14]. But our results also seem to indicate that "plateau" distributions are stable, when transmission delay is taken into account. Therefore, the system would exhibit bistability between the steady state with the lowest firing rate and the "plateau" distribution.
  - The limiting case $b = 1$ is especially interesting because the "plateau" profile (2.4.2) coincides with the stationary profile, with $N \to \infty$. Our results indicate that the system evolves to a "plateau" distribution under blow-up situations, either without synaptic delay or with a very small delay value. Nevertheless, for a high enough delay the system avoids blow-up and tends to the stationary state, instead of the "plateau".

From a neurophysiological point of view, the explosion phenomenon can be understood as the synchronization of the neural network, where all neurons spike at once. This phenomenon occurs if synaptic delay is not taken into account. However, when some transmission delay is included in the model, we show that the system moves into an asynchronous state (stationary distribution away from the threshold value) or towards a "plateau" distribution, which means that the membranes potential tend to be uniformly distributed in the interval (V_R, V_F). The system seems to evolve towards these "plateau" distributions, passing near the "pseudo-equilibria" caused by the transmission delay. The limiting case $b = 1$ has a "pseudo equilibrium" associated with $N \to \infty$, that matches the profile of a "limit steady-state" (with $N \approx \infty$). In this case, the "plateau" distribution is obtained without the need to include any transmission delay.

Chapter 3

Asymptotic behavior of the NNLIF neuron model for general connectivity strength

3.1 Introduction

In this chapter[2] we proof new results on the asymptotic behavior of the nonlinear integrate-and-fire neuron model. Among them, we give a criterion for the linearized stability or instability of equilibria, without restriction on the connectivity parameter, which provides a proof of stability or instability in some cases. In all cases, this criterion can be checked numerically, allowing us to give a full picture of the stable and unstable equilibria depending on the connectivity parameter b and transmission delay d. We also give further spectral results on the associated linear equation, and use them to give improved results on the nonlinear stability of equilibria for weak connectivity, and on the link between linearized and nonlinear stability. Although the nonlinear Fokker-Planck equation (1.2.7) that is the subject of this chapter was explained in detail in section 1.2.2, we will recall it so that the chapter is self-contained and does not have to refer to equations external to itself.

Let us consider the following nonlinear Fokker-Planck equation, which provides the evolution in time of the probability density $p(v,t) \geq 0$ of finding neurons at membrane potential $v \in (-\infty, V_F]$ and time $t \geq 0$:

$$\partial_t p(v,t) + \partial_v \left[(-v + bN_p(t-d))\, p(v,t) \right] - \partial_v^2 p(v,t) = \delta_{V_R} N(t), \tag{3.1.1a}$$

[2]This chapter compiles the work sent for publication, whose preprint is [12].

where $\delta_{V_R}(v) \equiv \delta(v - V_R)$ is a delta function at the point $v = V_R$, $-v + bN_p(t-d)$ is the drift parameter with b the connectivity parameter describing the excitatory or inhibitory behavior of the system, d the transmission delay and $N_p(t)$ the firing rate.

The spiking and reset effect explained in 1.2.1, where neurons spikes when its membrane voltage reaches the firing threshold value V_F, discharges immediately afterwards, and its membrane potential is restored to the reset value $V_R < V_F$, is described by the right hand side of (3.1.1), the boundary condition

$$p(V_F, t) = 0, \qquad \text{for } t > 0, \tag{3.1.1b}$$

and the definition of the firing rate $N_p(t)$ as the flux at V_F,

$$N_p(t) := -\partial_v p(V_F, t) \geq 0, \tag{3.1.1c}$$

which makes the system (3.1.1) nonlinear. In order to have unique solutions, the system must include an initial condition of the form

$$p(v, t) = p_0(v, t) \qquad \text{for } v \in (-\infty, V_F] \text{ and } t \in [-d, 0], \tag{3.1.1d}$$

where p_0 is a given function.

Given any nonnegative, integrable initial condition $p_0(v, t) \geq 0$, the system (3.1.1) satisfies the conservation law $\int_{-\infty}^{V_F} p(v, t)\, \mathrm{d}v = \int_{-\infty}^{V_F} p_0(v, t)\, \mathrm{d}v$ at any time t for which the solution is defined (we always assume $\lim_{v \to -\infty} p(v, t) = 0$, or other reasonable conditions which ensure appropriate decay of solutions as $v \to -\infty$). For simplicity, and since this does not entail any qualitative changes to the system, we will consider $\int_{-\infty}^{V_F} p_0(v, t)\, \mathrm{d}v = 1$ for $t \in [-d, 0]$ throughout this chapter.

The steady states or equilibria of the system (3.1.1) are integrable, nonnegative solutions to the following equation:

$$\begin{cases} \partial_v \left[(-v + bN_\infty)\, p_\infty(v) \right] - \partial_v^2 p_\infty(v) = \delta_{V_R} N_\infty, \\ N_\infty = -\partial_v p_\infty(V_F), \qquad p_\infty(V_F) = 0, \\ \text{and} \quad \int_{-\infty}^{V_F} p_\infty(v)\, \mathrm{d}v = 1. \end{cases} \tag{3.1.2}$$

These profiles are continuous in $(-\infty, V_F]$, differentiable in $(-\infty, V_R) \cup (V_R, V_F]$, and they are given by

$$p_\infty(v) = N_\infty e^{-\frac{(v - bN_\infty)^2}{2}} \int_{\max(v, V_R)}^{V_F} e^{\frac{(w - bN_\infty)^2}{2}}\, \mathrm{d}w, \tag{3.1.3}$$

where the stationary firing rate N_∞ is a solution of the implicit equation $N_\infty I(N_\infty) = 1$,

with $I(N)$ given by

$$I(N) = \int_{-\infty}^{V_F} e^{-\frac{(v-bN)^2}{2}} \int_{\max(v,V_R)}^{V_F} e^{\frac{(w-bN)^2}{2}} \, \mathrm{d}w \, \mathrm{d}v. \tag{3.1.4}$$

Figure 3.1 shows the function $N \mapsto 1/I(N)$, for different values of b. Each equilibrium of the nonlinear system (3.1.1) corresponds to a crossing of the function $N \mapsto 1/I(N)$ with the diagonal. Figure 3.2 illustrates, for each $b > 0$, the N_∞ values solving $N_\infty I(N_\infty) = 1$, that is, the values of N_∞ at the equilibria of (3.1.1).

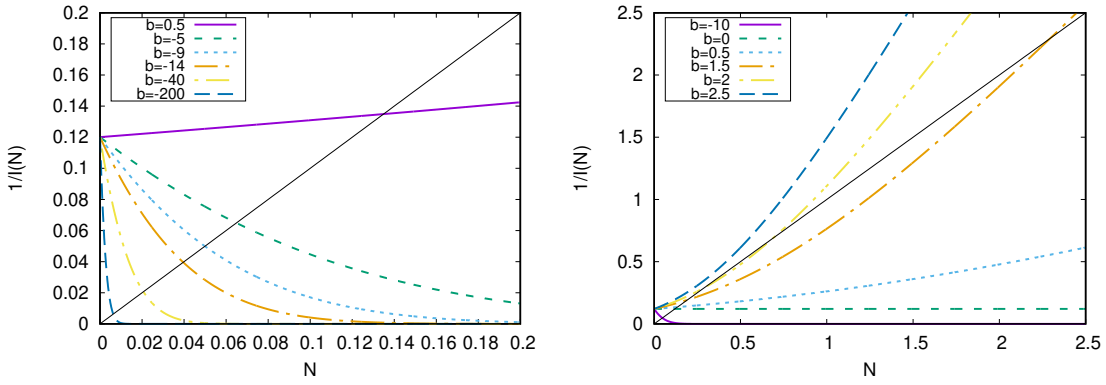

Figure 3.1: **Function $\frac{1}{I(N)}$ (see (3.1.4)) for different values of the connectivity parameter b.** Each crossing with the diagonal corresponds to an equilibrium of equation (3.1.1). Reset and firing potential are set to $V_R = 1$ and $V_F = 2$ respectively.

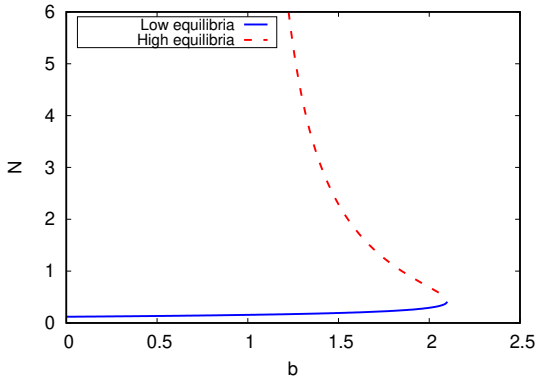

Figure 3.2: **Values of N solving $NI(N) = 1$, for each b.** Point $b = 1$ corresponds to $b = V_F - V_R$ for the selected parameter values. Therefore, there is only one equilibrium for $b < 1$, two equilibria for $1 < b < b_e$ with b_e a certain critical value, and none for $b > b_e$. The dashed line has a vertical asymptote at $b = 1$. Reset and firing potential are set to $V_R = 1$ and $V_F = 2$ respectively.

To improve the understanding of the results we will present in the different sections of this chapter, we will clarify the notation we will use and some useful definitions. First, given a fixed $N \geq 0$ and $b \in \mathbb{R}$ we define the linear operator L_N, acting on functions $u = u(v)$, by

$$L_N u := \partial_v^2 u + \partial_v((v - bN)u) + \delta_{V_R} N_u. \tag{3.1.5}$$

This operator is formally obtained by replacing N_p on the nonlinear term in the right hand side of (3.1.1a) by N. The associated linear PDE,

$$\partial_t p = L_N p, \tag{3.1.6}$$

with the same Dirichlet boundary condition as before and $N_u(t) := -\partial_v u(V_F, t)$, models a situation where neurons evolve with a fixed background firing rate. A central part of our strategy is based on a careful study of the linear operator L_N. The PDE (3.1.6) has a unique (probability) stationary state p_∞, explicitly given by a very similar expression to (3.1.3):

$$p_\infty^N(v) = \overline{N} e^{-\frac{(v-bN)^2}{2}} \int_{\max(v,V_R)}^{V_F} e^{\frac{(w-bN)^2}{2}} \, \mathrm{d}w, \tag{3.1.7}$$

where $\overline{N}$ is a normalizing factor to ensure that p_∞^N is a probability distribution. It is also known that solutions to this linear equation converge exponentially to equilibrium in the weighted norm $L^2(1/p_\infty)$, which is a natural norm when considering a quadratic entropy [14,25]. By studying some well-posedness and regularization bounds for the linear equation, we are able to show that this exponential decay is also true in the smaller space X given by

$$X := \{u \in \mathcal{C}(-\infty, V_F] \cap \mathcal{C}^1(-\infty, V_R] \cap \mathcal{C}^1[V_R, V_F] \mid u(V_F) = 0 \text{ and } \|u\|_X < \infty\}, \tag{3.1.8}$$

where

$$\|u\|_X := \|u\|_\infty + \|\partial_v u\|_\infty + \|u\|_{L^2(\varphi)} + \|\partial_v u\|_{L^2(\varphi)} \tag{3.1.9}$$

and

$$\varphi(v) := \exp\left(\frac{(v - bN)^2}{2}\right), \qquad v \in (-\infty, V_F].$$

It is understood that the $L^2(\varphi)$ norms are taken on $(-\infty, V_F]$. The linear space X is a Banach space with the above norm. We observe that $X \subseteq L^2((p_\infty^N)^{-1})$ since for some constant $C > 0$

$$\frac{1}{p_\infty^N(v)} = C\varphi(v) \qquad \text{for all } v \leq V_R, \tag{3.1.10}$$

and for any $u \in X$ we have

$$\int_{V_R}^{V_F} u(t,v)^2 p_\infty^N(v)^{-1}\,\mathrm{d}v \lesssim \int_{V_R}^{V_F} u(t,v)^2 \frac{1}{V_F - v}\,\mathrm{d}v \\ \leq \|\partial_v u(\cdot,t)\|_\infty^2 \int_{V_R}^{V_F} (V_F - v)\,\mathrm{d}v \lesssim \|u\|_X^2, \quad (3.1.11)$$

where we have used the estimate

$$|u(t,v)| \leq \|\partial_v u(t,\cdot)\|_\infty (V_F - v) \qquad \text{for } v \leq V_F,$$

easily obtained via the mean value theorem and the fact that $u(V_F) = 0$. Inequalities (3.1.10) and (3.1.11) show that $\|u\|_{L^2(p_\infty^{-1})} \lesssim \|u\|_X$, so $X \subseteq L^2(p_\infty^{-1})$.

Definition 3.1.1. Given $b \in \mathbb{R}$ and a probability equilibrium p_∞ of the PDE (3.1.1), we define the *linearized* equation at p_∞ by

$$\begin{aligned} \partial_t u =& \partial_v^2 u + \partial_v((v - bN_\infty)u) + \delta_{V_R} N_u - bN_u(t-d)\partial_v p_\infty \\ =& L_\infty u - bN_u(t-d)\partial_v p_\infty, \end{aligned} \quad (3.1.12)$$

where $L_\infty \equiv L_{N_\infty}$ is the linear operator from (3.1.5), with $N = N_\infty$. We notice that this equation has a delay d in the last term. We add the same boundary condition as before, that is,

$$u(V_F, t) = 0, \qquad \text{for } t > 0. \quad (3.1.13)$$

The property that the linear PDE decays exponentially to equilibrium in a certain space is often stated by saying that it has a *spectral gap* in that space. The technique we use to "shrink" the space where a given linear PDE has a spectral gap was used in [38] in relation to a coagulation-fragmentation PDE, and is linked to operator techniques described in [74] and [96]. A spectral gap in the space X allows us to carry out stability arguments in a more natural way, since now the firing rate N_p, considered as an operator $-\partial_v p(V_F)$ acting on p, is a *bounded* linear operator on X. This allows us to relate the linearized and the nonlinear equations, and to give more precise estimates on the range of parameters where stability or instability take place.

For the rest of the chapter, whenever p_∞ is an equilibrium of the nonlinear problem, we define

$$q(v,t) := e^{tL_\infty} \partial_v p_\infty, \quad (3.1.14)$$

where e^{tL_∞} denotes the flow of the linear problem (3.1.5) (that is: $e^{tL_\infty} u_0$ is the solution to problem (3.1.5) with initial condition u_0). In agreement with previous notation we set

$$N_q(t) := -\partial_v q(V_F, t), \qquad \text{for } t > 0, \quad (3.1.15)$$

and call $\hat{N}_q$ the Laplace transform of N_q,

$$\hat{N}_q(\xi) := \int_0^\infty e^{-\xi t} N_q(t)\,\mathrm{d}t. \tag{3.1.16}$$

The chapter is structured as follows: in Section 3.2 we carry out our study of the linear equation, giving well-posedness and regularization estimates in the space X, and showing that the linear PDE has a spectral gap in the space X. In Section 3.3 we lay out some groundwork on classical delay equations, needed for the arguments presented in later sections. In Section 3.4 we give a result on the nonlinear stability of the NNLIF model for weak interconnectivity, and we show that linearized stability implies nonlinear stability (that is, that linearized behavior dominates close to an equilibrium). Finally, in Section 3.5 we give a new criterion for linear stability or instability of equilibria with a given connectivity b and delay d, which implies corresponding results for the nonlinear equation, due to the results in Section 3.4.

Throughout the chapter we often use C to denote an arbitrary nonnegative constant which may change from line to line. We also use the symbol $\lesssim$ to denote inequality up to a positive multiplicative constant.

3.2 Study of the linear equation

In this section we study several aspects of the following linear equation, which results when we fix the firing rate N, independent on time, in the nonlinear term of equation (3.1.1):

$$\partial_t u(v,t) = \partial_v^2 u(v,t) + \partial_v[(v-bN)u(v,t)] + \delta_{V_R} N_u(t),\ v \in (-\infty, V_F]\,,\ t \geq 0, \tag{3.2.1a}$$

with the boundary condition

$$u(V_F, t) = 0, t \geq 0 \tag{3.2.1b}$$

and defining

$$N_u(t) := -\partial_v u(V_F, t). \tag{3.2.1c}$$

As usual, we also impose an initial condition at time $t = 0$:

$$u(v,0) = u_0(v), \qquad v \in (-\infty, V_F]. \tag{3.2.1d}$$

We will first study well-posedness bounds in several spaces, and then study its spectral gap properties in suitable "strong" spaces which will later be useful for the nonlinear theory.

3.2.1 Summary of results: well-posedness, regularity and spectral gap

Let us state our main results on the linear equation, leaving the proof of all technical estimates for Section 3.2.2. We recall that an existence theory for classical solutions to the nonlinear system (3.1.1) was given in [29], which covers in particular the linear case (3.2.1a) (as the case with $b = 0$ in their paper). Throughout this section we assume this existence theory, and we develop some more precise well-posedness estimates on these classical solutions. Actually, from our estimates below one could construct a linear existence theory for equation (3.2.1a) by using known tools from semigroup theory (see [64], in particular Section III.3 and the Desch-Schappacher theorem). We do not follow this path here since we think it is more direct to work with the already studied classical solutions, developing new estimates for them.

We also know from previous results [14] that equation (3.2.1), in the linear case, has a unique probability equilibrium p_∞^N (given by (3.1.7)), which in this section we denote simply by p_∞, since we work only with the linear equation in all of Section 3.2. This equilibrium is positive, and the linear equation has a spectral gap in the space $L^2(p_\infty^{-1})$: there exists $\lambda > 0$ such that for all probability distributions $p_0 \in L^2(p_\infty^{-1})$,

$$\|e^{tL}p_0 - p_\infty\|_{L^2(p_\infty^{-1})} \leq e^{-\lambda t}\|p_0 - p_\infty\|_{L^2(p_\infty^{-1})} \qquad \text{for all } t \geq 0. \tag{3.2.2}$$

In fact, the same reasoning from [14], based on a Poincaré's inequality, actually shows something slightly stronger: for any initial condition $u_0 \in L^2(p_\infty^{-1})$ such that $\int_{-\infty}^{V_F} u_0(v)\,\mathrm{d}v = 0$ we have

$$\|e^{tL}u_0\|_{L^2(p_\infty^{-1})} \leq e^{-\lambda t}\|u_0\|_{L^2(p_\infty^{-1})} \qquad \text{for all } t \geq 0. \tag{3.2.3}$$

Another straightforward consequence is that there exists $C \geq 1$ such that for any $u_0 \in L^2(p_\infty^{-1})$ (not necessarily with integral 0) we have

$$\|e^{tL}u_0\|_{L^2(p_\infty^{-1})} \leq C\|u_0\|_{L^2(p_\infty^{-1})} \qquad \text{for all } t \geq 0. \tag{3.2.4}$$

Due to (3.2.3), this is clearly true (with $C = 1$) if u_0 has integral 0. For a general $u_0 \in L^2(p_\infty^{-1})$, (3.2.4) may be obtained by writing $u_0 = (u_0 - mp_\infty) + mp_\infty$, with $m := \int_{-\infty}^{V_F} u_0(v)\,\mathrm{d}v$, applying (3.2.3), and noticing that $|m| \leq C\|u_0\|_{L^2(p_\infty^{-1})}$ for some $C > 0$:

$$\begin{aligned}
\|e^{tL}u_0\|_{L^2(p_\infty^{-1})} &\leq \|e^{tL}(u_0 - mp_\infty)\|_{L^2(p_\infty^{-1})} + |m|\|e^{tL}p_\infty\|_{L^2(p_\infty^{-1})} \\
&\leq e^{-\lambda t}\|u_0 - mp_\infty\|_{L^2(p_\infty^{-1})} + |m|\|p_\infty\|_{L^2(p_\infty^{-1})} \\
&\leq \|u_0\|_{L^2(p_\infty^{-1})} + |m|\|p_\infty\|_{L^2(p_\infty^{-1})} + |m|\|p_\infty\|_{L^2(p_\infty^{-1})} \\
&\leq (1 + 2C\|p_\infty\|_{L^2(p_\infty^{-1})})\|u_0\|_{L^2(p_\infty^{-1})}.
\end{aligned}$$

Our main aim is to have good estimates, similar to (3.2.3) and (3.2.4), in a linear space where the derivative of the solution is bounded (unlike $L^2(p_\infty^{-1})$). We consider the space X defined in (3.1.8) (associated to the unique probability equilibrium p_∞ of (3.2.1)). Here are the main estimates we wish to prove on this:

Lemma 3.2.1 (Well-posedness estimate)**.** *Let $u_0 \in X$ be any initial condition. Then the solution u to the linear equation (3.2.1) satisfies the following: there are constants $M, C > 0$ such that*

$$\|e^{tL}u_0\|_X \leq Me^{Ct}\|u_0\|_X \qquad \text{for all } t \geq 0. \tag{3.2.5}$$

And here is our main regularization estimate:

Lemma 3.2.2 (Regularization estimate)**.** *Let $u_0 \in X$ be any initial condition. Then the solution u to the linear equation (3.2.1) satisfies the following: there exists a constant $C > 0$ and $t_0 > 0$ (both independent of the initial condition u_0), such that*

$$\|e^{tL}u_0\|_X \leq Ct^{-3/4}\|u_0\|_{L^2(\varphi)} \qquad \text{for all } 0 < t \leq t_0. \tag{3.2.6}$$

and in particular

$$\|e^{tL}u_0\|_X \leq Ct^{-3/4}\|u_0\|_{L^2(p_\infty^{-1})} \qquad \text{for all } 0 < t \leq t_0. \tag{3.2.7}$$

Both of the lemmas above are a direct consequence of the bounds in Lemmas 3.2.11 and 3.2.12, proved at the end of Section 3.2.2. Notice that

$$\varphi(v) \lesssim \frac{1}{p_\infty(v)} \qquad \text{for all } v < V_F,$$

so (3.2.7) is clearly a consequence of (3.2.6).

Regarding spectral gap estimates, we show that the semigroup associated to the linear equation has a spectral gap in the space X. This is essentially deduced from the known spectral gap estimate (3.2.3) and Lemmas 3.2.1 and 3.2.2:

Proposition 3.2.3 (Spectral gap estimate)**.** *There exist constants $\lambda > 0$, $C \geq 1$ such that for all initial conditions $u_0 \in X$ such that $\int_{-\infty}^{V_F} u_0(v)\,\mathrm{d}v = 0$ it holds that*

$$\|e^{tL}u_0\|_X \leq Ce^{-\lambda t}\|u_0\|_X \qquad \text{for all } t \geq 0 \tag{3.2.8}$$

and also

$$\|e^{tL}u_0\|_X \leq Ct^{-\frac{3}{4}}e^{-\lambda t}\|u_0\|_{L^2(\varphi)} \qquad \text{for all } t > 0. \tag{3.2.9}$$

Remark 3.2.4. From the proof below one can see that the constant λ in (3.2.8) can be taken to be the same one as in (3.2.2) (usually obtained via a Poincaré's inequality [14]).

The constant λ in (3.2.9) can be taken to be any constant strictly smaller than the λ in (3.2.2) (or alternatively, one could keep the same λ and write $\max\{1, t^{-3/4}\}$ instead of $t^{-3/4}$ in (3.2.9)).

Proof. Call $Y \equiv L^2(p_\infty^{-1})$. Our regularization result in equation (3.2.7) gives

$$\|e^{tL}u_0\|_X \lesssim t^{-\frac{3}{4}}\|u_0\|_Y \qquad \text{for all } 0 < t \le t_0.$$

Now we can prove (3.2.8) for $t \ge t_0$ by using (3.2.3): for $t \ge t_0$ we have

$$\begin{aligned}\|e^{tL}u_0\|_X = \|e^{t_0 L}e^{(t-t_0)L}u_0\|_X &\lesssim t_0^{-\frac{3}{4}}\|e^{(t-t_0)L}u_0\|_Y \\ &\lesssim t_0^{-\frac{3}{4}}e^{-\lambda(t-t_0)}\|u_0\|_Y \lesssim t_0^{-\frac{3}{4}}e^{-\lambda(t-t_0)}\|u_0\|_X \lesssim e^{-\lambda t}\|u_0\|_X.\end{aligned}$$

Notice that we also used $\|u_0\|_Y \lesssim \|u_0\|_X$, since $X \subseteq Y$ (see the observation after (3.1.9) in the introduction). For $t \le t_0$ we can use the well-posedness estimate of Lemma 3.2.1, finally getting (3.2.8) for all $t \ge 0$.

In order to show (3.2.9) we take any $t > 0$ and any $0 < s < \min\{t_0, t\}$, and we use (3.2.8) and (3.2.6) to write

$$\|e^{tL}u_0\|_X = \|e^{(t-s)L}e^{sL}u_0\|_X \lesssim e^{-\lambda(t-s)}\|e^{sL}u_0\|_X \lesssim s^{-\frac{3}{4}}e^{-\lambda(t-s)}\|u_0\|_{L^2(\varphi)}.$$

For $t \ge t_0$ we take $s := t_0/2$ and this shows (3.2.9) (with a slightly smaller λ). For $t < t_0$ we take $s = t/2$, and this also gives the result on that range. □

3.2.2 Bounds for classical solutions

In order to study the linear equation (3.2.1a) we separate its terms as follows

$$\partial_t u = \partial_v^2 u + \partial_v[(v - bN)u] + \delta_{V_R}N_u(t) = Fu + L_1 u + L_2 u, \tag{3.2.10}$$

with

$$Fu := \partial_v^2 u + \partial_v[(v - V_F)u], \qquad L_1 u := \delta_{V_R}N_u(t), \qquad L_2 u := \partial_v[(V_F - bN)u].$$

We still consider the same boundary conditions (3.2.1b). In order, we prove estimates for the equation $\partial_t u = Fu$ in Section 3.2.2, then for $\partial_t u = Fu + L_1 u$ in Section 3.2.2, and finally for the full linear equation in Section 3.2.2.

Bounds for the Fokker-Planck equation

The Cauchy problem for the Dirichlet Fokker-Planck equation on the half-line, posed for $t \geq 0$ and $v \in (-\infty, 0]$,

$$\partial_t u = \partial_v^2 u + \partial_v(vu) \qquad \text{with} \qquad u(0,t) = 0 \quad \text{for } t \geq 0, \tag{3.2.11}$$

$$u(v,0) = u_0 \qquad \text{with} \qquad u_0 \colon (-\infty, 0] \to \mathbb{R},$$

has the explicit solution

$$u(v,t) = \int_{-\infty}^{\infty} \widetilde{u}_0(w)\Phi_t(v,w)\,\mathrm{d}w = \int_{-\infty}^{0} u_0(w)\Psi_t(v,w)\,\mathrm{d}w, \tag{3.2.12}$$

defined for $t > 0$ and $v \in (-\infty, 0]$. Here $\widetilde{u}_0 \colon \mathbb{R} \to \mathbb{R}$ is the anti-symmetrization of the initial condition

$$\widetilde{u}_0(x) := \begin{cases} u_0(x), & x \leq 0 \\ -u_0(-x), & x > 0, \end{cases}$$

$\Phi_t = \Phi_t(v,w)$ is the fundamental solution of the standard Fokker-Planck equation:

$$\Phi_t(v,w) = \frac{1}{\sqrt{2\pi(1-e^{-2t})}} \exp\left(-\frac{(v-e^{-t}w)^2}{2\,(1-e^{-2t})}\right), \qquad t > 0, \quad v, w \in \mathbb{R}, \tag{3.2.13}$$

and

$$\Psi_t(v,w) := \Phi_t(v,w) - \Phi_t(v,-w), \qquad t > 0,\ v, w \in (-\infty, 0]. \tag{3.2.14}$$

For later reference, we notice that $\Psi_t(v,w) \geq 0$, since $t > 0$ and $v, w \in (-\infty, 0]$, and

$$\partial_v \Phi_t(v,w) = (2\pi)^{-\frac{1}{2}}(1-e^{-2t})^{-\frac{3}{2}}(v-e^{-t}w)\exp\left(-\frac{(v-e^{-t}w)^2}{2\,(1-e^{-2t})}\right). \tag{3.2.15}$$

For an explicit solution to be available it is essential that the boundary condition is set at $v = 0$; otherwise we do not know of an explicit expression. From the expression (3.2.12) of the solution, it is easy to see that many estimates for the standard Fokker-Planck equation on $\mathbb{R}$ can be carried over to the Fokker-Planck equation (3.2.11), posed on $(-\infty, 0]$ and with a Dirichlet boundary condition.

It is then straightforward to translate equation (3.2.12) and obtain a solution to the translated Fokker-Planck equation

$$\partial_t u = Fu = \partial_v^2 u + \partial_v[(v - V_F)u] \tag{3.2.16}$$

posed for $t \geq 0$ and $v \in (-\infty, V_F]$ with the boundary condition

$$u(V_F, t) = 0, \qquad t \geq 0. \tag{3.2.17}$$

A solution to (3.2.16)–(3.2.17), with initial condition u_0, is then given by

$$u(v,t) = \int_{-\infty}^{\infty} \widetilde{u}_0(w)\Phi_t(v - V_F, w - V_F)\,\mathrm{d}w = \int_{-\infty}^{V_F} u_0(w)\Psi_t(v - V_F, w - V_F)\,\mathrm{d}w, \tag{3.2.18}$$

for $t > 0$ and $v \in (-\infty, V_F]$, where $\widetilde{u}_0$ is now the function

$$\widetilde{u}_0(x) := \begin{cases} u_0(x), & x \leq V_F \\ -u_0(2V_F - x), & x > V_F. \end{cases}$$

With this explicit expression we can obtain the following estimates:

Lemma 3.2.5. *Denote by $e^{tF}u_0$ the solution (3.2.18) to the Fokker-Planck equation (3.2.16)–(3.2.17) in the domain $v \in (-\infty, V_F]$, $t \geq 0$, with an initial condition u_0. Then, the following well-posedness inequalities hold for all $u_0 \in X$ and all $t \geq 0$:*

$$\|e^{tF}u_0\|_\infty \leq e^t\|u_0\|_\infty. \tag{3.2.19}$$
$$\|e^{tF}u_0\|_2 \leq \sqrt{2}e^{\frac{t}{2}}\|u_0\|_2. \tag{3.2.20}$$
$$\|\partial_v e^{tF}u_0\|_\infty \leq e^{2t}\|\partial_v u_0\|_\infty. \tag{3.2.21}$$
$$\|\partial_v e^{tF}u_0\|_2 \leq \sqrt{2}e^{\frac{3t}{2}}\|\partial_v u_0\|_2. \tag{3.2.22}$$

Also, the following "regularization" inequalities hold for some constants $C > 0$, all $u_0 \in X$ and t small enough:

$$\|e^{tF}u_0\|_\infty \leq Ct^{-1/4}\|u_0\|_2. \tag{3.2.23}$$
$$\|\partial_v e^{tF}u_0\|_\infty \leq Ct^{-1/2}\|u_0\|_\infty. \tag{3.2.24}$$
$$\|\partial_v e^{tF}u_0\|_\infty \leq Ct^{-3/4}\|u_0\|_2. \tag{3.2.25}$$
$$\|\partial_v e^{tF}u_0\|_2 \leq Ct^{-1/2}\|u_0\|_2. \tag{3.2.26}$$
$$\|\partial_v e^{tF}u_0\|_\infty \leq Ct^{-1/4}\|\partial_v u_0\|_2. \tag{3.2.27}$$

Proof. These estimates are obtained in a straightforward way from the explicit solution (3.2.18), and are a consequence of the corresponding estimates for the standard Fokker-Planck equation on $\mathbb{R}$. We use the standard properties

$$\int_{-\infty}^{+\infty} \Phi_t(v,w)\,\mathrm{d}v = 1, \qquad \int_{-\infty}^{+\infty} \Phi_t(v,w)\,\mathrm{d}w = e^t \tag{3.2.28}$$

and

$$\int_{-\infty}^{+\infty} (\Phi_t(v,w))^2 \,\mathrm{d}w = \frac{1}{2\sqrt{\pi}}(1-e^{-2t})^{-\frac{1}{2}}e^t. \tag{3.2.29}$$

In order to obtain (3.2.19), we directly apply the second part of (3.2.28) to the expression (3.2.18). To obtain (3.2.20) from (3.2.18) we use the Cauchy-Schwarz inequality and the second part of (3.2.28) to get

$$\begin{aligned}\left(\int_{-\infty}^{\infty} \widetilde{u}_0(w)\Phi_t(v-V_F,w-V_F)\,\mathrm{d}w\right)^2 \\ \leq \left(\int_{-\infty}^{\infty} \widetilde{u}_0(w)^2\Phi_t(v-V_F,w-V_F)\,\mathrm{d}w\right)\left(\int_{-\infty}^{\infty} \Phi_t(v-V_F,w-V_F)\,\mathrm{d}w\right) \\ = e^t\left(\int_{-\infty}^{\infty} \widetilde{u}_0(w)^2\Phi_t(v-V_F,w-V_F)\,\mathrm{d}w\right).\end{aligned} \tag{3.2.30}$$

Integrating now in v and taking into account that $\|\widetilde{u_0}\|_2^2 = 2\|u_0\|_2^2$ gives (3.2.20).

For the estimates involving the derivative ∂_v we note that

$$\partial_v\Phi_t(v,w) = -e^t\partial_w\Phi_t(v,w). \tag{3.2.31}$$

Using this, to obtain (3.2.21) we write

$$\begin{aligned}\partial_v u(v,t) = \int_{-\infty}^{\infty} \widetilde{u}_0(w)\partial_v\Phi_t(v-V_F,w-V_F)\,\mathrm{d}w \\ = e^t\int_{-\infty}^{\infty} \partial_w\widetilde{u}_0(w)\Phi_t(v-V_F,w-V_F)\,\mathrm{d}w,\end{aligned} \tag{3.2.32}$$

and now take the supremum of both sides and use the second part of (3.2.28). We can also obtain (3.2.22) from this same expression by using a very similar argument as in (3.2.30).

Regarding the regularization estimates, in order to show $\|e^{tF}u_0\|_\infty \leq Ct^{-1/4}\|u_0\|_2$, i.e. (3.2.23), from (3.2.18) we easily get

$$\|e^{tF}u_0\|_\infty \leq \sqrt{2}\|u_0\|_2\|\Phi_t(v,\cdot)\|_2,$$

and using (3.2.29) gives (3.2.23). To show (3.2.24), we take the supremum in the first expression of equation (3.2.32) and use the estimate

$$\int_{-\infty}^{+\infty} |\partial_v\Phi_t(v,w)|\,\mathrm{d}w = \frac{\sqrt{2}e^t}{\sqrt{\pi(1-e^{-2t})}}\int_{-\infty}^{+\infty} |z|e^{-z^2}\,\mathrm{d}z \lesssim Ct^{-\frac{1}{2}} \qquad \text{for } 0<t\leq 1. \tag{3.2.33}$$

To prove $\|\partial_v e^{tF}u_0\|_\infty \leq Ct^{-3/4}\|u_0\|_2$, i.e. (3.2.25), we use (3.2.32) to write

$$\|\partial_v e^{tF}u_0\|_\infty \leq e^t\sqrt{2}\|u_0\|_2\|\partial_v\Phi_t(v,\cdot)\|_2.$$

The fact that

$$\int_{-\infty}^{+\infty} (\partial_v \Phi_t(v,w))^2 \,\mathrm{d}w = \frac{\sqrt{2}}{\pi} e^t (1-e^{-t})^{-\frac{3}{2}} \int_{-\infty}^{+\infty} z^2 e^{-2z^2} \,\mathrm{d}z \tag{3.2.34}$$

now shows (3.2.25). To prove $\|\partial_v e^{tF} u_0\|_2 \le C t^{-1/2} \|u_0\|_2$, i.e. (3.2.26), we use the Cauchy-Schwarz inequality in (3.2.32) in a similar way as in equation (3.2.30) to get

$$\|\partial_v e^{tF} u_0\|_2 \le C e^{\frac{t}{2}} t^{-\frac{1}{4}} \left(\int_{-\infty}^{\infty} \int_{-\infty}^{\infty} \widetilde{u}_0(w)^2 |\partial_v \Phi_t(v - V_F, w - V_F)| \,\mathrm{d}v \,\mathrm{d}w \right)^{\frac{1}{2}},$$

where we also used (3.2.33). Now the bound

$$\int_{-\infty}^{\infty} |\partial_v \Phi_t(v,w)| \,\mathrm{d}v = \frac{\sqrt{2}}{\sqrt{\pi(1-e^{-2t})}} \int_{-\infty}^{+\infty} |z| e^{-z^2} \,\mathrm{d}z \lesssim C t^{-\frac{1}{2}} \qquad \text{for } 0 < t \le 1$$

completes the proof of (3.2.26). Finally, to prove (3.2.27), i.e. $\|\partial_v e^{tF} u_0\|_\infty \le C t^{-1/4} \|\partial_v u_0\|_2$, we take the supremum in the last expression of (3.2.32), apply the Cauchy-Schwarz inequality, and then use (3.2.29). □

We also need some additional weighted L^2 well-posedness and regularization estimates with Gaussian weight, which we state separately here:

Lemma 3.2.6 (L^2 Gaussian estimates for the Fokker-Planck equation)**.** *Take $v_0 \in \mathbb{R}$ and let $\varphi(v) := \exp((v-v_0)^2/2)$. There exist $t_0 > 0$ and $C > 0$ depending only on v_0 and V_F such that*

$$\|\partial_v e^{tF} u_0\|_{L^2(\varphi)} \le C \|\partial_v u_0\|_{L^2(\varphi)} \qquad \text{for all } 0 < t \le t_0, \tag{3.2.35}$$

and

$$\|\partial_v e^{tF} u_0\|_{L^2(\varphi)} \le C t^{-1/2} \|u_0\|_{L^2(\varphi)} \qquad \text{for all } 0 < t \le t_0, \tag{3.2.36}$$

both for any $u_0 \in X$.

Remark 3.2.7. Of course, estimate (3.2.35) (which has the same norm on both sides) can be iterated for later times to obtain

$$\|\partial_v e^{tF} u_0\|_{L^2(\varphi)} \le C e^{\sigma t} \|\partial_v u_0\|_{L^2(\varphi)} \qquad \text{for all } t \ge 0$$

for some (other) $C > 0$ and some $\sigma > 0$. We have chosen to state this kind of estimates only for a short time when we have no straightforward estimate on σ.

Proof of Lemma 3.2.6. **Proof of the first estimate when $v_0 = 0$.** By possibly changing v_0 it is enough to write the proof for $V_F = 0$. We will first prove the result also assuming

that $v_0 = 0$, and then point out the modifications needed to obtain the general case. Call $u(\cdot, t) = e^{tF} u_0$. From (3.2.18) we have

$$\begin{aligned}\partial_v u(v,t) &= \int_{-\infty}^{0} u_0(w)\partial_v \Psi_t(v,w)\,\mathrm{d}w \\ &= -e^t \int_{-\infty}^{0} u_0(w)\partial_w(\Phi_t(v,w) + \Phi_t(v,-w))\,\mathrm{d}w \\ &= e^t \int_{-\infty}^{0} \partial_w u_0(w)(\Phi_t(v,w) + \Phi_t(v,-w))\,\mathrm{d}w,\end{aligned}$$

where we have used the property (3.2.31) to change ∂_v by ∂_w. Hence,

$$|\partial_v u(v,t)| \le 2e^t \int_{-\infty}^{0} |\partial_w u_0(w)|\,\Phi_t(v,w)\,\mathrm{d}w. \tag{3.2.37}$$

We use this expression to write

$$\begin{aligned}\int_{-\infty}^{0} \varphi(v)(\partial_v u(v,t))^2\,\mathrm{d}v &\le 4e^{2t} \int_{-\infty}^{0} \varphi(v) \left(\int_{-\infty}^{0} \partial_w u_0(w)\Phi_t(v,w)\,\mathrm{d}w\right)^2 \mathrm{d}v \\ &\le 4e^{3t} \int_{-\infty}^{0} \varphi(v) \int_{-\infty}^{0} (\partial_w u_0(w))^2 \Phi_t(v,w)\,\mathrm{d}w\,\mathrm{d}v \\ &= 4e^{3t} \int_{-\infty}^{0} (\partial_w u_0(w))^2 \int_{-\infty}^{0} \varphi(v)\Phi_t(v,w)\,\mathrm{d}v\,\mathrm{d}w, \end{aligned} \tag{3.2.38}$$

where we have used the Cauchy-Schwarz inequality and also (3.2.28). In the case $v_0 = 0$ we can estimate the inner integral by (using the shorthand $r(t) := 1 - e^{-2t}$)

$$\begin{aligned}\int_{-\infty}^{+\infty} \varphi(v)\Phi_t(v,w)\,\mathrm{d}v &= \frac{1}{\sqrt{2\pi r(t)}} \int_{-\infty}^{+\infty} e^{\frac{v^2}{2}} \exp\left(-\frac{(v - e^{-t}w)^2}{2r(t)}\right) \mathrm{d}v \\ &= \frac{1}{\sqrt{1 - r(t)}} \exp\left(\frac{w^2}{2e^{2t}(1 - r(t))}\right) = e^{2t} \exp\left(\frac{w^2}{2}\right) = e^{2t}\varphi(w). \end{aligned} \tag{3.2.39}$$

In order to calculate the integral above we have used the following well-known formula for a Gaussian integral with $\alpha > 0$:

$$\int_{-\infty}^{+\infty} e^{-\alpha v^2 + \beta v + \gamma}\,\mathrm{d}v = \frac{\sqrt{\pi}}{\sqrt{\alpha}} e^{\frac{\beta^2}{4\alpha} + \gamma}. \tag{3.2.40}$$

In the previous calculation we used formula (3.2.40) with $\alpha = (1 - r(t))/(2r(t))$, $\beta = e^{-t}w/r(t)$ and $\gamma = -e^{-2t}w^2/2r(t)$. From (3.2.38) and (3.2.39) we immediately obtain (3.2.35).

Proof of the first estimate for a general v_0. Now, for any $v_0 \in \mathbb{R}$ we proceed in a similar way as before, but now choosing $p, q > 1$ such that $\frac{1}{p} + \frac{1}{q} = 1$ when applying the Cauchy-Schwarz inequality:

$$\begin{aligned}\left(\int_{-\infty}^{0} |\partial_w u_0(w)| \Phi_t(v,w)\,\mathrm{d}w\right)^2 & \\ \leq \left(\int_{-\infty}^{0} (\partial_w u_0(w))^2\, \Phi_t(v,w)^{\frac{2}{p}}\,\mathrm{d}w\right) & \left(\int_{-\infty}^{0} \Phi_t(v,w)^{\frac{2}{q}}\,\mathrm{d}w\right) \\ = \frac{1}{2\pi r(t)} \left(\int_{-\infty}^{0} (\partial_w u_0(w))^2\, e^{-\frac{(v-e^{-t}w)^2}{pr(t)}}\,\mathrm{d}w\right) & \left(\int_{-\infty}^{0} e^{-\frac{(v-e^{-t}w)^2}{qr(t)}}\,\mathrm{d}w\right) \\ \leq \frac{Ce^t}{\sqrt{r(t)}} \int_{-\infty}^{0} (\partial_w u_0(w))^2\, e^{-\frac{(v-e^{-t}w)^2}{pr(t)}}\,\mathrm{d}w. & \quad (3.2.41)\end{aligned}$$

Using this in (3.2.37) we get

$$\begin{aligned}\int_{-\infty}^{0} \varphi(v)(\partial_v u(v,t))^2\,\mathrm{d}v &\leq 4e^{2t} \int_{-\infty}^{0} \varphi(v) \left(\int_{-\infty}^{0} |\partial_w u_0(w)| \Phi_t(v,w)\,\mathrm{d}w\right)^2 \mathrm{d}v \\ &\leq \frac{Ce^{3t}}{\sqrt{r(t)}} \int_{-\infty}^{0} \varphi(v) \int_{-\infty}^{0} (\partial_w u_0(w))^2 e^{-\frac{(v-e^{-t}w)^2}{pr(t)}}\,\mathrm{d}w\,\mathrm{d}v \\ &= \frac{Ce^{3t}}{\sqrt{r(t)}} \int_{-\infty}^{0} (\partial_w u_0(w))^2 \int_{-\infty}^{0} \varphi(v) e^{-\frac{(v-e^{-t}w)^2}{pr(t)}}\,\mathrm{d}v\,\mathrm{d}w. \quad (3.2.42)\end{aligned}$$

An application of the integral formula (3.2.40) gives

$$\begin{aligned}\frac{1}{\sqrt{r(t)}} \int_{-\infty}^{0} \varphi(v) e^{-\frac{(v-e^{-t}w)^2}{pr(t)}}\,\mathrm{d}v &\leq \int_{-\infty}^{+\infty} e^{\frac{(v-v_0)^2}{2}} e^{-\frac{(v-e^{-t}w)^2}{pr(t)}}\,\mathrm{d}v \\ &\leq \frac{C}{\sqrt{1-\frac{p}{2}r(t)}} \exp\left(\frac{(e^{-t}w - v_0)^2}{2-pr(t)}\right).\end{aligned}$$

In order to conclude as before it is enough to show that there is some constant $C > 0$ such that

$$\exp\left(\frac{(e^{-t}w - v_0)^2}{2-pr(t)}\right) \leq C \exp\left(\frac{(w-v_0)^2}{2}\right) \qquad \text{for all } 0 \leq t \leq 1 \text{ and } w \leq 0.$$

Gathering terms one sees it is enough to show that there exists some (other) constant $C > 0$ such that

$$w^2 \left(\frac{1}{e^{2t}(2-pr(t))} - \frac{1}{2}\right) + |w||v_0| \left(1 - \frac{2e^{-t}}{2-pr(t)}\right) \leq C$$

for all $w \leq 0$ and all $0 \leq t \leq 1$. Choosing $p = 3/2$ (in fact, any $p \in (1,2)$ works) we may

find $a, b > 0$ such that

$$w^2 \left(\frac{1}{e^{2t}(2 - pr(t))} - \frac{1}{2} \right) + |w||v_0| \left(1 - \frac{2e^{-t}}{2 - pr(t)} \right) \leq -atw^2 + bt|w||v_0|$$

for all $w \leq 0$ and all $0 \leq t \leq 1$. These a,b are obtained easily by noticing that both of the terms in brackets are 0 at $t = 0$, and have simple linear bounds. We also notice that the factor of w^2 is negative whenever $t > 0$ and $p < 2$. Now by finding the maximum of this parabola in w it is easy to find $C > 0$ such that

$$-atw^2 + bt|w||v_0| \leq C$$

for all $w \leq 0$ and all $0 \leq t \leq 1$. This shows the result.

Proof of the second estimate. The second estimate in the statement can be obtained in a similar way. Choose $1 < p < 2$. By using the explicit expression of $\partial_v \Phi_t$ from (3.2.15) we first notice that

$$|\partial_v \Phi_t(v, w)| \lesssim \frac{1}{r(t)} e^{-\frac{(v - e^{-t}w)^2}{2pr(t)}}, \tag{3.2.43}$$

$$|\partial_v \Phi_t(v, -w)| \lesssim \frac{1}{r(t)} e^{-\frac{(v + e^{-t}w)^2}{2pr(t)}} \lesssim \frac{1}{r(t)} e^{-\frac{(v - e^{-t}w)^2}{2pr(t)}}, \tag{3.2.44}$$

which implies

$$|\partial_v \Psi_t(v, w)| \lesssim \frac{1}{r(t)} e^{-\frac{(v - e^{-t}w)^2}{2pr(t)}}.$$

Now we carry out a similar estimate as in (3.2.41) to get

$$\begin{aligned}
&\left(\int_{-\infty}^{0} u_0(w) \partial_v \Psi_t(v, w) \, \mathrm{d}w \right)^2 \\
&\qquad \leq \left(\int_{-\infty}^{0} u_0(w)^2 \left(\partial_v \Psi_t(v, w) \right)^{\frac{2}{p}} \mathrm{d}w \right) \left(\int_{-\infty}^{0} \left(\partial_v \Psi_t(v, w) \right)^{\frac{2}{q}} \mathrm{d}w \right) \\
&\qquad \lesssim \frac{1}{r(t)^2} \left(\int_{-\infty}^{0} u_0(w)^2 \, e^{-\frac{(v - e^{-t}w)^2}{p^2 r(t)}} \, \mathrm{d}w \right) \left(\int_{-\infty}^{0} e^{-\frac{(v - e^{-t}w)^2}{pqr(t)}} \, \mathrm{d}w \right) \\
&\qquad \lesssim \frac{1}{(r(t))^{\frac{3}{2}}} \int_{-\infty}^{0} u_0(w)^2 \, e^{-\frac{(v - e^{-t}w)^2}{p^2 r(t)}} \, \mathrm{d}w.
\end{aligned}$$

Proceeding as in (3.2.42),

$$\int_{-\infty}^{0} \varphi(v)(\partial_v u(v,t))^2 \,\mathrm{d}v \leq \int_{-\infty}^{0} \varphi(v) \left(\int_{-\infty}^{0} u_0(w) \partial_v \Psi_t(v,w) \,\mathrm{d}w \right)^2 \mathrm{d}v \\ \lesssim \frac{1}{(r(t))^{\frac{3}{2}}} \int_{-\infty}^{0} u_0(w)^2 \int_{-\infty}^{0} \varphi(v) e^{-\frac{(v-e^{-t}w)^2}{p^2 r(t)}} \,\mathrm{d}v \,\mathrm{d}w.$$

Choosing any $1 < p < 2$ such that also $1 < p^2 < 2$ we may carry out the same reasoning we did after (3.2.42) to get

$$\int_{-\infty}^{0} \varphi(v)(\partial_v u(v,t))^2 \,\mathrm{d}v \leq \int_{-\infty}^{0} \varphi(v) \left(\int_{-\infty}^{0} u_0(w) \partial_v \Psi_t(v,w) \,\mathrm{d}w \right)^2 \mathrm{d}v \\ \lesssim \frac{1}{r(t)} \int_{-\infty}^{0} u_0(w)^2 \varphi(w) \,\mathrm{d}w.$$

This finishes the result. □

Bounds for the Fokker-Planck equation plus the source term

In the following lemma, we show the bounds for the semigroup that adds the source term $\delta_{V_R} N_u(t)$ to the previous one.

Lemma 3.2.8. *Denote by $e^{tA}u_0$ the classical solution to*

$$\partial_t u = Fu + L_1 u = \partial_v^2 u + \partial_v[(v - V_F)u] + \delta_{V_R} N_u(t) \tag{3.2.45}$$

in the domain $v \in (-\infty, V_F]$, $t \geq 0$, with the Dirichlet boundary condition (3.2.1b) and with an initial condition $u_0 \in X$. Then there exist $C > 0$ and $t_0 > 0$ depending only on the system parameters such that the following well-posedness inequalities hold for all $0 \leq t \leq t_0$:

$$\|\partial_v e^{tA} u_0\|_\infty \leq C \|\partial_v u_0\|_\infty, \tag{3.2.46}$$

$$\|\partial_v e^{tA} u_0\|_2 \leq C \|\partial_v u_0\|_2, \tag{3.2.47}$$

$$\|e^{tA} u_0\|_\infty \leq C \|u_0\|_\infty, \tag{3.2.48}$$

$$\|e^{tA} u_0\|_2 \leq C \|u_0\|_2, \tag{3.2.49}$$

and the following "regularization" inequalities hold for all times $0 < t \leq t_0$*:*

$$\|\partial_v e^{tA} u_0\|_\infty \leq C t^{-3/4} \|u_0\|_2. \tag{3.2.50}$$

$$\|\partial_v e^{tA} u_0\|_\infty \leq C t^{-1/2} \|u_0\|_\infty. \tag{3.2.51}$$

$$\|\partial_v e^{tA} u_0\|_2 \leq C t^{-1/2} \|u_0\|_2. \tag{3.2.52}$$

$$\|e^{tA} u_0\|_\infty \leq C t^{-1/4} \|u_0\|_2. \tag{3.2.53}$$

As we mentioned in Remark 3.2.7, inequalities (3.2.46)–(3.2.49) can be iterated to obtain a bound for all times.

Proof. The solution to this equation can be written through Duhamel's formula by using the Fokker-Planck semi-group e^{tF} from Lemma 3.2.5 as follows:

$$\begin{aligned} u(v,t) = e^{tA} u_0(v) &= e^{tF} u_0(v) + \int_0^t e^{(t-s)F} \left[N_u(s) \delta_{V_R} \right] \mathrm{d}s \\ &= e^{tF} u_0(v) + \int_0^t \Psi_{t-s}(v - V_F, V_R - V_F) N_u(s) \, \mathrm{d}s, \end{aligned} \tag{3.2.54}$$

where we have explicitly written $e^{(t-s)F}\left[\delta_{V_R}\right]$ by using equation (3.2.18). We note that this Duhamel's formula is a possible definition of classical solutions to (3.2.45), similarly to the approach in [29].

Taking the derivative in terms of v of the previous equation, we can write the derivative of the solution to the incomplete linear equation as

$$\partial_v u(v,t) = \partial_v e^{tA} u_0(v) = \partial_v e^{tF} u_0(v) + \int_0^t \partial_v \Psi_{t-s}(v - V_F, V_R - V_F) N_u(s) \, \mathrm{d}s. \tag{3.2.55}$$

We are first going to show the bounds on the derivative of the solution u, which will be useful later to prove the bounds on u itself.

Step 1. Bounds on $N_u(t)$. We need to bound $N_u(t)$ by the three different norms contained in the norm of X. With this aim we compute $N_u(t)$ by evaluating equation (3.2.55) at V_F:

$$-N_u(t) = \partial_v e^{tF} u_0(V_F) + \int_0^t N_u(s) \partial_v \Psi_{t-s}(0, V_R - V_F) \, \mathrm{d}s, \tag{3.2.56}$$

where we recall that the kernel Ψ is given in (3.2.14)–(3.2.13). This kernel is easily seen to satisfy

$$|\partial_v \Psi_t(0, V_R - V_F)| < C \qquad \text{for all } t > 0,$$

for some constant $C > 0$. Using also the bound (3.2.25), from (3.2.56) we find

$$|N_u(t)| \leq Ct^{-3/4}\|u_0\|_2 + C\int_0^t |N_u(s)|\,\mathrm{d}s,$$

which can be also written as

$$t^{3/4}|N_u(t)| \leq C\|u_0\|_2 + Ct^{3/4}\int_0^t s^{-3/4}s^{3/4}|N_u(s)|\,\mathrm{d}s.$$

Now we write the previous equation as

$$z(t) \leq C\|u_0\|_2 + Ct^{3/4}\int_0^t s^{-3/4}z(s)\,\mathrm{d}s,$$

with $z(t) = t^{3/4}|N_u(t)|$, and we apply Lemma 3.2.13 with $\alpha = 3/4$, $\beta = 0$ and $\gamma = 3/4$, which leads to

$$|N_u(t)| \leq Ct^{-3/4}\|u_0\|_2 \tag{3.2.57}$$

for all t small enough. Proceeding as we have done so far, but using the bounds (3.2.24), (3.2.21) and (3.2.27) instead of (3.2.25), we end up with:

$$|N_u(t)| \leq Ct^{-1/2}\|u_0\|_\infty, \tag{3.2.58}$$

$$|N_u(t)| \leq C\|\partial_v u_0\|_\infty, \tag{3.2.59}$$

and

$$|N_u(t)| \leq Ct^{-1/4}\|\partial_v u_0\|_2, \tag{3.2.60}$$

all valid for all $t > 0$ small enough.

Step 2. Bounds on the second term in (3.2.54). We need to give some bounds for the term

$$\begin{aligned}\int_0^t &\partial_v\Psi_{t-s}(v - V_F, V_R - V_F)N_u(s)\,\mathrm{d}s \\ &= \int_0^t \partial_v\Phi_{t-s}(v - V_F, V_R - V_F)N_u(s)\,\mathrm{d}s + \int_0^t \partial_v\Phi_{t-s}(v - V_F, V_F - V_R)N_u(s)\,\mathrm{d}s.\end{aligned}$$

The main difficulty when bounding this lies on the first integral on the right-hand side. For this purpose we use the explicit expression of the derivative of the kernel, given by equation (3.2.15). We use inequality (3.2.57) for $N_u(s)$ as follows, with the notation $\tilde{v} \equiv v - V_F$, $\tilde{V_R} \equiv V_R - V_F$ and $r(t) := \left(1 - e^{-2t}\right)$, (notice that $\tilde{v}, \tilde{V_R} \in (-\infty, 0]$),

$$\begin{aligned}
&\left|\int_0^t \partial_v \Phi_{t-s}(v-V_F, V_R-V_F) N_u(s)\,\mathrm{d}s\right| \\
&\qquad \le (2\pi)^{-\frac{1}{2}} \int_0^t r(t-s)^{-3/2} |N_u(s)| \left|\tilde{v} - e^{-(t-s)}\tilde{V}_R\right| e^{-\frac{|\tilde{v}-e^{-(t-s)}\tilde{V}_R|^2}{2r(t-s)}}\,\mathrm{d}s \\
&\qquad \le (2\pi)^{-\frac{1}{2}} \|u_0\|_2 \int_0^t r(t-s)^{-3/2} s^{-3/4} \left|\tilde{v} - e^{-(t-s)}\tilde{V}_R\right| e^{-\frac{|\tilde{v}-e^{-(t-s)}\tilde{V}_R|^2}{2r(t-s)}}\,\mathrm{d}s \\
&\qquad\qquad \le Ct^{-3/4}\|u_0\|_2,
\end{aligned}$$

where in the last inequality we have applied the Lemma 3.2.9 with $\alpha = 3/4$. On the other hand, since $v - V_F$ and $V_R - V_F$ are both negative,

$$\begin{aligned}
&\left|\int_0^t \partial_v \Phi_{t-s}(v-V_F, V_F-V_R) N_u(s)\,\mathrm{d}s\right| \\
&\qquad \le (2\pi)^{-\frac{1}{2}} \int_0^t r(t-s)^{-3/2} |N_u(s)| \left|\tilde{v} + e^{-(t-s)}\tilde{V}_R\right| e^{-\frac{|\tilde{v}+e^{-(t-s)}\tilde{V}_R|^2}{2r(t-s)}}\,\mathrm{d}s \\
&\qquad\qquad \lesssim \int_0^t r(t-s)^{-1} |N_u(s)| e^{-\frac{|\tilde{v}+e^{-(t-s)}\tilde{V}_R|^2}{4r(t-s)}}\,\mathrm{d}s \\
&\qquad \lesssim \int_0^t r(t-s)^{-1} |N_u(s)| e^{-\frac{\tilde{V}_R^2}{4r(t-s)}}\,\mathrm{d}s \lesssim \int_0^t |N_u(s)|\,\mathrm{d}s \\
&\qquad\qquad \lesssim \|u_0\|_2 \int_0^t s^{-3/4}\,\mathrm{d}s = 4\|u_0\|_2 t^{1/4}.
\end{aligned}$$

From the last two equations we see that

$$\left|\int_0^t \partial_v \Psi_{t-s}(v-V_F, V_F-V_R) N_u(s)\,\mathrm{d}s\right| \lesssim t^{-3/4}\|u_0\|_2$$

for all $t > 0$ small enough. We can repeat this procedure using for $N_u(s)$ the bounds (3.2.58), (3.2.59) or (3.2.60) instead of (3.2.57), obtaining the following four bounds for the integral:

$$\left|\int_0^t \partial_v \Psi_{t-s}(v-V_F, V_R-V_F) N_u(s)\,\mathrm{d}s\right| \le \begin{cases} Ct^{-3/4}\|u_0\|_2 \\ Ct^{-1/2}\|u_0\|_\infty \\ C\|\partial_v u_0\|_\infty \\ Ct^{-1/4}\|\partial_v u_0\|_2 \end{cases} \tag{3.2.61}$$

Step 3. Bounds on $\partial_v u$. Now we can show the bounds for the derivative of the solution.

With this purpose, in equation (3.2.55) we take the absolute value, which leads to

$$|\partial_v u(v,t)| \leq \left|\partial_v e^{tF} u_0(v)\right| + \left|\int_0^t \partial_v \Psi_{t-s}(v - V_F, V_R - V_F) N_u(s)\, \mathrm{d}s\right| \tag{3.2.62}$$

First, by taking the supremum norm in the inequality (3.2.62) together with the first bound in (3.2.61) we obtain

$$\|\partial_v u(.,t)\|_\infty = \|\partial_v e^{tA} u_0\|_\infty \leq \|\partial_v e^{tF} u_0\|_\infty + Ct^{-3/4}\|u_0\|_2.$$

A direct application of the bound (3.2.25) for $\|\partial_v e^{tF} u_0\|_\infty$ gives inequality (3.2.50). Alternatively, using the second bound in (3.2.61) and (3.2.24) gives (3.2.51); and using the third bound in (3.2.61) and (3.2.21), we get to (3.2.46).

In order to bound the L^2 norms of $\partial_v u$ we take the L^2 norm in equation (3.2.55):

$$\|\partial_v e^{tA} u_0\|_2 \leq \|\partial_v e^{tF} u_0\|_2 + \int_0^t \|\partial_v \Psi_{t-s}(v - V_F, V_R - V_F)\|_2 |N_u(s)|\, \mathrm{d}s. \tag{3.2.63}$$

First we bound $\|\partial_v \Phi_t(v - V_F, V_R - V_F)\|_2$ as follows:

$$\begin{aligned}
&\|\partial_v \Phi_t(v - V_F, V_R - V_F)\|_2^2 \\
&\quad = \frac{1}{2\pi(1-e^{-2t})^3} \int_{-\infty}^{V_F} |v - V_F - e^{-t}(V_R - V_F)|^2 e^{-\frac{|v - V_F - e^{-t}(V_R - V_F)|^2}{1-e^{-2t}}}\, \mathrm{d}v \\
&\quad \leq \frac{1}{2\pi(1-e^{-2t})^{3/2}} \int_{\mathbb{R}} w^2 e^{-w^2}\, \mathrm{d}w = \frac{1}{4\sqrt{\pi}(1-e^{-2t})^{3/2}} \leq Ct^{-3/2},
\end{aligned} \tag{3.2.64}$$

where we used the change of variables $w = \frac{v - V_F - e^{-t}(V_R - V_F)}{(1-e^{-2t})^{1/2}}$. The reflected term $\|\partial_v \Phi_t(v - V_F, V_F - V_R)\|_2$ is in turn bounded in the same way by using $w = \frac{v - V_F - e^{-t}(V_F - V_R)}{(1-e^{-2t})^{1/2}}$ as change of variables in the previous process. Then we use equations (3.2.26) and (3.2.57) so that the previous inequality implies

$$\begin{aligned}
\|\partial_v e^{tA} u_0\|_2 &\leq Ct^{-1/2}\|u_0\|_2 + C\|u_0\|_2 \int_0^t (t-s)^{-3/4} s^{-3/4}\, \mathrm{d}s \\
&= Ct^{-1/2}\|u_0\|_2 + Ct^{-1/2}\|u_0\|_2 = Ct^{-1/2}\|u_0\|_2.
\end{aligned}$$

which is exactly the inequality (3.2.52). If, otherwise, in expression (3.2.63) we use the inequalities (3.2.22) and (3.2.60) we obtain

$$\|\partial_v e^{tA} u_0\|_2 \leq C\|\partial_v u_0\|_2 + C\|\partial_v u_0\|_2 \int_0^t (t-s)^{-3/4} s^{-1/4}\, \mathrm{d}s \leq C\|\partial_v u_0\|_2.$$

By directly solving the integral, which is constant in time, we get to inequality (3.2.47).

Step 4. Bounds on u. We now carry out similar estimates on the solution given in (3.2.54). First we take the supremum norm to get:

$$\|u(.,t)\|_\infty = \|e^{tA}u_0\|_\infty \leq \|e^{tF}u_0\|_\infty + \int_0^t \|\Psi_{t-s}(v-V_F, V_R-V_F)\|_\infty |N_u(s)|\,\mathrm{d}s,$$

now, using the definition of Ψ (see (3.2.14))

$$\Phi_{t-s}(v-V_F, V_R-V_F) = \Psi_{t-s}(v-V_F, V_R-V_F) + \Phi_{t-s}(v-V_F, V_F-V_R)$$

and the fact that three terms are nonnegative, we obtain

$$\|\Psi_{t-s}(v-V_F, V_R-V_F)\|_\infty < \|\Phi_{t-s}(v-V_F, V_R-V_F)\|_\infty,$$

and therefore

$$\|e^{tA}u_0\|_\infty \leq \|e^{tF}u_0\|_\infty + \int_0^t \|\Phi_{t-s}(v-V_F, V_R-V_F)\|_\infty |N_u(s)|\,\mathrm{d}s.$$

By using the explicit expression of the Fokker-Planck kernel $\Phi_{t-s}(v-V_F, V_R-V_F)$, together with the equations (3.2.23) and (3.2.57), we find the following inequality:

$$\|e^{tA}u_0\|_\infty \leq Ct^{-1/4}\|u_0\|_2 + C\|u_0\|_2 \int_0^t s^{-3/4}(1-e^{-2(t-s)})^{-1/2} e^{-\frac{|v-V_F-e^{-t}(V_R-V_F)|^2}{2(1-e^{2(t-s)})}}\,\mathrm{d}s,$$

where we can apply Lemma 3.2.9 (considering $\tilde{v} \equiv v - V_F$, $\tilde{V}_R \equiv V_R - V_F$) to bound the integral and obtain inequality (3.2.53).

Additionally, if we want to bound the norm infinity of the solution by the norm infinity of the initial condition, we can do as before, taking norm infinity in (3.2.54), but using equations (3.2.19) and (3.2.58), which gives the inequality (3.2.48).

Now we take norm L_2 of equation (3.2.54), resulting in

$$\|e^{tA}u_0\|_2 \leq \|e^{tF}u_0\|_2 + \int_0^t \|\Psi_{t-s}(v-V_F, V_R-V_F)\|_2 |N_u(s)|\,\mathrm{d}s,$$

where $|N_u(s)|$ can be bounded by using again the equation (3.2.57) and $\|\Psi_{t-s}(v-V_F, V_R-V_F)\|_2$ can be directly bounded using:

$$\|\Psi_{t-s}(v-V_F,V_R-V_F)\|_2^2 \le \|\Phi_{t-s}(v-V_F,V_R-V_F)\|_2^2 = \frac{1}{2\pi(1-e^{-2(t-s)})}\int_{\mathbb{R}} e^{-\frac{|v-V_F-e^{-(t-s)}(V_R-V_F)|^2}{(1-e^{-2(t-s)})}}\,\mathrm{d}v$$
$$= \frac{1}{2\pi\sqrt{1-e^{-2(t-s)}}}\int_{\mathbb{R}} e^{-w^2}\,\mathrm{d}w = \frac{1}{\sqrt{4\pi(1-e^{-2(t-s)})}},$$

having used the change of variables $w = \frac{v-V_F-e^{-(t-s)}(V_R-V_F)}{(1-e^{-(t-s)})^{1/2}}$. Using this bound, for small t, such that $t < 1-e^{-2t}$, and (3.2.20) for estimate $\|e^{tF}u_0\|_2$ and (see (3.2.57)) $|N_u(t)| \le Ct^{-3/4}\|u_0\|_2$, we get:

$$\|e^{tA}u_0\|_2 \le Ce^{t/2}\|u_0\|_2 + C\|u_0\|_2\int_0^t (t-s)^{-1/4}s^{-3/4}\,\mathrm{d}s \le C\|u_0\|_2.$$

where we have directly solved the integral, using the change of variable $\tau = s/t$ and the beta function $\beta(x,y) := \int_0^1 \tau^{x-1}(1-\tau)^{y-1}d\tau$, for $x,y \in \mathbb{C}$ with real part positive (we recall the relation with the gamma function, $\beta(x,y) = \frac{\Gamma(x)\Gamma(y)}{\Gamma(x+y)}$), to obtain inequality (3.2.49). This completes the proof of all inequalities. □

We finish this subsection with the proof of the lemma used to prove the previous result.

Lemma 3.2.9. *For $t > 0$, $v \in (-\infty, 0]$, $\tilde{V}_R < 0$ and $0 \le \alpha < 1$, let us consider the following integrals:*

$$I_1(v,t) := \int_0^t s^{-\alpha}(1-e^{-2(t-s)})^{-1/2}e^{-\frac{|v-e^{-(t-s)}\tilde{V}_R|^2}{2(1-e^{-2(t-s)})}}\,\mathrm{d}s,$$
$$I_2(v,t) := \int_0^t s^{-\alpha}(1-e^{-2(t-s)})^{-3/2}\left|v-e^{-(t-s)}\tilde{V}_R\right| e^{-\frac{|v-e^{-(t-s)}\tilde{V}_R|^2}{2(1-e^{-2(t-s)})}}\,\mathrm{d}s.$$

Then, there exists $C = C(\alpha)$ such that

$$I_1(v,t) \le Ct^{\frac{1}{2}-\alpha} \qquad \text{and} \qquad I_2(v,t) \le Ct^{-\alpha}$$

for t small enough and $v \in (-\infty, 0]$.

Proof. For both cases we will consider a sufficiently small t so that $t \le (1-e^{-2t})$. In the case of I_1 we use this bound and estimate the exponential by 1 to get

$$I_1 \le \int_0^t s^{-\alpha}(t-s)^{-1/2}\,\mathrm{d}s = t^{1/2-\alpha}\frac{\Gamma(1-\alpha)\sqrt{\pi}}{\Gamma(3/2-\alpha)},$$

where the last equality is seen through the change of variables $\tau = s/t$, as explained above.

Now we consider the second integral and we split it by using $v - e^{-t}\tilde{V}_R = (v - \tilde{V}_R) + \tilde{V}_R(1 - e^{-t})$ and therefore, $|v - e^{-t}\tilde{V}_R| \leq |\tilde{V}_R|t + |v - \tilde{V}_R|$ (valid for all $t \geq 0$, since $1 - e^{-t} \leq t$):

$$\begin{aligned} I_2 &\leq \int_0^t s^{-\alpha}(t-s)^{-3/2}|v - e^{-(t-s)}\tilde{V}_R| e^{-\frac{|v-e^{-(t-s)}\tilde{V}_R|^2}{2(t-s)}}\,\mathrm{d}s \\ &\leq |\tilde{V}_R| \int_0^t s^{-\alpha}(t-s)^{-1/2} e^{-\frac{|v-e^{-(t-s)}\tilde{V}_R|^2}{2(t-s)}}\,\mathrm{d}s \\ &\quad + \int_0^t s^{-\alpha}(t-s)^{-3/2}|v - \tilde{V}_R| e^{-\frac{|v-e^{-(t-s)}\tilde{V}_R|^2}{2(t-s)}}\,\mathrm{d}s =: I_{2.1} + I_{2.2}. \end{aligned}$$

The first integral, $I_{2,1}$, can be bounded as was done for I_1 by $Ct^{1/2-\alpha}$.

For the second one we use the inequality $(a+b)^2 \geq \frac{1}{2}a^2 - b^2$ (valid for any real a, b) to get

$$\begin{aligned} (v - e^{-(t-s)}\tilde{V}_R)^2 &= ((v - \tilde{V}_R) + \tilde{V}_R(1 - e^{-(t-s)}))^2 \\ &\geq \frac{1}{2}(v - \tilde{V}_R)^2 - \tilde{V}_R^2(1 - e^{-(t-s)})^2 \geq \frac{1}{2}(v - \tilde{V}_R)^2 - \tilde{V}_R^2(t-s)^2. \end{aligned}$$

As a consequence, for t small, we have

$$e^{-\frac{(v-e^{-(t-s)}\tilde{V}_R)^2}{2(t-s)}} \leq e^{-\frac{(v-\tilde{V}_R)^2}{4(t-s)}} e^{\frac{1}{2}\tilde{V}_R^2(t-s)} \lesssim e^{-\frac{(v-\tilde{V}_R)^2}{4(t-s)}}.$$

We can use this bound on the term $I_{2,2}$ and obtain

$$I_{2.2} \lesssim \int_0^t s^{-\alpha}(t-s)^{-3/2}|v - \tilde{V}_R| e^{-\frac{(v-\tilde{V}_R)^2}{4(t-s)}}\,\mathrm{d}s.$$

Now we use the change of variables $w = (v - \tilde{V}_R)^2/(t-s)$ and call $a := (v - \tilde{V}_R)^2$. After standard computations we have

$$I_{2.2} \lesssim \int_{\frac{a}{t}}^{\infty} \left(t - \frac{a}{w}\right)^{-\alpha} w^{-\frac{1}{2}} e^{-\frac{w}{4}}\,\mathrm{d}w = t^{-\alpha} \int_{\frac{a}{t}}^{\infty} \left(w - \frac{a}{t}\right)^{-\alpha} w^{\alpha-\frac{1}{2}} e^{-\frac{w}{4}}\,\mathrm{d}w.$$

Now, if $\alpha \geq \frac{1}{2}$ we write

$$\begin{aligned} t^{-\alpha} \int_{\frac{a}{t}}^{\infty} \left(w - \frac{a}{t}\right)^{-\alpha} w^{\alpha-\frac{1}{2}} e^{-\frac{w}{4}}\,\mathrm{d}w &\lesssim t^{-\alpha} \int_{\frac{a}{t}}^{\infty} \left(w - \frac{a}{t}\right)^{-\alpha} e^{-\frac{w}{8}}\,\mathrm{d}w \\ &\leq t^{-\alpha} \int_{\frac{a}{t}}^{\infty} \left(w - \frac{a}{t}\right)^{-\alpha} e^{-\frac{1}{8}(w-\frac{a}{t})}\,\mathrm{d}w = t^{-\alpha} \int_0^{\infty} w^{-\alpha} e^{-\frac{w}{8}}\,\mathrm{d}w = Ct^{-\alpha}\Gamma(1-\alpha). \end{aligned}$$

Otherwise, if $0 \le \alpha < 1/2$, we use that $w^{\alpha-\frac{1}{2}} \le \left(w - \frac{a}{t}\right)^{\alpha-\frac{1}{2}}$ to write

$$t^{-\alpha}\int_{\frac{a}{t}}^{\infty}\left(w-\frac{a}{t}\right)^{-\alpha} w^{\alpha-\frac{1}{2}} e^{-\frac{w}{4}}\,\mathrm{d}w \le t^{-\alpha}\int_{\frac{a}{t}}^{\infty}\left(w-\frac{a}{t}\right)^{-\frac{1}{2}} e^{-\frac{1}{4}\left(w-\frac{a}{t}\right)}\,\mathrm{d}w$$
$$= t^{-\alpha}\int_0^{\infty} w^{-\frac{1}{2}} e^{-\frac{w}{4}}\,\mathrm{d}w = Ct^{-\alpha}\Gamma(1/2).$$

In any of the two cases we obtain

$$I_{2,2} \lesssim Ct^{-\alpha} \qquad \text{for } t \text{ small enough.}$$

Together with the bound for $I_{2,1}$ we obtain the stated result. □

As in the previous section, we also need Gaussian estimates for the semigroup associated to the operator A:

Lemma 3.2.10 (L^2 Gaussian estimates including the source term)**.** *Take $v_0 \in \mathbb{R}$ and let $\varphi(v) := \exp((v-v_0)^2/2)$. There exists $C > 0$ and $t_0 > 0$ depending only on v_0 and V_F such that*

$$\|\partial_v e^{tA} u_0\|_{L^2(\varphi)} \le C\|\partial_v u_0\|_{L^2(\varphi)} \qquad \text{for all } 0 \le t \le t_0 \tag{3.2.65}$$

and

$$\|\partial_v e^{tA} u_0\|_{L^2(\varphi)} \le Ct^{-1/2}\|u_0\|_{L^2(\varphi)} \qquad \text{for all } 0 < t \le t_0, \tag{3.2.66}$$

both for any $u_0 \in X$.

Proof. For simplicity we show the estimates for $V_F = 0$, since the general case follows also from very similar calculations. Let us first show (3.2.65). We take the $L^2(\varphi)$ norm in (3.2.55) and obtain similar bound as in (3.2.63):

$$\|\partial_v e^{tA} u_0\|_{L^2(\varphi)} \le \|\partial_v e^{tF} u_0\|_{L^2(\varphi)} + \int_0^t \|\partial_v \Psi_{t-s}(v, V_R)\|_{L^2(\varphi)} |N_u(s)|\,\mathrm{d}s.$$

An explicit calculation along the lines of (3.2.64) shows that

$$\|\partial_v \Psi_t(v, V_R)\|^2_{L^2(\varphi)} \lesssim t^{-3/2}.$$

Using this bound, (3.2.60) and (3.2.35) from Lemma 3.2.6 we have

$$\|\partial_v e^{tA} u_0\|_{L^2(\varphi)} \lesssim \|\partial_v u_0\|_{L^2(\varphi)} + \|\partial_v u_0\|_{L^2(\varphi)} \int_0^t (t-s)^{-\frac{3}{4}} s^{-\frac{1}{4}}\,\mathrm{d}s \lesssim \|\partial_v u_0\|_{L^2(\varphi)},$$

valid for all times $t \ge 0$ small enough. This shows (3.2.65).

In order to prove (3.2.66) we follow the same path but use (3.2.57) and (3.2.36) instead of (3.2.60) and (3.2.35), respectively, to get

$$\|\partial_v e^{tA} u_0\|_{L^2(\varphi)} \lesssim t^{-\frac{1}{2}} \|u_0\|_{L^2(\varphi)} + \|u_0\|_{L^2(\varphi)} \int_0^t (t-s)^{-\frac{3}{4}} s^{-\frac{3}{4}} \, \mathrm{d}s \lesssim t^{-\frac{1}{2}} \|u_0\|_{L^2(\varphi)}.$$

This completes the proof. □

Bounds for the complete linear equation

Finally, using the bounds proved in Lemma 3.2.8 we can obtain the bounds for the complete linear equation.

Lemma 3.2.11. *Let us consider $u_0 \in X$ any initial condition to the equation:*

$$\partial_t u(v,t) = \partial_v^2 u(v,t) + \partial_v \left(v u(v,t)\right) + N_u(t)\delta_{V_R} - bN\partial_v u(v,t) =: Lu(v,t)$$

in the domain $v \in (-\infty, V_F)$, $t \geq 0$, with the boundary condition $u(V_F, t) = 0$ and whose associated semi-group is e^{tL}. We recall that b is the connectivity parameter and N is considered constant here. Then there exist $C \geq 1$ and $t_0 > 0$ depending only on N, V_R and V_F such that for all $u_0 \in X$ and all $0 \leq t \leq t_0$ the following well-posedness inequalities hold:

$$\|\partial_v e^{tL} u_0\|_2 \leq C \|\partial_v u_0\|_2, \tag{3.2.67}$$
$$\|\partial_v e^{tL} u_0\|_\infty \leq C \|\partial_v u_0\|_\infty, \tag{3.2.68}$$
$$\|e^{tL} u_0\|_\infty \leq C \|u_0\|_\infty, \tag{3.2.69}$$
$$\|e^{tL} u_0\|_2 \leq C \|u_0\|_2, \tag{3.2.70}$$

and the following "regularization" inequalities hold for all $0 < t \leq t_0$:

$$\|\partial_v e^{tL} u_0\|_2 \leq C t^{-1/2} \|u_0\|_2, \tag{3.2.71}$$
$$\|\partial_v e^{tL} u_0\|_\infty \leq C t^{-3/4} \|u_0\|_2, \tag{3.2.72}$$
$$\|\partial_v e^{tL} u_0\|_\infty \leq C t^{-1/2} \|u_0\|_\infty, \tag{3.2.73}$$
$$\|e^{tL} u_0\|_\infty \leq C t^{-1/4} \|u_0\|_2. \tag{3.2.74}$$

Proof. We use the splitting (3.2.10) for the PDE, $Lu = Fu + L_1 u + L_2 u$, which is rewritten as $Lu = Au + L_2 u$ and we recall that $L_2 u = \partial_v[(V_F - bN)u]$ and $V_F - bN$ is a constant.

Again, to prove the lemma, we use Duhamel's formula for the solution and its derivative:

$$u(v,t) = e^{tL}u_0(v) = e^{tA}u_0(v) + (V_F - bN)\int_0^t e^{(t-s)A}\left(\partial_v u(v,s)\right)\,\mathrm{d}s, \tag{3.2.75}$$

$$\partial_v u(v,t) = \partial_v e^{tL}u_0(v) = \partial_v e^{tA}u_0(v) + (V_F - bN)\int_0^t \partial_v e^{(t-s)A}\left(\partial_v u(v,s)\right)\,\mathrm{d}s, \tag{3.2.76}$$

and bounds obtained Lemma 3.2.8 for the semigroup e^{At}.

Step 1. Bounds on $\partial_v u$. If we take the L^2 norm in equation (3.2.76) we obtain the following inequality:

$$\|\partial_v e^{tL}u_0\|_2 \leq \|\partial_v e^{tA}u_0\|_2 + C\int_0^t \|\partial_v e^{(t-s)A}\left(\partial_v u(.,s)\right)\|_2\,\mathrm{d}s, \tag{3.2.77}$$

which, directly using inequality (3.2.52), $\|\partial_v e^{tA}u_0\|_2 \leq Ct^{-1/2}\|u_0\|_2$, implies

$$\|\partial_v e^{tL}u_0\|_2 \leq Ct^{-1/2}\|u_0\|_2 + C\int_0^t (t-s)^{-1/2}\,\|\partial_v u(.,s)\|_2\,\mathrm{d}s.$$

After that, taking into account that $\|\partial_v u(.,s)\|_2$ can be also written as $\|\partial_v e^{sL}u_0\|_2$, we use the change of variables $z(t) := t^{1/2}\|\partial_v e^{tL}u_0\|_2$ to write the previous expression as follows:

$$z(t) \leq C\|u_0\|_2 + Ct^{1/2}\int_0^t (t-s)^{-1/2}\,s^{-1/2}z(s)\,\mathrm{d}s,$$

where the application of the Lemma 3.2.13 with $\alpha = \beta = \gamma = 1/2$ gives us the proof for the inequality (3.2.71). Another way of bounding the l.h.s of (3.2.77) consists of using inequality (3.2.47), $\|\partial_v e^{tA}u_0\|_2 \leq C\|\partial_v u_0\|_2$, in the first term of the r.h.s and (3.2.52), $\|\partial_v e^{tA}u_0\|_2 \leq Ct^{-1/2}\|u_0\|_2$, in the second one, obtaining

$$\|\partial_v e^{tL}u_0\|_2 \leq C\|\partial_v u_0\|_2 + C\int_0^t (t-s)^{-1/2}\,\|\partial_v e^{sL}u_0\|_2\,\mathrm{d}s,$$

which proves inequality (3.2.67) after the application of Lemma 3.2.13 with $\alpha = 0, \beta = 1/2$ and $\gamma = 0$.

Now we are going to bound equation (3.2.76) by taking norm L^∞ on it, which leads to

$$\|\partial_v e^{tL}u_0\|_\infty \leq \|\partial_v e^{tA}u_0\|_\infty + C\int_0^t \|\partial_v e^{(t-s)A}\left(\partial_v u(.,s)\right)\|_\infty\,\mathrm{d}s, \tag{3.2.78}$$

where, using equation (3.2.50), $\|\partial_v e^{tA}u_0\|_\infty \leq Ct^{-3/4}\|u_0\|_2$, we obtain

$$\|\partial_v e^{tL}u_0\|_\infty \leq Ct^{-3/4}\|u_0\|_2 + C\int_0^t (t-s)^{-3/4}\,\|\partial_v e^{sL}u_0\|_2\,\mathrm{d}s.$$

Finally, by using the inequality (3.2.71), $\|\partial_v e^{tL}u_0\|_2 \leq Ct^{-1/2}\|u_0\|_2$, and by integrating the second term in the r.h.s, we prove inequality (3.2.72) as follows:

$$\begin{aligned}\|\partial_v e^{tL}u_0\|_\infty &\leq Ct^{-3/4}\|u_0\|_2 + C\int_0^t (t-s)^{-3/4}\,s^{-1/2}\|u_0\|_2\,\mathrm{d}s \\ &= Ct^{-3/4}\|u_0\|_2 + Ct^{-1/4}\|u_0\|_2 \leq Ct^{-3/4}\|u_0\|_2.\end{aligned}$$

If, instead of performing the latter procedure, we apply bound (3.2.51), $\|\partial_v e^{tA}u_0\|_\infty \leq Ct^{-1/2}\|u_0\|_\infty$, to inequality (3.2.78), we find

$$\|\partial_v e^{tL}u_0\|_\infty \leq Ct^{-1/2}\|u_0\|_\infty + C\int_0^t (t-s)^{-1/2}\|\partial_v e^{sL}u_0\|_\infty\,\mathrm{d}s,$$

which we can equivalently write, through the use of the change of variables $z(t) := t^{1/2}\|\partial_v e^{tL}u_0\|_\infty$, as

$$z(t) \leq C\|u_0\|_\infty + Ct^{1/2}\int_0^t (t-s)^{-1/2}s^{-1/2}z(s)\,\mathrm{d}s$$

where, the application of Lemma 3.2.13 with $\alpha = \beta = \gamma = 1/2$, implies inequality (3.2.73).

As a last estimate for the inequality (3.2.78), we apply the bounds (3.2.46), $\|\partial_v e^{tA}u_0\|_\infty \leq C\|\partial_v u_0\|_\infty$, in the first term on the r.h.s and (3.2.51), $\|\partial_v e^{tA}u_0\|_\infty \leq Ct^{-1/2}\|u_0\|_\infty$, in the second one, so that we obtain the following expression:

$$\|\partial_v e^{tL}u_0\|_\infty \leq C\|\partial_v u_0\|_\infty + C\int_0^t (t-s)^{-1/2}\|\partial_v e^{sL}u_0\|_\infty\,\mathrm{d}s,$$

which, proceeding as in the last case, through the same change of variable, and applying Lemma 3.2.13 as well, implies inequality (3.2.68).

Step 2. Bounds on u. Now that we have computed all the estimates for the derivative of the solution to the linear problem, we are able to control the second term of the Duhamel's formula given by equation (3.2.75). First we apply the norm L^∞ on it, getting to the following inequality:

$$\|e^{tL}u_0\|_\infty \leq \|e^{tA}u_0\|_\infty + C\int_0^t \|e^{(t-s)A}\left(\partial_v e^{sL}u_0\right)\|_\infty\,\mathrm{d}s, \tag{3.2.79}$$

where both terms in the r.h.s can be bounded by using the inequality (3.2.53), $\|e^{tA}u_0\|_\infty \leq Ct^{-1/4}\|u_0\|_2$, leading to the following expression:

$$\|e^{tL}u_0\|_\infty \leq Ct^{-1/4}\|u_0\|_2 + C\int_0^t (t-s)^{-1/4}\|\partial_v e^{sL}u_0\|_2\,\mathrm{d}s.$$

and then, given the impossibility of completing the estimate, by having inside the integral a different norm that the one in the l.h.s of the inequality, we need to control the integral term by applying the bound (3.2.71), $\|\partial_v e^{tL}u_0\|_2 \leq Ct^{-1/2}\|u_0\|_2$, so that we get:

$$\|e^{tL}u_0\|_\infty \leq Ct^{-1/4}\|u_0\|_2 + C\int_0^t (t-s)^{-1/4}s^{-1/2}\|u_0\|_2\,\mathrm{d}s = Ct^{-1/4}\|u_0\|_2,$$

where we solved the integral and we put the constants together, in order to proof the inequality (3.2.74).

Going backwards and starting again from inequality (3.2.79) the application of the estimate (3.2.48), $\|e^{tA}u_0\|_\infty \leq C\|u_0\|_\infty$, gives

$$\|e^{tL}u_0\|_\infty \leq C\|u_0\|_\infty + C\int_0^t \|\partial_v e^{sL}u_0\|_\infty\,\mathrm{d}s,$$

where, using the inequality (3.2.73), $\|\partial_v e^{tL}u_0\|_\infty \leq Ct^{-1/2}\|u_0\|_\infty$ and Lemma 3.2.13 with $\alpha = \beta = 0$ and $\gamma = 1/2$ proves the inequality (3.2.69).

To show the last estimate, let us take the L^2 norm in equation (3.2.75), getting to

$$\|e^{tL}u_0\|_2 \leq \|e^{tA}u_0\|_2 + C\int_0^t \|e^{(t-s)A}\left(\partial_v e^{sL}u_0\right)\|_2\,\mathrm{d}s.$$

First we use the inequality (3.2.49), $\|e^{tA}u_0\|_2 \leq C\|u_0\|_2$, in both terms of the r.h.s and then we apply the formula (3.2.71), $\|\partial_v e^{tL}u_0\|_2 \leq Ct^{-1/2}\|u_0\|_2$, to the term inside the integral, as it is shown below:

$$\begin{aligned}\|e^{tL}u_0\|_2 &\leq C\|u_0\|_2 + C\int_0^t \|\partial_v u(.,s)\|_2\,\mathrm{d}s \\ &\leq C\|u_0\|_2 + C\|u_0\|_2\int_0^t s^{-1/2}\,\mathrm{d}s \leq C\|u_0\|_2,\end{aligned}$$

thus proving inequality (3.2.70). □

Finally we give some Gaussian bounds for the complete linear equation:

Lemma 3.2.12 (L^2 Gaussian estimates for the full linear equation)**.** *Take $v_0 \in \mathbb{R}$ and let $\varphi(v) := \exp((v-v_0)^2/2)$. There exist $C > 0$ and $t_0 > 0$ depending only on N, v_0, V_R and V_F such that*

$$\|\partial_v e^{tL} u_0\|_{L^2(\varphi)} \leq C \|\partial_v u_0\|_{L^2(\varphi)} \qquad \text{for all } 0 \leq t \leq t_0. \tag{3.2.80}$$

and

$$\|\partial_v e^{tL} u_0\|_{L^2(\varphi)} \leq C t^{-1/2} \|u_0\|_{L^2(\varphi)} \qquad \text{for all } 0 < t \leq t_0, \tag{3.2.81}$$

both for any $u_0 \in X$.

Proof. As usual, call $u(\cdot,t) = e^{tL}u_0$. We prove the first estimate by taking the $L^2(\varphi)$ norm in (3.2.76), getting

$$\|\partial_v u(\cdot,t)\|_{L^2(\varphi)} \leq \|\partial_v u(\cdot,t)\|_{L^2(\varphi)} + C \int_0^t \|\partial_v e^{(t-s)A} \left(\partial_v u(\cdot,s)\right)\|_{L^2(\varphi)} \, \mathrm{d}s. \tag{3.2.82}$$

We use now (3.2.65) from Lemma 3.2.10 on the first term, and (3.2.66) on the term inside the integral:

$$\|\partial_v u(\cdot,t)\|_{L^2(\varphi)} \lesssim \|\partial_v u_0\|_{L^2(\varphi)} + \int_0^t (t-s)^{-\frac{1}{2}} \|\partial_v u(\cdot,s)\|_{L^2(\varphi)} \, \mathrm{d}s,$$

valid for t small enough. Lemma 3.2.83 applied to $z(t) = \|\partial_v u(\cdot,t)\|_{L^2(\varphi)}$, with $\beta = \frac{1}{2}$ and $\alpha = \gamma = 0$ immediately gives (3.2.80).

In order to get (3.2.81) we continue from (3.2.82) and use now (3.2.66) on both terms on the right hand side:

$$\|\partial_v u(\cdot,t)\|_{L^2(\varphi)} \lesssim t^{-\frac{1}{2}} \|u_0\|_{L^2(\varphi)} + \int_0^t (t-s)^{-\frac{1}{2}} \|\partial_v u(\cdot,s)\|_{L^2(\varphi)} \, \mathrm{d}s,$$

or equivalently, setting $z(t) := t^{\frac{1}{2}} \|\partial_v u(\cdot,t)\|_{L^2(\varphi)}$,

$$z(t) \lesssim \|u_0\|_{L^2(\varphi)} + t^{\frac{1}{2}} \int_0^t (t-s)^{-\frac{1}{2}} s^{-\frac{1}{2}} z(s) \, \mathrm{d}s,$$

again valid for small enough t. Lemma 3.2.83 with $\alpha = \beta = \gamma = \frac{1}{2}$ now proves the result. □

In the following lemma we prove the Gronwall-type inequality used in the previous results. The case with $\beta = 0$ can be deduced from the standard Gronwall's inequality, and the case $\alpha = \gamma$ can also be obtained as a consequence of the techniques in Section 3.3. However, since the focus of this result is the short-time behavior and the proof in that case is very straightforward, we prefer to give an independent proof now:

Lemma 3.2.13 (Short-time Gronwall-type inequality)**.** *Take $T > 0$ and $z \in L^\infty[0,T]$ which satisfies*

$$z(t) \le k + t^\alpha \int_0^t (t-s)^{-\beta}\, s^{-\gamma} z(s)\,\mathrm{d}s, \qquad \text{for all } t \in [0,T], \tag{3.2.83}$$

with k, α, β and γ constants such that $k > 0$; $\beta, \gamma \in [0,1)$ and $0 < \alpha - \beta - \gamma + 1$. Then there exist $t_0 \in (0,T]$ and $C > 0$ depending only on α, β and γ such that

$$z(t) < Ck \qquad \text{for all } t \in [0,t_0].$$

Proof. Let us define the function $y(t) := \max_{\tau\in[0,t]} z(\tau)$, for which equation (3.2.83) implies

$$y(t) \le k + y(t) t^\alpha \int_0^t (t-s)^{-\beta}\, s^{-\gamma}\,\mathrm{d}s = k + y(t) t^{\alpha-\beta-\gamma+1} C_{\beta,\gamma}$$

where $C_{\beta,\gamma} := B(1-\beta, 1-\gamma)$, the Beta function evaluated at $(1-\beta, 1-\gamma)$. Now, using that $\alpha - \beta - \gamma + 1 > 0$, we may take $t_0 \in (0,T]$ small enough so that $t_0^{\alpha-\beta-\gamma+1} C_{\beta,\gamma} < 1$. Then for any $t \in [0,t_0]$ we obtain $y(t) \le kC$ with $C := (1 - t_0^{\alpha-\beta-\gamma+1} C_{\beta,\gamma})^{-1}$. □

3.3 Asymptotics of Volterra-type equations

We devote this section to the following integral equation with unknown f:

$$f(t) = g(t) + \int_0^t f(s) h(t-s)\,\mathrm{d}s \qquad \text{for } t \ge 0. \tag{3.3.1}$$

Understanding this equation is essential to the proofs of some of the main results of this chapter, especially those in Sections 3.4 and 3.5. Equation (3.3.1) is a Volterra's convolution integral equation of the second kind, also known as the *renewal equation* in the context of delay differential equations [54, Chapter I].

3.3.1 Exact asymptotic behavior

The following result is a version of [54, Theorem 5.4], which we need to adapt since the technical assumptions on the functions g and h do not match our case. The strategy of the proof is however essentially the same. Our main result is the following:

Theorem 3.3.1. *Assume that $g, h\colon [0,+\infty) \to \mathbb{R}$ are given functions, with g being continuous and of bounded variation on compact subsets of $(0,+\infty)$, such that for some $\alpha \in \mathbb{R}$*

we have

$$h \in L^1([0,+\infty); e^{-\alpha t}) \cap L^p([0,+\infty); e^{-\alpha t}) \qquad \text{for some } p > 1, \tag{3.3.2}$$

$$t \mapsto g(t)e^{-\alpha t} \qquad \text{is bounded on } [0,+\infty). \tag{3.3.3}$$

Let f be the solution to equation (3.3.1), and consider the function

$$F(k) := \frac{\widehat{g}(k)}{1-\widehat{h}(k)} \qquad \text{for } \Re(k) \geq \alpha,$$

which is a meromorphic function on the set of k with $\Re(k) > \alpha$. Then:

1. *If F has no poles on the set $\{k \in \mathbb{C} \mid \Re(k) > \alpha\}$, then for every $\beta > \alpha$ there is a constant $C_\beta > 0$ (depending on g, h and β) such that*

$$|f(t)| \leq C_\beta e^{\beta t} \qquad \text{for all } t \geq 1.$$

2. *If F has some pole of order N on the set $R_\alpha := \{k \in \mathbb{C} \mid \Re(k) > \alpha\}$, then there is a polynomial $p = p(t)$ of degree $N-1$ such that*

$$f(t) \sim p(t)e^{\beta t} \qquad \text{as } t \to +\infty,$$

   where β is the largest real part of the poles of F on R_α.

In addition, the constant C_β and the coefficients $a_1, \ldots, a_N$ of p can be chosen so that

$$\max\{|a_1|, \ldots, |a_N|\} \leq C_h \sup_{t\geq 0} |g(t)|e^{-\alpha t}, \qquad C_\beta \leq C_{h,\beta} \sup_{t\geq 0} |g(t)|e^{-\alpha t},$$

where C_h is a constant which depends only on h, and $C_{h,\beta}$ depends only on h and β.

Proof. For $\Re(k)$ large enough (let us say for $\Re(k) \geq \gamma > \alpha$) we may take the Laplace transform of (3.3.1) and obtain

$$\widehat{f}(k) = \frac{\widehat{g}(k)}{1-\widehat{h}(k)} \qquad \text{for } \Re(k) \geq \gamma.$$

Notice that we know $\widehat{f}(k) = F(k)$ for $\Re(k) \geq \gamma$, but we cannot say that $\widehat{f}(k)$ even makes sense for a general k with $\Re(k) \geq \alpha$.

Take $R > 0$ large enough and let us define the positively oriented curve

$$\Gamma := [\gamma - iR, \gamma + iR] \cup [\gamma + iR, \alpha + iR] \cup [\alpha + iR, \alpha - iR] \cup [\alpha - iR, \gamma - iR].$$

The function F is analytic on its domain, so we may use Cauchy's integral theorem on the

curve Γ to obtain that, for any $t > 0$,

$$2\pi i \sum \operatorname{Res}(F(k)e^{kt}, z_n) = \int_\Gamma e^{kt}F(k)\,\mathrm{d}k = \int_{\gamma-iR}^{\gamma+iR} e^{kt}F(k)\,\mathrm{d}k - e^{iRt}\int_\alpha^\gamma e^{st}F(s+iR)\,\mathrm{d}s$$
$$- \int_{\alpha-iR}^{\alpha+iR} e^{kt}F(k)\,\mathrm{d}k + e^{-iRt}\int_\alpha^\gamma e^{st}F(s-iR)\,\mathrm{d}s =: I_1 + I_2 + I_3 + I_4, \quad (3.3.4)$$

where the residue sum is over all zeros of F inside the curve Γ. From equation (3.3.1) one can see that f must be continuous and of bounded variation on compact subsets of $[0, +\infty)$ (since h is locally integrable and g is continuous and locally of bounded variation). Hence we can apply the inversion theorem for the Laplace transform (Lemma 3.3.2) to get

$$\lim_{R\to+\infty} I_1 = 2\pi i f(t). \quad (3.3.5)$$

On the other hand, Riemann-Lebesgue's lemma shows that

$$\lim_{R\to+\infty} \widehat{g}(s+iR) = \sqrt{2\pi} \lim_{R\to+\infty} \mathscr{F}_t(e^{-st}g(t))(R) = 0,$$

uniformly for $s \in [\alpha, \gamma]$ (one can see that the arguments in the standard proof of the Riemann-Lebesgue lemma can be made uniformly for $s \in [\alpha, \gamma]$). For a similar reason we have

$$\lim_{R\to+\infty} \widehat{h}(s+iR) = 0$$

uniformly for $s \in [\alpha, \gamma]$. This shows that

$$\lim_{R\to+\infty} F(s+iR) = \lim_{R\to+\infty} \frac{\widehat{g}(s+iR)}{1-\widehat{h}(s+iR)} = 0$$

uniformly for $s \in [\alpha, \gamma]$, and hence that

$$\lim_{R\to+\infty} I_2 = 0. \quad (3.3.6)$$

By symmetric arguments applied to $s - iR$,

$$\lim_{R\to+\infty} I_4 = 0. \quad (3.3.7)$$

Finally, for the third integral we have (see Lemma 3.3.4)

$$\left|\lim_{R\to+\infty} I_3\right| = e^{\alpha t}\left|\lim_{R\to+\infty}\int_{-R}^{R} e^{i\xi t}F(\alpha+i\xi)\,\mathrm{d}\xi\right| \le Ce^{\alpha t}. \quad (3.3.8)$$

Regarding the residue of F around z_n, Lemma 3.3.3 shows that for some nontrivial poly-

nomial p_n,

$$\operatorname*{Res}_{k=z_n}(F(k)e^{kt}) = p_n(t)e^{z_n t}. \tag{3.3.9}$$

Using (3.3.5), (3.3.6), (3.3.7), (3.3.8) and (3.3.9) in (3.3.4) and passing to the limit as $R \to +\infty$ shows the result. □

The following result is a version of the Fourier inversion theorem taken from [56, Theorem 24.4]:

Lemma 3.3.2 (Inverse Laplace transform)**.** *Let $f\colon [0,+\infty) \to \mathbb{R}$ and $\alpha \in \mathbb{R}$ be such that $t \mapsto f(t)e^{-\alpha t}$ is absolutely integrable. Let $t > 0$ be a point where f has bounded variation in some neighbourhood of t. Then for every $\beta \geq \alpha$ we have*

$$\lim_{R\to+\infty} \frac{1}{2\pi i} \int_{\beta-iR}^{\beta+iR} e^{kt}\widehat{f}(k)\,\mathrm{d}k = \frac{1}{2}(f(t_+) + f(t-)),$$

where the integral is understood as a complex integral along the straight line with real part R.

Of course, if additionally f is continuous at t, then

$$\lim_{R\to+\infty} \frac{1}{2\pi i} \int_{\beta-iR}^{\beta+iR} e^{kt}\widehat{f}(k)\,\mathrm{d}k = f(t).$$

The following lemma gives the result of calculating the residue of the complex function F from the proof of Theorem 3.3.1 at a given pole. It is essentially the same as Lemma 5.1 in [54]:

Lemma 3.3.3 (Residue close to a pole)**.** *Under the assumptions of Theorem 3.3.1, define*

$$F(k) := \frac{\widehat{g}(k)}{1-\widehat{h}(k)} \qquad \text{for } \Re(k) \geq \alpha.$$

We notice F is analytic on $R_\alpha := \{w \in \mathbb{C} \mid \Re(w) > \alpha\}$, except for possibly a set of isolated poles. Let $z \in \mathbb{C}$ be a pole of F with $\Re(z) > \alpha$. There exists a nontrivial polynomial $p = p(t)$ of degree $N-1$ such that

$$\operatorname*{Res}_{k=z}(e^{kt}F(k)) = p(t)e^{zt}$$

for any $t \in \mathbb{R}$. All coefficients $a_1, \ldots, a_N$ of p can be bounded by

$$|a_n| \leq C \sup_{t\geq 0} |g(t)|e^{-\alpha t} \qquad \text{for } n = 1, \ldots, N,$$

for some constant C which depends only on h.

Proof. The residue at $k = z$ is equal to $2\pi i$ times the coefficient of the power -1 in the Laurent expansion of $e^{kt}F(k)$ around $k = z$. Expanding both $F(k)$ and e^{kt} close to $k = z$ we have

$$F(k) = \sum_{n=-N}^{\infty} a_n(k-z)^n, \qquad e^{kt} = e^{zt}e^{(k-z)t} = e^{zt}\sum_{n=0}^{\infty}\frac{t^n}{n!}(k-z)^n,$$

with $a_{-N} \neq 0$. Multiplying out these series we obtain that the coefficient of the power -1 in the Laurent expansion of $e^{kt}F(k)$ is

$$\frac{1}{2\pi i}p(t) := \sum_{j=0}^{N-1} a_{-j-1}\frac{t^j}{j!}.$$

We see that p is of degree $N-1$, since the coefficient a_{-N} is nonzero. Its coefficients can easily be bounded in the following way: choose a closed circle γ of radius $r > 0$, centered on z, and which does not enclose any other zero of $1 - \widehat{h}$. We may also choose γ such that it is contained in $\{w \in \mathbb{C} \mid \Re(w) \geq \beta\}$ for some $\beta > \alpha$. Then for $n = 1, \ldots, N$

$$\begin{aligned}|a_n| = \frac{1}{2\pi}\left|\int_\gamma \frac{F(w)}{(w-z)^{n+1}}\,\mathrm{d}w\right| &\leq \frac{1}{2\pi}r^{n+1}\int_\gamma |F(w)|\,\mathrm{d}w \\ &\leq \frac{1}{2\pi}r^{n+1}C_h\int_\gamma |\widehat{g}(w)|\,\mathrm{d}w \leq r^{n+2}C_h\int_0^\infty g(t)e^{-\beta t}\,\mathrm{d}t.\end{aligned}$$

We notice that $C_h := \inf_\gamma |1-\widehat{h}|$ only depends on h, and the choice of r and β also depends on h only. This easily gives the bound in the statement. □

Lemma 3.3.4. *Assume that $g, h\colon [0,+\infty) \to \mathbb{R}$ are given functions, with g being of bounded variation on compact subsets of $(0,+\infty)$, such that for some $\alpha_0 \in \mathbb{R}$ we have*

$$h \in L^1([0,+\infty); e^{-\alpha_0 t}) \cap L^p([0,+\infty); e^{-\alpha_0 t}) \qquad \text{for some } p > 1, \tag{3.3.10}$$

$$t \mapsto |g(t)|e^{-\alpha_0 t} \qquad \text{is bounded on } [0,+\infty). \tag{3.3.11}$$

Take any $\alpha > \alpha_0$, and assume there are no zeros of the function $1 - \widehat{h}(k)$ on the line with $\Re(k) = \alpha$. Then the function

$$F(k) := \frac{\widehat{g}(k)}{1-\widehat{h}(k)}$$

satisfies that there exists $C > 0$ such that

$$\left|\lim_{R\to+\infty}\int_{-R}^{R} e^{i\xi t}F(\alpha+i\xi)\,\mathrm{d}\xi\right| \leq C \qquad \text{for all } t > 0. \tag{3.3.12}$$

In addition, the constant C can be chosen as $C = C_h \sup_{t\geq 0}|g(t)|e^{-\alpha_0 t}$, where C_h depends only on h.

The difficulty in proving the above statement is that in general we do not know that $F(k)$ is absolutely integrable on the line with $\Re(k) = \alpha$; otherwise, we would bound the above integral by the integral of $|F(k)|$ over that line, ignoring $e^{i\xi t}$. Similarly, we do not know whether F on the line with $\Re(k) = \alpha$ is the Laplace transform of any function f; otherwise, we would use the inversion lemma 3.3.2 to say that the limit must be $e^{-\alpha t} f(t)$, and we would just need to check whether the latter is a bounded function. Instead, what we can do is write F as a sum of F_1 and F_2, where F_1 is absolutely integrable on the line and F_2 is the Laplace transform of a known function. That is the main idea of the following proof:

Proof of Lemma 3.3.4. We first observe that for any $\xi \in \mathbb{R}$,

$$\widehat{h}(\alpha + i\xi) = \sqrt{2\pi}\mathscr{F}_t(e^{-\alpha t}h(t))(\xi),$$

so by the Riemann-Lebesgue lemma we have $\widehat{h}(\alpha + i\xi) \to 0$ as $|\xi| \to +\infty$. Since $\xi \mapsto \widehat{h}(\alpha + i\xi)$ is continuous and $1 - \widehat{h}(\alpha + i\xi)$ has no zeros for $\xi \in \mathbb{R}$, it is clear that for some $C_2 > 0$,

$$\frac{1}{|1 - \widehat{h}(\alpha + i\xi)|} \leq C_2 \qquad \text{for all } \xi \in \mathbb{R}, \tag{3.3.13}$$

Choosing an integer $N \geq 1$ we can rewrite

$$F = \frac{\widehat{h}^N \widehat{g}}{1 - \widehat{h}} + \widehat{g} \sum_{n=0}^{N-1} \widehat{h}^n = F_1 + F_2.$$

The second term F_2 is the Laplace transform of $f_2 := g + g * (\sum_{n=1}^{N-1} h^{*n})$. Lemma 3.3.2 then shows that

$$\lim_{R \to +\infty} \frac{1}{2\pi i} \int_{\beta - iR}^{\beta + iR} e^{kt} F_2(k)\, \mathrm{d}k = \frac{1}{2}(f_2(t_+) + f_2(t_-)) \qquad \text{for all } t \geq 0.$$

Notice that Lemma 3.3.2 is applicable because f_2 is of bounded variation on compact sets (which can be seen from (3.3.10) and (3.3.11)). Hence for all $t > 0$ we have

$$\left| \lim_{R \to +\infty} \int_{-R}^{R} e^{i\xi t} F_2(\alpha + i\xi)\, \mathrm{d}\xi \right| = \pi e^{-\alpha t}(|f_2(t_+)| + |f_2(t_+)|) \leq C_3, \tag{3.3.14}$$

for some $C > 0$. (We notice that $t \mapsto |f_2(t)|e^{-\alpha t}$ is bounded for all $t > 0$ due to (3.3.10) and (3.3.11), so the same is true if we write t_+ or t_- instead of t.) Now for the term F_1, we use (3.3.13) to write

$$\begin{aligned}\int_{-\infty}^{+\infty} |F_1(\alpha+i\xi)|\,\mathrm{d}\xi &\le C_2 \int_{-\infty}^{+\infty} |\widehat{h}(\alpha+i\xi)|^N |\widehat{g}(\alpha+i\xi)|\,\mathrm{d}\xi \\ &= 2\pi C_2 \int_{-\infty}^{+\infty} \mathscr{F}_t(e^{-\alpha t}h)(\xi)^N \mathscr{F}_t(e^{-\alpha t}g)(\xi)\,\mathrm{d}\xi \\ &\le C_2 \|\mathscr{F}_t(e^{-\alpha t}h)\|_{2N}^N \|\mathscr{F}_t(e^{-\alpha t}g)\|_2 \le C_2 \|e^{-\alpha t}h\|_p^N \|e^{-\alpha t}g\|_2,\end{aligned}$$

where we have used the Hausdorff-Young inequality and p is such that $\frac{1}{p} + \frac{1}{2N} = 1$. Now, $\|g\|_2$ is finite, and we may choose N large enough to make p small enough so that $\|e^{-\alpha t}h\|_p$ is finite (by hypothesis). So we see that

$$\left| \int_{-R}^{R} e^{i\xi t} F_1(\alpha+i\xi)\,\mathrm{d}\xi \right| \le C_4$$

for all $t \ge 0$, and also that this integral has a limit as $R \to +\infty$, for all $t \ge 0$. From this and (3.3.14) we see that

$$\lim_{R\to+\infty} \left| \int_{-R}^{R} e^{i\xi t} F(\alpha+i\xi)\,\mathrm{d}\xi \right| \le C := \max\{C_3, C_4\},$$

for all $t > 0$. This shows the result. One may also check that all constants which appear above are consistent with the form $C = C_h \sup_{t\ge 0} |g(t)| e^{-\alpha_0 t}$ given in the statement. □

3.3.2 Comparison results and special cases

We also have a comparison result for solutions to inequalities of this type.

Lemma 3.3.5 (Comparison result)**.** *Take $T \in (0, +\infty]$ and let $g\colon [0,T) \to \mathbb{R}$ and $h\colon [0,T) \to [0,+\infty)$ be locally integrable functions. If $f_1, f_2\colon [0,T) \to \mathbb{R}$ are locally bounded functions (i.e., L^∞ on compact intervals) such that*

$$\begin{aligned} f_2(t) &\ge g(t) + \int_0^t f_2(s)h(t-s)\,\mathrm{d}s \qquad \text{for } t \in [0,T), \\ f_1(t) &\le g(t) + \int_0^t f_1(s)h(t-s)\,\mathrm{d}s \qquad \text{for } t \in [0,T), \end{aligned}$$

then

$$f_1(t) \le f_2(t) \qquad \text{for } t \in [0,T).$$

Proof. Choose $t_0 < T$ such that

$$\delta := \int_0^{t_0} h(s)\,\mathrm{d}s < 1.$$

The function $w(t) := f_1(t) - f_2(t)$ satisfies

$$w(t) \leq \int_0^t w(s)h(t-s)\,\mathrm{d}s.$$

Our aim is to show that $w(t) \leq 0$ for all $t \in [0,T)$. Taking the essential supremum on $[0,t_0]$ and calling $M := \operatorname{ess\,sup}_{t\in[0,t_0]} w(t)$ gives

$$M \leq M \int_0^{t_0} h(t-s)\,\mathrm{d}s = M\delta,$$

which implies $M \leq 0$ and hence $w(t) \leq 0$ for almost all $t \in [0,t_0]$. But then the inequality is also true for all $t \in [0,t_0]$ since

$$w(t) \leq \int_0^t w(s)h(t-s)\,\mathrm{d}s \leq 0 \qquad \text{for all } t \in [0,t_0].$$

One can then repeat the same argument for the function $w_{t_0}\colon [0,T-t_0) \to \mathbb{R}$ defined by $w_{t_0}(t) := w(t+t_0)$, which satisfies

$$\begin{aligned} w_{t_0}(t) &\leq \int_0^{t_0} w(s)h(t+t_0-s)\,\mathrm{d}s + \int_{t_0}^{t+t_0} w(s)h(t+t_0-s)\,\mathrm{d}s \\ &\leq \int_0^t w_{t_0}(s)h(t-s)\,\mathrm{d}s. \end{aligned}$$

With this we obtain that $w(t) \leq 0$ for $t \in [0,2t_0) \cap [0,T)$. Iterating this argument we obtain the result. □

Lemma 3.3.6 (Comparison result with delay)**.** *Take $d > 0$, $T \in (0,+\infty]$ and let $g\colon [-d,T) \to \mathbb{R}$ and $h\colon [-d,T) \to [0,+\infty)$ be locally integrable functions. If $f_1, f_2\colon [-d,T) \to \mathbb{R}$ are locally bounded functions (i.e., L^∞ on compact intervals) such that*

$$f_1(t) \leq f_2(t) \qquad \textit{for } t \in [-d,0]$$

and

$$\begin{aligned} f_2(t) &\geq g(t) + \int_0^t f_2(s-d)h(t-s)\,\mathrm{d}s \qquad \textit{for } t \in [0,T), \\ f_1(t) &\leq g(t) + \int_0^t f_1(s-d)h(t-s)\,\mathrm{d}s \qquad \textit{for } t \in [0,T), \end{aligned}$$

then

$$f_1(t) \leq f_2(t) \qquad \textit{for } t \in [-d,T).$$

Proof. The proof is easier in this case and can be done by induction: we show that $f_1(t) \leq f_2(t)$ for $t \in [-d, nd] \cap [0, T)$, for all integers $n \geq 0$. The case $n = 0$ holds by assumption, and if the case n holds then for $t \in [nd, (n+1)d] \cap [0, T)$ we have

$$f_1(t) \leq g(t) + \int_0^t f_1(s-d)h(t-s)\,\mathrm{d}s \leq g(t) + \int_0^t f_2(s-d)h(t-s)\,\mathrm{d}s \leq f_2(t),$$

where the intermediate inequality holds because $s - d$ is always in $[-d, nd]$, where the inequality is already assumed to hold. □

As a consequence we obtain a "modified Gronwall's inequality" which is needed below. It can also be deduced as a consequence of Theorem 3.3.1, but we give a direct proof since it is easier in this case:

Lemma 3.3.7 (Convolution Gronwall inequality)**.** *Let $0 < \alpha < 1$ and $0 < T \leq \infty$. If $f\colon [0, T) \to [0, \infty)$ is a locally bounded function which satisfies*

$$f(t) \leq A + B \int_0^t (t-s)^{-\alpha} f(s)\,\mathrm{d}s \qquad \text{for all } t \in [0, T), \tag{3.3.15}$$

for some constants $A, B > 0$, then there exists $\mu = \mu(\alpha) > 0$ such that

$$f(t) \leq 2A \exp\left(B^{\frac{1}{1-\alpha}} \mu t\right) \qquad \text{for all } t \in [0, T).$$

Proof. We first notice that it is enough to prove the result for $A = B = 1$. Then the general case can be obtained by noticing that if f satisfies (3.3.15) then the function $g(t) := \frac{1}{A} f(\beta t)$ satisfies the same inequality with $A = B = 1$ if we choose $\beta := B^{-\frac{1}{1-\alpha}}$.

In order to prove the result when $A = B = 1$, let us find C and μ such that $F(t) := Ce^{\mu t}$ is a supersolution of the corresponding Volterra's equation; that is, such that

$$F(t) \geq 1 + \int_0^t (t-s)^{-\alpha} F(s)\,\mathrm{d}s \qquad \text{for all } t \in [0, \infty). \tag{3.3.16}$$

This is not hard, since

$$\begin{aligned}\int_0^t (t-s)^{-\alpha} F(s)\,\mathrm{d}s &= C \int_0^t (t-s)^{-\alpha} e^{\mu s}\,\mathrm{d}s \\ &= Ce^{\mu t} \int_0^t (t-s)^{-\alpha} e^{-\mu(t-s)}\,\mathrm{d}s \leq Ce^{\mu t} \mu^{\alpha-1} \Gamma(1-\alpha) =: K_{\alpha,\mu} F(t),\end{aligned}$$

where $K_{\alpha,\mu} := \mu^{\alpha-1}\Gamma(1-\alpha)$. Hence

$$1 + \int_0^t (t-s)^{-\alpha} F(s)\,\mathrm{d}s \leq \frac{1}{C} F(t) + K_{\alpha,\mu} F(t) = \left(\frac{1}{C} + K_{\alpha,\mu}\right) F(t).$$

So equation (3.3.16) holds if $\frac{1}{C} + K_{\alpha,\mu} \leq 1$. It is enough to take $C = 2$ and

$$K_{\alpha,\mu} = \mu^{\alpha-1}\Gamma(1-\alpha) = \frac{1}{2}, \qquad \text{that is,} \qquad \mu := (2\Gamma(1-\alpha))^{\frac{1}{1-\alpha}}.$$

For this choice of C and μ, the function $F(t)$ is a supersolution of the Volterra's equation in the statement, and then Lemma 3.3.5 shows that $f(t) \leq F(t)$ on $[0,T)$. □

Lemma 3.3.8 (Convolution Gronwall's inequality with delay)**.** *Let $d \geq 0$, $0 < \alpha < 1$ and $0 < T \leq \infty$. If $f\colon [-d,T) \to [0,\infty)$ is a locally bounded function which satisfies*

$$f(t) \leq A + B\int_0^t (t-s)^{-\alpha} f(s-d)\,\mathrm{d}s \qquad \text{for all } t \in [0,T), \tag{3.3.17}$$

for some constants $A, B > 0$, then

$$f(t) \leq (2A + M_0)\, e^{\mu t} \qquad \text{for all } t \in [0,T),$$

where μ is any positive number satisfying

$$Be^{-\mu d}\mu^{\alpha-1} \leq \frac{1}{2\Gamma(1-\alpha)}$$

and

$$M_0 := \sup_{t\in[-d,0]} f(t).$$

Proof. Let us find C and μ such that $F(t) := Ce^{\mu t}$ is a supersolution of the corresponding Volterra's equation; that is, such that $F(t) \geq f(t)$ for $t \in [-d,0]$ and

$$F(t) \geq A + B\int_0^t (t-s)^{-\alpha} F(s-d)\,\mathrm{d}s \qquad \text{for all } t \in [0,\infty). \tag{3.3.18}$$

The condition $F(t) \geq f(t)$ for $t \in [-d,0]$ is satisfied if we take $C \geq \sup_{t\in[-d,0]} f(t) =: M_0$. And the second condition can also be satisfied, since

$$\begin{aligned}\int_0^t (t-s)^{-\alpha} F(s-d)\,\mathrm{d}s &= Ce^{-\mu d}\int_0^t (t-s)^{-\alpha} e^{\mu s}\,\mathrm{d}s \\ &= Ce^{-\mu d}e^{\mu t}\int_0^t (t-s)^{-\alpha} e^{-\mu(t-s)}\,\mathrm{d}s \leq Ce^{-\mu d}e^{\mu t}\mu^{\alpha-1}\Gamma(1-\alpha) =: K_{\alpha,\mu}F(t),\end{aligned}$$

where $K_{\alpha,\mu} := e^{-\mu d}\mu^{\alpha-1}\Gamma(1-\alpha)$. Hence for $t \geq 0$,

$$A + B\int_0^t (t-s)^{-\alpha} F(s-d)\,\mathrm{d}s \leq \frac{A}{C}F(t) + BK_{\alpha,\mu}F(t) = (\frac{A}{C} + BK_{\alpha,\mu})F(t).$$

So equation (3.3.18) holds if $\frac{A}{C} + BK_{\alpha,\mu} \leq 1$. It is enough to take $C \geq 2A$ and $\mu > 0$ such that

$$BK_{\alpha,\mu} = Be^{-\mu d}\mu^{\alpha-1}\Gamma(1-\alpha) \leq \frac{1}{2},$$

Hence for this choice of μ and with $C := \max\{2A, M_0\}$, the function $F(t)$ is a supersolution of the Volterra's equation in the statement, and then Lemma 3.3.5 shows that $f(t) \leq F(t)$ on $[0, T)$. □

3.4 Behavior of the nonlinear equation

In this section we consider the solution of the Cauchy problem associated with (3.1.1) with delay $d \geq 0$, whose related stationary problem is given by (3.1.2), with solution (3.1.3). We assume in this section that $|b|$ is small enough for the solution to this stationary problem to be unique.

3.4.1 Weakly excitatory case

Theorem 3.4.1 (Long-time behavior for weakly coupled systems)**.** *Consider $b \in \mathbb{R}$ with $|b|$ small enough for the equilibrium p_∞ of (3.1.1) to be unique, $V_R < V_F$, $d \geq 0$, a nonnegative initial data $p_0 \in \mathcal{C}([-d, 0], X)$, and p the corresponding solution to the nonlinear system (3.1.1). Let $K > 0$ and assume that the initial data p_0 satisfies*

$$K_0 := \sup_{t\in[-d,0]} \|p_0(\cdot, t) - p_\infty\|_X \leq K,$$

where p_∞ is the (unique) probability stationary solution of the nonlinear system (3.1.1). There exist $C \geq 1$ depending only on V_R and V_F and $b_0 > 0$ depending on V_R, V_F and K such that if $|b| < b_0$ then

$$\|p(., t) - p_\infty\|_X \leq Ce^{-\frac{\lambda}{2+d}t}\|p_0(\cdot, 0) - p_\infty\|_X \qquad \text{for all } t \geq 0. \tag{3.4.1}$$

We emphasize that b_0 is independent of d.

Proof. We consider $u(v, t) := p(v, t) - p_\infty(v)$ with $N_u(t) := N_p(t) - N_{p_\infty}$. From (3.1.1) we see that u satisfies

$$\partial_t u = \partial_v^2 u + \partial_v(vu) + N_u(t)\delta_{V_R} - bN_{p_\infty}\partial_v u - bN_u(t-d)\partial_v p =: Lu - bN_u(t-d)\partial_v p.$$

By Duhamel's formula we get the following expression for $u(v, t)$:

$$u(v, t) = e^{tL}u_0(v) - b\int_0^t N_u(s-d)e^{(t-s)L}\partial_v p(v, s)\,\mathrm{d}s, \tag{3.4.2}$$

where e^{tL} refers to the semigroup of the linear problem described in Section 3.2, and we denote $u_0(v) := u(v,0) = p_0(v,0) - p_\infty(v)$. We can apply the norm $\|.\|_X$ to find

$$\|u(.,t)\|_X \leq \|e^{tL}u_0\|_X + |b| \int_0^t |N_u(s-d)| \|e^{(t-s)L}\partial_v p(.,s)\|_X \, \mathrm{d}s.$$

We can apply (3.2.8) to the first term, and the spectral gap / regularization result (3.2.9) to the norm inside the integral, which leads to

$$\|u(.,t)\|_X \leq Ce^{-\lambda t}\|u_0\|_X + C|b| \int_0^t e^{-\lambda(t-s)}(t-s)^{-3/4}|N_u(s-d)| \|\partial_v p(.,s)\|_2 \, \mathrm{d}s.$$

Considering that, for any t, $|N_u(t)| \leq \|\partial_v u(.,t)\|_\infty \leq \|u(.,t)\|_X$ and $\|\partial_v p(.,t)\|_2 \leq \|p(.,t)\|_X \leq \|u(.,t)\|_X + \|p_\infty\|_X$, from our previous estimate for $\|u(.,t)\|_X$ we obtain

$$\|u(.,t)\|_X \leq Ce^{-\lambda t}\|u_0\|_X + C|b| \int_0^t e^{-\lambda(t-s)}(t-s)^{-3/4}\|u(.,s-d)\|_X \left(\|u(.,s)\|_X + \bar{C}\right) \, \mathrm{d}s,$$

where $\bar{C} := \|p_\infty\|_X$. Let us now take $K_1 := (4C+1)K_0$ and define

$$T := \sup\{t \geq 0 \mid \|u(\cdot,s)\|_X \leq K_1 \text{ for } s \in [0,t]\}.$$

This T must be strictly positive, and it may be $+\infty$; we will show later that with an appropriate choice of b it must be $+\infty$. Calling $C_b := C|b|\left(K_1 + \bar{C}\right)$, we get to

$$\|u(.,t)\|_X \leq Ce^{-\lambda t}\|u_0\|_X + C_b \int_0^t e^{-\lambda(t-s)}(t-s)^{-3/4}\|u(.,s-d)\|_X \, \mathrm{d}s,$$

for all $0 \leq t < T$. We can now define $f(t) := e^{\lambda t}\|u(.,t)\|_X$ in order to simplify previous expression, which becomes

$$f(t) \leq Cf(0) + C_b e^{\lambda d} \int_0^t (t-s)^{-3/4} f(s-d) \, \mathrm{d}s.$$

By our modified Gronwall's Lemma 3.3.8 with $A = Cf(0)$, $B = C_b e^{\lambda d}$, $M_0 = \sup_{t\in[-d,0]} f(t)$ and $\alpha = 3/4$, we find the following bound for $f(t)$:

$$f(t) \leq (2Cf(0) + M_0)\exp(\mu t) \qquad \text{for all } 0 \leq t < T,$$

for any $\mu > 0$ satisfying

$$C_2|b|e^{\lambda d}e^{-\mu d}\mu^{\alpha-1} \leq \frac{1}{2\Gamma(1-\alpha)}, \tag{3.4.3}$$

with $C_2 := C(K_1 + \bar{C})$. Notice that $\sup_{t\in[-d,0]} f(t) = \sup_{t\in[-d,0]} e^{\lambda t}\|u(\cdot,t)\|_X \leq K_0$, and

also $f(0) \leq K_0$. In terms of $\|u(.,t)\|_X$ this implies

$$\|u(.,t)\|_X \leq (2C+1)K_0 \exp(-(\lambda-\mu)t) \qquad \text{for all } 0 \leq t < T,$$

Whenever $\mu < \lambda$, this shows in particular that $\|u(.,t)\|_X \leq (2C+1)K_0$ on $[0,T)$, which in fact shows that T cannot be finite (otherwise, there would be a slightly larger T' for which $\|u(.,t)\|_X \leq (4C+1)K_0$ on $[0,T']$, contradicting the definition of T).

Now it only remains to show that for $|b|$ small enough one can choose μ so that $\mu < \lambda$ for all $d \geq 0$. First, notice that for $\mu := \lambda - \frac{\lambda}{d}$ equation (3.4.3) reads

$$C_2|b|e^{\lambda}\left(\lambda - \frac{\lambda}{d}\right)^{\alpha-1} \leq \frac{1}{2\Gamma(1-\alpha)},$$

which is valid for $|b|$ small enough (depending also on K) and all $d \geq 2$. For all $0 \leq d \leq 2$ it is clear that we can also choose $|b|$ small enough, independent of $d \in [0,2]$, for which (3.4.3) holds with $\mu := \lambda/2$. Hence the statement is proved. □

3.4.2 Linearized stability implies nonlinear stability

Given an equilibrium of the nonlinear equation, the linearized equation close to p_∞ is given by

$$\partial_t u = \partial_v\left[(v - bN_\infty)u\right] + \partial_v^2 u + \delta_{V_R} N_u(t) - bN_u(t-d)\partial_v p_\infty(v).$$

The link between this and the solution of the nonlinear system is that we expect $p \approx u + p_\infty$ as long as the solution p is close to the equilibrium p_∞. When there is no delay ($d = 0$) we denote by T the operator on the right hand side of the previous equation:

$$Tu := \partial_v\left[(v - bN_\infty)u\right] + \partial_v^2 u + \delta_{V_R} N_u(t) - bN_u(t)\partial_v p_\infty(v). \tag{3.4.4}$$

We will assume that the PDE $\partial_t u = Tu$, with boundary condition $u(V_F,t) = 0$ and an initial condition $u_0 \in X$ is well posed, and we denote the associated solution by $e^{tT}u_0$. As far as we know there are no previous results on this, and we realize that this is a gap that needs to be filled in order to make the theory fully rigorous. However, assuming a solution exists which satisfies the usual Duhamel's formula, it is easy to give *a priori* estimates which could then be used to give a full proof of existence of solutions. We will not develop this existence theory in this chapter since it would add a long technical part, but we will show two straightforward a priori estimates. Call $u(t,\cdot) = e^{tT}u_0$. Since $Tu = Lu - bN_u\partial_v p_\infty$, and assuming we may apply Duhamel's formula, we have

$$u(\cdot,t) = e^{tL}u_0 + \int_0^t N_u(s)e^{(t-s)L}(\partial_v p_\infty)\,\mathrm{d}s. \tag{3.4.5}$$

Taking the $\|\cdot\|_X$ norm and using equations (3.2.8) and (3.2.9) from Proposition 3.2.3 gives

$$\begin{aligned}\|u(\cdot,t)\|_X &\leq \|e^{tL}u_0\|_X + |b|\int_0^t |N_u(s)|\|e^{(t-s)L}(\partial_v p_\infty)\|_X \,\mathrm{d}s \\ &\lesssim e^{-\lambda t}\|u_0\|_X + |b|\|\partial_v p_\infty\|_{L^2(\varphi)}\int_0^t \|u(\cdot,s)\|_X (t-s)^{-\frac{3}{4}} e^{-\lambda(t-s)}\,\mathrm{d}s,\end{aligned}$$

valid for all $t \geq 0$. Calling $z(t) := e^{\lambda t}\|u(\cdot,t)\|_X$ we have

$$z(t) \lesssim \|u_0\|_X + \int_0^t z(s)(t-s)^{-\frac{3}{4}}\,\mathrm{d}s.$$

Lemma 3.2.13 now shows that there exists $C > 0$ and $t_0 > 0$ such that

$$\|u(\cdot,t)\|_X \leq C\|u_0\|_X \qquad \text{for all } 0 \leq t \leq t_0.$$

This is an apriori estimate on the well-posedness of the linearized equation. Similarly, we can obtain a regularization estimate: taking again the $\|\cdot\|_X$ norm in (3.4.5) and using now Lemma 3.2.2 we have

$$\begin{aligned}\|u(\cdot,t)\|_X &\lesssim t^{-\frac{3}{4}}\|u_0\|_{L^2(\varphi)} + |b|\|\partial_v p_\infty\|_{L^2(\varphi)}\int_0^t \|u(\cdot,s)\|_X (t-s)^{-\frac{3}{4}} e^{-\lambda(t-s)}\,\mathrm{d}s \\ &\lesssim t^{-\frac{3}{4}}\|u_0\|_{L^2(\varphi)} + \int_0^t \|u(\cdot,s)\|_X (t-s)^{-\frac{3}{4}}\,\mathrm{d}s.\end{aligned}$$

Lemma 3.2.13 now shows that there exist $C > 0$ and $t_0 > 0$ such that

$$\|u(\cdot,t)\|_X \leq Ct^{-\frac{3}{4}}\|u_0\|_{L^2(\varphi)} \qquad \text{for all } 0 \leq t \leq t_0. \tag{3.4.6}$$

This regularization estimate will be needed for the proof of the next result.

Theorem 3.4.2 (Linearized stability implies nonlinear stability)**.** *Let us consider $b \in \mathbb{R}$, $V_R < V_F \in \mathbb{R}$, a nonnegative initial condition $p_0 \in X$ and p the corresponding solution to the nonlinear system (3.1.1). Let p_∞ be an equilibrium of the nonlinear system. Assume that the flow $(e^{tT})_{t\geq 0}$ associated to the linearized operator T given in (3.4.4) has a spectral gap of size $\lambda > 0$ in the space X; that is, there exist $\lambda > 0$ and $C \geq 1$ such that for all $u_0 \in X$ with $\int_{-\infty}^{V_F} u_0(v)\,\mathrm{d}v = 0$ we have*

$$\|e^{tT}u_0\|_X \leq Ce^{-\lambda t}\|u_0\|_X \qquad \textit{for all } t \geq 0. \tag{3.4.7}$$

Then there exists $\epsilon > 0$ (depending on b, V_R, V_F, p_∞ and λ) such that if $\|p_0 - p_\infty\|_X \leq \epsilon$ we have

$$\|p(.,t) - p_\infty(\cdot)\|_X \leq 2Ce^{-\frac{\lambda t}{2}}\|p_0 - p_\infty\|_X \qquad \textit{for all } t \geq 0. \tag{3.4.8}$$

The above result is given for systems without delay. Though we believe the analogous result holds for systems with delay, in that case there are technical difficulties in carrying out the same argument (in particular in stating the Duhamel's formula). We also point out that from the proof below one can easily obtain a decay rate with $e^{-(\lambda-\delta)t}$ for any $\delta > 0$ instead of $e^{-(\lambda t)/2}$, but we have chosen the latter for readability.

Proof of Theorem 3.4.2. The proof goes along the lines of the one for the Theorem 3.4.1, using this time our assumption on the linearized operator. As a preliminary step, we notice that due to (3.4.7), the semigroup e^{tT} satisfies

$$\|e^{tT}u_0\|_X \leq Ct^{-\frac{3}{4}}e^{-\lambda t}\|u_0\|_{L^2(\varphi)} \tag{3.4.9}$$

for all $u_0 \in X$, all $t > 0$ and some $C > 0$, $\lambda > 0$. For $0 < t \leq t_0$ this is a consequence of (3.4.6); and for $t > t_0$ we can carry out the same argument as in the proof of (3.2.9).

We call $u(v,t) := p(v,t) - p_\infty(v)$ with $N_u(t) := N_p(t) - N_{p_\infty}$, and we write the nonlinear equation (3.1.1a) as

$$\begin{aligned}\partial_t u = \partial_v^2 u + \partial_v(vu) + N_u(t)\delta_{V_R} - bN_{p_\infty}\partial_v u - bN_u(t)\partial_v p_\infty - bN_u(t)\partial_v u \\ =: Tu(v,t) - bN_u(t)\partial_v u,\end{aligned}$$

where e^{tT} refers to the semigroup of the linearized equation (with no delay). By Duhamel's formula we have

$$u(\cdot,t) = e^{tT}u_0 - b\int_0^t N_u(s)e^{(t-s)T}(\partial_v u(\cdot,s))\,\mathrm{d}s.$$

Taking the $\|\cdot\|_X$ norm, using (3.4.7), (3.4.9) and the fact that $\|\partial_v u\|_{L^2(\varphi)} \leq \|u\|_X$ we have

$$\begin{aligned}\|u(.,t)\|_X &\leq Ce^{-\lambda t}\|u_0\|_X + C|b|\int_0^t \|u(.,s)\|_X e^{-\lambda(t-s)}(t-s)^{-3/4}\|\partial_v u(.,s)\|_{L^2(\varphi)}\,\mathrm{d}s. \\ &\leq Ce^{-\lambda t}\|u_0\|_X + C|b|\int_0^t e^{-\lambda(t-s)}(t-s)^{-3/4}\|u(.,s)\|_X^2\,\mathrm{d}s.\end{aligned}$$

Let us now take $K_1 := 4C\|u_0\|_X$ and define

$$T_0 := \sup\{t \geq 0 \mid \|u(\cdot,s)\|_X \leq K_1 \text{ for } s \in [0,t]\}.$$

This T_0 must be strictly positive, and it may be $+\infty$; we will show later that with an appropriate choice of b it must be $+\infty$. Defining $C_b := C|b|K_1$ we get

$$\|u(.,t)\|_X \leq Ce^{-\lambda t}\|u_0\|_X + C_b\int_0^t e^{-\lambda(t-s)}(t-s)^{-3/4}\|u(.,s)\|_X\,\mathrm{d}s. \tag{3.4.10}$$

We define now $f(t) := e^{\lambda t}\|u(.,t)\|_X$ and write the previous equation as

$$f(t) \leq Cf(0) + C_b \int_0^t (t-s)^{-3/4} f(s)\,\mathrm{d}s.$$

Using the modified Gronwall's Lemma 3.3.7 with $A = C, B = C_b$ and $\alpha = 3/4$ we find the following bound for $f(t)$:

$$f(t) \leq 2Cf(0)\exp(C_b^4 \mu t),$$

which in terms of $\|u(.,t)\|_X$ is written as

$$\|u(.,t)\|_X \leq 2C\|u_0\|_X \exp(-(\lambda - C_b^4\mu)t). \tag{3.4.11}$$

As in the proof of Theorem 3.4.1, this shows that $T_0 = +\infty$ whenever $C_b^4\mu \leq \lambda$, that is, when

$$4C^2|b|\|u_0\|_X \leq \lambda^{\frac{1}{4}}\mu^{-\frac{1}{4}}.$$

The latter condition is satisfied if $\|u_0\|_X$ is small enough. If we additionally take $\|u_0\|_X$ so that

$$4C^2|b|\|u_0\|_X \leq 2^{-\frac{1}{4}}\lambda^{\frac{1}{4}}\mu^{-\frac{1}{4}}$$

then $\lambda - C_b^4\mu \leq \lambda/2$ and eq. (3.4.11) shows that

$$\|u(.,t)\|_X \leq 2C\|u_0\|_X \exp(-\frac{\lambda}{2}t) \qquad \text{for all } t \geq 0. \qquad \square$$

3.5 Spectral gap of the linearized equation

Consider equation (3.1.1) with delay $d \geq 0$; that is,

$$\partial_t p = \partial_v\left[(v - bN_p(t-d))p\right] + \partial_v^2 p + \delta_{V_R} N_p(t), \tag{3.5.1}$$

where $p = p(v,t)$ is the unknown and $N_p(t) := -\partial_v p(v,t)\big|_{v=v_F}$. We recall that the corresponding linear equation studied in Section 3.2 corresponds to the case in which $N_p(t)$ is fixed to a given constant in the nonlinear term:

$$\partial_t u = \partial_v\left[(v - bN)u\right] + \partial_v^2 u + \delta_{V_R} N_u(t) := Lu(v,t), \tag{3.5.2}$$

where it is understood that $N_u(t) := -\partial_v u(v,t)\big|_{v=V_F}$. The *linear* equation is inherently an equation without any delay. On the other hand, we may also consider the *linearized* (see definition 3.1.1) version of equation (3.5.1): if p_∞ is a stationary state of this equation (nonnegative, with integral equal to 1), we may search for solutions "close to p_∞", of the form $p(v,t) = p_\infty(v) + \epsilon u(v,t)$; for small ϵ, u must approximately solve the linearization

of this partial differential equation close to p_∞, given by

$$\partial_t u = \partial_v \left[(v - bN_\infty)u\right] + \partial_v^2 u + \delta_{V_R} N_u(t) - bN_u(t-d)\partial_v p_\infty,$$

that is,

$$\partial_t u = L_\infty u - bN_u(t-d)\partial_v p_\infty, \tag{3.5.3}$$

where L_∞ is the linear operator (3.5.2) corresponding to $N = N_\infty := -\partial_v p_\infty(V_F)$. The linearized equation (3.5.3) inherits the mass-preservation property from the nonlinear equation (3.5.1), and it is natural to always assume that $\int_{-\infty}^{V_F} u(t,v)\,\mathrm{d}v = 0$. Equation (3.5.3) is fundamental in the study of the behavior of the nonlinear equation (3.5.1) close to equilibrium.

Definition 3.5.1. Take $b \in \mathbb{R}$ and $d \geq 0$. We say that a probability equilibrium p_∞ of system (3.1.1) is *linearly stable* if there exist $C \geq 1$ and $\lambda > 0$ such that all solutions u to the linearized equation (3.5.3) with an initial condition $u_0 \in \mathcal{C}([-d,0];X)$ such that

$$\int_{-\infty}^{0} u_0(v,t)\,\mathrm{d}v = 0 \qquad \text{for all } t \in [-d,0] \tag{3.5.4}$$

satisfy

$$\|u(\cdot,t)\|_X \leq Ce^{-\lambda t} \sup_{\tau\in[-d,0]} \|u_0(\cdot,\tau)\|_X \qquad \text{for all } t \geq 0. \tag{3.5.5}$$

We say that p_∞ is *linearly unstable* if this is not true for $\lambda = 0$ and any $C \geq 1$; that is, if for any $C \geq 1$ there exists u_0 satisfying (3.5.4) and $t > 0$ such that

$$\|u(\cdot,t)\|_X \geq C \sup_{\tau\in[-d,0]} \|u_0(\cdot,\tau)\|_X.$$

The purpose of this section is to give conditions under which solutions to (3.5.3) converge to 0 as $t \to +\infty$, always assuming that $v \mapsto u(t,v)$ has integral zero for all t.

Our first observation is that assuming we know the solution to the linear equation (3.5.2), equation (3.5.3) becomes a closed equation for $N_u(t) := -\partial_v u(t,V_F)$. To see this, consider first the case with delay $d = 0$. By the Duhamel's formula, the solution to (3.5.3) is given by

$$u(v,t) = e^{tL_\infty}u_0 - b\int_0^t N_u(s)e^{(t-s)L_\infty}(\partial_v p_\infty)\,\mathrm{d}s.$$

Taking the derivative at $v = V_F$ we obtain

$$N_u(t) = g(t) + \int_0^t N_u(s)h(t-s)\,\mathrm{d}s, \tag{3.5.6}$$

where we define

$$h(t) := -bN(e^{tL_\infty}\partial_v p_\infty), \qquad g(t) := N(e^{tL_\infty}u_0). \tag{3.5.7}$$

Equation (3.5.6) is a type of integral equation sometimes known as the *renewal equation* or *Volterra's integral equation of the second kind*. It can be solved and its asymptotic behavior as $t \to +\infty$ can be characterized in terms of the Laplace transform of h; see Section 3.3.

Now, in the case of a positive delay $d > 0$, we consider an initial condition $u_0 \in \mathcal{C}([-d, 0], X)$. Duhamel's formula applied to equation (3.5.3) gives

$$u_t = e^{tL_\infty}u_0 - b\int_0^t N_u(s-d)e^{(t-s)L_\infty}(\partial_v p_\infty)\,\mathrm{d}s, \tag{3.5.8}$$

where it is understood that $e^{tL_\infty}u_0$ means e^{tL_∞} applied to the initial condition $u_0(0)$. Taking the derivative at $v = V_F$ we obtain

$$N_u(t) = g(t) + \int_0^t N_u(s-d)h(t-s)\,\mathrm{d}s,$$

where we define h and g just as before. We now rewrite this equation in a form closer to the convolution equation (3.5.6). For $t \geq d$ we have

$$N_u(t) = g(t) + \int_0^d N_u(s-d)h(t-s)\,\mathrm{d}s + \int_0^{t-d} N_u(s)h(t-s-d)\,\mathrm{d}s.$$

If we define $h(t) := 0$ for $t < 0$, the above equation can be written as

$$N_u(t) = g(t) + \int_0^d N_u(s-d)h(t-s)\,\mathrm{d}s + \int_0^t N_u(s)h(t-s-d)\,\mathrm{d}s,$$

and this can actually be checked to hold for all $t \geq 0$. Hence we have

$$N_u(t) = g_1(t) + \int_0^t N_u(s)h(t-s-d)\,\mathrm{d}s, \tag{3.5.9}$$

where

$$g_1(t) := g(t) + \int_0^d N_u(s-d)h(t-s)\,\mathrm{d}s.$$

Notice that the values of N_u which appear in the definition of g_1 are only for negative times, and are hence given by the initial condition of the delay equation for u.

We prove in Section 3.2 that $|N_q(t)| \leq Ce^{-\lambda t}$ for some $C, \lambda > 0$, and hence $\hat{N}_q(\xi)$ is well defined for $\Re(\xi) > -\lambda$. A study of the integral equations (3.5.6) and (3.5.9) (see Theorem 3.3.1 in Section 3.3) leads to the following theorem:

Theorem 3.5.2. *Take $b \in \mathbb{R}$ and $d \geq 0$, and let p_∞ be a (probability) stationary state of system (3.1.1), and define $\hat{N}_q$ by (3.1.14)–(3.1.16). The steady state p_∞ is linearly stable if and only if all zeros of the analytic function*

$$\Phi_d(\xi) := 1 + b\hat{N}_q(\xi)\exp(-\xi d)$$

(defined for $\Re(\xi) > -\lambda$) are located on the real negative half-plane $\{\xi \in \mathbb{C} \mid \Re(\xi) < 0\}$.

Proof. First, assume that the zeros of Φ_d (if any) are all on the real negative half-plane. Since Φ_d has a finite number of zeros on any strip with bounded real part, we know then that there exists $\lambda_0 > 0$ such that F, the function which appears in Theorem 3.3.1, does not have any poles with real part $\geq -\lambda_0$. Let u be any solution to the linearized equation (3.5.3) with delay $d \geq 0$, with initial data $u_0 \in X$ (if $d = 0$) or $u_0 \in \mathcal{C}([-d, 0], X)$ (if $d > 0$). In both cases it is enough to show (3.5.5) in the definition of linearized stability when $u_0(\cdot, 0)$ is a regular function (say $\mathcal{C}^2$), since the general case can be obtained by density. For the same reason, we may assume $N[u_0(\cdot, t)]$ is a $\mathcal{C}^1$ function on $[-d, 0]$.

The firing rate N_u associated to the solution u satisfies the renewal-type equation (3.5.9) (which is (3.5.6) in the particular case $d = 0$). The functions g_1 and $h(\cdot - d)$ satisfy the hypotheses of Theorem 3.3.1 (with g_1 playing the role of g in its statement):

1. The function g satisfies $|g(t)| = |N(e^{tL_\infty}u_0)| \leq \|e^{tL_\infty}u_0\|_X \leq Ce^{-\lambda t}\|u_0\|_X$ due to Theorem 3.2.3. Hence the bound (3.3.3) is satisfied. Since we may assume $u_0(0)$ is regular enough, it is known from [29] that g is $\mathcal{C}^1$ on $[0, +\infty)$, so it is continuous and of bounded variation on compact intervals of $[0, +\infty)$.

2. Since we have assumed the function N_u to be $\mathcal{C}^1$ on $[-d, 0]$, the integral term in the definition of g_1 is easily seen to be of bounded variation on compact sets, and satisfies (3.3.3).

3. Due to (3.2.9) in Proposition 3.2.3, the function h can be bounded by $|h(t)| \leq Ct^{-\frac{3}{4}}e^{-\lambda t}$ for some $C, \lambda > 0$, so h satisfies (3.3.2).

We note that Φ_d is precisely the denominator of the function F which appears in Theorem 3.3.1, so we have proved that F does not have any poles with real part $\geq \max\{-\lambda, -\lambda_0\}$. Then the theorem shows that, for some $C \geq 1$ and $\lambda > 0$,

$$|N_u(t)| \leq Ce^{-\frac{\lambda}{2}t}\|u_0\|_X \qquad \text{for } t \geq 0.$$

(Or any positive constant strictly smaller than λ instead of $\lambda/2$.) This shows the decay of N_u as $t \to +\infty$. The decay of $\|u(\cdot, t)\|_X$ is obtained by taking the $\|\cdot\|_X$ norm in eq. (3.5.8) and using the decay of N_u. This gives the spectral gap result, since the constants C and λ can be taken to depend only on h.

Reciprocally, assume that there is a zero ξ_0 of Φ_d with $\Re(\xi_0) \geq 0$. One can choose an initial condition u_0 on $[-d, 0]$ such that ξ_0 is a pole of the function F in Theorem 3.3.1. For the solution associated to this initial condition, Theorem 3.3.1 shows that $N_u(t)$ does not decay exponentially as $t \to +\infty$, so the equation does not have a spectral gap in this case. □

This result simplifies the numerical study of the stability of equilibria, and gives some theoretical consequences. For example, we have:

Corollary 3.5.3. *Take $b \in \mathbb{R}$. If a probability stationary state p_∞ of system (3.1.1) is linearly stable for $d = 0$, then it is linearly stable also for small enough $d > 0$.*

Proof. If p_∞ is linearly stable for $d = 0$, it means that for some $\mu > 0$, the function Φ_0 does not have any zeros on $\mathbb{C}_\mu := \{\xi \in \mathbb{C} \mid \Re(\xi) \geq -\mu\}$. By properties of the Laplace transform, $\hat{N}_q(\xi)$ tends to zero both when $\Im(\xi) \to \pm\infty$ and when $\Re(\xi) \to +\infty$. Hence all possible zeros of Φ_d in $\mathbb{C}_\mu$, for any $d \geq 0$, must be in some fixed compact subset $K \subseteq C_\mu$. Since the functions Φ_d are continuous and $\Phi_d(\xi) \to \Phi_0(\xi)$ uniformly as $d \to 0$, we see that for d small, the function Φ_d cannot have any zeros on K, and hence cannot have zeros on $\mathbb{C}_\mu$. □

There is a specific value of $\hat{N}_q$ which is linked to the function $I(N)$: in Lemma 3.5.5 we show that

$$b\hat{N}_q(0) = \frac{\mathrm{d}}{\mathrm{d}N}\Big|_{N=N_\infty} \left(\frac{1}{I(N)}\right).$$

As a consequence, analyzing the zeros of $\Phi_d(\xi)$ gives us the following criterion of stability/instability, often easier to check:

Theorem 3.5.4. *Let us set $V_R < V_F \in \mathbb{R}$, $b \in \mathbb{R}$, and let p_∞ be a probability equilibrium of the nonlinear equation (3.1.1). Call $N_\infty := -\partial_v p_\infty(V_F)$ its associated firing rate.*

1. *If*
$$\frac{\mathrm{d}}{\mathrm{d}N}\Big|_{N=N_\infty} \left(\frac{1}{I(N)}\right) > 1$$
then p_∞ is a linearly unstable equilibrium, for any delay $d \geq 0$.

2. *If*
$$|b| \int_0^\infty |N_q(t)| \, \mathrm{d}t < 1$$
then the equilibrium p_∞ is linearly stable, for any delay $d \geq 0$.

3. *If*
$$\frac{\mathrm{d}}{\mathrm{d}N}\Big|_{N=N_\infty} \left(\frac{1}{I(N)}\right) < -1 \tag{3.5.10}$$
then the equilibrium p_∞ is linearly unstable when the delay d is large enough.

Proof. **Proof of point 1.** Due to Lemma 3.5.5, the inequality in point 1 means that

$$\hat{h}(0) = \int_0^\infty h(t)\,\mathrm{d}t > 1.$$

Hence the function $\Phi_d(\xi)$ satisfies $\Phi_d(0) = 1 - \hat{h}(0) < 0$, it is real and analytic for $\xi \in [0, +\infty)$, and satisfies $\lim_{\xi\to+\infty,\ \xi\in\mathbb{R}} \Phi_d(\xi) = 1$. Hence Φ_d must have a zero at some $\xi_0 \in \mathbb{R}$ with positive real part, and by Theorem 3.5.2 the linearized equation (3.5.3) must have a solution whose associated N diverges to $+\infty$. Hence p_∞ is linearly unstable.

Proof of point 2. In the second case it holds that, for purely imaginary $\xi = ik$ (with $k \in \mathbb{R}$) we have

$$|\hat{h}(\xi)\exp(-ikd)| = \left|\int_0^\infty h(t)e^{-ikt}\,\mathrm{d}t\right| \le \int_0^\infty |h(t)|\,\mathrm{d}t < 1.$$

Hence, the function $\hat{h}$ is analytic on the real positive half-plane $\mathbb{C}_{\Re\ge 0} := \{\xi \in \mathbb{C} \mid \Re(\xi) \ge 0\}$, has modulus strictly less than one on the imaginary axis, and converges to 0 as $|\xi| \to +\infty$ on $\mathbb{C}_{\Re\ge 0}$. Hence $\hat{h}$ never has modulus 1 on $\mathbb{C}_{\Re\ge 0}$, and as a consequence the function Φ_d does not have any zeros on $\mathbb{C}_{\Re\ge 0}$. By Theorem 3.5.2, p_∞ is linearly stable.

Proof of point 3. In order to use Theorem 3.5.2 to prove that p_∞ is an unstable equilibrium for large d, we will find a root $\xi \in \mathbb{C}_{\Re\ge 0}$ of the function Φ_d (that is, a root with $\Re(\xi) > 0$). Equivalently, we need to find $\xi \in \mathbb{C}_{\Re\ge 0}$ with $\hat{h}(\xi)e^{-\xi d} = 1$. We will first show (in steps 1-4) that there exists $\xi \in \mathbb{C}$ with $\hat{h}(\xi)e^{-\xi d} = 1$ and $\Re(\xi) \ge 0$, and then we will slightly modify the argument (in step 5) to find a root ξ with strictly positive real part.

Step 1: Link to the winding number of a certain curve. Due to Lemma 3.5.5, the inequality (3.5.10) means that

$$\hat{h}(0) = \int_0^\infty h(t)\,\mathrm{d}t < -1.$$

For any $y \ge 0$, consider the curve $\alpha_y\colon [0, +\infty) \to \mathbb{C}$ defined by

$$\alpha_y(k) := \hat{h}(y + ik)\exp(-(y + ik)d) \qquad \text{for } k \in \mathbb{R}.$$

This curve satisfies $\alpha_y(0) = \hat{h}(y)e^{-yd}$ and $\lim_{k\to+\infty} \alpha_y(k) = 0$. We may complete this curve to a closed, continuous curve $\beta_y\colon [0, 2] \to \mathbb{C}$ by joining these endpoints, for example by defining

$$\beta_y(x) := \begin{cases} \alpha_y(\tan(\frac{\pi x}{2})) & \text{if } x \in [0, 1), \\ (x - 1)\alpha_y(0) & \text{if } x \in [1, 2]. \end{cases}$$

Assume the opposite of what we want to prove; that is, assume that

$$\hat{h}(\xi)e^{-\xi d} \neq 1 \qquad \text{for all } \xi \in \mathbb{C}_{\Re \geq 0}. \tag{3.5.11}$$

Equivalently, the curve α_y never touches the point 1, for any $y \geq 0$. As a further consequence, notice that $\alpha_y(0) = \hat{h}(y)e^{-yd}$ must always be strictly less than 1 for $y \geq 0$, since it is real and continuous, it is less than -1 for $y = 0$, and it never touches 1. Hence, the curves β_y never touch the point 1.

Since the curves β_y give a homotopy from the curve β_0 to the single point 0, all curves β_y must have winding number 0 about the point 1. Our proof by contradiction is complete if we prove that β_0 has nonzero winding number about 1 for d large.

Step 2: For large d, all crossings of β_0 with $(1, +\infty)$ are negatively oriented. That is, we will show that any time β_0 crosses the line $R := (1, \infty)$ in the complex plane, it does so by traversing it from above. Since $\alpha_0(0) < -1$, it is clear that $\beta_y(x)$ never touches R for $x \in [1, 2]$, so we only need to study the way in which the curve α_0 crosses R. We have, for $k > 0$,

$$\frac{\mathrm{d}}{\mathrm{d}k}\alpha_0(k) = i\hat{h}'(ik)e^{-ikd} - id\alpha_0(k).$$

Notice that for all $k \geq 0$,

$$|\hat{h}'(ik)| = \left| \int_0^\infty it\, h(t) e^{-ikt}\, \mathrm{d}t \right| \leq \int_0^\infty t\, |h(t)|\, \mathrm{d}t =: M.$$

Hence, if $\alpha_0(k) > 1$ at a certain point $k > 0$ then

$$\Im\left(\frac{\mathrm{d}}{\mathrm{d}k}\alpha_0(k)\right) \leq |\hat{h}'(ik)| - d\alpha_0(k) \leq M - d\alpha_0(k),$$

where $\Im(\cdot)$ denotes the imaginary part. If $d \geq M$ then this is a negative number, and hence the crossing is negatively oriented.

Step 3: For large d, the curve β_0 crosses the line $(1, +\infty)$ at least once. This is easy to see, since the curve $\gamma(k) := \alpha_0(k/d)$ converges to the curve $\alpha_0(0)e^{-ik}$, uniformly in compact sets. Since $\alpha_0(0) < -1$ by assumption, the curve γ must cross the interval $(1, +\infty)$ for large enough d, hence the same is true of α_0.

Step 4: The winding number of β_0 is nonzero for d large. The crossing number can be equivalently defined as the total number of crossings of the curve β_0 with $(1, +\infty)$, counting each one with its orientation. Since β_0 crosses $(1, +\infty)$ at least once, and all crossings are negatively oriented, this means that its winding number around 1 must be negative. This completes the contradiction, and shows that for d large, Φ_d must have at least one root on the positive complex half plane $\mathbb{C}_{\Re \geq 0}$.

Step 5: End of the proof. It only remains to show that (for d large) there must actually be a root of Φ_d with strictly positive real part. But all the previous steps can be carried out with the slightly perturbed curve α_y, instead of α_0, for small y, hence obtaining the conclusion. □

This criterion is also in agreement with the prediction of the pseudo equilibria sequence given in chapter 4 for networks with large transmission delay. It strikes us that the criterion is given in terms of the slope of $\frac{1}{I(N)}$ (see (3.1.4) for an explicit expression of I), which determines the behaviour of the discrete sequence of firing rates studied in chapter 4.

The function $1/I(N)$ is explicit (see (3.1.4)) and the only obstacle to checking analytically whether the conditions in Theorem 3.5.4 hold is that the expression of $I(N)$ is cumbersome to work with. Some rigorous properties of I are given in [14] and chapter 4, but in any case the following is clearly seen numerically (Figure 3.1):

- Case 1 in Theorem 3.5.4 holds in the excitatory case $b > 0$, assuming there are two equilibria. The higher equilibrium satisfies $\frac{\mathrm{d}}{\mathrm{d}N}\Big|_{N=N_\infty}\left(\frac{1}{I(N)}\right) > 1$ (with N_∞ the highest stationary firing rate). Hence assuming there are two equilibria, the higher equilibrium is unstable.

- Case 2 in Theorem 3.5.4 seems hard to check analytically, though numerical checks are straightforward. This case takes place for the lower equilibrium if there are two of them, and for the single equilibrium whenever there is a unique one.

- Case 3 in Theorem 3.5.4 can be rigorously proved to hold when $b < 0$ is sufficiently negative. Hence there is some $b^* < 0$ such that for $b < b^*$ and large enough $d > 0$, the unique equilibrium p_∞ is linearly unstable.

We note that Theorem 3.5.4 may not be fully exhaustive. First, because it does not speak about the critical cases where $\frac{\mathrm{d}}{\mathrm{d}N}\Big|_{N=N_\infty}(1/I(N)) = \pm 1$. And second, even ignoring these cases, it may still happen that none of its three possibilities are satisfied. However, from our simulations we suspect that the criterion is in fact exhaustive except at the critical cases, since we expect $N_q(t)$ to have a fixed sign for all $t > 0$ (which seems clear numerically), and then

$$|b| \int_0^\infty |N_q(t)| \, \mathrm{d}t = \left| \frac{\mathrm{d}}{\mathrm{d}N}\Big|_{N=N_\infty} \left(\frac{1}{I(N)}\right) \right|.$$

On the other hand, point 3 of Theorem 3.5.4 does not give information on the case of strongly inhibitory systems with small delay. For those cases we must study the zeros of Φ_d, as indicated by Theorem 3.5.2, and the best we can say is Corollary 3.5.3.

In Figure 3.3 we see a numerical description of the different cases in Theorem 3.5.4, depending on the connectivity parameter b. This gives a global description of the long-time behavior of the solutions to the linearized equation (3.5.3). However, in cases where the value of the delay is key to the stability of the equilibria, no quantitative results are shown with respect to the delay. For this purpose we have made Figure 3.4, where the stability or instability of equilibria to the linearized equation stated in Theorems 3.5.2 and 3.5.4 can be checked numerically is shown in a two-dimension map (b, d).

Though it is not contained in Theorem 3.5.4, we point out that the expected behavior of the nonlinear system (3.1.1) when (b, d) is in the unstable region with $b < 0$ should be periodic, as shown consistently in simulations shown in [87] and chapter 4. That is, we expect solutions to converge to a unique (up to time translations) periodic solution with period approximately equal to $2d$. Since the analysis leading to Theorem 3.5.4 is based on the linearized equation, we are not able to show a global behavior such as periodic solutions, but the mechanism for their appearance seems to be given by the presence of delayed negative feedback: in the literature on delay equations there are many instances of periodic behavior, arising due to a delayed system in which the driving force works against the displacement that the system has experienced in the previous delay period. See for example the books [54] (especially chapter XV) or [65] for an exposition of this topic.

We end the section by proving the relationship between $\hat{h}(0)$ and $\frac{d}{dN}\left(\frac{1}{I(N)}\right)_{|N=N_\infty}$ used in proof of Theorem 3.5.4.

Lemma 3.5.5. *Take $b \in \mathbb{R}$, and let $p_\infty \colon (-\infty, V_F] \to [0, +\infty)$ be a nonnegative equilibrium with unit mass of the nonlinear integrate-and-fire equation (3.5.1). The following equality holds:*

$$\hat{h}(0) = bN(L_\infty^{-1}(\partial_v p_\infty)) = \frac{d}{dN}\left(\frac{1}{I(N)}\right)_{|N=N_\infty}. \tag{3.5.12}$$

(We recall that $I \colon [0, \infty) \to \mathbb{R}^+$ was defined in (3.1.4) and $h(t) = -bN_q(t)$ was defined in (3.5.7).)

Proof. **Proof of the first equality.** Due to our well-posedness inequalities in Section 3.2 we have

$$\|e^{tL_\infty} u_0\|_X \lesssim Ce^{\mu t}\|u_0\|_X$$

for some $C, \mu > 0$, where $e^{tL_\infty} u_0$ denotes the classical solution to the linear problem with a sufficiently regular initial condition u_0. By density we may then extend the map e^{tL_∞} to all of X, defining a strongly continuous semigroup in this space. Due to mass conservation, this semigroup may be restricted to the space X_0 of functions in X with integral 0, which

we do in the following. By a general result on semigroups [64, Theorem 1.10] we have

$$L_\infty^{-1}(u_0) = -\int_0^\infty e^{tL_\infty} u_0 \, \mathrm{d}t$$

for any $u_0 \in X_0$. Applying the operator N (which is continuous in X) to both sides,

$$N\left[L_\infty^{-1}(u_0)\right] = -\int_0^\infty N\left[e^{tL_\infty} u_0\right] \, \mathrm{d}t$$

for all $u_0 \in X_0$. Approximating $\partial_v p_\infty$ by functions in X_0 and multiplying by b we obtain

$$bN\left[L_\infty^{-1}(\partial_v p_\infty)\right] = -b\int_0^\infty N\left[e^{tL_\infty}\partial_v p_\infty\right] \, \mathrm{d}t = \int_0^\infty h(t)\, \mathrm{d}t = \hat{h}(0).$$

Proof of the second equality. We denote $\phi \equiv L_\infty^{-1}(\partial_v p_\infty)$, so $\phi\colon (-\infty, V_F] \to [0, +\infty)$ is a function which satisfies

$$\partial_v p_\infty = L_\infty(\phi),\ \phi(V_F) = 0,\ N_\phi := -\phi'(V_F),\ \text{and} \int_{-\infty}^{V_F} \phi(v)dv = 0,$$

or equivalently, $\phi(V_F) = 0$, $N_\phi := -\phi'(V_F)$, $\int_{-\infty}^{V_F} \phi(v)dv = 0$ and

$$\partial_v p_\infty(v) = \phi''(v) + (v\phi)'(v) - bN_\infty \phi'(v) + \delta_{V_R}.$$

Therefore,

$$\left(\phi' + (v - bN_\infty)\phi + H(v - V_R)N_\phi - p_\infty\right)'(v) = 0$$

and using the boundary condition $\phi(V_F) = 0$, we obtain

$$\phi'(v) = -(v - bN_\infty)\phi(v) - H(v - V_R)N_\phi + p_\infty(v),$$

which can be solved and we get, in terms of N_ϕ,

$$\phi(v) = \frac{N_\phi}{N_\infty} p_\infty - N_\infty e^{-\frac{(v-bN_\infty)^2}{2}} \int_v^{V_F} \int_w^{V_F} e^{\frac{(y-bN_\infty)^2}{2}} H(y - V_R)\, \mathrm{d}y\, \mathrm{d}w.$$

To determine N_ϕ we integrate in $(-\infty, V_F)$ and we impose that the integral is zero

$$\begin{aligned}
N_\phi &= N_\infty^2 \int_{-\infty}^{V_F} e^{-\frac{(v-bN_\infty)^2}{2}} \int_v^{V_F} \int_w^{V_F} e^{\frac{(y-bN_\infty)^2}{2}} H(y - V_R)\, \mathrm{d}y\, \mathrm{d}w\, \mathrm{d}v \\
&= N_\infty^2 \int_{-\infty}^{V_F} e^{-\frac{(v-bN_\infty)^2}{2}} \int_v^{V_F} e^{\frac{(y-bN_\infty)^2}{2}} H(y - V_R) \int_v^y \mathrm{d}w\, \mathrm{d}y\, \mathrm{d}v \\
&= N_\infty^2 \int_{-\infty}^{V_F} e^{-\frac{(v-bN_\infty)^2}{2}} \int_v^{V_F} e^{\frac{(y-bN_\infty)^2}{2}} H(y - V_R)(y - v)\, \mathrm{d}y\, \mathrm{d}v.
\end{aligned}$$

So we have proved

$$N(L_\infty^{-1}(\partial_v p_\infty)) = N_\phi = N_\infty^2 \int_{-\infty}^{V_F} e^{-\frac{(v-bN_\infty)^2}{2}} \int_v^{V_F} e^{\frac{(y-bN_\infty)^2}{2}} H(y-V_R)(y-v)\,\mathrm{d}y\,\mathrm{d}v. \tag{3.5.13}$$

To conclude the proof we calculate $\frac{d}{dN}\left(\frac{1}{I(N)}\right)_{|N=N_\infty}$. To do that we recall the definition of I (see (3.1.4))

$$I(N) = \int_{-\infty}^{V_F} e^{-\frac{(v-bN)^2}{2}} \int_v^{V_F} e^{\frac{(y-bN)^2}{2}} H(y-V_R)\,\mathrm{d}y\,\mathrm{d}v. \tag{3.5.14}$$

and write $g(N) := \frac{1}{I(N)}$, and we want to prove that

$$g'(N_\infty) = bN_\phi. \tag{3.5.15}$$

We know that $N_\infty I(N_\infty) = 1$, because N_∞ is the firing rate of the equilibrium (see (3.1.3)), thus

$$g'(N_\infty) = \frac{-I'(N_\infty)}{I(N_\infty)^2} = -I'(N_\infty)N_\infty^2. \tag{3.5.16}$$

We differentiate $I(N)$

$$\begin{aligned}
I'(N) &= b\int_{-\infty}^{V_F} (v-bN)e^{-\frac{(v-bN)^2}{2}} \int_v^{V_F} e^{\frac{(y-bN)^2}{2}} H(y-V_R)\,\mathrm{d}y\,\mathrm{d}v \\
&\quad -b\int_{-\infty}^{V_F} e^{-\frac{(v-bN)^2}{2}} \int_v^{V_F} (y-bN)e^{\frac{(y-bN)^2}{2}} H(y-V_R)\,\mathrm{d}y\,\mathrm{d}v \\
&= b\int_{-\infty}^{V_F} v\, e^{-\frac{(v-bN)^2}{2}} \int_v^{V_F} e^{\frac{(y-bN)^2}{2}} H(y-V_R)\,\mathrm{d}y\,\mathrm{d}v \\
&\quad -b\int_{-\infty}^{V_F} e^{-\frac{(v-bN)^2}{2}} \int_v^{V_F} y\, e^{\frac{(y-bN)^2}{2}} H(y-V_R)\,\mathrm{d}y\,\mathrm{d}v \\
&= b\int_{-\infty}^{V_F} e^{-\frac{(v-bN)^2}{2}} \int_v^{V_F} e^{\frac{(y-bN)^2}{2}} H(y-V_R)(v-y)\,\mathrm{d}y\,\mathrm{d}v,
\end{aligned}$$

and evaluating in N_∞ and using (3.5.16) we obtain (3.5.15), which concludes the proof. □

3.6 Conclusions

Applications of entropy methods have only given results for weakly connected networks (small $|b|$) so far, i.e. almost linear systems. Building on these results, in this chapter we increase the existing knowledge on the long-time behavior of the Fokker-Planck equation (3.1.1), either in its linear, linearized or non-linear forms.

In section 3.2 we give further properties of the linear operator, and thus we restrict the spectral gap known from entropy methods to a space that includes part of the nonlinear term. This allows us to prove in section 3.4.1 that, on the loosely connected system, for small $|b|$, the (unique) equilibrium is stable. Our proof works for a given small $|b|$, and any delay $d \geq 0$; this should be compared to [18], where a condition on d was needed. In addition, similar arguments to those used in this proof will allow us in chapter 4 to present results on the global behavior of the NNLIF system for small b. With a similar proof, in section 3.4.2 we show that linearized stability of an equilibrium implies its nonlinear stability without delay, which is a new result as far as we know. We expect the same to be true also for any positive delay, but the proof runs into technical difficulties that we have not been able to overcome. Furthermore, the study of the linear equation performed in section 3.2 may be useful for its subsequent extension to an alternative theory of existence to the one offered in [29], and its use as a basis for the rigorous analysis of variants of the PDE (3.1.1).

In our knowledge, the most important finding of this chapter is what is developed in section 3.5 with the support of results in sections 3.2 and 3.3. There we give explicit criteria to study whether a given equilibrium is linearly stable or not. That is, for each equilibrium of the non-linear system, we linearize the equation around it, and we give a rigorous criteria, easy to check numerically, about the stability or instability of this equilibrium. Moreover, we use the extension between stability of the linearized and the nonlinear equation provided in Section 3.4.2, thus giving a rather complete picture of the asymptotic behavior of the PDE (3.1.1). These criteria are intimately related to the slope at which the curve $N \mapsto (I(N))^{-1}$ crosses the diagonal in Figure 3.1, which also determines the behavior of the firing rate sequence, which provides the pseudo-equilibria sequence (see chapter 4 for more details).

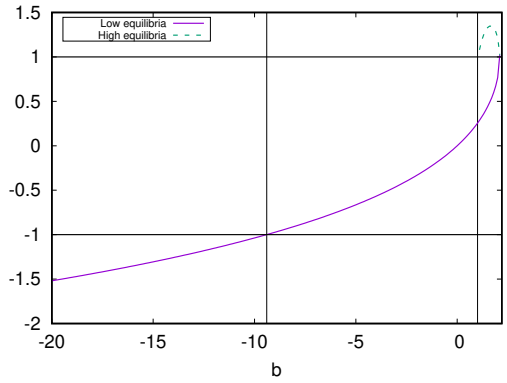

Figure 3.3: **Value of** $S(b) := -b\int_0^\infty N_q(t)\,\mathrm{d}t = \frac{\mathrm{d}}{\mathrm{d}N}\Big|_{N=N_\infty}\left(\frac{1}{I(N)}\right)$ **for different values of** b**.** Vertical lines at $b = -9.4$ and $b = 1$ separate regions with different behaviors in terms of stability for equilibria of equation (3.5.3): for $b < -9.4$ (one equilibrium) we find that $S(b) < -1$, which coincides with point 3 of Theorem 3.5.4, i.e. the region of b where equilibria stability depends on the delay value; in the case $-9.4 < b < 1$ (one equilibrium), we get $|S(b)| = |b|\int_0^\infty |N_q(t)|\,\mathrm{d}t < 1$ (since the function $N_q(t)$ is numerically seen to be always monotone), leading us to the scenario in point 2 of Theorem 3.5.4, where regardless of the delay value, the equilibrium is stable. For any $b > 1$ there are two equilibria: for the lower equilibrium (solid line) the situation is the same as in the previous case, while for the higher equilibrium (dashed line), $S(b) > 1$ and point 1 of Theorem 3.5.4 is fulfilled. Reset and firing potential are set to $V_R = 1$ and $V_F = 2$ respectively.

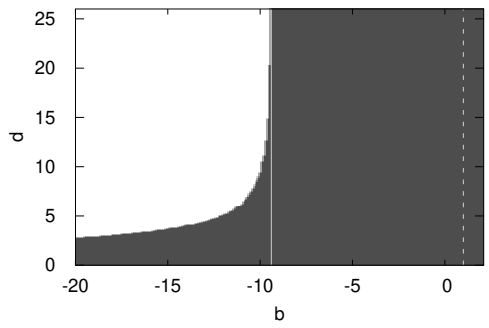

Figure 3.4: **Stability map of the linearized equation.** For each pair of values of the connectivity parameter and transmission delay (b, d), this color map shows the stability (dark) or instability (white) for the solutions of the linearized equation (3.1.12). The vertical black solid line placed at $b_p \approx -9.4$ separates the region of unconditional stability (for any delay d), from that where stability depends on the value of d. The vertical dashed line at $b = 1$ separates the region with a unique steady state (left) from the one with two steady states (right). For cases with two steady states (that is, to the right of the vertical dashed line) we consider the lower one. The stability condition considered to make this map is based on Theorems 3.5.2 and 3.5.4: for each b we find its related equilibrium p_∞, choosing the lower one if there are two equilibria; we differentiate p_∞ and use it as initial condition for the linear system given by equation (3.1.1a), thus obtaining $q(v,t) = e^{tL_\infty}\partial_v p_\infty$ and $N_q(t)$. Cases 1 and 2 of Theorem 3.5.4 account for all cases with $b > b_p$. In order to tell apart the cases with $b < b_p$, for each $d > 0$ we compute $Q(k) := -be^{-ikd}\int_0^\infty N_q(t)e^{ikt}\,\mathrm{d}t$, with $k \in \mathbb{R}$; finally we count the number of times that $Q(k)$ crosses the line $(1, \infty)$ taking into account its orientation. If the net balance of crossings is different from 0, the equilibrium p_∞ related to (b, d) is unstable (see the proof of Theorem 3.5.4 in Section 3.5 for a better understanding of this). Otherwise we need to compute the zeros of function $\Phi_d(\xi) := 1 + b\hat{N}_q(\xi)\exp(-\xi d)$, given in Theorem 3.5.2 in order to check whether the equilibrium is stable or not. Reset and firing potential are set to $V_R = 1$ and $V_F = 2$ respectively.

Chapter 4

The sequence of pseudo-equilibria describes the long-time behavior of the NNLIF model with large delay

4.1 Introduction

We introduce a set of novel states, which we call "pseudo-equilibria"[3], and give evidence of their defining role in the behavior of the NNLIF system when a significant synaptic delay is considered. The advantage is that these states are determined solely by the system's parameters and are derived from a sequence of firing rates that result from solving a recurrence equation. We propose a new strategy to show convergence to an equilibrium for a weakly connected system with large transmission delay, based on following the sequence of pseudo-equilibria. Unlike with the direct entropy dissipation method, this technique allows us to see how a large delay favors convergence. We also present a detailed numerical study to support our results. This study explores the overall behavior of the NNLIF system and helps us understand, among other phenomena, periodic solutions in strongly inhibitory networks.

The mathematical description of the model studied is given in section 1.2.2, so we will make a quick reminder of it:

$$\partial_t p(v,t) + \partial_v \left[(-v + bN(t-d))\, p(v,t) \right] - \partial_v^2 p(v,t) = \delta_{V_R} N(t), \tag{4.1.1}$$

This Fokker-Planck PDE provides the evolution in time $t \geq 0$ of the probability density $p(v,t) > 0$ of finding neurons at voltage $v \in (-\infty, V_F]$. The right hand side of the equation

[3]This chapter compiles the work sent for publication, whose preprint is [13].

and the boundary condition $p(V_F, t) = 0$ describe the firing mechanism of neurons between the firing potential V_F, to the reset potential $V_R < V_F$. The firing rate $N(t)$ is computed as

$$N(t) := -a\,\partial_v p(V_F, t) \geq 0,$$

making the system nonlinear. The parameter b, shows how excitatory or inhibitory the network is: $b = 0$ means that neurons are not connected with each other and the system becomes linear; if $b > 0$ the network is average-excitatory; and if $b < 0$ the network is average-inhibitory. The transmission delay is represented by a parameter d in the drift. Finally, assuming also $p(-\infty, t) = 0$ the solution to the related Cauchy problem satisfies the conservation law:

$$\int_{-\infty}^{V_F} p(v,t)dv = \int_{-\infty}^{V_F} p_0(v)dv, \quad \text{for } t \in [0, T),$$

for a given non-negative, integrable initial condition $p(v, 0) = p_0(v) \geq 0$, with $N(t) = -a\partial_v p_0(V_F)$ for $t \in [-d, 0]$, where $T > 0$ is the maximal time of existence. For the sake of simplicity, we consider that $\int_{-\infty}^{V_F} p_0(v)\,\mathrm{d}v = 1$.

The probability stationary states, steady states, or equilibria, $p_\infty(v)$, of system (4.1.1) are non negative solutions to

$$\begin{cases} \partial_v \left[(-v + bN_\infty)\, p_\infty(v)\right] - \partial_v^2 p_\infty(v) = \delta(v - V_R)N_\infty, \\ N_\infty := -\partial_v p_\infty(V_F), \text{ and } \int_{-\infty}^{V_F} p_\infty(v)\,\mathrm{d}v = 1, \end{cases} \tag{4.1.2}$$

which are given by

$$p_\infty(v) = N_\infty e^{-\frac{(v-bN_\infty)^2}{2}} \int_{\max(v,V_R)}^{V_F} e^{\frac{(w-bN_\infty)^2}{2}}\,\mathrm{d}w. \tag{4.1.3}$$

The stationary firing rate N_∞ is implicitly given by the requirement of unit mass, which is translated into the condition $N_\infty I(N_\infty) = 1$, where

$$I(N) := \int_{-\infty}^{V_F} e^{-\frac{(v-bN)^2}{2}} \int_{\max(v,V_R)}^{V_F} e^{\frac{(w-bN)^2}{2}}\,\mathrm{d}w\,\mathrm{d}v. \tag{4.1.4}$$

Every stationary state corresponds to a solution of the implicit equation $N_\infty I(N_\infty) = 1$ for N_∞. The number of steady states depends on the connectivity parameter b [14]: for $b \leq 0$ (inhibitory case) there is only one, while for $b > 0$ (excitatory case) there is more variety; there is only one, if b is small, there are no steady states, if b is large, and there are at least two for intermediate values of b. In the latter scenario, only two equilibria have been observed numerically.

So far the analysis of the asymptotic behavior of the model (4.1.1) has been carried out essentially by means of the entropy dissipation method (see [14,16,18,19,25]), considering the following relative entropy functional, between the solution p and the stationary solution p_∞:

$$H(p(\cdot,t)|p_\infty) := \int_{-\infty}^{V_F} \frac{(p(v,t)-p_\infty(v))^2}{p_\infty(v)} dv = \|p(.,t)-p_\infty(.)\|_{L^2(p_\infty^{-1})}.$$

This strategy has given results only for weakly connected networks (small values of the connectivity parameter b), that is, almost linear systems. The main difficulty in applying these techniques to strongly connected systems lies in the necessary control over the firing rate, $N(t)$. We partly overcome that problem in chapter 3 and analyze the long-term local behavior of the NNLIF system for general connectivity strength by proposing a new strategy based on: studying the spectral gap properties of the linearized problem in a space with a "strong" norm.

In this chapter we propose new ideas to complement the study of the global asymptotic behavior of the NNLIF model, which are based on examining a discrete system solely determined by the parameters of the nonlinear system (4.1.1). In chapter 2 we numerically observed the formation of a new profile, which describes networks with uniformly distributed membrane potentials between the reset value V_R and the threshold value V_F. We called these states "plateau" distributions. These profiles appear in two situations: 1) strongly connected systems (high connectivity parameter b) with synaptic delay, $d > 0$, and 2) systems with $b = V_F - V_R$, without delay ($d = 0$) or with very small transmission delay value. Numerically we observe that plateau states appear to be related to what we call "pseudo-equilibria". For a given $N \in \mathbb{R}^+$

$$p_{\text{pseudo}}(v) := \tilde{N} e^{-\frac{(v-bN)^2}{2}} \int_{\max(v,V_R)}^{V_F} e^{\frac{(w-bN)^2}{2}}\, \mathrm{d}w, \quad \text{with} \quad \tilde{N} = \frac{1}{I(N)}, \tag{4.1.5}$$

is an equilibrium corresponding to the linear equation for *fixed* N. We refer to this as a *pseudo-equilibrium*. The constant $\tilde{N}$ guarantees unit mass: $\int_{-\infty}^{V_F} p_{\text{pseudo}}(v)\,\mathrm{d}v = 1$. We notice that given $N_\infty \in \mathbb{R}^+$, the pseudo-equilibrium (4.1.5) is a steady state of the NNLIF system (4.1.1) (see (4.1.3)), if and only if, $\tilde{N}_\infty = N_\infty$, that is, if and only if $N_\infty I(N_\infty) = 1$.

Figure 4.1 shows the comparison of the plateau distributions found for $b = 1.5$ (left plot) and $b = 2.2$ (right plot), with delay transmission, and several pseudo-equilibria. There is a high coincidence between the plateau distributions and the profiles (4.1.5) as N increases. Furthermore, the dynamics of the particle system appears to go through states with the form (4.1.5) with increasing N, during the formation of its plateau states. For $b = 1.5$ the system (4.1.1) exhibits two steady states, and it can evolve towards a plateau

distribution, as shown in the left plot, if the initial condition is far from the stationary state with lowest firing rate. For $b = 2.2$ there are no stationary solutions and the system evolves towards a plateau distribution.

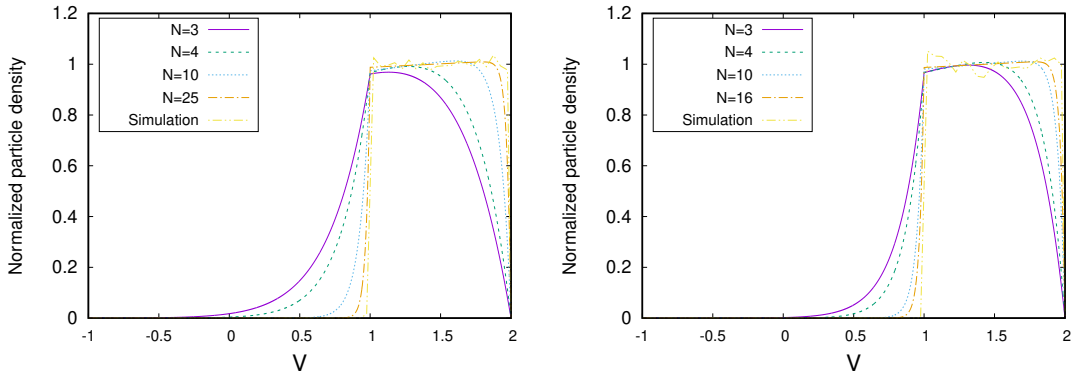

Figure 4.1: **Comparison of "plateau" distributions with profiles** (4.1.5). Pictures of [17]. *L*eft: $b = 1.5$. *R*ight: $b = 2.2$.

That behavior suggests that we may think of the pseudo-equilibria sequence as a tool to analyze the asymptotic behavior of the system when a large synaptic delay is taken into account. The aims of this chapter are twofold: 1) to analyze the sequence of pseudo-equilibria determined by the associated discrete system, and 2) to establish a connection between the long-term behavior of the pseudo-equilibria sequence and the solutions of the nonlinear system (4.1.1).

Section 4.2 extends result of the linear PDE studied in section 3.2 so that they can be applied in this chapter. In section 4.3 we define and analyze the discrete model, i.e, the firing rate and the pseudo-equilibria sequences. In section 4.4 we prove the exponential convergence to equilibrium for the nonlinear system (4.1.1) for small connectivity parameter b and large delay d, by "following" the sequence of pseudo-equilibria. This approach looks promising to study a broader range of phenomena, such as periodic solutions or the approach of the plateau state, and served as a catalyst for the main ideas in chapter 3. In section 4.5 we provide the numerical evidence to support the connection between the sequence of pseudo-equilibria studied in section 4.3 with the nonlinear system. This numerical work also suggests several conjectures on the possible extension of the results of section 4.4 to cases with an arbitrary value of the parameter b. Hence our numerical results explore the global behavior of the NNLIF system away from the cases which have been analytically studies in chapter 3. Lastly section 4.6 is devoted to conclusions, discussion and possible extensions of our work.

4.2 Results for the linear integrate-and-fire Fokker-Planck equation

This is an extension of the analytical results obtained in chapter 3 on the linear integrate-and-fire model. The linear model is obtained by fixing the firing rate as a constant $\overline{N}$, in the drift term of equation (4.1.1):

$$\partial_t u(v,t) = \partial_v^2 u(v,t) + \partial_v[(v - b\overline{N})u(v,t)] + \delta_{V_R} N_u(t),\ v \in (-\infty, V_F]\,,\ t \geq 0, \tag{4.2.1}$$

where we recall that $N_u(t) := -\partial_v u(V_F, t)$, for $t \geq 0$, and the boundary condition $u(V_F, t) = 0$. The existence theory for classical solutions to the nonlinear system (4.1.1) is given in [29] (including the linear case with constant $\overline{N}$).

We consider the family of spaces:

$$X_{\overline{N}} := \{u \in \mathcal{C}(-\infty, V_F] \cap \mathcal{C}^1(-\infty, V_R] \cap \mathcal{C}^1[V_R, V_F] \mid u(V_F) = 0 \text{ and } \|u\|_X < \infty\}, \tag{4.2.2}$$

where

$$\|u\|_{X_{\overline{N}}} := \|u\|_\infty + \|\partial_v u\|_\infty + \|u\|_{L^2(\varphi_{\overline{N}})} + \|\partial_v u\|_{L^2(\varphi_{\overline{N}})} \tag{4.2.3}$$

and

$$\varphi_{\overline{N}}(v) := \exp\left(\frac{(v - b\overline{N})^2}{2}\right), \qquad v \in (-\infty, V_F].$$

In chapter 3 we show that the evolution semigroup associated to the operator L (which depends on the parameter $\overline{N}$) has a spectral gap in the space $X_{\overline{N}}$. In the proof of Theorem 4.4.1 (see section 4.4) we need to have a *common* space X where all semigroups associated to all operators L have a spectral gap, for all $\overline{N}$ in a neighbourhood of a given value N. We choose the space $X \equiv X_0$, with norm

$$\|u\|_X := \|u\|_\infty + \|\partial_v u\|_\infty + \|u\|_{L^2(\varphi)} + \|\partial_v u\|_{L^2(\varphi)} \tag{4.2.4}$$

and

$$\varphi(v) := \exp\left(\frac{v^2}{2}\right), \qquad v \in (-\infty, V_F].$$

The analytical results obtained in chapter 3 on the linear integrate-and-fire model can be extended to this space using the following lemma:

Lemma 4.2.1 (Regularization estimates between $L^2(\varphi_{\overline{N}})$ and $L^2(\varphi)$)**.** *If $b \leq 0$ then there exists a function $\alpha\colon (0,1) \to (0, +\infty)$ depending on $\overline{N}$ such that*

$$\|e^{tL} u_0\|_X \leq \alpha(t) \|u_0\|_{X_{\overline{N}}} \qquad \textit{for all } t \in (0,1), \tag{4.2.5}$$

for all initial conditions $u_0 \in X_{\overline{N}}$. *Similarly, if* $b \geq 0$ *we have*

$$\|e^{tL}u_0\|_{X_{\overline{N}}} \leq \alpha(t)\|u_0\|_X \qquad \text{for all } t \in (0,1), \tag{4.2.6}$$

for all initial conditions $u_0 \in X$.

Observe that for $b \leq 0$ we have $\varphi_{\overline{N}} \leq C\varphi$ for some constant $C > 0$, so $X \subseteq X_{\overline{N}}$; while for $b \geq 0$ we have $\varphi \leq C\varphi_{\overline{N}}$ for some constant $C > 0$, so $X_{\overline{N}} \subseteq X$. The proof of this lemma follows the same steps as lemma 3.2.12. The main difficulty is proving a corresponding estimate for the standard Fokker-Planck equation, which can be proved following similar calculations as in the proof of lemma 3.2.6.

One can similarly obtain the following well-posedness results, where the only change with respect to lemmas 3.2.1 and 3.2.2 is the weight φ in the space X:

Lemma 4.2.2 (Well-posedness estimate)**.** *Let us consider any initial condition* $u_0(v) \in X$, *where* X *is given by* (4.2.2). *Then the solution to the Cauchy problem related to the linear equation* (4.2.1) *satisfies the following: there are constants* $M, C > 0$ *such that*

$$\|e^{tL}u_0\|_X \leq Me^{Ct}\|u_0\|_X, \ \forall\, t \geq 0. \tag{4.2.7}$$

Lemma 4.2.3 (Regularization estimate)**.** *Let us consider any initial condition* $u_0(v) \in L^2(\varphi_{\overline{N}})$. *Then the solution to the Cauchy problem related to the linear equation* (4.2.1) *satisfies the following: there exist constants* $C > 0$ *and* $t_0 > 0$, *such that*

$$\|e^{tL}u_0\|_X \leq Ct^{-3/4}\|u_0\|_{L^2(\varphi)}, \ \forall\, 0 < t \leq t_0, \tag{4.2.8}$$

We know from previous results [14] that equation (4.2.1) has a unique equilibrium p_∞ with unit mass. This equilibrium is positive, and the operator L has a spectral gap in the space $L^2(p_\infty^{-1})$. More precisely, there exists $\lambda > 0$ such that for all probability distributions $p_0 \in L^2(p_\infty^{-1})$,

$$\|e^{tL}p_0 - p_\infty\|_{L^2(p_\infty^{-1})} \leq e^{-\lambda t}\|p_0 - p_\infty\|_{L^2(p_\infty^{-1})} \qquad \text{for all } t \geq 0. \tag{4.2.9}$$

In chapter 3 this is proved also for the smaller space $X_{N_\infty} \subseteq L^2(p_\infty^{-1})$, with N_∞ the equilibrium firing rate $N_\infty := -\partial_v p_\infty(V_F)$. We can in fact state the result also for the space X ($\equiv X_0$), with a similar proof which uses our lemmas 4.2.2 and 4.2.3:

Proposition 4.2.4 (Spectral gap)**.** *The operator* L *associated to the linear equation* (4.2.1) *has a spectral gap in the space* X. *That is, there exist constants* $\lambda > 0$, $C \geq 1$ *such that for all initial condition* $u_0 \in X$ *with zero integral, it holds that*

$$\|e^{tL}u_0\|_X \leq Ce^{-\lambda t}\|u_0\|_X \qquad \text{for all } t \geq 0. \tag{4.2.10}$$

Proof. From chapter 3 we know that for all $u_0 \in X_{N_\infty}$ with zero integral,

$$\|e^{tL}u_0\|_{X_{N_\infty}} \leq Ce^{-\lambda t}\|u_0\|_{X_{N_\infty}} \qquad \text{for all } t \geq 0. \tag{4.2.11}$$

We write the proof in the two cases $b \leq 0$ and $b \geq 0$:

Proof for $b \leq 0$. In this case we have $X \subseteq X_{N_\infty}$. We will use (4.2.11) and the regularization result (4.2.5). For any fixed $0 < t_0 < 1$ and any $u_0 \in X_{N_\infty}$ we have the following for any $t \geq t_0$:

$$\begin{aligned}\|e^{tL}u_0\|_X = \|e^{t_0L}e^{(t-t_0)L}u_0\|_X &\leq \alpha(t_0)\|e^{(t-t_0)L}u_0\|_{X_{N_\infty}} \\ &\leq C\alpha(t_0)e^{-\lambda(t-t_0)}\|u_0\|_{X_{N_\infty}} \leq C\alpha(t_0)e^{-\lambda(t-t_0)}\|u_0\|_X.\end{aligned}$$

By density we obtain the result for any $u_0 \in X$. This proves the result for any $t \geq t_0$. For $0 \leq t \leq t_0$ it is enough to use the well-posedness result in lemma 4.2.2.

Proof for $b \geq 0$. In this case we have $X_{N_\infty} \subseteq X$. We will use (4.2.11) and the regularization result (4.2.6). For any fixed $0 < t_0 < 1$ and any $u_0 \in X$ we have the following for any $t \geq t_0$:

$$\begin{aligned}\|e^{tL}u_0\|_X = \|e^{(t-t_0)L}e^{t_0L}u_0\|_X &\lesssim \|e^{(t-t_0)L}e^{t_0L}u_0\|_{X_{N_\infty}} \\ &\leq Ce^{-\lambda(t-t_0)}\|e^{t_0L}u_0\|_{X_{N_\infty}} \leq Ce^{-\lambda(t-t_0)}\alpha(t_0)\|u_0\|_X.\end{aligned}$$

This proves the result for any $t \geq t_0$. For $0 \leq t \leq t_0$ it is enough to use the well-posedness result in lemma 4.2.2. □

With this and the regularization result in lemma 4.2.3 one can obtain the following:

Corollary 4.2.5 (Regularization and spectral gap)**.** *Let us consider operator L, associate to the linear equation (4.2.1). There exists constants $\lambda > 0$, $\tilde{C} \geq 1$ such that for all initial condition $u_0 \in L^2(\varphi)$ with zero integral, the following inequality holds:*

$$\|e^{tL}u_0\|_X \leq \tilde{C}t^{-3/4}e^{-\lambda t}\|u_0\|_{L^2(\varphi)} \qquad \textit{for all } t > 0. \tag{4.2.12}$$

4.3 Firing rate and pseudo-equilibria sequences

This section deals with the study of sequences of firing rates, $\{N_{k,\infty}\}_{k\geq 0}$, and pseudo-equilibria, $\{p_{k,\infty}\}_{k\geq 0}$. Let us first give their definition:

Definition 4.3.1 (Firing rate sequence)**.** Given $b, V_R, V_F \in \mathbb{R}$, with $V_R < V_F$, and I the function (4.1.4), the *firing rate sequence* $\{N_{k,\infty}\}_{k\geq 0}$ associated to an initial firing rate $N_{0,\infty} > 0$ is recursively defined by

$$N_{k+1,\infty} := \frac{1}{I(N_{k,\infty})} \qquad k = 0, 1, 2, \dots \tag{4.3.1}$$

This sequence is well defined since $I(N) > 0$ for all $N > 0$. Associated to a firing rate sequence $\{N_{k,\infty}\}_{k\geq 0}$ we define the following pseudo-equilibria sequence:

Definition 4.3.2 (Pseudo-equilibria sequence)**.** Given a firing rate sequence $\{N_{k,\infty}\}_{k\geq 0}$ its associated *pseudo-equilibria sequence* is the sequence

$$p_{k,\infty}(v) = N_{k,\infty} e^{-\frac{\left(v - bN_{k-1,\infty}\right)^2}{2}} \int_{\max(v,V_R)}^{V_F} e^{\frac{\left(w - bN_{k-1,\infty}\right)^2}{2}} dw, \quad k = 1, 2, \dots \tag{4.3.2}$$

The behavior of these sequences depends only on the values of the connectivity parameter b, the diffusion coefficient a (which we consider to be 1), the reset potential V_R and the threshold potential V_F. Their definition is completely detached from the dynamics of the nonlinear system (4.1.1).

Before presenting the main results of this section, let us establish an auxiliary lemma that will be useful in subsequent demonstrations.

Lemma 4.3.3. *Let us consider $b \in (-\infty, 0]$ and $N(b)$ the solution to the equation $NI(b, N) = 1$, then, $g(b) := \frac{-\partial_N I(b,N(b))}{I(b,N(b))^2}$ is an increasing function, defined in $(-\infty, 0]$.*

Proof. We consider $v(s) := s^{-1} e^{-s^2/2} e^{-sbN(b)} \left(e^{sV_F} - e^{sV_R}\right)$, $w(s) := e^{-s^2/2} e^{-sbN(b)} \left(e^{sV_F} - e^{sV_R}\right)$ and $u(s) := se^{-s^2/2} e^{-sbN(b)} \left(e^{sV_F} - e^{sV_R}\right)$, and rewrite the function $I(b, N(b))$ and some of its useful derivatives as follows:

$$I(b, N(b)) = \int_0^\infty v(s) ds > 0,$$

$$\partial_N I(b, N(b)) = -b \int_0^\infty w(s) ds > 0, \quad \partial_b I(b, N(b)) = -N(b) \int_0^\infty w(s) < 0,$$

$$\partial_N^2 I(b, N(b)) = b^2 \int_0^\infty u(s) ds > 0, \text{ and } \partial_b \partial_N I(b, N(b)) = bN(b) \int_0^\infty u(s) ds - \int_0^\infty w(s) ds < 0,$$

In the following, to shorten the notation we write I instead of $I(b, N(b))$, N instead of $N(b)$ and N' instead of $\frac{\mathrm{d}N}{\mathrm{d}b}(b)$. Thus

$$g'(b) = \frac{-I\partial_b\partial_N I - N'I\partial_N^2 I + 2\partial_N I\partial_b I + 2N'\left(\partial_N I\right)^2}{I^3}. \tag{4.3.3}$$

We derive implicitly in $I(b, N(b))N(b) = 1$, and obtain $N' = \frac{-\partial_b I}{I^2+\partial_N I}$. Using it in (4.3.3)

$$g'(b) = \frac{-I^2\partial_b\partial_N I - \partial_N I\partial_b\partial_N I + \partial_b I\partial_N^2 I + 2I\partial_b I\partial_N I}{I^2(I^2+\partial_N I)}.$$

The denominator is positive, so we conclude the proof if we prove that the numerator is also positive.

$$\begin{aligned} g'(b)I^2(I^2+\partial_N I) = &-\left(\int_0^\infty v(s)ds\right)^2\left(bN\int_0^\infty u(s)ds - \int_0^\infty w(s)ds\right) \\ &+ b\int_0^\infty w(s)ds\left(bN\int_0^\infty u(s)ds - \int_0^\infty w(s)ds\right) \\ &- Nb^2\int_0^\infty w(s)ds\int_0^\infty u(s)ds + 2Nb\int_0^\infty v(s)ds\left(\int_0^\infty w(s)ds\right)^2 \\ = &-b\int_0^\infty v(s)ds\int_0^\infty u(s)ds + \left(\int_0^\infty v(s)ds\right)^2\int_0^\infty w(s)ds + b\left(\int_0^\infty w(s)ds\right)^2, \end{aligned}$$

where in the first and last terms we have used the equality $N = I^{-1} = \left(\int_0^\infty v(s)ds\right)^{-1}$. It can be easily seen by observing the sign of the different parameters, the only negative term is the last one, so that though the following Cauchy-Schwarz inequality

$$\int_0^\infty v(s)ds\int_0^\infty u(s)ds \geq \left(\int_0^\infty w(s)ds\right)^2, \quad \text{as} \quad w(s) = \sqrt{v(s)u(s)},$$

we cancel the last term with the first one and show that $\frac{\mathrm{d}}{\mathrm{d}b}\partial_N f(b, N(b)) > 0 \;\forall\, b < 0$. □

In the following theorems we show the monotonicity of the firing rates sequence $\{N_{k,\infty}\}_{k\geq 0}$, in terms of the number of solutions to the implicit equation

$$NI(N) = 1, \text{ with } 0 \leq N. \tag{4.3.4}$$

We have denoted the unknown in equation (4.3.4) by N and hope that it will not cause any confusion with the firing rate of the nonlinear system (4.1.1). In this section we never consider the system (4.1.1), since we are only concerned with the behavior of the firing rate sequence.

The number of solutions to equation (4.3.4) was studied in [14]. Analytically it was shown that for $b < 0$ or for a small positive value of b there is only one solution, there is no solution if $b > 0$ is large, and there are at least two for intermediate positive values of b. The proof is based on the study of the monotone function $1/I(N)$ (increasing if $b > 0$ and decreasing if $b < 0$). However, rigorously proving the exact number of solutions in the excitatory case ($b > 0$) is not easy, due to the complexity of I. Numerically we observe that for positive b there are a maximum of two solutions, and at the point where the equation switches from having two solutions to none the function $1/I(N)$ has slope equal to 1 and positive second derivative (see right plot of figure 4.2). These are the scenarios we consider in the following theorem for the case $b > 0$:

Theorem 4.3.4 (Monotonicity of the firing rate sequence $\{N_{k,\infty}\}_{k\geq 0}$ for excitatory networks)**.** *Let us consider $0 < b$ and a firing rate sequence $\{N_{k,\infty}\}_{k\geq 0}$ (as given by definition 4.3.1).*

1. *If N^* is the only solution to equation (4.3.4), then:*
   - (a) *If $N \to 1/I(N)$ crosses the line $N \to N$ at $N = N^*$ ($N < 1/I(N)$ if $N < N^*$ and $1/I(N) < N$ if $N^* < N$):*
     - *If $N^* \leq N_{0,\infty}$ then $\{N_{k,\infty}\}_{k\geq 0}$ is a decreasing sequence tending to N^*.*
     - *If $N_{0,\infty} \leq N^*$ then $\{N_{k,\infty}\}_{k\geq 0}$ is an increasing sequence tending to N^*.*
   - (b) *If $N \to 1/I(N)$ cut tangentially the line $N \to N$ at $N = N^*$ being $N < 1/I(N)$ if $N \neq N^*$:*
     - *If $N^* \leq N_{0,\infty}$ then $\{N_{k,\infty}\}_{k\geq 0}$ diverges.*
     - *If $N_{0,\infty} \leq N^*$ then $\{N_{k,\infty}\}_{k\geq 0}$ is an increasing sequence tending to N^*.*
2. *If equation (4.3.4) has no solutions, then $\{N_{k,\infty}\}_{k\geq 0}$ diverges.*
3. *If equation (4.3.4) has two solutions: N_1^* and N_2^* ($N_1^* < N_2^*$), then:*
   - *If $N_{0,\infty} \leq N_1^*$ then $\{N_{k,\infty}\}_{k\geq 0}$ is an increasing sequence which tends to N_1^*.*
   - *If $N_1^* \leq N_{0,\infty} \leq N_2^*$ then $\{N_{k,\infty}\}_{k\geq 0}$ is a decreasing sequence which tends to N_1^*.*
   - *If $N_2^* \leq N_{0,\infty}$ then $\{N_{k,\infty}\}_{k\geq 0}$ diverges.*

Proof. The function I (see (4.1.4)) is a $C^\infty(0,\infty)$ function, which was studied in the proof of [14, Theorem 3.1], and can be rewritten as $I(N) = \int_0^\infty e^{-s^2/2} e^{-sbN} \frac{e^{sV_F} - e^{sV_R}}{s}\ \mathrm{d}s$. Its k-th order derivative is

$$I^{(k)}(N) = (-b)^k \int_0^\infty s^{k-1} e^{-s^2/2} e^{-sbN} \left(e^{sV_F} - e^{sV_R}\right)\ \mathrm{d}s, \tag{4.3.5}$$

and for b positive:

- $\frac{1}{I(N)}$ is an increasing function.
- $\frac{1}{I(0)} < \infty$.
- $\lim_{N\to\infty} \frac{1}{I(N)} = \infty$.

The firing rate sequence is a solution to the recursive equation

$$N_{k+1,\infty} = f(N_{k,\infty}), \quad f : \mathbb{R}_0^+ \to \mathbb{R}^+, \ f(x) := \frac{1}{I(x)}, \tag{4.3.6}$$

and we have seen that f is an increasing function. The behavior of this type of discrete system is well known: its solutions are monotonic, and either diverge or converge to an equilibrium of the system. With the hypotheses of the theorem we have the following possibilities, since $f(0) > 0$:

- If N^* is the only solution to equation (4.3.4) then:
  - If $f(N)$ crosses the line $N \to N$ at $N = N^*$.
    - $N < f(N)$ if $N < N^*$.
    - $f(N) < N$ if $N^* < N$.
  - If $f(N)$ cut tangentially the line $N \to N$ at $N = N^*$ being $N < f(N)$ if $N \neq N^*$.
    - $N < f(N)$ if $N \neq N^*$.
- If equation (4.3.4) has two solutions, N_1^* and N_2^*, with $N_1^* < N_2^*$, then:
  - $N < f(N)$ if $N \in [0, N_1^*) \cup (N_2^*, +\infty)$.
  - $f(N) < N$ if $N \in (N_1^*, N_2^*)$.
- If equation (4.3.4) has no solutions, then $N < f(N)$ for all $N \geq 0$, because $0 < f(0)$.

The proof is easily done by analyzing the monotonicity of the sequence in each interval bounded by equilibria.

1. If the initial condition is taken in an interval in which $N < f(N)$ then the sequence is increasing, because $N_{k,\infty} < f(N_{k,\infty}) = N_{k+1,\infty}$.
2. If the initial condition is taken in an interval in which $f(N) < N$ then the sequence is decreasing, because $N_{k+1,\infty} = f(N_{k,\infty}) < N_{k,\infty}$.

Whenever the sequence is decreasing, it is bounded below by a constant solution of equation (4.3.6) and therefore converges to it (because there are no more equilibria in that interval). If the sequence is increasing, it either converges to an equilibrium, if bounded, or diverges. □

Remark 4.3.5. As a consequence of the convergence of the firing rate sequences, given in theorem 4.3.4, it follows:

1. If N^* is the only solution to equation (4.3.4), then:

   (a) In case 1.(a) of theorem 4.3.4, $\frac{d}{dN}\frac{1}{I(N)}|_{N^*} < 1$.

   (b) In case 1.(b) of theorem 4.3.4, $\frac{d}{dN}\frac{1}{I(N)}|_{N^*} = 1$.

   This behavior is shown in right plot of figure 4.2 with $b = 0$ or $b = 0.5$ for the first case and $b = 2.1$ the second case.

2. If equation (4.3.4) has two solutions: N_1^* and N_2^* ($N_1^* < N_2^*$), then:

   - $0 \leq \frac{d}{dN}\frac{1}{I(N)}|_{N_1^*} \leq 1$.
   - $1 < \frac{d}{dN}\frac{1}{I(N)}|_{N_2^*}$.

   This behavior is shown in right plot of figure 4.2 with $b = 1.5$.

We analyze the inhibitory case ($b < 0$) in the following theorem, where two different behaviors appear although in this case equation (4.3.4) has only one solution.

Theorem 4.3.6 (Monotonicity of the firing rates sequence $\{N_{k,\infty}\}_{k\geq 0}$ for inhibitory networks)**.** *Assume $b < 0$ and consider a firing rate sequence $\{N_{k,\infty}\}_{k\geq 0}$. Then there exists a value $b^* < b$ of the connectivity parameter b such that:*

- *If $b^* < b < 0$ the sequence $\{N_{k,\infty}\}_{k\geq 0}$ tends to the unique solution to equation (4.3.4), N^*.*
- *If $b < b^*$, there exist two values N^-, N^+, $0 \leq \min(N^-, N^+) < N^* < \max(N^-, N^+)$, such that the sequence $\{N_{k,\infty}\}_{k\geq 0}$ tends to the 2-cycle $\{N^-, N^+\}$.*

Proof. The proof, as in theorem 4.3.4, is based on the study of the recursive equation:

$$N_{k+1,\infty} = f(N_{k,\infty}), \qquad f(x) := \frac{1}{I(x)}, \tag{4.3.7}$$

where the function I, defined in (4.1.4), is a $C^\infty(0,\infty)$ increasing function if $b < 0$ (see (4.3.5) with $k = 1$). Therefore, for the inhibitory case, $f : \left[0, \frac{1}{I(0)}\right] \to \left[0, \frac{1}{I(0)}\right]$ since the function $1/I$ is decreasing, and, with the possible exception of the initial datum,

$N_{0,\infty}$, all the other terms in the sequence fall within the interval $\left[0, \frac{1}{I(0)}\right]$. Moreover, in this case, equation (4.3.4) has an unique solution, N^*, because $1/I(N)$ is a decreasing continuous function, which tends towards 0 and $0 < 1/I(0)$. The behavior of this type of discrete system is easy to study, because f is an decreasing function and the solutions are bounded; they tend to the unique equilibrium or towards 2-cycle. The proof of this result is as follows: we denote by N^* the equilibrium of (4.3.7) and suppose $N_{0,\infty} \neq N_{2,\infty}$ (otherwise, the solution would be a 2 cycle, which would be trivial if $N_{0,\infty} = N_{2,\infty} = N^*$). Thus, using that f is a decreasing function and $F := f \circ f$ is increasing:

- If $N_{0,\infty} \leq N_{2,\infty}$, then $N_{3,\infty} = f(N_{2,\infty}) \leq N_{1,\infty} = f(N_{0,\infty})$ and $N_{2,\infty} = F(N_{0,\infty}) \leq N_{4,\infty} = F(N_{2,\infty})$. Therefore, by induction we prove that $\{N_{2k,\infty}\}_{\{k\geq 0\}}$ is an increasing sequence and $\{N_{2k+1,\infty}\}_{\{k\geq 0\}}$ is a decreasing sequence.
- If $N_{0,\infty} \geq N_{2,\infty}$, then $N_{3,\infty} = f(N_{2,\infty}) \geq N_{1,\infty} = f(N_{0,\infty})$ and $N_{2,\infty} = F(N_{0,\infty}) \geq N_{4,\infty} = F(N_{1,\infty})$. Therefore, by induction we prove that $\{N_{2k,\infty}\}_{\{k\geq 0\}}$ is a decreasing sequence and $\{N_{2k+1,\infty}\}_{\{k\geq 0\}}$ is an increasing sequence.

Moreover:

- If $N_{0,\infty} \leq N^*$, then $N^* = f(N^*) \leq f(N_{0,\infty}) = N_{1,\infty}$ and $N_{2,\infty} = f(N_{1,\infty}) \leq f(N^*) = N^*$. Therefore, by induction we prove that $0 \leq N_{2k,\infty} \leq N^* \leq N_{2k+1,\infty} \leq \frac{1}{I(0)}$ for $k = 0, 1, 2, \ldots$.
- If $N^* \leq N_{0,\infty}$, then $f(N_{0,\infty}) = N_{1,\infty} \leq N^* = f(N^*)$ and $f(N^*) = N^* \leq N_{2,\infty} = f(N_{1,\infty})$. Therefore, by induction we prove that $0 \leq N_{2k+1,\infty} \leq N^* \leq N_{2k,\infty} \leq \frac{1}{I(0)}$ for $k = 0, 1, 2, \ldots$.

So that in either case, both sequences, $\{N_{2k,\infty}\}_{\{k\geq 0\}}$ and $\{N_{2k+1,\infty}\}_{\{k\geq 0\}}$, are monotonic and bounded, hence convergent. Thus, considering $N^- := \lim_{k\to\infty} N_{2k+1,\infty}$ and $N^+ := \lim_{k\to\infty} N_{2k,\infty}$ we obtain, since f is a continuous function, that $f(N^+) = N^-$ and there are two possibilities:

1. $N^- = N^+ = N^*$, so that the system tends towards the equilibrium.
2. $N^- \neq N^+$, so that the system tends towards the 2-cycle $\{N^-, N^+\}$, where $\min(N^-, N^+) < N^* < \max(N^-, N^+)$.

The remainder of the proof concentrates on determining b^*, which turns out to be the largest value at which N^* is asymptotically stable. We consider I as a function that also depends on b and use the notation $I(b, N)$, in case of referring to its dependency. We note that I is a decreasing function of b, since $\partial_b I(b, N) = -N \int_0^\infty e^{-s^2/2} e^{-sbN} \left(e^{sV_F} - e^{sV_R}\right) ds$, and consequently $1/I$ is increasing as function of b (see figure 4.2).

Therefore, if $b_1 < b_2 < 0$, then $\frac{1}{I(b_1,N)} < \frac{1}{I(b_2,N)}$ and the solution to equation (4.3.4) for value b_1, is less than the solution for b_2, that is $N^*_{b_1} < N^*_{b_2}$. We can also prove that N^*_b is increasing in b by deriving implicitly in the equation $N^*_b I(b, N^*_b) = 1$ and observing that the derivative is positive, as follows

$$\frac{dN^*_b}{db} = \frac{-N\partial_b I(b, N^*_b)}{I(b, N^*_b) + N^*_b \partial_N I(b, N^*_b)} \geq 0.$$

Consequently, N^*_b is an increasing function bounded from below by 0, so it has a limit when b tends to $-\infty$. On the other hand, when b tends to $-\infty$, $\frac{1}{I(b,N)}$ loses continuity at $N = 0$, because $\frac{1}{I(b,0)} > 0$, while it vanishes for $0 < N < 1/I(b, 0)$. Therefore, $\overline{N}^* := \lim_{b\to-\infty} N^*_b = 0$, because, if that limit is positive, we get a contradiction, since $0 = \lim_{b\to-\infty} \frac{1}{I(b,\overline{N}^*)} = \lim_{b\to-\infty} \frac{1}{I(b,N^*_b)} = \lim_{b\to-\infty} N^*_b = \overline{N}^* > 0$ (this limit was also proven in [87, Lemma 2.2]). Thus, in a certain sense, we can understand that the system loses its equilibrium, when b tends to $-\infty$, due to loss of continuity of function $1/I$.

To determine whether or not the equilibrium of equation (4.3.7), N^*_b, is asymptotically stable, we check if $|f'(N^*_b)|$ is less than or greater than 1. With this aim, we define

$$g(b) := f'(N^*_b) = \frac{d}{dN}\frac{1}{I(N)}|_{N^*_b} = \frac{-\partial_N I(b, N^*_b)}{I(b, N^*_b)^2} = -N^{*2}_b \partial_N I(b, N^*_b),$$

which is a continuous increasing function in $(-\infty, 0]$, due to the positivity of $g'(b)$, as proved in lemma 4.3.3. We note that $\lim_{b\to-\infty} g(b) = -\infty$ and $g(0) = f'(N^*_0) = 0$, thus there exists b^* such that $g(b^*) = -1$. Then, if $b < b^*$, thus $g(b) < -1$, which means that N^*_b is unstable, while for $b > b^*$, $g(b) > -1$ and N^*_b is stable. And from what has been proven above, if the equilibrium is unstable, the system tends to a 2-cycle. □

Remark 4.3.7. Two details could not be proved in theorem 4.3.6, due to the complexity of the function I: the stability of the equilibrium in the critical case, $b = b^*$, and the uniqueness of the two cycles, in the case $b < b^*$. However, we can check both numerically. Figure 4.3 shows the function $F(N) = f \circ f(N)$, for cases with $b < b^*$. F has only 3 fixed points, i.e., the equilibrium N^* and cycle $\{N^-, N^+\}$ corresponding to each value of b. Moreover, the 2-cycles appear as a bifurcation of the equilibrium, which is asymptotically stable for $b = b^*$, as this value is the starting point for the formation of 2-cycles. We also note that the 2-cycle $\{N^-, N^+\}$ becomes $\left\{0, \frac{1}{I(0)}\right\}$, approximately $\{0, 0.12\}$, when b tends to $-\infty$, as N^*_b tends to 0. For $b > b^*$ we observe an unique fixed point for $F(N)$, corresponding with the equilibrium N^*.

Remark 4.3.8. As a consequence of the convergence of the firing rate sequences, given in theorem 4.3.6, it follows:

1. If $b_* < b < 0$, then $-1 \leq \frac{d}{dN}\frac{1}{I(N)}|_{N^*} < 0$, for N^*, the only solution to equation (4.3.4).

2. If $b < b_*$, then $\frac{d}{dN}\frac{1}{I(N)}|_{N^*} \leq -1$, for N^*, the only solution to equation (4.3.4).

We have estimated numerically b^* around -9.4 (see figure 4.3), the left plot of figure 4.2 shows the function $\frac{1}{I(N)}$ for $b < -9.4$ and for $b > -9.4$, where we can observe its slope at N^*.

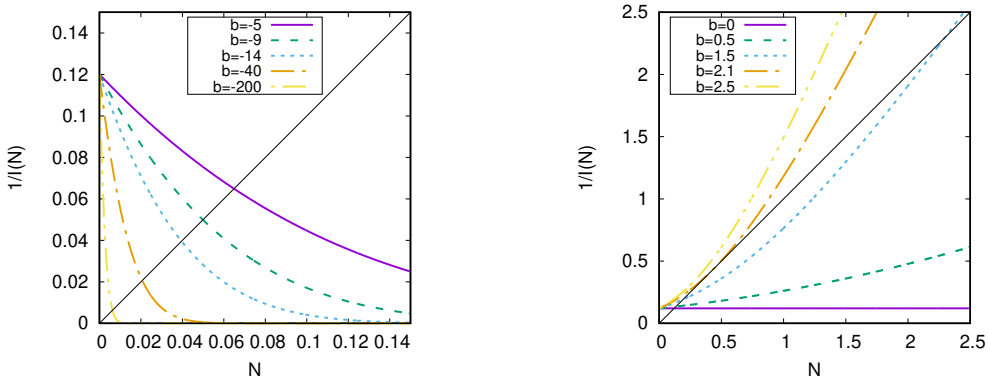

Figure 4.2: **Function $\frac{1}{I(N)}$ (see (4.1.4)) for different values of the connectivity parameter b.**

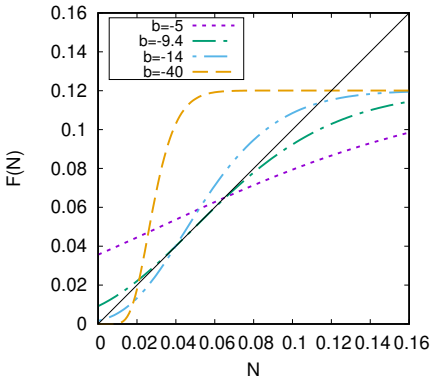

Figure 4.3: **Function $F := f \circ f$ with $f = 1/I(N)$ (see (4.1.4)) for different values of the connectivity parameter b.**

We recall that the number of solutions to the equation (4.3.4) gives us the number of steady states of the nonlinear system (4.1.1). And that number depends on the value of b (see [14]). For the excitatory case ($b > 0$) there is only one steady state if $b \leq V_F - V_R$, if $V_F - V_R < b$ there are two possibilities: there are at least two steady states (numerically

no more than two steady states have been observed), or, if b is large enough, there is not steady states. The case $b = V_F - V_R$ is very interesting because this is the limit value for which the notion of physical solutions makes sense. Numerically this case was analyzed in chapter 2 and without delay ($d = 0$) the particle system evolves to a plateau distribution, if the initial condition is concentrated enough around V_F. In a limit sense, this plateau profile is a stationary state of the system for $b = V_F - V_R$. However, the system tends to the unique steady state with bounded firing rate, if a large transmission delay is considered. For the inhibitory case ($b < 0$) there is only one steady state. Therefore, theorems 4.3.4 and 4.3.6 can also be read in terms of the number of the steady states of the nonlinear system (4.1.1).

Remark 4.3.9. theorem 4.3.4 does not include the case with more than two equilibria, which can be easily extended following the same strategy. For instance, if equation (4.3.4) has three solutions (i.e. the nonlinear system (4.1.1) has three steady states), $N_1^* < N_2^* < N_3^*$, the sequence $\{N_{k,\infty}\}_{k\geq 0}$ tends to N_1^*, if $N_{0,\infty} \in (0, N_2^*)$, and to N_3^*, if $N_{0,\infty} \in (N_2^*, +\infty)$. In general, the behavior of the sequence $\{N_{k,\infty}\}_{k\geq 0}$ depends on whether $N_k I(N_k) < 1$ or $1 < N_k I(N_k)$. In the first case the sequence is increasing, while in the second case the sequence is decreasing. When the sequence is decreasing it converges to some solution to equation (4.3.4), while if the sequence is increasing it converges or diverges depending on whether it is bounded by a solution to the implicit equation or not.

The following theorem shows that the pseudo-equilibria sequence $\{p_{k,\infty}(v)\}_{k\geq 0}$ described in (4.3.2) tends to a stationary solution p_∞ of the nonlinear system (4.1.1) if its related sequence $\{N_{k,\infty}\}_{k\geq 0}$ (see (4.3.1)) converges to a finite value N_∞, which is the firing rate of p_∞.

Theorem 4.3.10. *Considering the firing rate sequence $\{N_{k,\infty}\}_{k\geq 0}$ given in (4.3.1), and its related pseudo-equilibria sequence $\{p_{k,\infty}(v)\}_{k\geq 0}$ described in (4.3.2), if $\lim_{k\to\infty} N_{k,\infty} = N_\infty$ and $N_\infty < \infty$, then $\exists\ k_0 \in \mathbb{N}$ such that for all $k \geq k_0$ the following inequalities hold:*

$$|p_{k+1,\infty}(v) - p_{k,\infty}(v)| \leq C_{N_\infty} |N_{k,\infty} - N_{k-1,\infty}|, \quad \forall v \in (-\infty, V_F], \tag{4.3.8}$$

$$|\partial_v p_{k+1,\infty}(v) - \partial_v p_{k,\infty}(v)| \leq C_{N_\infty} |N_{k,\infty} - N_{k-1,\infty}|, \quad \forall v \in (-\infty, V_F], \tag{4.3.9}$$

where $C_{N_\infty} > 0$ is a constant that depends on N_∞. Consequently,

$$\lim_{k\to\infty} \|p_{k,\infty}(.) - p_\infty(.)\|_\infty = 0 \quad \textit{and} \quad \lim_{k\to\infty} \|\partial_v p_{k,\infty}(.) - \partial_v p_\infty(.)\|_\infty = 0,$$

with $p_\infty(v)$ a steady state of the nonlinear system (4.1.1) with firing rate N_∞. Moreover, $\{p_{k,\infty}(v)\}_{k\geq 0}$ and $\{\partial_v p_{k,\infty}(v)\}_{k\geq 0}$ converge to p_∞ and $\partial_v p_\infty$, respectively, in the $L^2(\varphi_N)$ norm, with $\varphi_N(v) = e^{\frac{(v-bN)^2}{2}}$, and $N \in \mathbb{R}$.

Proof. We recall the expression of the pseudo-equilibrium

$$p_{k,\infty}(v) = N_{k,\infty} e^{-\frac{\left(v-bN_{k-1,\infty}\right)^2}{2}} \int_{\max(v,V_R)}^{V_F} e^{\frac{\left(w-bN_{k-1,\infty}\right)^2}{2}} dw,$$

where $N_{k,\infty} = I(N_{k-1,\infty})^{-1}$ and $I(N) = \int_{-\infty}^{V_F} e^{-\frac{(v-bN)^2}{2}} \int_{\max(v,V_R)}^{V_F} e^{\frac{(w-bN)^2}{2}} dwdv$. We also note that, if N_∞ is the limit of $\{N_{k,\infty}\}_{k\geq 0}$, it is a fixed point of the implicit equation $NI(N) = 1$ and

$$p_\infty(v) = N_\infty e^{-\frac{(v-bN_\infty)^2}{2}} \int_{\max(v,V_R)}^{V_F} e^{\frac{(w-bN_\infty)^2}{2}} dw,$$

is a steady state of the nonlinear system (4.1.1).

For a fixed value of v, we define the function $h(v, N_{k-1,\infty}) := p_{k,\infty}(v)$, which is written as $h(v, N_{k-1,\infty}) = \frac{g(v,N_{k-1,\infty})}{I(N_{k-1,\infty})}$ defining $g(v, N) := e^{-\frac{(v-bN)^2}{2}} \int_{\max(v,V_R)}^{V_F} e^{\frac{(w-bN)^2}{2}} dw$. Through a first order Taylor's expansion, in N variable, we can write the difference between two consecutive elements of the sequence $\{p_{k,\infty}\}_{k\geq 0}$ as

$$p_{k+1,\infty}(v) - p_{k,\infty}(v) = \partial_N h(v, \xi_k) \left(N_{k,\infty} - N_{k-1,\infty}\right),$$

where ξ_k is a value located between $N_{k-1,\infty}$ and $N_{k,\infty}$. By computing $\partial_N h(v, N)$ we obtain

$$\partial_N h(v, N) = \frac{\partial_N g(v, N)}{I(N)} - \frac{I'(N)}{I(N)^2} g(v, N). \tag{4.3.10}$$

Given $\epsilon > 0$, $\exists\ k_0 \in \mathbb{N}$ such that $N_{k-1,\infty}$ and $N_{k,\infty} \in (N_\infty - \epsilon, N_\infty + \epsilon)$ for all $k \geq k_0$, because $\lim_{k\to\infty} \{N_{k,\infty}\}_{k\geq 0} = N_\infty < \infty$. In particular, $\xi_k \in (N_\infty - \epsilon, N_\infty + \epsilon)$ for all $k \geq k_0$. Therefore, if $|\partial_N h(v, N_\infty)| < \infty$ we obtain that $|\partial_N h(v, \xi_k)| < C_{N_\infty}$ for all $k \geq k_0$ (by continuity) and inequality (4.3.8) is proven, since constant C_{N_∞} only depends on N_∞. Then, we compute

$$\partial_N h(v, N_\infty) = N_\infty \partial_N g(v, N_\infty) - N_\infty I'(N_\infty) p_\infty(v) \tag{4.3.11}$$

using that $N_\infty I(N_\infty) = 1$, since N_∞ is the stationary firing rate. We observe that $p_\infty(v) = N_\infty e^{-\frac{(v-bN_\infty)^2}{2}} \int_{\max(v,V_R)}^{V_F} e^{\frac{(w-bN_\infty)^2}{2}} dw$ is a smooth equilibrium of the (4.1.1), with $vp_\infty(v) = 0$ at $v = -\infty$ and then it is bounded on $(-\infty, V_F]$. Moreover, $I \in C^\infty((0,\infty))$, thus $I'(N_\infty) < \infty$ (see (4.3.5) and [14]). Consequently, to prove $|\partial_N h(v, N_\infty)| < \infty$ we need to show that $\partial_N g(v, N_\infty) < \infty$. For that purpose, we explicitly write $N_\infty \partial_N g(v, N_\infty)$ as

$$N_\infty \partial_N g(v, N_\infty) = \begin{cases} b(v - bN_\infty)p_\infty - bN_\infty e^{-\frac{(v-bN_\infty)^2}{2}} \left(e^{\frac{(V_F-bN_\infty)^2}{2}} - e^{\frac{(V_R-bN_\infty)^2}{2}} \right) \text{ if } v < V_R, \\ b(v - bN_\infty)p_\infty - bN_\infty \left(e^{-\frac{(v-bN_\infty)^2}{2}} e^{\frac{(V_F-bN_\infty)^2}{2}} - 1 \right) \text{ if } V_R \leq v \leq V_F. \end{cases}$$

We note that $N_\infty \partial_N g(v, N_\infty) < \infty$ since N_∞, $p_\infty(v)$, $v p_\infty(v)$ and $e^{-\frac{(v-bN_\infty)^2}{2}}$ are bounded, and therefore, (4.3.8) has been proven.

In analogous way we can prove for all $v \in (-\infty, V_F]$

$$|p_{k,\infty}(v) - p_\infty(v)| \leq C_\infty \left| N_{k,\infty} - N_\infty \right|,$$

and then $\lim_{k\to\infty} \|p_{k,\infty}(v) - p_\infty(v)\|_\infty = 0$, because $\{N_{k,\infty}\}_{k>0}$ tends to N_∞.

In order to control the $L^2(\varphi_N)$ norm we analyze the dependence on v of $\partial_N h(v, N_\infty)^2$ (see (4.3.11)),

$$\partial_N h(v, N_\infty)^2 = (N_\infty \partial_N g(v, N_\infty))^2 + \left(N_\infty I'(N_\infty) p_\infty(v)\right)^2 - 2N_\infty^2 I'(N_\infty) p_\infty(v) \partial_N g(v, N_\infty),$$

in comparison with $\varphi_N(v)$. To be more precise we can prove that

$$\int_{-\infty}^{V_F} \varphi_N(v) \partial_N h(v, N_\infty)^2 \, dv$$

is bounded by a constant depending on N_∞, because the integrals of type $e^{-(v-bN_\infty)^2}\varphi_N(v)$, $(c_1 v^2 + c_2 v) p_\infty(v)^2 \varphi_N(v)$, and $(c_1 v^2 + c_2 v) p_\infty(v) e^{-\frac{(v-bN_\infty)^2}{2}} \varphi_N(v)$, with $c_1, c_2 \in \mathbb{R}$, are bounded.

Finally, we need to study the sequence of $\partial_v p_{k,\infty}(v)$

$$\partial_v p_{k,\infty}(v) = \begin{cases} -(v - bN_{k-1,\infty}) p_{k,\infty}(v) & \text{if } v < V_R, \\ -(v - bN_{k-1,\infty}) p_{k,\infty}(v) - N_{k,\infty} & \text{if } V_R < v \leq V_F. \end{cases}$$

Thus, using the pointwise convergence of $\{p_{k,\infty}(v)\}_{k\geq 0}$, already proved, and the convergence of $\{N_{k,\infty}\}_{k\geq 0}$, we prove the pointwise convergence of $\{\partial_v p_{k,\infty}(v)\}_{k\geq 0}$ to $\partial_v p_\infty(v)$. And, finally, in analogous way as before, we obtain the converge in the $L^2(\varphi_N)$ norm, using

$$\begin{aligned} \partial_N \partial_v h(v, N_\infty) &= b p_\infty(v) - b(v - bN_\infty)^2 p_\infty(v) \\ &+ bN_\infty (v - bN_\infty) e^{\frac{-(v-bN_\infty)^2}{2}} \left(e^{\frac{(V_F - bN_\infty)^2}{2}} - e^{\frac{(\max(v, V_R) - bN_\infty)^2}{2}} \right) \\ &- N_\infty I'(N_\infty) \partial_v p_\infty(v). \end{aligned}$$

□

For the inhibitory case, the firing rate sequences can converge to 2-cycles (see theorem 4.3.6). We show the long-term behavior of the pseudo-equilibria sequences in those cases in the following theorem.

Theorem 4.3.11. *Let us consider the firing rate sequence* $\{N_{k,\infty}\}_{k\geq 0}$ *given in* (4.3.1)*, and its related pseudo-equilibria sequence* $\{p_{k,\infty}(v)\}_{k\geq 0}$ *described in* (4.3.2)*, if the sequence* $\{N_{k,\infty}\}_{k\geq 0}$ *tends to the 2-cycle* $\{N^-, N^+\}$*, then* $\exists\ k_0 \in \mathbb{N}$ *such that for all* $k \geq k_0$ *the following inequality holds:*

$$|p_{2k,\infty}(v) - p_{2k-2,\infty}(v)| \leq C_{N^-}|N_{2k-1,\infty} - N_{2k-3,\infty}|, \quad \forall v \in (-\infty, V_F], \tag{4.3.12}$$

$$|p_{2k+1,\infty}(v) - p_{2k-1,\infty}(v)| \leq C_{N^+}|N_{2k,\infty} - N_{2k-2,\infty}|, \quad \forall v \in (-\infty, V_F], \tag{4.3.13}$$

where $C_{N^-}, C_{N^+} > 0$ *depend on* N^- *and* N^+*, respectively. Consequently,*

$$\{p_{2k-1,\infty}(v)\}_{k\geq 1} \to p^-(v) \text{ when } k \to \infty,\ \forall v \in (-\infty, V_F]\,,$$

$$\{p_{2k,\infty}(v)\}_{k\geq 0} \to p^+(v) \text{ when } k \to \infty,\ \forall v \in (-\infty, V_F]\,,$$

where $p^-(v), p^+(v)$ *are pseudo-equilibria of the nonlinear system* (4.1.1) *(see* (4.1.5)*), given by*

$$p^-(v) = N^- e^{-\frac{\left(v-bN^+\right)^2}{2}} \int_{\max(v,V_R)}^{V_F} e^{\frac{\left(w-bN^+\right)^2}{2}} dw, \quad N^- = \frac{1}{I(N^+)} \tag{4.3.14}$$

and

$$p^+(v) = N^+ e^{-\frac{\left(v-bN^-\right)^2}{2}} \int_{\max(v,V_R)}^{V_F} e^{\frac{\left(w-bN^-\right)^2}{2}} dw, \quad N^+ = \frac{1}{I(N^-)}, \tag{4.3.15}$$

respectively, (see (4.1.4) *for a reminder of what* I *is).*

Proof. The proof is analogous to that of the theorem 4.3.10, so we follow the same notation as in it. We note that the properties of the equilibria used in the previous theorem for $p_\infty(v)$ and $N_\infty I(N_\infty)$, such as $p_\infty(v)$ bounded in $v \in (-\infty, V_F]$ and $N_\infty I(N_\infty) = 1$, will be also true for the pseudo-equilibria $p^+(v)$, $p^-(v)$ and $N^+I(N^-)$, $N^-I(N^+)$. The main ingredient here is to consider the corresponding subsequences with even and odd terms. In this way, we write the difference between two odd or even consecutive elements of the sequence $\{N_{k,\infty}\}_{k\geq 0}$, for all $v \in (-\infty - V_F]$, by using first order Taylor expansions over expression (4.3.2):

$$p_{2k,\infty}(v) - p_{2k-2,\infty}(v) = \partial_N h\left(v, \xi_k^-\right)\left(N_{2k-1,\infty} - N_{2k-3,\infty}\right),$$

$$p_{2k+1,\infty}(v) - p_{2k-1,\infty}(v) = \partial_N h\left(v, \xi_k^+\right)\left(N_{2k,\infty} - N_{2k-2,\infty}\right),$$

with ξ_k^-, ξ_k^+ real values between $N_{2k-1,\infty}$ and $N_{2k-3,\infty}$, or $N_{2k,\infty}$ and $N_{2k-2,\infty}$, respectively. Given $\epsilon > 0$, $\exists\ k_0 \in \mathbb{N}$ such that $N_{2k-1,\infty}$ and $N_{2k-3,\infty} \in (N^- - \epsilon, N^- + \epsilon)$, while $N_{2k,\infty}$ and $N_{2k-2,\infty} \in (N^+ - \epsilon, N^+ + \epsilon)$ for all $k \geq k_0$, because $\lim_{k\to\infty}\{N_{2k-1,\infty}\}_{k\geq 1} = N^- < \infty$ and $\lim_{k\to\infty}\{N_{2k,\infty}\}_{k\geq 0} = N^+ < \infty$. This means that $\xi_k^- \in (N^- - \epsilon, N^- + \epsilon)$ and

$\xi_k^+ \in (N^+ - \epsilon, N^+ + \epsilon)$ for all $k \geq k_0$. Thus, the proof of this theorem lies in proving that $|\partial_N h(v, N^-)| < \infty$ and $|\partial_N h(v, N^+)| < \infty$, because, as a consequence (by continuity), we obtain that $|\partial_N h(v, \xi_k^-)| < C_{N^-}$ and $|\partial_N h(v, \xi_k^+)| < C_{N^+}$ for all $k > k_0$, and certain $k_0 \geq 2$.

As we did in the calculations for theorem 4.3.10 we write $\partial_N h(v, N)$ (see (4.3.10)) as

$$\partial_N h(v, N) = \frac{\partial_N g(v, N)}{I(N)} - \frac{I'(N)}{I(N)^2} g(v, N),$$

what can be rewritten for N^- and N^+ as follows:

$$\partial_N h(v, N^-) = N^+ \partial_N g(v, N^-) - N^+ I'(N^-) p^+(v),$$

$$\partial_N h(v, N^+) = N^- \partial_N g(v, N^+) - N^- I'(N^+) p^-(v).$$

As stated in the proof of theorem 4.3.10, the only terms that we do not directly control are $\partial_N g(v, N^-)$ and $\partial_N g(v, N^+)$, whose explicit forms can be written, multiplied by N^- and N^+ respectively, as

$$N^+ \partial_N g(v, N^-) = \begin{cases} b(v - bN^-)p^+ - bN^- e^{-\frac{\left(v - bN^-\right)^2}{2}} \left(e^{\frac{\left(V_F - bN^-\right)^2}{2}} - e^{\frac{\left(V_R - bN^-\right)^2}{2}} \right) \text{ if } v < V_R \\ b(v - bN^-)p^+ - bN^- \left(e^{-\frac{\left(v - bN^-\right)^2}{2}} e^{\frac{\left(V_F - bN^-\right)^2}{2}} - 1 \right) \text{ if } V_R \leq v \leq V_F, \end{cases}$$

and

$$N^- \partial_N g(v, N^+) = \begin{cases} b(v - bN^+)p^- - bN^+ e^{-\frac{\left(v - bN^+\right)^2}{2}} \left(e^{\frac{\left(V_F - bN^+\right)^2}{2}} - e^{\frac{\left(V_R - bN^+\right)^2}{2}} \right) \text{ if } v < V_R \\ b(v - bN^+)p^- - bN^+ \left(e^{-\frac{\left(v - bN^+\right)^2}{2}} e^{\frac{\left(V_F - bN^+\right)^2}{2}} - 1 \right) \text{ if } V_R \leq v \leq V_F. \end{cases}$$

In an analogous way we show that they are bounded, using that N^-, N^+, $p^-(v)$, $p^+(v)$, $vp^-(v)$ are $vp^+(v)$ are bounded.

□

We point out that the behavior of the pseudo-equilibria sequence is determined by the limit of the firing rate sequence, in case it exists, for all $b \in \mathbb{R}$. And there is a relation between the nonlinear system (4.1.1) and that long-term behavior:

- For the excitatory case ($b > 0$) the pseudo-equilibria sequence $\{p_{k,\infty}(v)\}_{k \geq 0}$:
  - converges to the unique steady state of the nonlinear system (4.1.1), if b is small.

  - converges to the steady state with lower firing rate of the nonlinear system (4.1.1), if the system has two stationary solutions and if $\{N_{k,\infty}\}_{k\geq 0}$ has finite limit.

- For the inhibitory case ($b < 0$) the pseudo-equilibria sequence $\{p_{k,\infty}(v)\}_{k\geq 0}$ tends to the unique stationary solution $p_\infty(v)$ of the nonlinear system (4.1.1), if $b^* < b$. Otherwise, if $b < b^*$, it tends to a 2-cycle $\{p^-(v), p^+(v)\}$, which are pseudo-equilibria of the nonlinear system (4.1.1).

To prove the convergence of the pseudo-equilibria sequence we use the fact that the limit of $\{N_{k,\infty}\}_{k\geq 0}$ is finite or is a 2-cycle, so it could not be used in case the sequence diverges. However, in that case, it could be prove that the sequence of pseudo-equilibria $\{p_{k,\infty}(v)\}_{k\geq 0}$ tends to plateau distribution (point-wise in $(-\infty, V_R) \cup (V_R, V_F)$).

In the following section we use theorem 4.3.10 to prove the convergence to equilibrium of solutions to the nonlinear system (4.1.1) in the weakly connected case, by following the associated pseudo-equilibria sequence. As presented, this technique only works in weakly connected networks, but it might be possible to use it for a wider range of b. The strategy in chapter 3 was suggested by this sequence, and is valid for a general connectivity parameter b.

4.4 Convergence to equilibrium along the pseudo equilibria sequence for weakly connected networks

In this section we study the long-term behavior of the nonlinear system (4.1.1), considering large transmission delay values, by following the pseudo-equilibria (4.3.2) for weakly connected networks. To do this, we consider the solution to the Cauchy problem associated with (4.1.1) (remember we assume $a = 1$):

$$\begin{cases} \partial_t p(v,t) + \partial_v \left[(-v + bN(t-d))\, p(v,t)\right] - \partial_v^2 p(v,t) = \delta(v - V_R)N(t), \\ N(t) = -\partial_v p(V_F, t), \text{ for } t \geq 0, \\ p(0,v) = p_0(v), \text{ and, } N(t) = -\partial_v p_0(V_F) \quad t \in [-d, 0], \end{cases} \tag{4.4.1}$$

as a sequence of functions, considering time in intervals of length d. Our initial condition is always a constant on $[-d, 0]$, and we observe that the system becomes linear for $0 \leq t < d$, since $N(t-d)$ is constant.

Therefore, for $0 \leq t < d$, the Cauchy problem (4.4.1) behaves like a linear problem of the form

$$\begin{cases} \partial_t p(v,t) + \partial_v \left[\left(-v + b\overline{N} \right) p(v,t) \right] - \partial_v^2 p(v,t) = \delta(v - V_R) N(t), \\ N(t) = -\partial_v p(V_F, t), \quad t \geq 0, \\ p(0,v) = p_0(v), \text{ with } \overline{N} = -\partial_v p_0(V_F) \geq 0. \end{cases}$$

During that interval of time, $[0, d)$, we obtain $N(t)$, which is necessary for the drift term, in the following period of time with size d, $[d, 2d)$. Consequently, proceeding in the same way in the following time intervals $[kd, (k+1)d)$ with $k = 2, 3, \ldots$, the behavior of the nonlinear problem (4.4.1) is described in terms of a sequence of linear problems of the type

$$\begin{cases} \partial_t p(v,t) + \partial_v \left[h\left(v, \overline{N}(t)\right) p(v,t) \right] - \partial_v^2 p(v,t) = \delta(v - V_R) N(t), \\ N(t) = -\partial_v p(V_F, t), \quad t \geq 0, \end{cases}$$

where $\overline{N}(t)$ is a known function. To describe the idea more simply, let us consider the following notation (see figure 4.4):

$$p_{k+1}(v,t) := p(v, t + kd), \text{ with } t \in [0, d], \ v \in (-\infty, V_F] \text{ and } k = 0, 1, 2... \tag{4.4.2}$$

In other words, $p_{k+1}(v,t) \equiv p(v, \bar{t})$, with $\bar{t} := t + kd \in [kd, (k+1)d)$. Similarly,

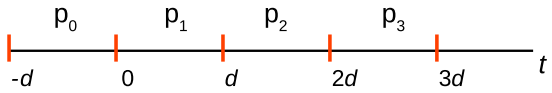

Figure 4.4: **Schematic representation of the solution to the Cauchy problem (4.4.1) in time through the sequence $p_k(v,t)$ given by (4.4.2).**

$$N_k(t) := N(t + kd), \qquad t \in [-d, 0], k = 0, 1, 2, \ldots$$

Hence we write the nonlinear problem (4.4.1) in any interval $(kd, (k+1)d)$, as follows: for $t \in (0, d)$ and $k = 1, 2, \ldots$

$$\begin{cases} \partial_t p_k(v,t) + \partial_v \left[(-v + bN_{k-1}(t-d)) \, p_k(v,t) \right] - \partial_v^2 p_k(v,t) = \delta(v - V_R) N_k(t), \\ N_k(t) = -\partial_v p_k(V_F, t), \ p_k(V_F) = 0, \end{cases} \tag{4.4.3}$$

Its related stationary problem is given by

$$\begin{cases} \partial_v \left[(-v + bN_{k-1,\infty})\, p_{k,\infty}(v)\right] - \partial_v^2 p_{k,\infty}(v) = \delta(v - V_R) N_{k,\infty}, \\ N_{k,\infty} = -\partial_v p_{k,\infty}(V_F), \text{ and } \int_{-\infty}^{V_F} p_{k,\infty}(v) dv = 1, \end{cases} \tag{4.4.4}$$

whose unique solution is the pseudo-equilibrium sequence (see (4.3.2))

$$p_{k,\infty}(v) = N_{k,\infty} e^{-\frac{\left(v - bN_{k-1,\infty}\right)^2}{2}} \int_{\max(v,V_R)}^{V_F} e^{\frac{\left(w - bN_{k-1,\infty}\right)^2}{2}} \, \mathrm{d}w, \tag{4.4.5}$$

given in terms of the firing rate sequence (4.3.1), with $N_{0,\infty} := -\partial_v p_0(V_F)$. Finally, we consider the space X given by

$$X := \{u \in \mathcal{C}(-\infty, V_F] \cap \mathcal{C}^1(-\infty, V_R] \cap \mathcal{C}^1[V_R, V_F] \mid u(V_F) = 0 \text{ and } \|u\|_X < \infty\}, \tag{4.4.6}$$

where

$$\|u\|_X := \|u\|_\infty + \|\partial_v u\|_\infty + \|u\|_{L^2(\varphi)} + \|\partial_v u\|_{L^2(\varphi)} \tag{4.4.7}$$

and

$$\varphi(v) := \exp\left(\frac{v^2}{2}\right), \qquad v \in (-\infty, V_F].$$

With this notation we will prove the following result:

Theorem 4.4.1. *Take $b \in \mathbb{R}$. Let us consider an initial condition $p_0 \in X$ for the nonlinear system (4.1.1) such that the firing rate sequence $\{N_{k,\infty}\}_{k\geq 0}$ with initial condition $N_{0,\infty} = -\partial_v p_0(V_F)$ converges to a certain value $N_\infty > 0$ (which must then satisfy $N_\infty I(N_\infty) = 1$). Let p_∞ be the stationary solution to (4.1.1) with firing rate N_∞. Let us assume that there exists $K > 0$ such that*

$$\|p_k(.,t) - p_{k,\infty}(.)\|_X \leq K \qquad \text{for all } k \geq 1 \text{ and all } t \in [0, d].$$

Then there exist $d_0, b_0, Q, \mu > 0$ such that the solution p to the nonlinear system (4.1.1) with $d > d_0$, $|b| < b_0$, and initial condition p_0 satisfies

$$\|p(.,t) - p_\infty(.)\|_X \leq Q e^{-\mu t} \|p_0 - p_\infty\|_X \qquad \text{for all } t \geq 0. \tag{4.4.8}$$

The proof is based on: 1) Proposition 4.2.4, which gives a spectral gap for linear systems; 2) Theorem 4.3.10, which shows

$$\|p_{k+1,\infty} - p_{k,\infty}\|_X \leq C_{N_\infty} |N_{k,\infty} - N_{k-1,\infty}|, \tag{4.4.9}$$

and, therefore $\|p_{k+1,\infty} - p_{k,\infty}\|_X \to 0$ as $\lim_{k\to\infty} N_{k,\infty} = N_\infty$; and, 3) the following two lemmas. The first lemma is a discrete version of the variation of constants technique:

Lemma 4.4.2 (Discrete variation of constants)**.** *Let M be a linear operator on a certain vector space E, and $\{b_k\}_{k\geq 0}$ any sequence in E. Then, given $a_0 \in E$, the sequence*

$$a_k := M^k a_0 + \sum_{i=0}^{k-1} M^{k-i-1} b_i, \quad k = 1, 2, \dots$$

is the (unique) solution to the linear equation

$$a_k = M a_{k-1} + b_{k-1}, \quad k = 1, 2, \dots. \tag{4.4.10}$$

Proof. We easily prove that $a_k = M^k a_0 + \sum_{i=0}^{k-1} M^{k-i-1} b_i$ fulfills equation (4.4.10):

$$M\left[M^{k-1}a_0 + \sum_{i=0}^{k-2} M^{k-i-2} b_i\right] + b_{k-1} = M^k a_0 + \sum_{i=0}^{k-1} M^{k-i-1} b_i.$$

□

The last lemma needed for the proof of theorem 4.4.1 is a discrete version of Gronwall's Lemma.

Lemma 4.4.3 (Discrete Gronwall's Lemma)**.** *If ϕ_k is a positive sequence and $W \in \mathbb{R}$, $V \geq 0$ are constants such that $\phi_k \leq W + V \sum_{i=0}^{k-1} \phi_i$ for $k \geq 0$, then $\phi_k \leq W e^{kV}$ for all $k \geq 0$.*

Proof. To prove the result we define the sequence $\psi_k := W + V \sum_{i=0}^{k-1} \phi_i$ for $k \geq 1$ and $\psi_0 := W$. We compute de difference between two consecutive elements of that sequence and then we write it down in terms of the sequence ϕ_k:

$$\psi_k - \psi_{k-1} = V\phi_{k-1} \leq V\left(W + V\sum_{i=0}^{k-2} \phi_i\right) = V\psi_{k-1},$$

which leads to

$$\phi_{k-1} \leq \psi_{k-1},$$

and

$$\psi_k \leq (1+V)\psi_{k-1} \implies \psi_k \leq (1+V)^k \psi_0 = (1+V)^k W.$$

Then we have the result, since $(1+V) \leq e^V$:

$$\phi_k \leq (1+V)^k W < W e^{kV}.$$

□

Proof of theorem 4.4.1. The proof is based on the study of the nonlinear system (4.1.1) in time intervals of size d, in which the system becomes linear. To do that we start with the

nonlinear system (4.4.3) for $t \in (0, d)$ and $k = 1, 2, \ldots$, and define

$$u_k(v,t) := p_k(v,t) - p_{k,\infty}(v),$$

the differences to the pseudo-equilibria $p_{k,\infty}(v)$. With this notation we rewrite the nonlinear system (4.4.3), splitting the equation in a linear part plus a nonlinear part:

$$\partial_t u_k(v,t) = L_{k-1}u_k(v,t) + b(N_{k-1,\infty} - N_{k-1})\partial_v p_k(v,t),$$

with the same Dirichlet boundary condition as before and defining the linear operator L_{k-1}, associated to the firing rate $N_{k-1,\infty}$, acting on $u = u(v)$, by

$$L_{k-1}u := \partial_v(v - bN_{k-1,\infty}u) + \partial_v^2 u + \delta(v - V_R)N_u,$$

where $N_u := -\partial_v u(V_F)$ emphasizes that N_u is the firing rate associated to u. By Duhamel's formula we get

$$u_k(v,t) = e^{tL_{k-1}}u_k(v,0) + b\int_0^t (N_{k-1,\infty} - N_{k-1}(s))e^{(t-s)L_{k-1}}\partial_v p_k(v,s)\,\mathrm{d}s.$$

Taking the X norm we note that $|N_{k-1,\infty} - N_{k-1}(t)| \leq \|u_k(.,t)\|_X$, and using the spectral gap of L_{k-1} in X (see proposition 4.2.4):

$$\|e^{tL_{k-1}}u_0\|_X \leq Ce^{-\lambda t}\|u_0\|_X, \quad 1 \leq C,$$

we have, for all $t \geq 0$:

$$\begin{aligned}
\|u_k(.,t)\|_X &\leq Ce^{-\lambda t}\|u_k(.,0)\|_X + |b|\int_0^t |N_{k-1,\infty} - N_{k-1}(s)|\,\|e^{(t-s)L_{k-1}}\partial_v p_k(.,s)\|_X\,\mathrm{d}s \\
&\leq Ce^{-\lambda t}\|u_k(.,0)\|_X + |b|\int_0^t \|u_{k-1}(.,s)\|_X\,\|e^{(t-s)L_{k-1}}\partial_v p_k(.,s)\|_X\,\mathrm{d}s \\
&\leq Ce^{-\lambda t}\|u_k(.,0)\|_X + \tilde{C}|b|\int_0^t e^{-\lambda(t-s)}(t-s)^{-3/4}\|u_{k-1}(.,s)\|_X\|\partial_v p_k(.,s)\|_{L^2(\varphi)}ds,
\end{aligned}$$

where in the last inequality we used corollary 4.2.5, written in this particular case as

$$\|e^{(t-s)L_{k-1}}\partial_v p_k(.,s)\|_X \leq \tilde{C}(t-s)^{-3/4}e^{-\lambda(t-s)}\|\partial_v p_k(.,s)\|_{L^2(\varphi)}.$$

Remark 4.4.4. We are considering the same value of λ for all the spectral gaps of the operators L_k with $k = 1, 2, ...$, because these values come from the Poincare's like inequality used to prove the spectral gap of the linear equation in the space $L^2_{(p_\infty^{-1})}$ (see [14, Appendix]). These values depend only on the tails of the pseudo-equilibria $p_{k,\infty}$ and, considering that they convergence to p_∞ (see theorem 4.3.10)), we may take a value λ valid for all k.

After this we can bound the $L^2(\varphi)$ norm of the derivative of p_k as

$$\|\partial_v p_k(.,t)\|_{L^2(\varphi)} \leq \|\partial_v u_k(.,t)\|_{L^2(\varphi)} + \|\partial_v p_{k,\infty}(.)\|_{L^2(\varphi)} \leq \|u_k(.,t)\|_X + \bar{C},$$

with $\bar{C} > 0$, and, by assuming that $\|u_k(.,s)\|_X \leq K < \infty \; \forall s \in [0,t] \subseteq [0,d]$, taking the constant out of the integral and renaming it as $C_b := \tilde{C}|b| \left(K + \bar{C}\right)$, we get

$$\|u_k(.,t)\|_X \leq Ce^{-\lambda t}\|u_k(.,0)\|_X + C_b \int_0^t e^{-\lambda(t-s)}(t-s)^{-3/4}\|u_{k-1}(.,s)\|_X \, \mathrm{d}s. \tag{4.4.11}$$

Taking into account that $p_k(v,d) = p_{k-1}(v,0)$, $u_{k-1}(v,d) := p_{k-1}(v,d) - p_{k-1,\infty}(v)$, and $u_k(v,0) := p_k(v,0) - p_{k,\infty}(v)$, we can write $u_k(v,0) = u_{k-1}(v,d) + (p_{k-1,\infty}(v) - p_{k,\infty}(v))$, which, taking the X norm in v, leads to

$$\|u_k(.,0)\|_X \leq \|u_{k-1}(.,d)\|_X + \delta_k$$

with $\delta_k := \|p_{k-1,\infty} - p_{k,\infty}\|_X$. By using the definitions $f_k(t) := e^{\lambda t}\|u_k(.,t)\|_X$ and $\epsilon(t) := e^{-\lambda t}$, we rewrite the previous inequality as $f_k(0) \leq e^{-\lambda d} f_{k-1}(d) + \delta_k$, and (4.4.11) as

$$f_k(t) \leq C\epsilon(d) f_{k-1}(d) + C\delta_k + C_b \int_0^t f_{k-1}(s)(t-s)^{-3/4} \, \mathrm{d}s, \tag{4.4.12}$$

which can be rewritten, in terms of the linear operators $Af_k(t) := Cf_k(d)$, $Bf_k := C_b \int_0^t f_k(s)(t-s)^{-3/4} \, \mathrm{d}s$ and $hf_{k-1} := \epsilon(d)Af_{k-1}$, in the following way:

$$f_k \leq (\epsilon(d)A + B) \, f_{k-1} + C\delta_k = h_{k-1} + Bf_{k-1} + C\delta_k, \tag{4.4.13}$$

To prove the decay of $\|u_k(.,t)\|_X$ we shall proceed in two steps: first we study the solution to $f_k \leq h_{k-1} + Bf_{k-1}$ and prove its convergence. Secondly we extend the converge to the complete sequence f_k, using that $\delta_k \to 0$ (see theorem 4.3.10 and previous comments before the proof).

First step: Study of $f_k \leq h_{k-1} + Bf_{k-1}$.
We note that if f_k satisfies the inequality $f_k \leq h_{k-1} + Bf_{k-1}$, then $f_k \leq x_k$, where x_k is the solution to the recursive equation $x_k = h_{k-1} + Bx_{k-1}$ with initial condition $x_k = f_0$. Then, using the lemma 4.4.2 to x_k we obtain

$$f_k \leq B^k f_0 + \sum_{i=0}^{k-1} B^{k-i-1} h_i.$$

Therefore we need to estimate $B^k f_0$ for $k = 1, 2, \ldots$. After some computations we obtain

$$B^k(f_0) \leq \|f_0\|_\infty t^{\frac{k}{4}} \frac{\left(C_b \Gamma\left(\frac{1}{4}\right)\right)^k}{\Gamma(1+\frac{k}{4})}, \quad 0 < t < d,$$

by using

$$\int_0^t s^n (t-s)^{-3/4} \, \mathrm{d}s = t^{n+\frac{1}{4}} \beta(n+1, \frac{1}{4}), \quad n = 1, 2, \ldots$$

and properties of the Gamma, Γ, and Beta, β, functions, as

$$B^k(f_0) \leq (C_b)^k \|f_0\|_\infty t^{\frac{k}{4}} \prod_{i=0}^{k-1} \beta\left(1+\frac{k}{4}, \frac{1}{4}\right) = (C_b)^k \|f_0\|_\infty t^{\frac{k}{4}} \prod_{i=0}^{k-1} \frac{\Gamma(1+\frac{k}{4})\Gamma(\frac{1}{4})}{\Gamma(1+\frac{k+1}{4})}.$$

Then we use the $\|.\|_\infty$ norm in $t \in [0, d]$ so that the following inequality holds:

$$\|f_k\|_\infty \leq \frac{\left(d^{1/4} C_b \Gamma\left(\frac{1}{4}\right)\right)^k}{\Gamma(1+\frac{k}{4})} \|f_0\|_\infty + \sum_{i=0}^{k-1} \frac{\left(d^{1/4} C_b \Gamma\left(\frac{1}{4}\right)\right)^{k-i-1}}{\Gamma\left(1+\frac{k-i-1}{4}\right)} \|h_i\|_\infty,$$

or, equivalently

$$\|f_k\|_\infty \leq \frac{\left(d^{1/4} C_b \Gamma\left(\frac{1}{4}\right)\right)^k}{\Gamma(1+\frac{k}{4})} \|f_0\|_\infty + C\epsilon(d) \sum_{i=0}^{k-1} \frac{\left(d^{1/4} C_b \Gamma\left(\frac{1}{4}\right)\right)^{k-i-1}}{\Gamma\left(1+\frac{k-i-1}{4}\right)} \|f_i\|_\infty. \tag{4.4.14}$$

Bearing in mind that $C > 1$, we consider $C \frac{\left(d^{1/4} C_b \Gamma(1/4)\right)^k}{\Gamma(1+\frac{k}{4})} \leq \eta_{b,d} e^{-k}$ for an appropriate $\eta_{b,d}$, which can be computed by finding the maximum of the function

$$g(k) := \frac{\left(d^{1/4} C_b e \Gamma(1/4)\right)^k}{\Gamma(1+\frac{k}{4})} = \frac{M^k}{\Gamma(1+\frac{k}{4})} \quad \text{with} \quad M := d^{1/4} C_b e \Gamma(1/4).$$

We take the logarithm of $g(k)$ and then we find a quantity that bounds the maximum of function $g(k)$ by approximating the gamma function using the Stirling's formula

$$\Gamma\left(1+\frac{k}{4}\right) \geq \left(\frac{k}{4}\right)^{\frac{k}{4}} e^{-\frac{k}{4}},$$

such that

$$\log g(k) \leq k \log M + \frac{k}{4} - \frac{k}{4} \log \frac{k}{4} =: \hat{g}(k).$$

Studying the first derivative of function $\hat{g}(k)$ we compute the maximum, given by $\hat{g}(4M^4)$ and then bounding the function $g(k)$ as $g(k) \leq e^{M^4}$. This procedure allows us to define the quantity $\eta_{b,d}$ as

$$\eta_{b,d} := C e^{M^4} = C e^{d\left(|b| \tilde{C}(\bar{C}+K) e \Gamma(1/4)\right)^4} = C e^{d|b|^4 \hat{C}},$$

having unified all constants in the exponential as $\hat{C} := \tilde{C}(\bar{C} + K)e\Gamma(1/4)$.

Now we can rewrite expression (4.4.14) through the following inequality:

$$\|f_k\|_\infty \leq \eta_{b,d} e^{-k} \|f_0\|_\infty + \eta_{b,d}\epsilon(d) \sum_{i=0}^{k-1} e^{-(k-i-1)} \|f_i\|_\infty.$$

Finally, if we define $\phi_k := e^k \|f_k\|_\infty$, $W := \eta_{b,d}\|f_0\|_\infty$ and $V := \eta_{b,d}\epsilon(d)e$, we can write the previous inequality as

$$\phi_k \leq W + V \sum_{i=0}^{k-1} \phi_i. \tag{4.4.15}$$

Now we use the discrete Gronwall's Lemma 4.4.3 to turn the equation (4.4.15) into the following $\phi_k \leq W e^{kV}$, which leads to

$$\|f_k\|_\infty \leq W e^{k(V-1)}. \tag{4.4.16}$$

Equation (4.4.16) implies that V must be less than 1 in order to obtain convergence to 0 of the sequence $\|u_k(t)\|_X$, so that the condition over the delay is the following:

$$d > \frac{1 + log\,(\eta_{b,d})}{\lambda} = \frac{1 + \log C + \hat{C} d b^4}{\lambda},$$

or, equivalently

$$d > \frac{1 + \log C}{\lambda - \hat{C} b^4} \tag{4.4.17}$$

This inequality requires a smallness condition on b, since $\lambda - \hat{C}b^4$ needs to be positive. That is: we can take d satisfying (4.4.17), only if $|b|^4 < \lambda/\hat{C}$.

Second step: Study of $f_k \leq h_{k-1} + Bf_{k-1} + C\delta_k$.
We write inequality (4.4.13) in terms of linear operator $\mathcal{M} := (\epsilon(d)A + B)$ as

$$f_k \leq \mathcal{M} f_{k-1} + C\delta_k.$$

Using the lemma 4.4.2 as before, we get to

$$f_k \leq \mathcal{M}^k f_0 + \sum_{i=0}^{k} \mathcal{M}^{k-i} C \delta_i. \tag{4.4.18}$$

We already know from equation (4.4.16) that $\|\mathcal{M}^k f_0\|_\infty \leq C\|f_0\|_\infty e^{k(V-1)}$, so that we can

take norm infinity in equation (4.4.18) and then write it as

$$\|f_k\|_\infty \leq Ce^{k(V-1)}\|f_0\|_\infty + C^2 \sum_{i=0}^{k} e^{(k-i)(V-1)}\|\delta_i\|_\infty. \tag{4.4.19}$$

Then, the condition to obtain convergence to 0 of f_k as $k \to \infty$ is given by two different requirements. First, as before, condition (4.4.17) should be satisfied. Secondly, $\|\delta_k\|_\infty$ has to converges to 0 as $k \to \infty$, which is proven in theorem 4.3.10. □

Remark 4.4.5. Convergence to the equilibrium was also proven using the entropy method in [18, Theorem 5.3] in weakly connected networks. In particular, the required smallness of the connectivity parameter was $8b^2e^{\lambda d} \leq \epsilon/N_\infty$, for ϵ a small constant, depending on N_∞ and constants of Sobolev injection of $H^1(I)$ in $L^\infty(I)$ (I is a small neighbourhood of V_R) . Our bound is $b^4 < \lambda/\hat{C}$. With this strategy we obtain the convergence for any large d if the smallness of b is satisfied. This should also be compared to a similar result in theorem 3.4.1.

On the other hand, the assumption $\|p_k(.,t) - p_{k,\infty}(.)\|_X \leq K \ \forall t \in [0,d]$ is quite natural for the cases to which we restrict ourselves in this chapter. First, taking into account that we consider synaptic delay, and therefore there is global existence of solution (see [18]). Secondly, the type of pseudo-equilibria $p_{k,\infty}$ we are considering are bounded in norm X.

4.5 Numerical results: Global perspective on the long-time behavior of the delayed NNLIF model

In this section we illustrate numerically the relationship between the discrete pseudo equilibrium model (4.3.2) and the highly delayed NNLIF model (4.1.1). We give numerical evidence that the long-time behaviors of the two models are closely related. In particular, in the long run, we can predict the behavior of the nonlinear system by knowing the behavior of the discrete system, which was studied in section 4.3.

The numerical approximation of equation (4.1.1) has been carried out by means of a fifth order finite difference flux-splitting WENO scheme [41] for the advection term, a standard second order finite differences for the diffusion term, and an explicit third order TVD Runge-Kutta method for the time evolution. This scheme has been used previously to simulate NNLIF models [20] and a detailed explanation of the scheme can be found in [15]. Other numerical schemes, such as those based on a Scharfetter-Gummel reformulation, have also been used to carry out numerical simulations of this model [86,87].

Our discretization is composed of a mesh in voltage with $v_i = v_{min} + i\Delta v,\ i = 0, 1, 2, ..., n_v$ with a suitable minimum value v_{min}, which ensures the mass is approximately 0 to the left of v_{min}; and a threshold value V_F as the maximum mesh value v_{n_v}. The mesh in time is given by $t_j = j\Delta t,\ j = 0, 1, 2, ..., n_t$ where the value of Δt is chosen so that it complies with the CFL condition imposed for a correct approximation of the drift and diffusion terms

$$\Delta t < \min\left(\frac{a(\Delta v)^2}{2}, \frac{C_{CFL}\Delta v}{\max|bN(t-d)-v|}\right).$$

The reset value V_R is one of the nodes of the mesh in voltage, and the delta function in the right term of (4.1.1) is approximated by a very sharp Maxwellian centered in V_R, of the form:

$$m(x) = \frac{1}{\sqrt{2\pi}\sigma} e^{-\frac{(x-V_R)^2}{2\sigma^2}}, \tag{4.5.1}$$

with $\sigma = 10^{-6}$. The initial conditions we have considered for these simulations are approximations of:

- The pseudo-equilibria profiles (see (4.3.2))

$$p(v) = \overline{N} e^{-\frac{(v,bN)^2}{2}} \int_{\max(v,V_R)}^{V_F} e^{\frac{(w-bN)^2}{2}} dw, \tag{4.5.2}$$

  fulfilling the condition $\int_{-\infty}^{V_F} p(v)dv = 1$, with the particular cases p^- (see (4.3.14)) and p^+ (see (4.3.15)), the 2-cycle of pseudo-equilibria sequence.

- Double Maxwellians:

$$\frac{1}{\sqrt{8\pi}\sigma}(e^{\frac{-(v-\mu)^2}{2\sigma^2}} + e^{\frac{-(v+\mu+2)^2}{2\sigma^2}}) \quad \mu \in \mathbb{R}, \sigma > 0. \tag{4.5.3}$$

Three system parameters are fixed: $a = 1$, $V_R = 1$ and $V_F = 2$. The connectivity parameter b and the delay d will change depending on the simulation, displaying different phenomena for this model.

We analyze in detail two different situations: bi-stability between the lower equilibrium and the plateau distribution for excitatory networks with two equilibria; and the emergence of periodic solutions for highly inhibitory systems. The rest of the system behavior is well represented by the above study, as we shall explain below.

The case with two equilibria: Bi-stability between the lower equilibrium and the plateau distribution

We consider in this case the regime in which the implicit equation $NI(N) = 1$ has two solutions ($N_1^* < N_2^*$), which determine the stationary firing rates of the nonlinear system (4.1.1). This regime corresponds to values of the connectivity parameter b between $V_F - V_R = 1$ and approximately 2.3. Specifically, we take $b = 1.5$ for which $N_1^* \approx 0.194$ and $N_2^* \approx 2.294$, but we emphasize that other values of b in that range appear to show an equivalent behavior. For this connectivity value, figure 4.5 shows the firing rate sequence $N_{k,\infty}$ (see (4.3.1)) for different initial conditions $N_{0,\infty}$. The behavior of the sequence was analyzed in theorem 4.3.4. Thus, we know that in that case (with two equilibria) the firing rate sequence tends to N_1^* or diverges, as we can see in figure 4.5.

In figure 4.6 we show that the behavior of the discrete system is reproduced for the nonlinear system. It is determined by the value of the initial firing rate $N_0 := -\partial_v p_0(V_F)$, depending on the position with respect to N_1^* and N_2^*. The threshold value between both regimes is $N_2^* \approx 2.294$: for a lower value of N_0 the nonlinear system is seen to converge to N_1^*, while for $N_0 > N_2^*$, the firing rate seems to diverge.

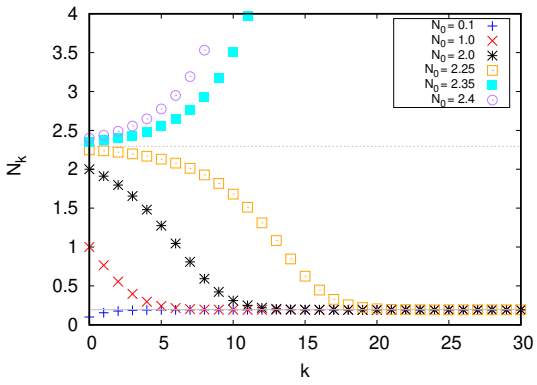

Figure 4.5: **Firing rate sequence $N_{k,\infty}$ (4.3.1) with $b = 1.5$ and different values of initial condition $N_{0,\infty}$.** Solid and dashed straight horizontal lines represent equilibria N_1^* and N_2^* respectively.

In figure 4.6 we consider two different initial conditions of the type (4.5.2), with the respective values of $N_0 = 2.233348$ and $N_0 = 2.365824$, which serve as representatives of two different regimes for the delayed nonlinear system: convergence to the low steady state or formation of the plateau distribution, when considering transmission delay $d = 10$. This illustrates bi-stability between the low steady state and the plateau distribution, depending only on the initial condition (see chapter 2 for a better understanding of the plateau distribution).

As we also mention in chapter 2, no matter what the size of the delay is, we shall find that the nonlinear system seems to behave according to the pseudo-equilibria sequence. This appears to indicate that the long-term behavior of the system can be decided only on the basis of the value of N_0. In the upper graphs, we see the time evolution of the firing rates and on the bottom, we see the shape of the voltage distributions at the end of the two simulations ($t = 220$). When the system starts with an initial condition whose N_0 is less than N_2^*, the firing rate convergences to N_1^* (left plot). However, if the system starts with $N_2^* < N_0$, then $N(t)$ increases in time (right plot). This behavior is consistent with that of the firing rate and pseudo-equilibria sequences described in theorem 4.3.4; if $N_{0,\infty} = N_0$ is below the high stationary firing rate N_2^* then $\{N_{k,\infty}\}_{k\geq 0}$ converges to the lower one N_1^*, and, if $N_{0,\infty} = N_0$ is higher than N_2^* then $\{N_{k,\infty}\}_{k\geq 0}$ diverges.

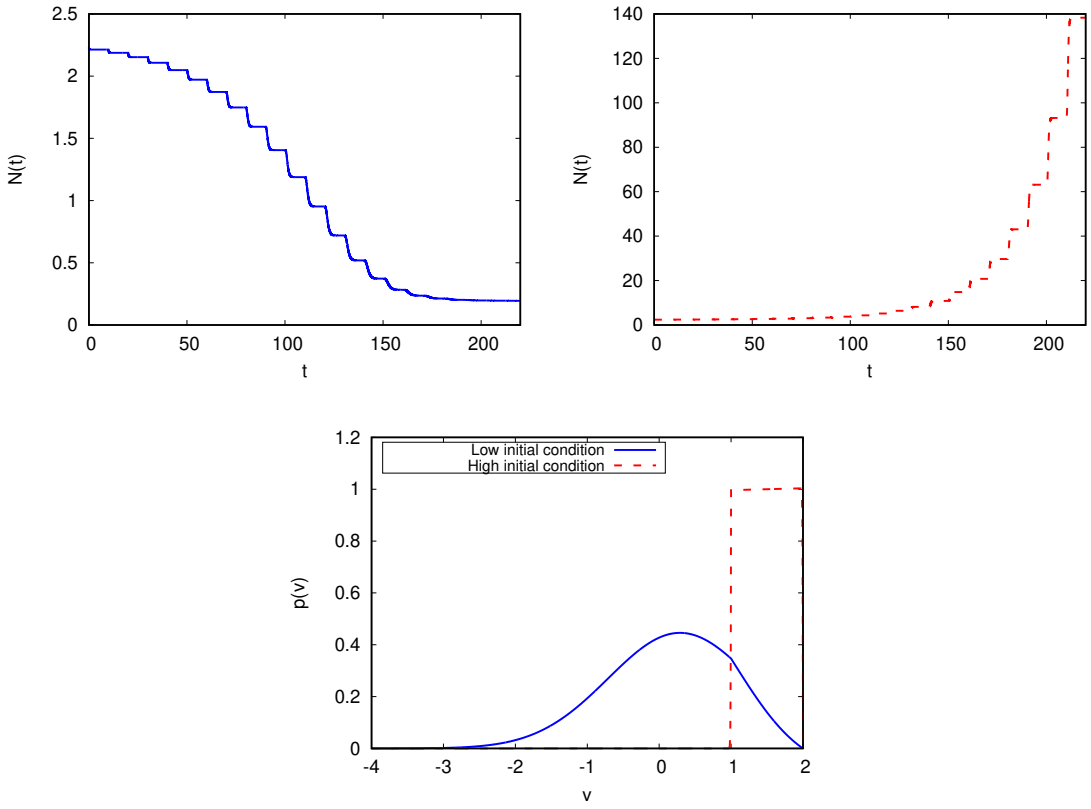

Figure 4.6: **Nonlinear system** (4.1.1) **with $b = 1.5$ and $d = 10$.**
Top: Evolution on time of the firing rate, $N(t)$, with initial conditions given by equation (4.5.2) with $N = 2.25$, $\overline{N} = 2.233348$, chosen to be smaller than N_2^* (left) and $N = 2.35$, $\overline{N} = 2.365824$, greater than N_2^* (right).
Bottom: Comparison of distributions $p(v, t)$ at the end of the simulations ($t = 220$).

We have compared the discrete and the nonlinear systems in figure 4.7. Here we have used the same simulations shown in figure 4.6 for the nonlinear system, and we have calculated the sequences $\{N_{k,\infty}\}_k$ and $\{p_{k,\infty}\}_k$ by starting with the same initial condition as for the simulations, $N_{0,\infty} = N_0 = 2.233348$ in the left plots and $N_{0,\infty} = N_0 = 2.365824$ in the right ones. In the top plots we observe the comparison between $N(t)$ and $\{N_{k,\infty}\}_k$ until $t = 200$, while in the bottom plots we show the comparison between $p(v, t = 20)$, $p(v, t = 120)$ and the pseudo-equilibria $p(v, t = 200)$ with $p_{2,\infty}(v)$, $p_{12,\infty}(v)$ and $p_{20,\infty}(v)$ respectively. We can observe that the delay $d = 10$ is large enough so that the simulation results, both $p(v, t)$ and $N(t)$, almost completely coincide with the elements of the pseudo equilibrium and firing rate sequences starting from the same initial condition.

In [18] a global existence theory was developed for the nonlinear system (4.1.1) with a transmission delay $d > 0$, by extending the results of [29]. So the sequence of pseudo-equilibria suggests that the firing rate of the nonlinear system should diverge and the theory tells us that this cannot happen in finite time. The only possibility is then that $N(t)$ diverges in infinite time, giving rise to the plateau distribution as $N(t)$ grows. This is precisely the behavior seen in our simulations.

So that in cases where the firing rate sequence diverges, we expect the following to be true: *Let us consider* $0 < b$, *an initial condition* $p_0 \in X$ *(and* $N(t) = -\partial_v p(V_F)$ *for* $t \in [-d, 0]$*) and* p *its related solution to the nonlinear system* (4.1.1). *Assuming that the firing rate sequence* $\{N_{k,\infty}\}_{k\geq 0}$, *with initial value* $N_{0,\infty} := -\partial_v p_0(V_F)$ *(see* (4.3.1)*) diverges, then the solution,* p, *to the nonlinear system* (4.1.1) *with transmission delay* $d > 0$ *and initial condition* p_0 *evolves to a plateau distribution, i.e, the membrane potential of the system tends to be uniformly distributed between* V_R *and* V_F.

The numerical results in figures 4.5 and 4.6 and numerical experiments in the literature also illustrate the behavior of the nonlinear system when the firing rate sequence converges. Theorems 4.3.4 and 4.3.6 give conditions on the initial value of the firing rate sequence to converge to an equilibrium of the system (in both cases, excitatory and inhibitory). In figures 4.6 and 4.7 we see that the nonlinear system tends to an equilibrium when the discrete system also tends to equilibrium. In the following experiments below we shall see it for the inhibitory case and in [14, 17, 20, 86] it can also be seen for the excitatory case with only one equilibrium.

So that in case where firing rate sequence converges, we expect the following to be true:

Let us consider $b \in \mathbb{R}$, an initial condition $p_0 \in X$ (and $N(t) = -\partial_v p(V_F)$ for $t \in [-d, 0]$) and p its related solution to the nonlinear system (4.1.1). Assuming that the firing rate sequence $\{N_{k,\infty}\}_{k\geq 0}$, with initial value $N_{0,\infty} := -\partial_v p_0(V_F)$ (see (4.3.1)) converges to $N_\infty > 0$, then there exists $d_0 > 0$ large enough and $Q, \mu > 0$, such that the solution, p, to the nonlinear system (4.1.1) with transmission delay $d > d_0$ and initial condition p_0 fulfills

$$\|p(.,t) - p_\infty(.)\|_X \leq Qe^{-\mu t}\|p_0 - p_\infty\|_X \quad \forall t \geq 0, \tag{4.5.4}$$

where p_∞ is the stationary solution to the nonlinear system (4.1.1) with firing rate N_∞.

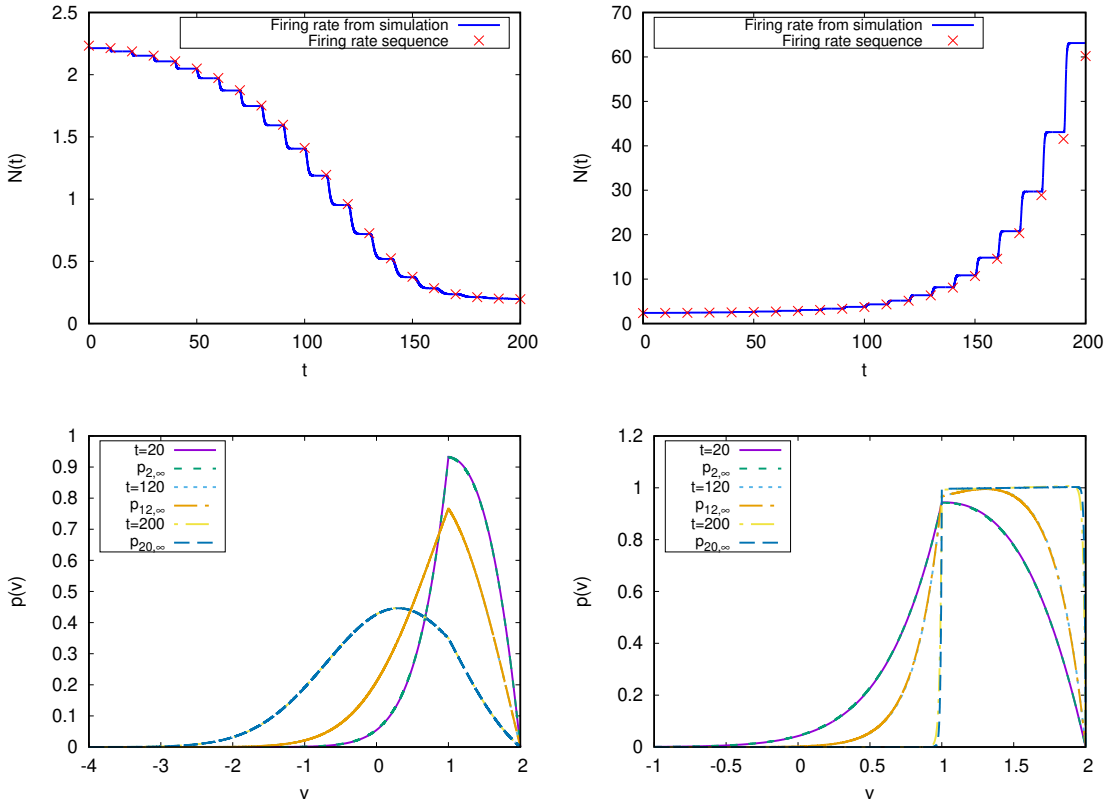

Figure 4.7: **Comparison between the nonlinear system (4.1.1) and the discrete system with $b = 1.5$ and $d = 10$.** *Top:* Comparison between the firing rate of the approximated solution to the nonlinear equation, $N(t)$ and the sequence of firing rates $N_{k,\infty}$. *Bottom:* Solutions of the nonlinear problem, $p(v,t)$ at different times, compared with the pseudo-equilibria $p_{k,\infty}(v)$ which correspond to those times. *Left:* initial condition given by equation (4.5.2) with $N = 2.25$, $\overline{N} = 2.233348$, chosen to be smaller than N_2^*. *Right:* initial condition given by equation (4.5.2) with $N = 2.35$, $\overline{N} = 2.365824$, greater than N_2^*.

Periodic states in the highly inhibitory case with large delay

In this second experiment we discover conditions under which periodic solutions appear in an inhibitory system. This phenomenon was observed numerically in [87]. We have determined the value of parameter b for which the periodic states appear for large delay, in the light of the behavior of the sequence of pseudo-equilibria. Here we find an important difference with the excitatory case, where the size of the delay is not essential to determine whether the long-term behavior of the system conforms to that described by the pseudo equilibrium sequence. For highly inhibitory systems the size of the transmission delay is key. We recall that for the inhibitory case the nonlinear system has only one steady state p_∞, with its associated stationary firing rate N_∞, and the behavior of the firing rate sequence $N_{k,\infty}$ (the discrete system) is given by theorem 4.3.6: $N_{k,\infty}$ tends to the equilibrium or to 2-cycle.

Our first aim is to find appropriate values of the parameters for which periodic states emerge. Then we shall focus on the study of periodic solutions. Figure 4.8 suggests which values we should choose for b in order to find periodic states. We see that the bifurcation value b^* is around the value $b^* \approx -9.4$ (in the sense of theorem 4.3.6). Thus, the firing rate sequence $N_{k,\infty}$ converges to N_∞ if $b^* < b$ and tends towards a 2-cycle $\{N^-, N^+\}$, if $b < b^*$. This tells us that a sufficiently large delay will allow us to observe the same behavior when simulating the nonlinear system. We must emphasize that for all cases with $b \leq 0$, the choice of initial condition $N_{0,\infty}$ does not appear to change the long-term values of the firing rate sequence $N_{k,\infty}$.

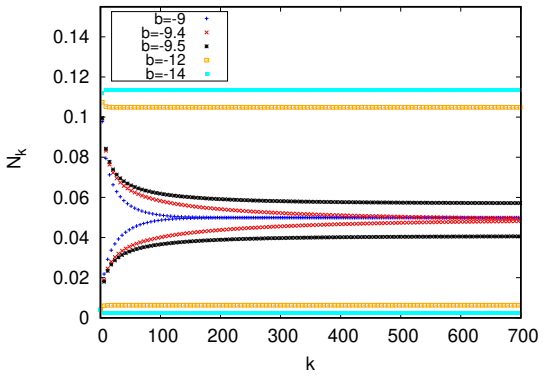

Figure 4.8: **Firing rate sequence $N_{k,\infty}$ (4.3.1) for different values of $b < 0$ with $N_{0,\infty} = 0.004$. For $b < -9.4$ the sequence tends towards a 2-cycle.**

Due to the numerical study of the firing rate sequence, we have a good guess for the values of b needed to find periodic states. Let us test different values of b and d and observe the behavior of the nonlinear system. The following simulations have been performed using as initial condition the profile given by equation (4.5.2), with $N = 0$, letting the system evolve up to $t = 300$. In the left plot of figure 4.9 we show the firing rate $N(t)$ of the nonlinear system, with delay $d = 10$, testing three different values of b to find stable oscillations. For b not sufficiently negative, the amplitude of the oscillations is observed to be damped in time, suggesting a tendency towards the single steady state of the system, as we showed earlier in the study of the sequence of pseudo-equilibria (see theorem 4.3.6). For a sufficiently negative value of b, as shown for $b = -12$, we observe fairly stable oscillations in time. Thus, to be sure of the stability of the solutions without the need for an excessively large delay, we will choose $b = -14$ for the following experiments. In the right plot of figure 4.9 we can see, for $b = -14$, how the choice of a large enough delay permits the system to evolve towards a periodic state. This picture shows the evolution in time of the firing rate $N(t)$ with different delay values d. If d is small ($d = 2$) the firing rates tends to a stationary value, while if d is large ($d = 10$, $d = 25$), its behavior tends to be periodic. We must emphasize that, when we do not set a sufficiently high delay, even if the value of b is very negative and therefore the pseudo-equilibria sequence in theorem 4.3.6 points to periodic behavior, we shall observe convergence to the steady state, as it is shown with solid line in the right graph, for $d = 2$. This is a strong difference between the inhibitory case with periodic state and the excitatory case with plateau state, where the size of the delay was irrelevant.

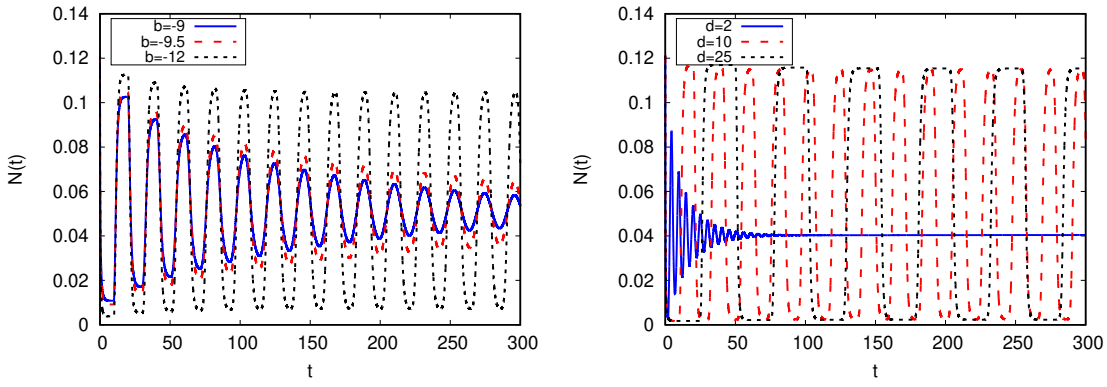

Figure 4.9: **Nonlinear system** (4.1.1) Time evolution of the firing rate, $N(t)$. The initial condition is given by equation (4.5.2) with $N = 0$.
Left: Different values of the connectivity parameter b with delay $d = 10$. *Right:* Connectivity parameter $b = -14$ with different values of the delay.

To study the periodic solutions of the highly inhibitory nonlinear system, we shall set $b = -14$ and $d = 25$ for the rest of the simulations.

For these parameters, the steady state of the nonlinear system $p_\infty(v)$ has firing rate $N_\infty = 0.0396$. When we study numerically the firing rate sequence $N_{k,\infty}$ we find a tendency towards the values $N^- = 0.0022$ and $N^+ = 0.1136$ in the sense of theorem 4.3.6, as shown above in figure 4.8 for $b = -14$.

In figure 4.10 we compare the solution to the nonlinear system (4.1.1) with the 2-cycle, $\{p^-(v), p^+(v)\}$, found in theorems 4.3.6 and 4.3.11 for the succession of pseudo-equilibria $\{p_{k,\infty}\}_{k\geq 0}$. In the left graph we observe the comparison between the lower state $p^-(v)$ and the approximated solution to the Fokker-Planck equation, starting with an initial condition given by an approximation of $p^-(v)$. The times shown in the graphs have been selected so that the distribution should coincide with $p^-(v)$, since they are even multiples of the delay. In the graph on the right we see a similar comparison between $p^+(v)$ and the approximated $p(v)$, starting now with an approximation of $p^+(v)$, also in the times they should overlap. We can see that in the left graph there is a small difference between the values of $p(v,t)$ for the different times represented with respect to $p^-(v)$, but in the right graph the difference is practically negligible. This may be due to the fact that the observed period for the periodic state is not exactly $2d$, as can be seen in the bottom plot, where we show the firing rate of the system, computed for a simulation with initial condition given by equation (4.5.2) with $N = 0$.

Finally, in figure 4.11, we analyze how the initial condition influences the evolution of the nonlinear system. We consider four different initial conditions shown in the top left graph: $p^-(v)$, $p^+(v)$ and two double Maxwellians distributions, as (4.5.3), with $\mu_{\text{low}} = -1$, $\mu_{\text{high}} = 0.4$ and $\sigma = 0.5$ in both cases. Our purpose is to provide evidence that regardless of the initial condition, with these values of b and d, the system will end up in a periodic state between the pseudo-equilibria $p^-(v)$ and $p^+(v)$, with pseudo-stationary firing rates N^- and N^+. Nevertheless, it is worth noting how the initial condition determines which pseudo equilibrium is going to be reached first, determining the times at which the distribution $p(v,t)$ will be close to $p^-(v)$ and $p^+(v)$.

In top right plot of figure 4.11, we can see the evolution on time of the four firing rates of the different simulations. We note that for $t > 150$ the firing rates of the simulations starting with the low state and the double Maxwellians low ($\mu_{\text{low}} = -1$) are synchronised, and the same is true for the firing rates of the simulations starting with the high state and the double Maxwellians high ($\mu_{\text{high}} = 0.4$). We also see, in the bottom graphs, these synchronies of the corresponding distributions $p(v,t)$, "passing" through $p^-(v)$ and $p^+(v)$ at the same times ($t = 250$ left and $t = 264$ right), and describing, in this way, a periodic behavior.

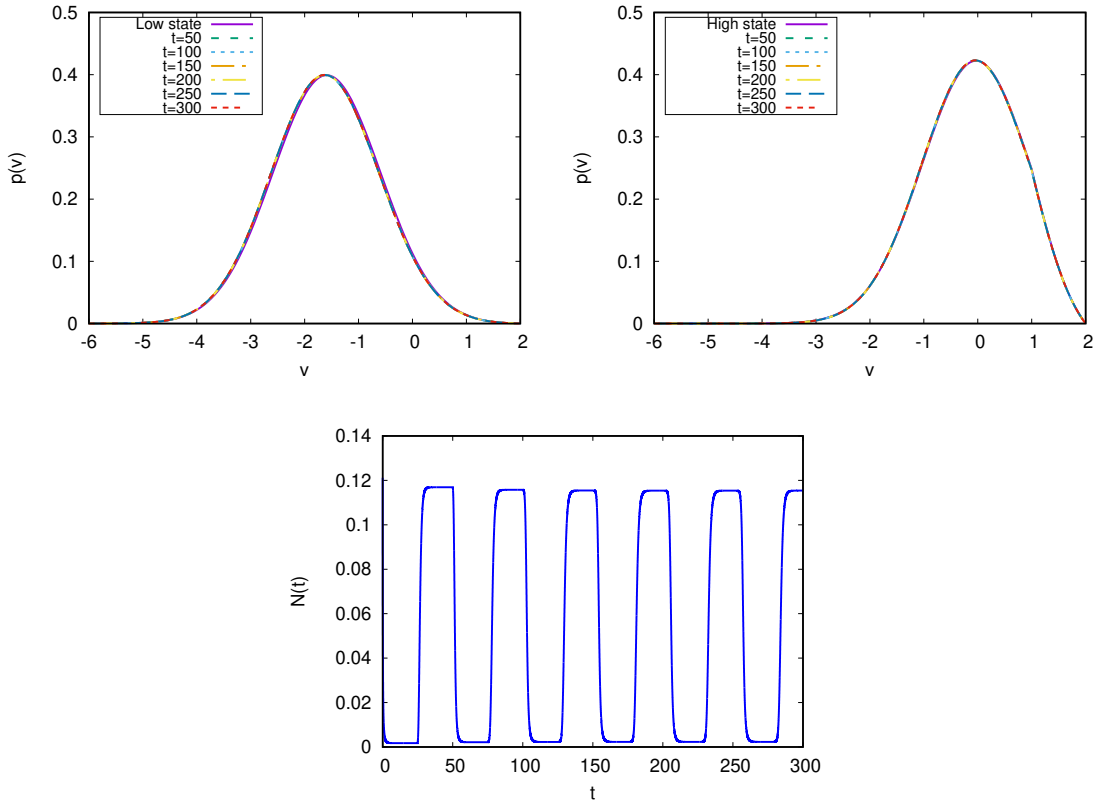

Figure 4.10: **Nonlinear system (4.1.1) with $b = -14$ and delay value $d = 25$.** *Top left:* Initial condition given by the pseudo equilibrium $p^-(v)$, from equation (4.3.14). Approximated solution to the nonlinear system, $p(v,t)$, at different times, compared with $p^-(v)$. *Top right:* Initial condition given by the pseudo equilibrium $p^+(v)$, from equation (4.3.15). Approximated $p(v,t)$ at different times, compared with $p^+(v)$. *Bottom:* Initial condition given by (4.5.2) with $N = 0$. Time evolution of the firing rate $N(t)$.

The behaviors shown in figures 4.9 and 4.10 agree with that of the firing rate and pseudo-equilibria sequences described in theorems 4.3.6 and 4.3.11; if $b^* \approx 9.5 < b < 0$ we find convergence to the steady state, no matter what the initial condition is. If $b < b^*$ then d should be sufficiently large to find a periodic state. Otherwise, there will be convergence to equilibrium. Finally, figure 4.11 helps us to understand which are the different options for the possible periodic states to which the nonlinear system tends, as well as their dependence on the initial condition.

The periodic states seem to be determined by the solutions starting from one of the two pseudo-equilibria. These solutions, when the delay is large, approach the other pseudo equilibrium at the end of each delay period. In the next delay period they return to the initial pseudo equilibrium, and so continue in the following periods of length d. And they tends to a periodic state, which we can call $p^-_\infty(v,t)$ and $p^+_\infty(v,t)$, depending if the initial

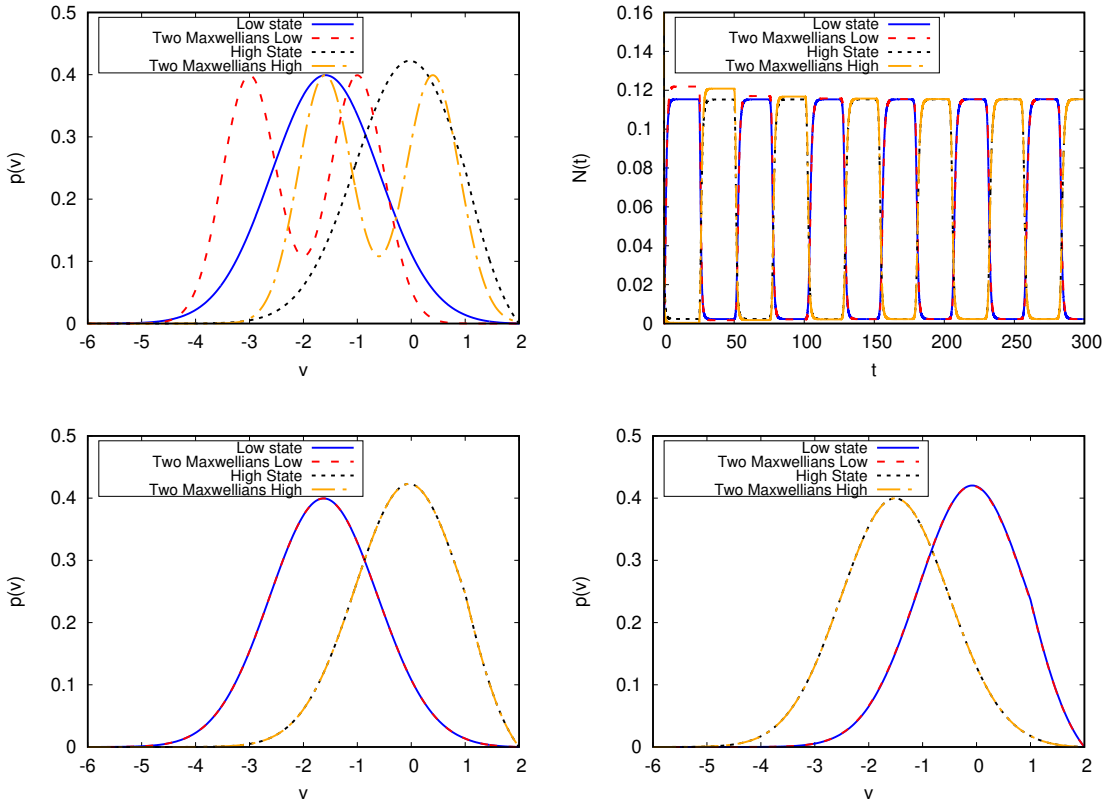

Figure 4.11: **Nonlinear system** (4.1.1) **with $b = -14$ and $d = 25$** using four different initial conditions. *Top left:* Initial conditions: we consider the low pseudo equilibrium given by equation (4.3.14), the high pseudo equilibrium given by equation (4.3.15) and two configurations of double Maxwellians given by equation (4.5.3), with $\mu_{\text{low}} = -1$, $\mu_{\text{high}} = 0.4$ and $\sigma = 0.5$ in both cases. *Top right:* Comparison between the time evolution of the firing rate $N(t)$ depending on the initial condition. *Bottom left and right:* Distribution $p(v)$ at times $t = 250$ and $t = 264$ respectively, for both initial conditions.

condition is $p^-(v)$ or $p^+(v)$, respectively. Simulations lead us to suspect that the period is $2d + \epsilon$, because of the time it takes to move from one pseudo equilibrium to another, and $p^-_\infty(v,t) = p^+_\infty(v, t + d + \epsilon/2)$.

To be more precise what we would expect to be demonstrated in the nonlinear system, in cases where the firing rate sequence tends to 2-cycle, i.e $b < b^*$, can be stated as follows: *Let us consider $b < 0$, an initial condition $p_0 \in X$ (and $N(t) = -\partial_v p(V_F)$ for $t \in [-d, 0]$) and p its related solution to the nonlinear system* (4.1.1). *Assuming that the firing rate sequence $\{N_{k,\infty}\}_{k\geq 0}$, with initial value $N_{0,\infty} := -\partial_v p_0(V_F)$ (see* (4.3.1)*) tends to a 2-cycle, $\{N^-, N^+\}$, then there exist $d_0 > 0$ large enough, such that the solution, p, to the nonlinear system* (4.1.1) *with transmission delay $d > d_0$ and initial condition p_0 has the following behavior:*

1. *If the initial datum, p_0, is p^-, (see (4.3.14)), thus, the solution tends to a periodic function, $p^-_\infty(v,t)$.*

2. *If the initial datum, p_0, is p^+, (see (4.3.15)), thus, the solution tends to a periodic function, $p^+_\infty(v,t)$.*

3. *For a general initial condition $N_0 := -\partial_v p_0(V_F)$:*

   (a) *If $N_0 < N_\infty$, thus, the system tends to $p^-_\infty(v, t+\delta_{N_0})$.*

   (b) *If $N_\infty < N_0$, thus, the system tends to $p^+_\infty(v, t+\delta_{N_0})$,*

   with fixed $\delta_{N_0} \in \mathbb{R}$ for each initial condition N_0.

4.6 Conclusions

In this chapter we show how a discrete system helps us to better understand the nonlinear leaky integrate and fire (NNLIF) models when large transmission delay is considered. This discrete system is defined only in terms of the system parameters. And it allows to build a firing rate and pseudo-equilibria sequences, that determine the long run of the nonlinear system (4.1.1). We have analytically studied the related discrete system. Our results give a global view of the asymptotic behavior of the discrete system for all possible values of the connectivity parameter b. Analytically, the link with the nonlinear system (4.1.1) has been proved in theorem 4.4.1, but it only works if b is small enough, in which case the system converges to its unique equilibrium. The long-term behavior for weakly connected networks was already known using the entropy dissipation method [18, 19, 25]. However, our strategy is different and new, as it describes the behavior in relation to the pseudo-equilibria sequence (4.3.2).

In addition to our analytical results we show a numerical study, that leads us to think that the nonlinear system should behave as shown by the sequence of pseudo-equilibria in all cases with high delay. The motivation for that conjecture is clear: large delay means that the nonlinear system is piecewise linear and with enough time to reach linear equilibria. The numerical results of this chapter describe the existence of periodic states for the nonlinear system, in the case of large delay and very negative connectivity parameter, as has been observed previously by other authors [87]. We offer range of values for the parameters b and d from which this phenomenon should occur. Moreover, we can link the numerical part with our study of the sequence of pseudo-stationary states, giving a plausible theoretical explanation for the existence of these oscillations, and shedding some light on the subsequent analytical test of them, which will be carried out in future work.

We can also relate the study of the sequence of pseudo-equilibria to the behavior of the system for b positive. Finding here a possible explanation for the emergence of the plateau state, observed in chapter 2.

As a final conclusion, we point out that this chapter completes the results given in chapter 3, since we have clarified the global behavior of systems with large delay in terms of its initial firing rate, $N_0 = -\partial_v p_0(V_F)$:

1. Excitatory networks ($0 < b$) show two possibilities: they can evolve to:
   (a) A stationary distribution, the single steady state or the steady profile with lower firing rate, in case of two equilibria.
   (b) The uniform distribution between V_R and V_F (plateau state). This case could occur even with small transmission delay value, d, if there is no steady state (b large), and in cases with two equilibria.
2. Inhibitory networks ($b < 0$) also show two possibilities: they can evolve towards:
   (a) The stationary distribution, if $b^* < b$.
   (b) A periodic solution between the 2-cycle $\{p^-, p^+\}$, if $b < b^*$.

Chapter 5

NNLIF model with refractory period: multi-scale study, pseudo-equilibria sequence and physical solutions

5.1 Introduction

In this chapter we apply the techniques developed in chapters 2 and 4 to the NNLIF model with refractory period described in section 1.2.3. This variant of the NNLIF model is characterized by considering that after synapsis, neurons remain for a certain time ($\tau > 0$) without interacting with the rest of the network. From the analytical point of view, we will define a succession of pseudo-equilibria equivalent to the one defined in chapter 4 for the model without refractory state, and we will study its monotonicity. After which, we will perform two types of numerical experiments:

- Simulations of the microscopic system associated with this model, through the numerical scheme designed in section 2.3, to observe what happens after the blow-up.
- Simulations of the mesoscopic system, using the numerical scheme developed in [118], in order to study the global long-time behavior of the system and its suitability to the behavior of the pseudo-equilibrium sequence.

Although the NNLIF model with refractory state has been explained in more detail in section 1.2.3, we will make a brief introduction to it to recall its main features. Taking into account that in this chapter we will not encounter notation problems for the firing rate, since we always deal with the nonlinear equation, we will denote it by $N(t)$ instead of $N_p(t)$.

Additionally, we will always consider constant initial conditions, so we will denote them by their value at time $t = 0$.

The NNLIF model with refractory state is described by:

$$\begin{cases} \partial_t p(v,t) + \partial_v \left[(-v + bN(t-d))\, p(v,t) \right] + \partial_v^2 p(v,t) = \frac{R(t)}{\tau} \delta \left(v - V_R \right), & v \leq V_F, \\ \frac{dR(t)}{dt} = N(t) - \frac{R(t)}{\tau}, & t \geq 0 \\ N(t) := -\frac{\partial p}{\partial v}\left(V_F, t \right) \geq 0, \end{cases} \tag{5.1.1}$$

together with the boundary and initial conditions: $p(V_F, t) = 0$, $p(-\infty, t) = 0$, $p(v, 0) = p_0(v) \geq 0$, $R(0) = R_0 > 0$. Here $p(v,t)$ represents the probability density of finding non-refractory neurons with voltage $v \in (-\infty, V_F]$ at time $t > 0$, $R(t)$ is the proportion of refractory neurons at time t, $N(t)$ represents the flux of neurons in the threshold V_F (firing potential), V_R represents the reset potential, d is the transmission delay and b is the connectivity parameter, whose value determines if the network is inhibitory or excitatory in average.

By integrating the equation (5.1.1) we derive the following mass conservation law:

$$\int_{-\infty}^{V_F} p_0(v) dv + R_0 = \int_{-\infty}^{V_F} p(v,t) dv + R(t), \tag{5.1.2}$$

where we will set the value of the integral of the initial conditions to 1. This means that the sum of the active neurons and those in a refractory state is preserved at all times.

The time stationary solutions to equation (5.1.1) are given by

$$(v - bN_\infty) p_\infty(v) + \frac{\partial p_\infty}{\partial v}(v) + \frac{R_\infty}{\tau} H(v - V_R) = 0, \quad R_\infty = \tau N_\infty, \tag{5.1.3}$$

where $H(x)$ is the Heaviside function, which means $H(x) = 0$ for $x < 0$ and $H(x) = 1$ for $x \geq 0$.

The solution to this equation can be directly computed as

$$p_\infty(v) = N_\infty e^{-\frac{(v - bN_\infty)^2}{2}} \int_{\max(v, V_R)}^{V_F} e^{\frac{(w - bN_\infty)^2}{2}} dw, \quad R_\infty = \tau N_\infty \tag{5.1.4}$$

After which we can computed the stationary firing rate N_∞ by imposing the conservation law (5.1.2), as follows:

$$1 = \int_{-\infty}^{V_F} p_\infty(v) dv + R_\infty = N_\infty \int_{-\infty}^{V_F} e^{-\frac{(v - bN_\infty)^2}{2}} \int_{\max(v, V_R)}^{V_F} e^{\frac{(w - bN_\infty)^2}{2}} dw dv + \tau N_\infty,$$

which, by using the definition

$$I(N) := \int_{-\infty}^{V_F} e^{-\frac{(v-bN)^2}{2}} \int_{\max(v,V_R)}^{V_F} e^{\frac{(w-bN)^2}{2}} dwdv, \tag{5.1.5}$$

can be rewritten as

$$1 = N_\infty(I(N_\infty) + \tau) \tag{5.1.6}$$

The number of solutions to this equation, which depends implicitly on b, will determine the number of steady states of the system. An analytical study of this equation was stated in theorem 4.1 [16], so that it is convenient to remember this result:

Theorem 5.1.1 (Number of Equilibria. Theorem 4.1 in [16])**.** *Depending on the value of the connectivity parameter b, the number of solutions of equation (5.1.6) will be:*

- *Inhibitory case ($b < 0$): there is only one solution.*
- *Excitatory case ($b > 0$): there is an odd number of solutions (considering multiplicity).*

For positive values of b, the number of solutions to equation (5.1.6) is not clear analytically, so that we have calculated them numerically, for each b and fixed $\tau = 0.06$, in the figure 5.1.

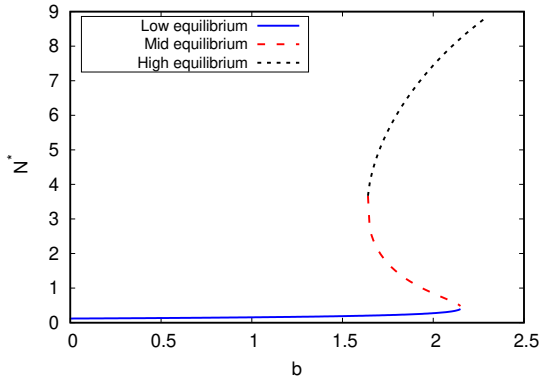

Figure 5.1: **Values N^* solving $N(I(N) + \tau) = 1$, for each b.** The refractory time is set to $\tau = 0.06$. There is one solution in $(-\infty, 1.64)$ and $(2.15, +\infty)$ and three solutions in $(1.64, 2.15)$. Firing and reset potentials are set to $V_F = 2$ and $V_R = 1$ respectively.

5.2 Behavior of the pseudo-equilibria sequence

This section is the logical extension of the results presented in chapter 4 for the NNLIF model without refractory state. The demonstrations of the results stated here for the model with refractory state, are strongly based on those performed in section 4, and therefore we will be more brief and concise in the developments.

We call firing rate sequence $\{N_{k,\infty}\}_{k\geq 0}$, for an initial condition $N_{0,\infty} > 0$ and a fixed refractory period $\tau > 0$, to the solution to the recursive equation

$$N_{k+1,\infty} := \frac{1}{I(N_{k,\infty}) + \tau} \quad k = 0, 1, 2, \ldots, \text{ where } I \text{ is the function (5.1.5)}, \tag{5.2.1}$$

Associated to each firing rate sequence, we find a sequence of pseudo-equilibria, given by

$$p_{k,\infty}(v) := N_{k,\infty} e^{-\frac{\left(v - bN_{k-1,\infty}\right)^2}{2}} \int_{\max(v,V_R)}^{V_F} e^{\frac{\left(w - bN_{k-1,\infty}\right)^2}{2}} dw, \quad k = 1, 2, \ldots \tag{5.2.2}$$

together with a sequence of refractory states, given by

$$R_{k,\infty} := \tau N_{k,\infty} \quad k = 0, 1, 2, \ldots. \tag{5.2.3}$$

Remark 5.2.1. Since $\tau \geq 0$ the monotonicity of sequence $\{R_{k,\infty}\}_{k\geq 0}$ is given by that of $\{N_{k,\infty}\}_{k\geq 0}$.

Next we will study, according to the number of solutions of the equation

$$N\left(I(N) + \tau\right) = 1, \text{ with } 0 \leq N, \tag{5.2.4}$$

depending on the value of the parameter b, the monotonicity and convergence properties of the sequence of firing rates and its associated sequence of pseudo-equilibria.

The study of the number of steady states to equation (5.2.4) was synthesized in theorem 5.1, which, together with the numerical results shown in figures 5.1, 5.2 points to the existence of only one or three equilibria. In some particular cases, for instance $\tau = 0.06$ and $b = 1.64$ or $b = 2.15$, we see in figure 5.2 how the function $N \to (I(N) + \tau)$ cut the straight line 1 in a tangential form, leading to two solutions of equation (5.2.4), where one solution has zero first derivative and non-zero second derivative at the cut-point. Thus, in the following results shown in this section, we will assume as number of solutions to the equation (5.2.4), the one that arise from the results described above.

Theorem 5.2.2 (Monotonicity of the firing rate sequence $\{N_{k,\infty}\}_{k\geq 0}$ for excitatory networks)**.** *Let us consider $b > 0$, a fixed $\tau > 0$, and the sequence $\{N_{k,\infty}\}_{k\geq 0}$ given by (5.2.1).*

1. *If N^* is the unique solution of equation (5.2.4), thus:*
   - *If $N^* \leq N_{0,\infty}$ then $\{N_{k,\infty}\}_{k\geq 0}$ is a decreasing sequence which tends to N^*.*
   - *If $N_{0,\infty} \leq N^*$ then $\{N_{k,\infty}\}_{k\geq 0}$ is an increasing sequence which tends to N^*.*
2. *If equation (5.2.4) has two solutions $N_1^* < N_2^*$, one of them due to a tangential cut between function $N \to N\,(I(N) + \tau)$ and straight line 1:*
   - *If $N_{0,\infty} \leq N_1^*$ then $\{N_{k,\infty}\}_{k\geq 0}$ is an increasing sequence which tends to N_1^*.*
   - *If $N_1^* \leq N_{0,\infty} \leq N_2^*$, there are two mutually exclusive possibilities:*
     - *If there is a tangential cut between function $N \to N\,(I(N) + \tau)$ and straight line 1 at $N = N_1^*$ with non-zero second derivative, $\{N_{k,\infty}\}_{k\geq 0}$ is an increasing sequence which tends to N_2^*.*
     - *If there is a tangential cut between function $N \to N\,(I(N) + \tau)$ and straight line 1 at $N = N_2^*$ with non-zero second derivative, $\{N_{k,\infty}\}_{k\geq 0}$ is a decreasing sequence which tends to N_1^*.*
   - *If $N_2^* < N_{0,\infty}$ then $\{N_{k,\infty}\}_k \geq 0$ is a decreasing sequence which tends to N_2^*.*
3. *If equation (5.2.4) has three solutions: N_1^*, N_2^* and N_3^* such that $N_1^* < N_2^* < N_3^*$, thus:*
   - *If $N_{0,\infty} \leq N_1^*$ then $\{N_{k,\infty}\}_{k\geq 0}$ is an increasing sequence which tends to N_1^*.*
   - *If $N_1^* \leq N_{0,\infty} \leq N_2^*$ then $\{N_{k,\infty}\}_{k\geq 0}$ is a decreasing sequence which tends to N_1^*.*
   - *If $N_2^* \leq N_{0,\infty} \leq N_3^*$ then $\{N_{k,\infty}\}_{k\geq 0}$ is an increasing sequence which tends to N_3^*.*
   - *If $N_3^* < N_{0,\infty}$ then $\{N_{k,\infty}\}_k \geq 0$ is a decreasing sequence which tends to N_3^*.*

Proof. First we present the following useful properties of the function $f(N) := \frac{1}{I(N)+\tau}$, which can be directly deducted from those shown in [14].

1. $f(N)$ is an increasing function,
2. $f(0) > 0$,
3. $\lim_{N\to\infty} f(N) = \infty$.

Due to the properties of function $f(N)$, concerning its monotonicity and behavior in 0 and ∞, together with the assumption that equation (5.2.4), for $b > 0$, has one or three solutions (two solutions in special cases mentioned above), the following cases arise:

- If N^* is the only solution of equation (5.2.4), thus:
  - $N < f(N)$ if $N < N^*$.
  - $f(N) < N$ if $N^* < N$.
- If equation (5.2.4) has two solutions, N_1^* and N_2^*, with $N_1^* < N_2^*$, thus:
  - If there is a tangential cut between function $N \to N\,(I(N) + \tau)$ and straight line 1 at $N = N_1^*$:
    - $N < f(N)$ if $N \in [0, N_1^*) \cup (N_1^*, N_2^*)$.
    - $f(N) < N$ if $N \in (N_2^*, +\infty)$.
  - If there is a tangential cut between function $N \to N\,(I(N) + \tau)$ and straight line 1 at $N = N_2^*$:
    - $N < f(N)$ if $N \in [0, N_1^*)$.
    - $f(N) < N$ if $N \in (N_1^*, +\infty)$.
- If equation (5.2.4) has three solutions, N_1^*, N_2^* and N_3^* such that $N_1^* < N_2^* < N_3^*$, thus:
  - $N < f(N)$ if $N \in [0, N_1^*) \cup (N_2^*, N_3^*)$.
  - $f(N) < N$ if $N \in (N_1^*, N_2^*) \cup (N_3^*, +\infty)$.

As stated in the proof of theorem 4.3.4:

1. If the initial condition is taken in an interval in which $N < f(N)$ then the sequence is increasing, because $N_{k,\infty} < f(N_{k,\infty}) = N_{k+1,\infty}$.
2. If the initial condition is taken in an interval in which $f(N) < N$ then the sequence is decreasing, because $N_{k+1,\infty} = f(N_{k,\infty}) < N_{k,\infty}$.

In each case, $\{N_{k,\infty}\}_{k\geq 0}$ is a bounded decreasing or increasing function, so that it converges. It must converge to the equilibrium that bounds it in each case, depending on whether it is increasing or decreasing. Otherwise, there would be another equilibrium to equation (5.2.4), and that would go against the hypotheses stated in the theorem. □

Theorem 5.2.3 (Monotonicity of the firing rate sequence $\{N_{k,\infty}\}_{k\geq 0}$ for inhibitory networks)**.** *Let us consider a fixed $\tau > 0$, $b < 0$ and the firing rate sequence $\{N_{k,\infty}\}_{k\geq 0}$ (see equation 5.2.1), then there exists a value of the connectivity parameter b, $b^* < 0$, such that:*

- *If $b^* < b < 0$ the sequence $\{N_{k,\infty}\}_{k\geq 0}$ tends to the unique solution of equation (5.2.4), N^*.*

- *If $b < b^*$, there exist two values N^-, N^+, $0 \leq \min(N^-, N^+) < N^* < \max(N^-, N^+)$, such that the sequence $\{N_{k,\infty}\}_{k\geq 0}$ tends to the 2-cycle $\{N^-, N^+\}$.*

Proof. In contrast to theorem 5.2.2, where there are different numbers of equilibria between models with and without refractory state, for $b \leq 0$ there is only one equilibrium for both models [14, 16], so that the proof in this case is even more similar to that of the theorem 4.3.6. Thus, we will present the idea of the proof and the differences with the case without refractory state, without going into the details already mentioned above. The proof is based on the study of the recursive equation:

$$N_{0,\infty} \geq 0 \quad \text{and} \quad N_{k+1,\infty} = \frac{1}{I(N_{k,\infty}) + \tau} \quad k = 0, 1, \ldots,$$

where the function I, defined in (5.1.5), is a $C^\infty(0,\infty)$ function that can be rewritten as

$$I(N) = \int_0^\infty e^{-s^2/2} e^{-sbN} \frac{e^{sV_F} - e^{sV_R}}{s} \, \mathrm{d}s,$$

and its k-order derivative is

$$I^{(k)}(N) = (-b)^k \int_0^\infty s^{k-1} e^{-s^2/2} e^{-sbN} \left(e^{sV_F} - e^{sV_R}\right) \, \mathrm{d}s. \tag{5.2.5}$$

For the inhibitory case, the recursive equation can be written as

$$N_{k+1,\infty} := f(N_{k,\infty}), \quad f : \left[0, \frac{1}{I(0)+\tau}\right] \to \left[0, \frac{1}{I(0)+\tau}\right], \; f(x) := \frac{1}{I(x)+\tau}, \tag{5.2.6}$$

since the function f is decreasing, also implying that the equation $N(I(N)+\tau) = 1$ has a unique solution. Under these conditions the sequence $\{N_{k,\infty}\}_{k\geq 0}$ may tend to equilibrium or to a periodic state of the 2-cycle type. Then we can determine the existence of a value of the connectivity parameter b^* that separates the equilibrium stability regime from the 2-cycle regime. The first part of the proof, which determines the occurrence of this two situations, is identical to the proof of theorem 5.2.2 and can therefore be consulted there.

To determine b^*, the main difference with theorem 5.2.2 is that

$$g(b) := f'(N_b^*) = \frac{d}{dN} \frac{1}{I(N)+\tau}\Big|_{N_b^*} = \frac{-\partial_N I(b, N_b^*)}{\left(I(b, N_b^*) + \tau\right)^2} = -{N_b^*}^2 \partial_N I(b, N_b^*),$$

Nevertheless lemma 4.3.3 can be also applied to study its monotonicity, because adding a positive constant in the denominator of the function $f(N)$ does not change the monotonicity of its derivative.

Having verified that $g(b)$ is a continuous increasing function in $(-\infty, 0]$, as $\lim_{b\to-\infty} g(b) = -\infty$ and $g(0) = f'(N_0^*) = 0$, there exists b^* such that $g(b^*) = -1$. Then, if $b < b^*$, thus $g(b) < -1$, which means that N_b^* is unstable and system (5.2.6) tends to a 2-cycle, while for $b > b^*$, $g(b) > -1$ and N_b^* is stable. □

Remark 5.2.4 (Numerical evidence for b^* stability and 2-cycle uniqueness). As in chapter 4 for the model without refractory state, we could not prove two things in 5.2.3, due to the complexity of the function I: the stability of the equilibrium in the critical case, $b = b^*$, and the uniqueness of the two cycles, in the case $b < b^*$. However we can provide numerical evidence to support both statements: Figure 5.3 shows the function $F(N) = f \circ f(N)$, for cases with $b < b^*$ and two different values of τ. F has only 3 fixed points, i.e., the equilibrium N^* and cycle $\{N^-, N^+\}$ corresponding to each value of b. Moreover, the 2-cycles appear as a bifurcation of the equilibrium, which is asymptotically stable for $b = b^*$, as this value is the starting point for the formation of 2-cycles. We also note that the 2-cycle $\{N^-, N^+\}$ becomes $\left\{0, \frac{1}{I(0)+\tau}\right\}$ when b tends to $-\infty$, as N_b^* tends to 0. For $b > b^*$ we observe an unique fixed point for $F(N)$, corresponding with the equilibrium N^*.

Remark 5.2.5 (τ dependence on b^*). As we have shown in theorem 5.2.3, using the same notation, there is a value b^* which represents a transition between stability and instability of the equilibrium to equation (5.2.6). At b^* the equilibrium to equation (5.2.6) is $N_{b^*}^*$ and

$$f'(N_{b^*}^*) = \frac{-\partial_N I(b^*, N_{b^*}^*)}{\left(I(b^*, N_{b^*}^*) + \tau\right)^2} = -1. \tag{5.2.7}$$

We know from lemma 4.3.3 that function $g(b) = f'(N_b^*)$ is increasing on b, but if we consider τ as another variable, it can easily be verified that $g(b, \tau)$ is also increasing in τ. Thus, for some values $\tau, b^*, N_{b^*}^*$ fulfilling equation (5.2.7), an increase in the value of τ will require a decrease in the value of b^* to fulfill the equality. In short, b^* is implicitly a decreasing function of τ, as shown in figure 5.13, where b^* is the projection on the horizontal axis of the line separating the stability region from the instability region. This dependence between b^* and τ can also be observed in the figure 5.3, where a bigger value of τ in the right plot involves lower values of b to get three fixed points to function $F(N)$, in comparison with the left plot.

We have proved that the sequence of firing rates given by (5.2.1) converges in some cases to a value N^*, which is an steady state of the system (5.1.1), i.e. we can call it N_∞ and it fulfills equation (5.2.4). Relying on this result, we are able to prove the pointwise convergence of the sequence of pseudo-equilibria given by (5.2.2) to the steady state $p_\infty(v)$ associated to N_∞.

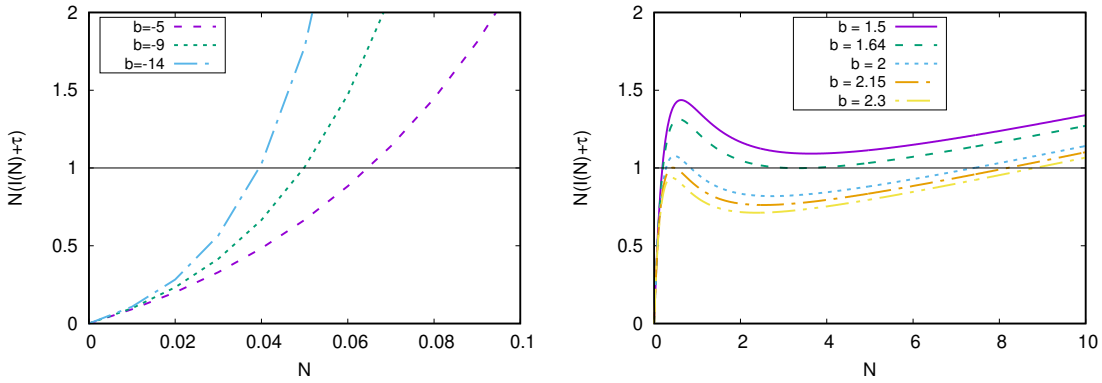

Figure 5.2: **Function $N\,(I(N)+\tau)$ (see (5.1.5)) for $\tau = 0.06$ and different values of the connectivity parameter b.** Intersections between the curves relative to each value of b and the straight line 1 mean solutions of the equation (5.1.6).

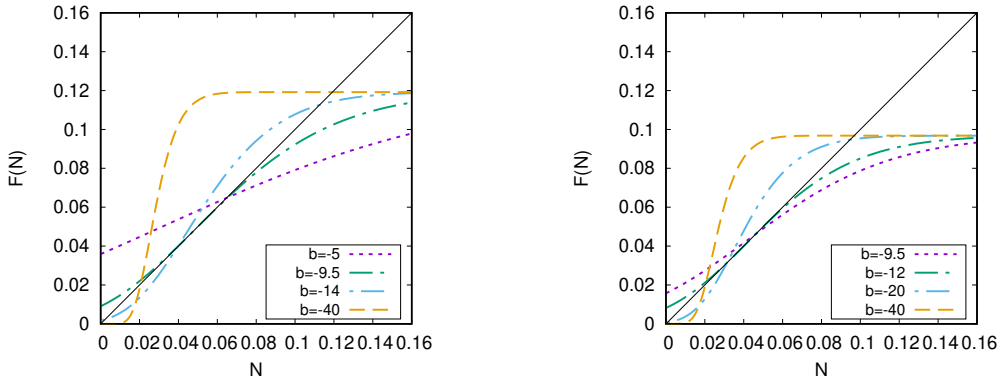

Figure 5.3: **Function $F := f \circ f$ with $f = \frac{1}{I(N)+\tau}$ (see (5.1.5)) for different values of the connectivity parameter b.** *Left:* $\tau = 0.06$. *Right:* $\tau = 2$.

Theorem 5.2.6. *Considering the firing rate sequence $\{N_{k,\infty}\}_{k\geq 0}$ given in (5.2.1), and its related pseudo-equilibria sequence $\{p_{k,\infty}(v)\}_{k\geq 0}$ described in (5.2.2), if $\lim_{k\to\infty} N_{k,\infty} = N_\infty$ and $N_\infty < \infty$, then $\exists\ k_0 \in \mathbb{N}$ such that for all $k \geq k_0$ the following inequality holds:*

$$|p_{k+1,\infty}(v) - p_{k,\infty}(v)| \leq C_{N_\infty} |N_{k,\infty} - N_{k-1,\infty}|, \quad \forall v \in (-\infty, V_F], \tag{5.2.8}$$

where $C_{N_\infty} > 0$ and depends on N_∞. Consequently,

$$\{p_{k,\infty}(v)\}_{k\geq 0} \to p_\infty(v) \text{ when } k \to \infty,\ \forall v \in (-\infty, V_F]\,,$$

and $p_\infty(v)$ is a steady state of the non-linear system (5.1.1), with N_∞ its related firing rate.

Proof. This proof is complementary to the one of theorem 4.3.10, so we will be brief and focus only on the differences that arise from taking into account the refractory state.

We note that, if N_∞ is the limit of the sequence of firing rates $\{N_{k,\infty}\}_{k\geq 0}$, it is a fixed point of the implicit equation $N\left(I(N)+\tau\right)=1$ and

$$p_\infty(v) = N_\infty e^{-\frac{(v-bN_\infty)^2}{2}} \int_{\max(v,V_R)}^{V_F} e^{\frac{(w-bN_\infty)^2}{2}} dw,$$

is a steady state of the non-linear system (5.1.1).

For a fixed value of v, we define the functions $h_v(N_{k-1,\infty}) := p_{k,\infty}(v)$ and $g(v,N) := e^{-\frac{(v-bN)^2}{2}} \int_{\max(v,V_R)}^{V_F} e^{\frac{(w-bN)^2}{2}} dw$, so that we can write $h_v(N_{k-1,\infty}) = \frac{g(v,N_{k-1,\infty})}{I(N_{k-1,\infty})+\tau}$. We use a first order Taylor's expansion to write the difference between two consecutive elements of the sequence of pseudo-equilibria, $\{p_{k,\infty}\}_{k\geq 0}$, as

$$p_{k+1,\infty}(v) - p_{k,\infty}(v) = h_v'(\xi_k)\left(N_{k,\infty} - N_{k-1,\infty}\right),$$

where ξ_k is some value between $N_{k-1,\infty}$ and $N_{k,\infty}$. By computing the derivative of $h_v(N)$ we obtain

$$h_v'(N) = \frac{\partial_N g(v,N)\left(I(N)+\tau\right) - I'(N)g(v,N)}{\left(I(N)+\tau\right)^2} = \frac{\partial_N g(v,N)}{\left(I(N)+\tau\right)} - \frac{I'(N)g(v,N)}{\left(I(N)+\tau\right)^2}. \quad (5.2.9)$$

Given $\epsilon > 0$, $\exists\ k_0 \in \mathbb{N}$ such that $N_{k-1,\infty}$, $N_{k,\infty} \in (N_\infty - \epsilon, N_\infty + \epsilon)$ for all $k \geq k_0$, because $\lim_{k\to\infty}\{N_{k,\infty}\}_{k\geq 0} = N_\infty < \infty$. In particular, $\exists\ k_0$ such that $\xi_k \in (N_\infty - \epsilon, N_\infty + \epsilon)$ for all $k \geq k_0$. Therefore, if $|h_v'(N_\infty)| < \infty$ we obtain that $|h_v'(\xi_k)| < C_{N_\infty}$ for all $k \geq k_0$ (by continuity) and inequality (5.2.8) is proven, since constant C_{N_∞} only depends on N_∞. With the aim of bound $|h_v'(N_\infty)|$, we compute

$$h_v'(N_\infty) = N_\infty \partial_N g(v,N_\infty) - N_\infty I'(N_\infty) p_\infty(v) \quad (5.2.10)$$

using that $N_\infty\left(I(N_\infty)+\tau\right) = 1$ for the stationary firing rate N_∞. Using the bounds showed in the proof of theorem 4.3.10, we prove that $h_v'(N_\infty) < \infty$. □

The following theorem extends previous result to inhibitory cases $b < 0$, taking into account possible convergence of the firing rate sequence $\{N_{k,\infty}\}_{k\geq 0}$ towards 2-cycle $\{N^-, N^+\}$.

Theorem 5.2.7. *Let us consider the firing rate sequence* $\{N_{k,\infty}\}_{k\geq 0}$ *given in* (5.2.1)*, and its related pseudo-equilibria sequence* $\{p_{k,\infty}(v)\}_{k\geq 0}$ *described in* (5.2.2)*, if the sequence* $\{N_{k,\infty}\}_{k\geq 0}$ *tends to the 2-cycle* $\{N^-, N^+\}$*, then* $\exists\ k_0 \in \mathbb{N}$ *such that for all* $k \geq k_0$ *the following inequality holds:*

$$|p_{2k,\infty}(v) - p_{2k-2,\infty}(v)| \leq C_{N^-}|N_{2k-1,\infty} - N_{2k-3,\infty}|, \quad \forall v \in (-\infty, V_F], \tag{5.2.11}$$

$$|p_{2k+1,\infty}(v) - p_{2k-1,\infty}(v)| \leq C_{N^+}|N_{2k,\infty} - N_{2k-2,\infty}|, \quad \forall v \in (-\infty, V_F], \tag{5.2.12}$$

where $C_{N^-}, C_{N^+} > 0$ *depend on* N^- *and* N^+*, respectively. Consequently,*

$$\{p_{2k-1,\infty}(v)\}_{k\geq 1} \to p^-(v) \text{ when } k \to \infty,\ \forall v \in (-\infty, V_F]\,,$$

$$\{p_{2k,\infty}(v)\}_{k\geq 0} \to p^+(v) \text{ when } k \to \infty,\ \forall v \in (-\infty, V_F]\,,$$

where $p^-(v), p^+(v)$ *are pseudo-equilibria of the non-linear system* (5.1.1)*, given by*

$$p^-(v) = N^- e^{-\frac{\left(v-bN^+\right)^2}{2}} \int_{\max(v,V_R)}^{V_F} e^{\frac{\left(w-bN^+\right)^2}{2}} dw, \quad N^- = \frac{1}{I(N^+)+\tau} \tag{5.2.13}$$

and

$$p^+(v) = N^+ e^{-\frac{\left(v-bN^-\right)^2}{2}} \int_{\max(v,V_R)}^{V_F} e^{\frac{\left(w-bN^-\right)^2}{2}} dw, \quad N^+ = \frac{1}{I(N^-)+\tau}, \tag{5.2.14}$$

respectively.

Proof. The proof is analogous to that of the theorem 5.2.6, so we follow the same notation as in it. We note that the properties of the equilibria used in the previous theorem for $p_\infty(v)$ and $N_\infty\left(I(N_\infty)+\tau\right)$, such as $p_\infty(v)$ bounded in $v \in (-\infty, V_F]$ and $N_\infty\left(I(N_\infty)+\tau\right) = 1$, will be also true for the pseudo-equilibria $p^+(v)$, $p^-(v)$ and $N^+I(N^-)$, $N^-I(N^+)$. The main ingredient here is to consider the corresponding subsequences with even and odd terms. In this way, we write the difference between two odd or even consecutive elements of the sequence $\{N_{k,\infty}\}_{k\geq 0}$, for all $v \in (-\infty - V_F]$, by using first order Taylor expansions over expression (5.2.2):

$$p_{2k,\infty}(v) - p_{2k-2,\infty}(v) = h_v'\left(\xi_k^-\right)\left(N_{2k-1,\infty} - N_{2k-3,\infty}\right),$$

$$p_{2k+1,\infty}(v) - p_{2k-1,\infty}(v) = h_v'\left(\xi_k^+\right)\left(N_{2k,\infty} - N_{2k-2,\infty}\right),$$

with ξ_k^-, ξ_k^+ real values between $N_{2k-1,\infty}$, $N_{2k-3,\infty}$, and $N_{2k,\infty}$, $N_{2k-2,\infty}$, respectively. Given $\epsilon > 0$, $\exists\ k_0 \in \mathbb{N}$ such that $N_{2k-1,\infty}$ and $N_{2k-3,\infty} \in (N^- - \epsilon, N^- + \epsilon)$, while $N_{2k,\infty}$ and $N_{2k-2,\infty} \in (N^+ - \epsilon, N^+ + \epsilon)$ for all $k \geq k_0$, because $\lim_{k\to\infty}\{N_{2k-1,\infty}\}_{k\geq 1} = N^- < \infty$

and $\lim_{k\to\infty}\{N_{2k,\infty}\}_{k\geq 0} = N^+ < \infty$. This means that $\xi_k^- \in (N^- - \epsilon, N^- + \epsilon)$ and $\xi_k^+ \in (N^+ - \epsilon, N^+ + \epsilon)$ for all $k \geq k_0$. Thus, the proof of this theorem lies in proving that $|h_v'(N^-)| < \infty$ and $|h_v'(N^+)| < \infty$, because, as a consequence (by continuity), we obtain that $|h_v'(\xi_k^-)| < C_{N^-}$ and $|h_v'(\xi_k^+)| < C_{N^+}$ for all $k > k_0$, and certain $k_0 \geq 2$.

We write $h_v'(N)$ as

$$h_v'(N) = \frac{\partial_N g(v,N)\,(I(N)+\tau) - I'(N)g(v,N)}{(I(N)+\tau)^2} = \frac{\partial_N g(v,N)}{(I(N)+\tau)} - \frac{I'(N)g(v,N)}{(I(N)+\tau)^2}.$$

Having verified that introduction of the refractory period has no influence on the terms to be bounded, the final part of the proof is identical to the one made for theorem 4.3.11, so that it can be consulted there.

□

5.3 Numerical study of the refractory NNLIF model

In this section we perform a numerical study of the integrate-and-fire model with refractory period (5.1.1), to compare the results with the behaviors predicted in section 5.2 by the pseudo-equilibria sequence study (5.2.2) and observe what happens in blow-up situations. By performing this comparison we expect to find agreement between the numerical results and the sequence of pseudo-equilibria, when the delay is sufficiently large, as explained in chapter 4. For this task we will use two different schemes: a microscopic point of view through a system of stochastic differential equations (SDE) whose detailed explanation of which can be found in the section 2.3, and a mesoscopic description consisting of approximating the Fokker-Planck equation through a WENO type scheme (see the appendix of [118] for a detailed explanation). The use of both microscopic and mesoscopic scales for a more complete description of the NNLIF neural network model has already been done by other authors [58]. This will allow us to relate the solution of the model with refractory period to the notion of physical solution (see section 2.2) given by Delarue et. al. in [52].

The initial conditions considered in our simulations are constructed though the pseudo-equilibria profiles (see (5.2.2))

$$p(v) = \bar{N} e^{-\frac{(v,bN)^2}{2}} \int_{\max(v,V_R)}^{V_F} e^{\frac{(w-bN)^2}{2}} dw, \quad R = 1 - \int_{-\infty}^{V_F} p(v)dv. \tag{5.3.1}$$

The procedure for the construction of the initial conditions consists of the following steps:

- We fix N, b and the refractory time τ.
- We compute $\bar{N}$ by solving the equation $\bar{N} = (I(N) + \tau)^{-1}$, with $I(N)$ defined in (5.1.5) as
$$I(N) = \int_{-\infty}^{V_F} e^{-\frac{(v-bN)^2}{2}} \int_{\max(v,V_R)}^{V_F} e^{\frac{(w-bN)^2}{2}} dwdv.$$
- This ensures N and $\bar{N}$ to be consecutive element of the firing rate sequence $N_{k+1,\infty} = 1/\left(I(N_{k,\infty}) + \tau\right)$, given in (5.2.1), and likewise $p(v)$ to be the element of the pseudo-equilibria sequence related with N and $\bar{N}$, as shown in equation (5.3.1).
- We set $R(0) = 1 - \int_{-\infty}^{V_F} p(v)dv$ and therefore the mass is conserved.
- For the Fokker-Planck equation approximation we directly used the discretization in v of this profile as initial condition. However, for the microscopic approximation, we need to use the profile as a probability to give values to the voltage of the particle sample.

Throughout the different simulations, we will consider the following fixed values for the system parameters: $V_R = 1$, $V_F = 2$ and $\tau = 0.06$. While, the connectivity parameter b and the delay d will change depending on the simulation, showing us different phenomena. Specifically, we are going to study two different regimes according to the value of b. The excitatory regime, $b > 0$ and the inhibitory one, $b < 0$. The value of τ has been chosen to be of the same order of magnitude as the values used previously in published papers on this model [16, 86].

5.3.1 Excitatory case

Within the excitatory regime, there are two possibilities in terms of the number of steady states of the system (5.1.1). This means that there are two ranges of values of b for which there are different numbers of solutions of the equation

$$N\left(I(N) + \tau\right) = 1, \quad N > 0.$$

In the right plot of figure 5.2 we see representative values for both the case with one steady state, $b = 2.3$, and the case with three steady states, $b = 2$.

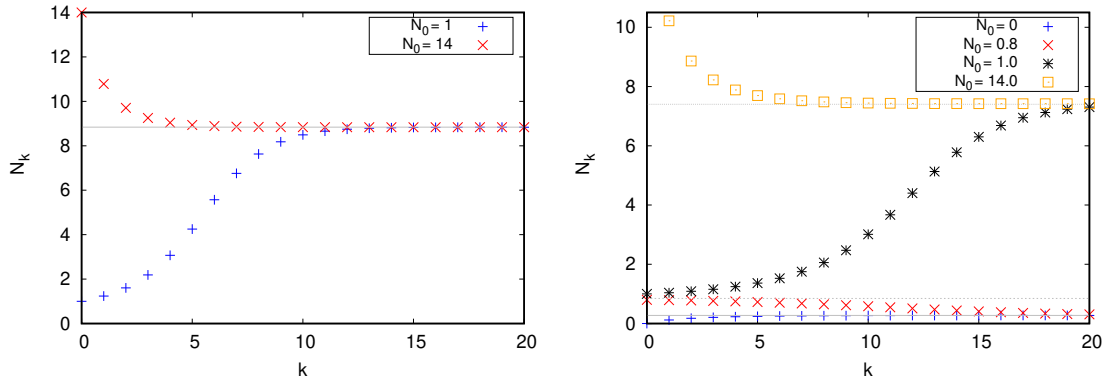

Figure 5.4: **Firing rate sequence $N_{k,\infty}$ (5.2.1) with different values of the initial condition $N_{0,\infty}$.** Gray lines represents the value of stationary firing rates associated with equilibria. *Left:* $b = 2.3$. *Right:* $b = 2$.

One steady state

According to figure 5.2, the steady state of the non-linear system (5.1.1) for $b = 2.3$, has firing rate $N^* \approx 8.84$. Left plot of figure 5.4 shows the behavior of the firing rate sequence $\{N_{k,\infty}\}_{k\geq 0}$ with initial condition $N_{0,\infty} = 1 < N^*$ or $N_{0,\infty} = 14 > N^*$. We observe convergence to the steady state, in agreement with theorem 5.2.2.

In the numerical simulations of the non-linear model we construct the initial condition with profiles (5.3.1), following the procedure stated at the beginning of the section. We set $N = 1$ in the first case and $N = 14$ in the second one. For each initial condition we simulate the solution to the equation (5.1.1) with transmission delay $d = 2$. In figure 5.5 we show the results related to the initial condition build with $N = 1$. In the left plot, we observe convergence to equilibrium for the firing rate, although oscillations appear when the delay interval changes, for high values of N. In the right plot we observe the initial condition, the equilibrium profile and $p(v, t)$ at the end of the simulation, which is very close to the equilibrium. Figure 5.6 shows the same numerical experiment, performed for the initial condition with $N = 14$. We see a similar behavior as before, but with such strong oscillations in between delay intervals that the simulation may break down before reaching equilibrium. Because of these oscillations, which can be clearly seen in the bottom of figure 5.6, we can say that at the end of each delay interval the solution of the linear system is close to the corresponding pseudo-equilibrium, or to the equilibrium if enough time has passed, but we cannot say that there are no periodic solutions or persistent oscillations.

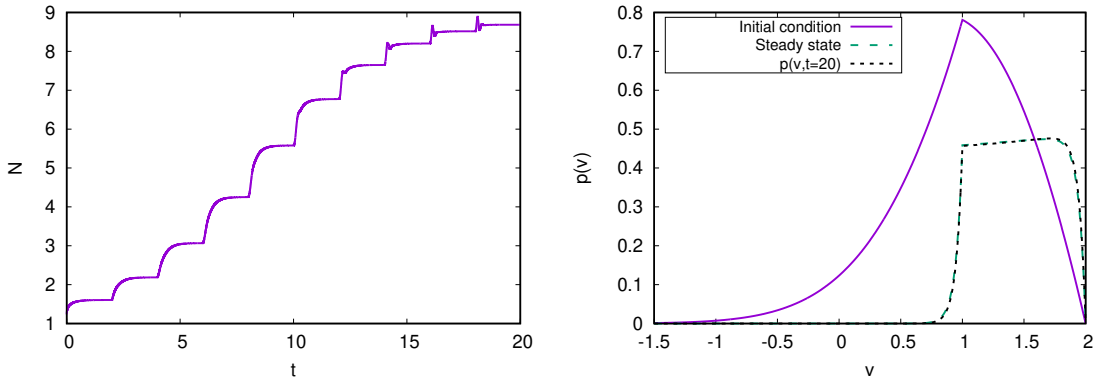

Figure 5.5: **Non-linear system** (5.1.1) **with** $b = 2.3$ **and** $d = 2$. $N_0 < N^*$. *Left:* Firing rate $N(t)$ computed for the Fokker-Planck equation, up to $t = 20$. *Right:* Initial condition given by profiles (5.3.1) with $N = 1$, $\bar{N} < N^*$, steady state $p_\infty(v)$ and approximated $p(v,t)$ at time $t = 20$.

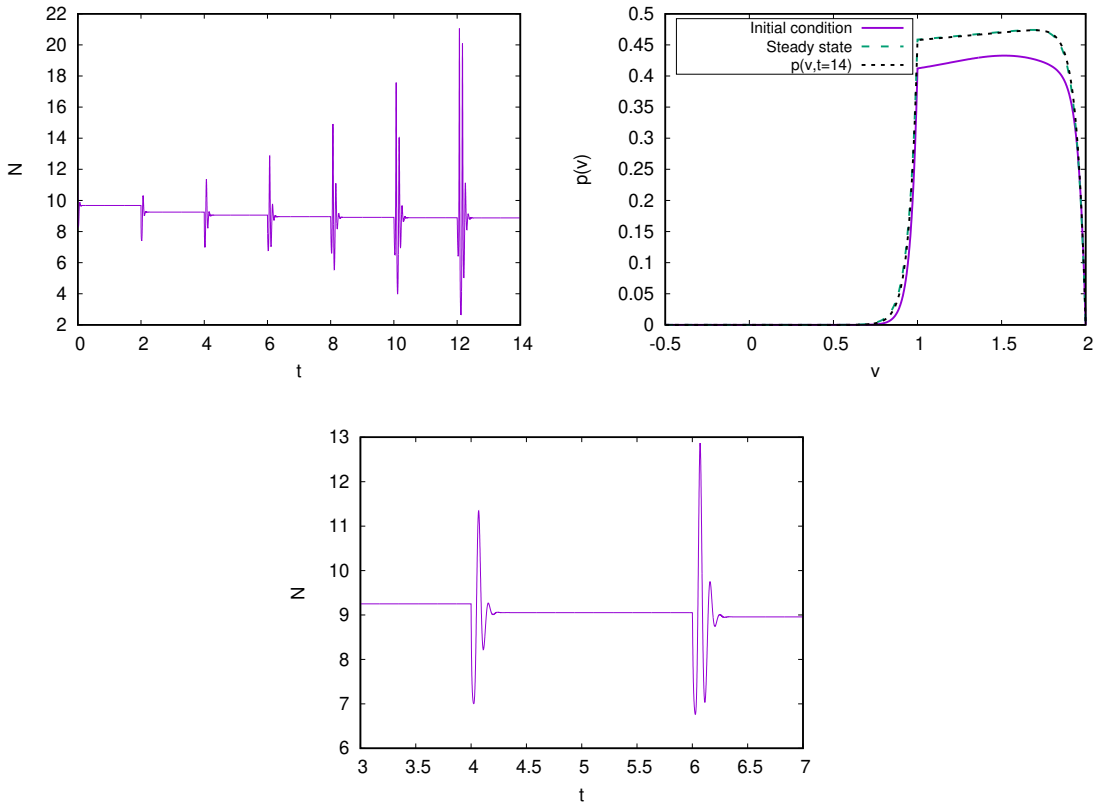

Figure 5.6: **Non-linear system** (5.1.1) **with** $b = 2.3$ **and** $d = 2$. $N_0 > N^*$. *Left:* Firing rate $N(t)$ computed for the Fokker-Planck equation, up to $t = 14$. *Right:* Initial condition given by profiles (5.3.1) with $N = 14$, $\bar{N} > N^*$, steady state $p_\infty(v)$ and approximated $p(v,t)$ at time $t = 14$. *Bottom:* Enlarged part of the left plot.

Three steady states

For the value $b = 2$ there are three equilibria to the nonlinear system (5.1.1), whose associated firing rates are $N_1^* \approx 0.274$, $N_2^* \approx 0.847$ and $N_3^* \approx 7.4$. The right plot of figure 5.4 shows numerically the content of theorem 5.2.2, concerning the sequence of firing rates: if $N_{0,\infty}$ is placed between N_1^* and N_2^*, the sequences tend to N_1^*. If $N_{0,\infty}$ is between N_2^* and N_3^* or it is greater than N_3^*, $\{N_{k\infty}\}_{k\geq 0}$ tends to N_3^*. Therefore, there is bi-stability between low and high equilibria, while intermediate equilibrium is unstable and serves as boundary between the zones of attraction of the others equilibria.

In the simulations of the nonlinear system, we are going to use four different initial conditions, which are constructed through profiles (5.3.1), using the same values of N that we used for the succession of firing rates in figure 5.4 ($N = 0, 0.8, 1, 14$). The transmission delay will be $d = 2$ and the connectivity parameter $b = 2$. Figure 5.7 shows the results obtained for the lowest initial condition. On the left plot of the figure, we observe the convergence to the low equilibria in terms of the firing rate. The right plot shows the shapes of the initial condition, low steady state and $p(v, t)$ at the end of the simulation, which coincides with the low steady state. For the simulation performed with initial condition relative to $N = 0.8$, shown in figure 5.8, the same tendency towards the low equilibrium as in the previous case is observed. In the last two cases the firing rate of the initial condition is higher than the one of the intermediate equilibrium, $N_0 = 1 < N_3^*$ as shown in figure 5.9 and $N_0 = 14 > N_3^*$ as shown in figure 5.10. In the first case there is convergence towards high equilibrium, as would be expected after studying the sequence of pseudo-equilibria. In the second case there also seems to be convergence to high equilibrium, but as in the cases with $b = 2.3$, oscillations appear between delay intervals.

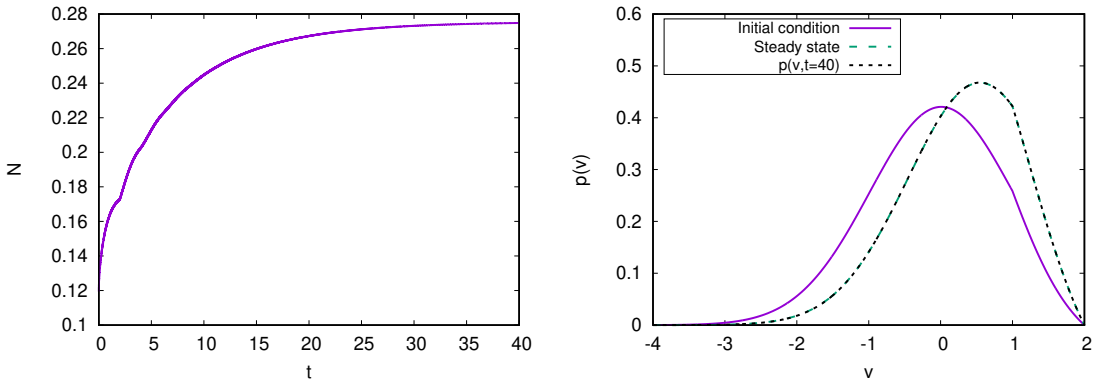

Figure 5.7: **Non-linear system (5.1.1) with $b = 2$ and $d = 2$. $N_0 < N_1^*$.** *Left:* Firing rate $N(t)$ computed for the Fokker-Planck equation, up to $t = 40$. *Right:* Initial condition given by profiles (5.3.1) with $N = 0$, $\bar{N} < N_1^*$. Steady state $p_\infty(v)$ corresponding to N_1^*. Approximated distribution $p(v, t = 40)$, computed by the Fokker-Planck equation.

Summarizing, for the excitatory case with three equilibria, when the delay is sufficiently high, theorem 5.2.2 for the sequence of pseudo-equilibria is fulfilled, with an oscillatory issue that appear in between delay intervals, for very excitatory cases.

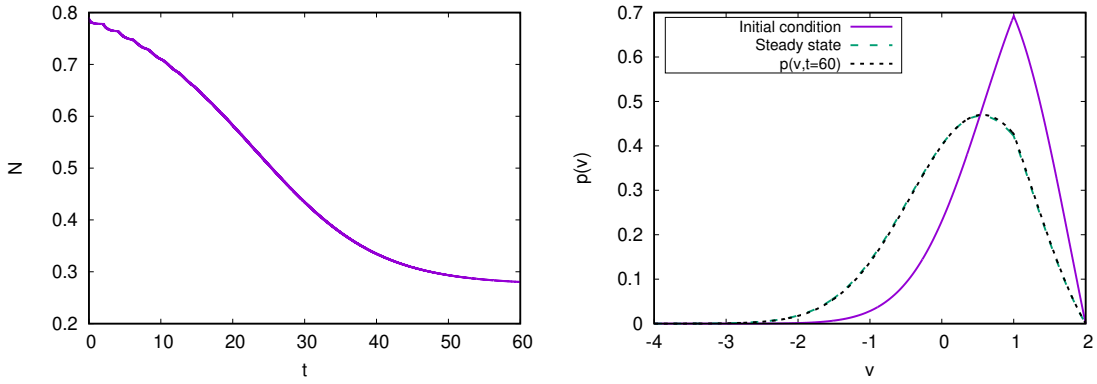

Figure 5.8: **Non-linear system (5.1.1) with $b = 2$ and $d = 2$. $N_1^* < N_0 < N_2^*$.** *Left:* Firing rate $N(t)$ computed for the Fokker-Planck equation, up to $t = 60$. *Right:* Initial condition given by profiles (5.3.1) with $N = 0.8$, $N_1^* < \bar{N} < N_2^*$. Steady state $p_\infty(v)$ corresponding to N_1^*. Approximated distribution $p(v, t = 60)$, computed by the Fokker-Planck equation.

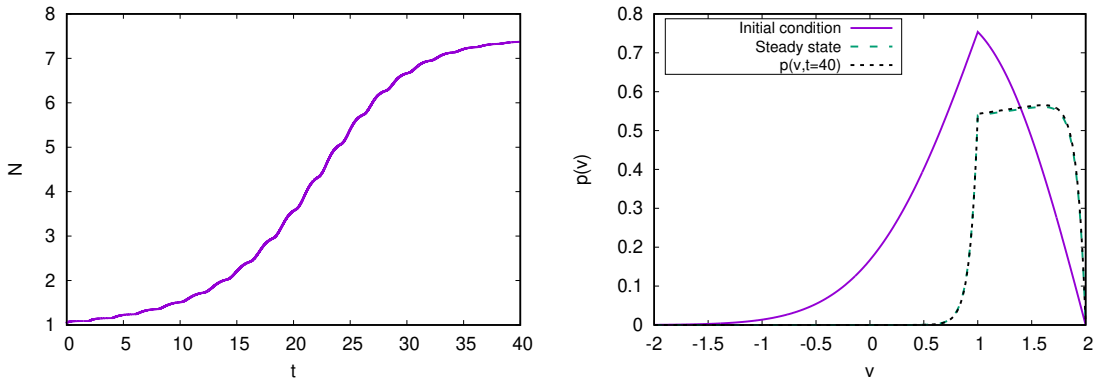

Figure 5.9: **Non-linear system (5.1.1) with $b = 2$ and $d = 2$. $N_2^* < N_0 < N_3^*$.** *Left:* Firing rate $N(t)$ computed for the Fokker-Planck equation, up to $t = 40$. *Right:* Initial condition given by profiles (5.3.1) with $N = 1$, $N_2^* < \bar{N} < N_3^*$. Steady state $p_\infty(v)$ corresponding to N_3^*. Approximated distribution $p(v, t = 40)$, computed by the Fokker-Planck equation.

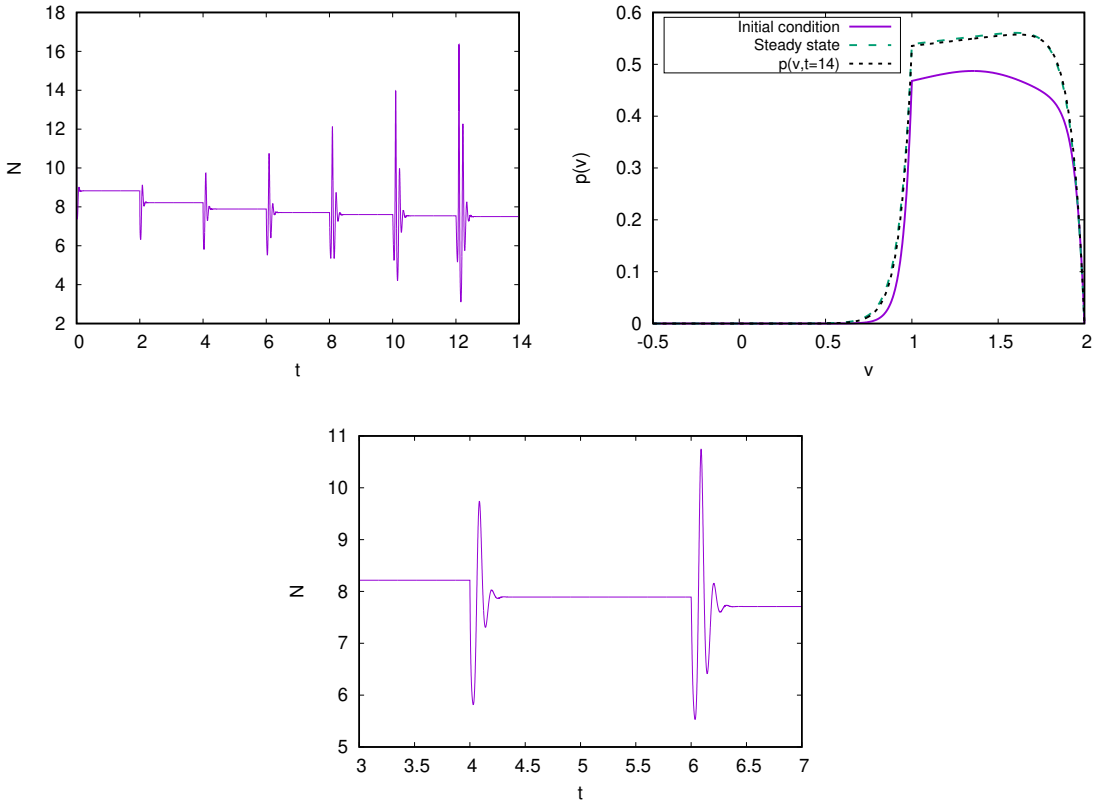

Figure 5.10: **Non-linear system (5.1.1) with $b = 2$ and $d = 2$. $N_0 > N_3^*$.** *Left:* Firing rate $N(t)$ computed for the Fokker-Planck equation, up to $t = 14$. *Right:* Initial condition given by profiles (5.3.1) with $N = 14$, $\bar{N} > N_3^*$. Steady state $p_\infty(v)$ corresponding to N_3^*. Approximated distribution $p(v, t = 14)$, computed by the Fokker-Planck equation. *Bottom:* Enlarged part of the left plot.

Periodic solutions arising after blow-up

Apart from the simulations performed with the scheme for the Fokker-Planck equation, the scheme for the system of SDEs used in chapter 2 has helped us to study what happens in blow-up situations for the model with refractory state, with and without delay. As stated in [16] the NNLIF model with refractory state may blows-up if $b > 0$ and the initial condition is concentrated near to the firing threshold. With this aim we have used initial conditions that simulate Dirac delta functions near the firing threshold, and we have simulated the microscopic system with two different values of delay, $d = 0$ and $d = 0.01$. In figure 5.11 we observe the results in terms of the firing rate. We have performed this same experiment for both $b = 2$ and $b = 2.3$ and the result obtained is basically the same, apart from the different size of the oscillations. We found periodic states both with small delay and without delay. With small delay this phenomenon has been observed before [20, 86].

However, to our knowledge, this is the first time it has been observed without delay.

The fact of finding after the blow-up, behaviors other than a numerical break in the simulation, or a trivial state as observed in chapter 2, where the neurons were firing constantly, allows us to relate the microscopic system with refractory state to the physical solutions [52]. We defined and studied numerically this kind of solutions to the microscopic system without refractory state in chapter 2. The fundamental property of physical solutions is that solution after the blow-up can be defined by controlling the size of the impulse it produces in the network, ensuring no neuron fires twice at the same time. So we could say that the solutions to the microscopic system with a refractory state are physical in the sense that they continue after blow-up and no neuron can spike twice at same time.

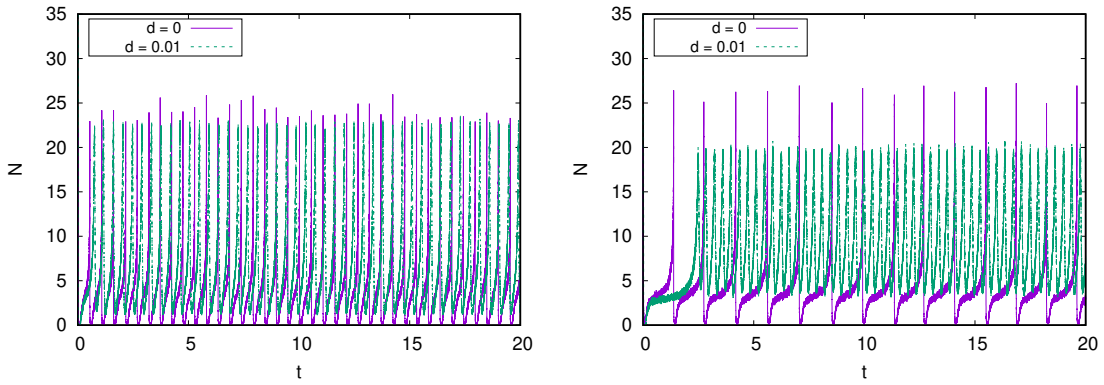

Figure 5.11: **Non-linear system (5.1.1) with periodic solutions.** Firing rate $N(t)$ computed for the particle system, up to $t = 20$, with different values of delay. Initial condition given by a Gaussian distribution with mean and standard deviation $\mu = 1.88$ and $\sigma = 0.003$, approaching a Dirac's delta near to the firing threshold. *Left:* $b = 2.3$. *Right:* $b = 2$.

Inhibitory case with large delay

For the cases considered within the inhibitory regime, those with $b < 0$, there is only one equilibrium to the nonlinear system (5.1.1), as shown in figure 5.2 and proved in [16]. Thus, for each negative value of b and fixed τ, there will be an equilibrium $p_\infty(v)$ with associated firing rate N_∞. Then a question arises: for a fixed b, what is the effect of the refractory time and delay on the equilibrium stability? First we answer this question for the sequence of pseudo-equilibria, by means of theorems 5.2.3 and 5.2.7 and the numerical work given below. Then we simulate the non-linear system (5.1.1) using a sufficiently large delay, and compare the results with the obtained for the sequence of pseudo-equilibria.

Theorems 5.2.3 and 5.2.7 show that, for any fixed $\tau > 0$ it is possible to find a value b^* such that the sequence of firing rates $\{N_{k,\infty}\}_{k\geq 0}$ converges to N_∞ for $b > b^*$, or it converges to a 2-cycle $\{N^-, N^+\}$ for $b < b^*$. This behavior, for $\tau = 0.06$ and different values of b, can be observed in figure 5.12, setting the approximated value of b^* around -9.5, that is a little higher than for $\tau = 0$, where $b^* \approx -9.4$ (see figure 4.8). This leads us to think that the increase in the value of the refractory time implies a decrease in the value of b^* (see remark 5.2.5). In figure 5.13 we show for which values of b, τ there is convergence of the firing rate sequence to a unique equilibrium or a 2-cycle.

For the simulations of the nonlinear system we will consider different values of b and two possible values for the delay, $d = 0$ and $d = 25$. The refractory time will be set to $\tau = 0.06$ and the initial condition will be always given by the profile (5.3.1) with $N = 0$ and $\bar{N} = 0.12$, because in the inhibitory cases the initial condition does not change the long range behavior of the non-linear system, as we point out in chapter 4. Figure 5.14 shows how, for $d = 0$, all values of b lead to the same asymptotic behavior, the system converges to its unique equilibrium. The left side of the figure shows the convergence in terms of $N(t)$ and the right side shows the final shapes of the distributions $p(v, t)$, which coincide with the respective equilibria for each b. However, in figure 5.15 it is observed that, when we consider a sufficiently large delay, specifically $d = 25$, the value of b determines the convergence to the equilibrium or to the 2-cycle $\{N^-, N^+\}$. On the left we see how the oscillatory behavior increases as b decreases, in terms of the firing rates. On the right we observe a clear overlapping between $p(v, t)$ and the pseudo-equilibria $\{p^-, p^+\}$, at different times, for $b = -14$.

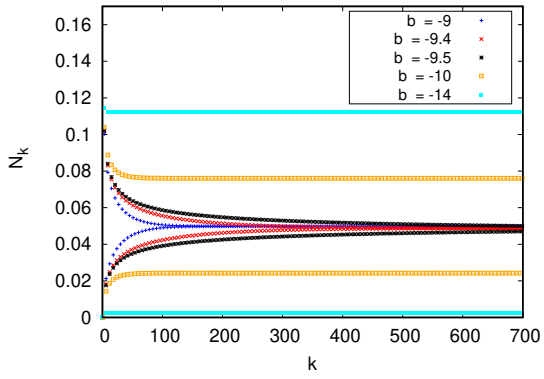

Figure 5.12: **Firing rate sequence $N_{k,\infty}$ (5.2.1) for different values of $b < 0$ with $N_{0,\infty} = 0$.** The approximated value for which the sequence of firing rates no longer converges to a unique equilibrium, but rather to a 2-cycle, is $b = -9.4$.

Summarizing the results regarding the inhibitory case, we can say that oscillatory behavior is observed for the NNLIF model with refractory period, in similar conditions to those observed for the model without refractory period. An inverse proportionality relationship is also observed between the value of the refractory period and the required value of the connectivity parameter to find periodic states, b^*.

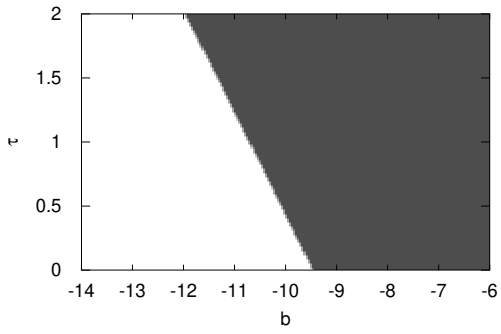

Figure 5.13: **Convergence of the firing rate sequence $N_{k,\infty}$ (5.2.1) for different values of $b < 0$ with $N_{0,\infty} = 0$, depending on b and τ.** Black means that $N_{k,\infty}$ converges to a unique value N_∞. White means that $N_{k,\infty}$ converges to a 2-cycle $\{N^-, N^+\}$. To determine the type of convergence, we compute 200 elements of $N_{k,\infty}$ (for each pair b, τ) and we examine the difference between the last two elements in absolute value. If this quantity is less than 0.001 we consider it as stable (convergence to N_∞), otherwise it is considered unstable (2-cycle).

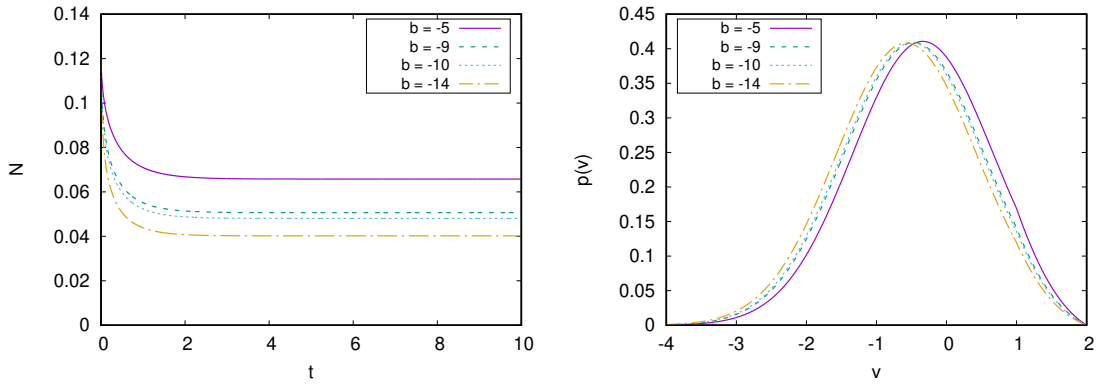

Figure 5.14: **Non-linear system (5.1.1) with $b < 0$ and $d = 0$. Initial condition given by (5.3.1) with $N = 0$ and $\bar{N} = 0.12$.** *Left:* Firing rate $N(t)$ for different values of b, up to time $t = 10$. *Right:* Approximated $p(v, t)$ for different values of b at $t = 300$.

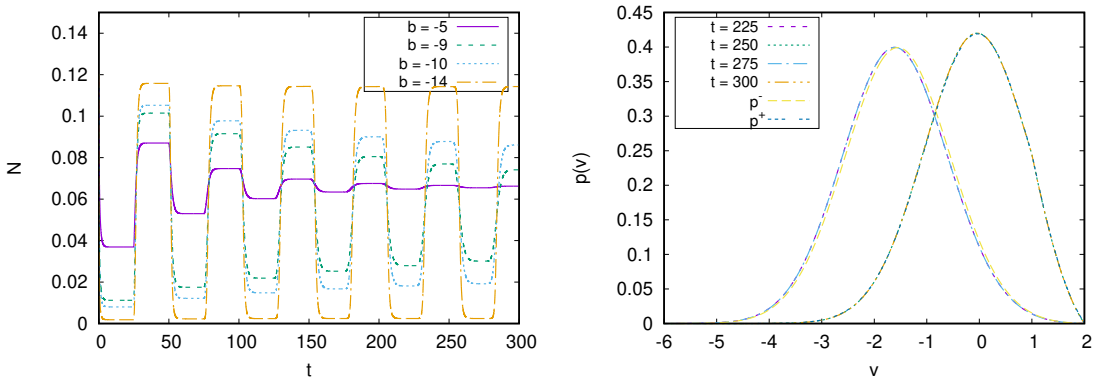

Figure 5.15: **Non-linear system (5.1.1) with $b < 0$ and $d = 25$. Initial condition given by (5.3.1) with $N = 0$ and $\bar{N} = 0.12$.** *Left:* Firing rate $N(t)$ for different values of b, up to time $t = 300$. *Right:* Approximated $p(v, t)$ at times $9d, 10d, 11d$ and $12d$, compared with the pseudo-equilibria $p^-(v)$ and $p^+(v)$.

5.4 Conclusions

This chapter is devoted to study the long-term behavior of the NNLIF model with refractory period, as it was proposed in [16]. For this purpose, we have performed the analysis of the sequence of pseudo-equilibria (5.2.2) with the associated sequence of firing rates (5.2.1). In addition, we have carried out several numerical experiments on the non-linear system (5.1.1). Our guess, which was numerically corroborated in chapter 4 for the non-refractory model, is that the monotonicity of the sequence of pseudo-equilibria should completely govern the long-term behavior of the nonlinear model with large delay. We complete this study using the tools developed in chapter 2 to observe what happens in blow-up situations for the NNLIF model with refractory period, from the point of view of the microscopic explained in 1.2.1 with refractory state.

In section 5.2 we make a complete characterization of the monotony and convergence of the firing rate and pseudo-equilibria sequences for any possible range of the connectivity parameter. For the excitatory regime ($b > 0$), in the case of one equilibrium, it should be stable regardless of the initial condition. However, in the case of three equilibria, there is bi-stability between the low and high equilibria, depending on the value of the firing rate of the initial condition. For the inhibitory case ($b < 0$), where there is always a unique equilibrium, the sequence of pseudo-equilibria tends towards a 2-cycle.

In contrast to the results obtained in chapter 4, no situations are observed where the sequence of firing rates diverges, thus avoiding the possibility of forming plateau distributions in the conditions where it could occur in the model without refractory state. A graphical representation of the behavior observed for the firing rate sequence, both in the excitatory and inhibitory cases, can be seen in the figures 5.4 and 5.12.

The numerical results presented in section 5.3 checked the predictions established by the pseudo-equilibrium sequence, for the non-linear system with refractory period and large delay. In the excitatory case we find:

- In the case with a high unique steady state, stability of the equilibrium, which is what we would expect after studying the sequence of pseudo-equilibria, presents some problems. We can say that as the sequence of pseudo-equilibria points out, at the end of each delay interval the system is close to its pseudo-equilibrium, which will coincide with the equilibrium if enough time has passed. However, the appearance of oscillations may imply that there are numerical problems with our scheme, such as the difficulty of preserving the equilibrium, or the existence of periodic states.

- In the case with three equilibria, convergence to low equilibrium is guaranteed if the initial condition is below the intermediate equilibrium in terms of firing rate. In cases where the initial condition is between intermediate and high equilibrium, convergence to high is also observed, as expected. Nevertheless, in the cases with initial condition higher than the high equilibrium, we observed oscillatory phenomena similar to those of the case with a single equilibrium.

Oscillations with certain similarities to ours were observed in [86], although the authors themselves emphasize that this phenomenon is not sufficiently studied, and we aim to investigate this further as future work.

For the inhibitory case, the equilibrium is stable without delay, for any b, and it becomes unstable as the delay increase, when $b < b^*$. Numerically, we have observed a linear inverse relationship between the value of the refractory period and the value of b^* (the connectivity at which periodic solutions appear), so that the larger the τ, the smaller the b^* (see figure 5.13).

In the excitatory cases, considering initial conditions that force a blow-up situation, we observe oscillatory solutions. This was found before in [20, 86] for small delay. However, this is the first time that this is observed for zero delay. This leads us to think in the extension of the notion of physical solution, established by Delarue et al. in [52], to the microscopic system with refractory state.

Chapter 6

Discrete minimizers of the interaction energy in collective behavior: a brief numerical and analytic review

6.1 Introduction

Finding configurations[4] with minimum potential energy for a set of particles is a common mathematical problem found across several fields. In its simplest version we consider a potential $V\colon \mathbb{R}^d \to \mathbb{R}\cup\{+\infty\}$ and a number $N \geq 2$ of particles. The problem then consists in finding the configurations $X = \{x_1, \dots, x_N\} \subseteq \mathbb{R}^d$ such that the energy

$$E_N(X) = \sum_{i=1}^{N} \sum_{\substack{j=1 \\ j\neq i}}^{N} V(x_i - x_j) \tag{6.1.1}$$

is as small as possible. These configurations are called *minimizers* or *ground states*. In a broader sense, the problem also involves understanding the structure of these minimizers: their shape, the distribution of their points, and their asymptotic properties for large N. The energy (6.1.1) is clearly invariant by a translation of the points $\{x_1, \dots, x_N\}$, and consequently any translation of a minimizer is also a minimizer. One usually removes this invariance by looking for minimizers with some fixed property, most often by fixing the mean position $\sum_{i=1}^{N} x_i$ to be 0. If V is radially symmetric, then E_N is also invariant by rotations of the points $\{x_1, \dots, x_N\}$, and by their inversion $\{-x_1, \dots, -x_N\}$ (and hence by

[4] This chapter compiles the work sent for publication, whose preprint is [22].

any rigid motion of these points). In all cases, minimizers are the same if V is substituted by $V + C$ for some constant C, so some normalization on V is usually assumed (often, either $\lim_{|x|\to+\infty} V(x) = 0$ or $V(0) = 0$, but not necessarily).

In this chapter we give a short review of numerical methods to calculate these minimizers, and report on some results in dimension $d = 2$ using the publicly available GMIN software developed by David J. Wales (see [130]). We carry out numerical simulations in 2D for potentials of the form

$$V(x) = \frac{|x|^a}{a} - \frac{|x|^b}{b}, \tag{6.1.2}$$

where $a > b$. Due to our choice of coefficients, the term with the a power always represents an attractive potential, and the term with the b power is repulsive. We will also give a short review of the available rigorous results to date.

In the previous statement of the problem, the particles are all identical: they interact with others in an identical way through the pair potential V. More complicated versions of the problem may allow for particles of different types, interacting in different ways with one another. One of the better known contexts where this problem is relevant is chemical physics, where one often wants to find the configuration of minimum possible energy for a given molecule. This is important for example in the study of protein folding, where the natural structure of a protein may be related to its minimum-energy configuration. In the context of molecular structure, the Lennard-Jones interaction potential

$$V(x) = \frac{A}{|x|^{12}} - \frac{B}{|x|^6}, \tag{6.1.3}$$

with $A, B > 0$ given constants, is often taken as a test case. The study of its minimizers (in dimension $d = 3$) has received a lot of attention, and is a notable example of a hard global optimization problem.

In addition to these problems in physics, this chapter is motivated by several collective behavior models where these minimizers are relevant. Among them, perhaps the simplest is the so-called *aggregation equation*,

$$\partial_t u = \operatorname{div}(u(\nabla u * V)), \tag{6.1.4}$$

which is a partial differential equation for $u = u(t, x)$, which represents the density of a certain population which interacts through the potential V. Equilibria of (6.1.4) (if any) must satisfy $\nabla u * V = 0$ on the support of u, which is a property shared by the minimizers of the *continuous interaction energy*

$$E(u) := \int_{\mathbb{R}^d} \int_{\mathbb{R}^d} u(x)u(y)V(x-y)\,\mathrm{d}x\,\mathrm{d}y \tag{6.1.5}$$

in the set of probability measures (or positive measures with a fixed total mass). Hence probability minimizers of the energy (6.1.5) are particular examples of stationary solutions to (6.1.4). To avoid repetition, whenever we speak of minimizers of E it is understood that we always refer to minimizers in the set of probability measures. Finding minimizers of E is a "continuous version" of the problem of minimizing E_N. The link between these problems is interesting, especially if we consider that numerical studies of the continuous problem must inevitably carry out some sort of discretization of the equation, which often leads to some version of the discrete minimization problem of E_N. Hence a proper understanding of the large-N behavior of minimizers of E_N is also useful to justify numerical methods for calculating minimizers of the continuous energy E.

There are also many individual-based models whose "organized states" share similarities with minimizers of E_N. As an example we mention a model from [57]: we consider N individuals with positions and velocities given by (x_i, v_i) for $i = 1, \dots, N$, and the system of ordinary differential equations

$$\begin{aligned} \frac{\mathrm{d}}{\mathrm{d}t} x_i &= v_i, \\ \frac{\mathrm{d}}{\mathrm{d}t} v_i &= (\alpha - \beta |v_i|^2) v_i - \sum_{\substack{j=1 \\ j \neq i}}^{N} \nabla V(x_i - x_j). \end{aligned}$$

This models a set of individuals which interact through a potential V, but also have a preferred movement speed $|v| = (\alpha/\beta)^{1/2}$. It is easy to see that if $X = (y_1, \dots, y_N)$ is a critical point of the energy E_N, then $(x_i(t), v_i(t)) := (y_i + tv, v)$ is a solution to the previous system of equations. In particular, minimizers of E_N yield coherent states or *flocking states* for this model. Minimizers (or critical points) of E_N appear similarly in other models, and this has motivated interest in types of potentials different from the ones usually encountered in physics problems.

Existence of minimizers of E_N For a very general family of potentials it is easy to show that minimizers must exist. If one assumes that V is lower semicontinuous and radially strictly increasing whenever $|x| > R$ for some given $R > 0$, then one may carry out an argument like that in [21, Theorem 4.1] to show their existence: it is not hard to argue that there cannot be "gaps" of size larger than R between the particles of a minimizer, which gives a simple estimate on their diameter. A different argument is given in [26, Lemma 2.1] for power-law potentials, and in [8, Section 1.2] for potentials satisfying $\lim_{|x| \to +\infty} V(x) = 0$.

6.2 Numerical methods

In general the energy E_N from (6.1.1), as a function $E_N\colon \mathbb{R}^{Nd} \to \mathbb{R}\cup\{+\infty\}$, is not convex, and the global optimization problem of finding its minima cannot use the comparatively simpler methods of convex optimization. As mentioned before, there's the problem of invariance by translations, easily avoided by fixing the mean position of particles. The problem of invariance by rotations is harder to avoid, and hence algorithms usually find one of any possible rotations of the minimizer. It can then be hard to decide whether two runs of the same algorithm have given a rotation of the same minimizer, or a fundamentally different minimizer. However, the deeper problem is that there are usually a huge number of stationary states for the energy E_N; that is, points $\{x_1, \dots, x_N\}$ at which

$$\sum_{i=1}^{N} \sum_{\substack{j=1 \\ j\neq i}}^{N} \nabla V(x_i - x_j) = 0 \qquad \text{for all } j = 1, \dots, N. \tag{6.2.1}$$

Many of these are local minima, and runs of standard local minimization algorithms will most often fall into one of these states, and not get to a minimizer. Hence simple descent algorithms such as variants of conjugate gradient descent, or Newton-type methods like LBFGS, will almost surely not find minimizers even for small N. Global minimization algorithms must somehow avoid these "traps" by more clever search techniques. We will give a short overview of numerical methods used for this kind of problems, and then describe the algorithm we use, implemented in the program GMIN by D. Wales [130].

Most numerical methods found in the literature have been tested with the Lennard-Jones potential (6.1.3), and most often in 3D, which is a challenging problem of physical interest and has been the subject of many publications in chemistry journals. A database with all currently available minima of E_N for several potentials in 3D (and molecular minimization problems of other kinds) is available online [132], among them Lennard-Jones and Morse potentials. This database contains references of the first publication for each minimizer, and the reader may also check the unpublished paper [135] for a good list of historical references.

Early methods such as those in [79–82] are *biased* methods, in the sense that they work by "guessing" that minimizers have some kind of regular crystal structure. Initial guesses for a minimizer are obtained by placing particles at the sites of an appropriate lattice, and then running local minimization algorithms to optimize the positions. Then one carries out some kind of random perturbation of these positions in order to find "nearby" local minima which may have a lower energy. In addition to guessing initial candidates by using the sites of a lattice, one may also start by finding minimizers for small N, and add particles to build candidates for larger N. These methods were quite

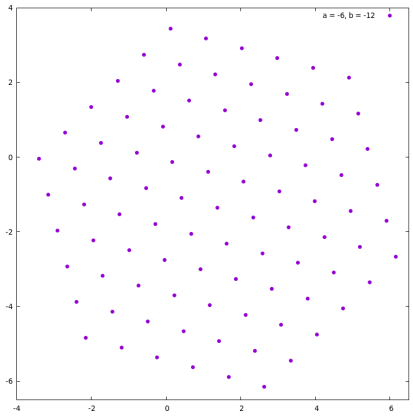

Figure 6.1: **Minimizer for the Lennard-Jones potential with 91 particles.**

successful in finding many candidates for minimizers which are still standing today, but there are several "hard" values of N for which better (lower energy) configurations were found later [101,131]. An important step of many of these methods, used for the "random perturbation" we mentioned, is *simulated annealing* [90], a global optimization method which has an appealing physical motivation for chemistry problems. Roughly speaking, in simulated annealing a random perturbation X' of a given configuration X is considered, and then:

1. It is accepted if X' has lower energy than X, or
2. It is accepted with a probability proportional to $\exp(-\frac{E_N(X')-E_N(X)}{T})$ if X' has higher energy than X.

Here T is a parameter which has an analogy to temperature, and governs how probable it is to jump "far" from the current state. In the literature on this, performing this algorithm any number of times for a fixed T is sometimes referred to as a MONTE CARLO SIMULATION, and each step as a *Monte Carlo step*. Simulated annealing methods then work by running many steps of this random perturbation, and gradually reducing T until departures from the current state become very unlikely. Methods focused on this technique have had some success [133,134], and are also part of more recent methods.

Another family of methods is that of evolutionary algorithms, which have also been quite successful in finding minima for Lennard-Jones potentials, even for the values of N considered harder [51,100]. Genetic algorithms are a particular kind of evolutionary algorithms, though the naming is not completely precise. These methods are based on an analogy with natural selection, and are also an example of biased methods which make informed guesses on the structure of minimizers. We refer to the more recent paper by [55] for a list of references on the use of this kind of algorithms for Lennard-Jones energy minimization.

The paper [6] contains a good presentation of related minimization problems, and describes a simple algorithm for minimizing E_N for the Lennard-Jones potential, which is tested in 2D. It is also a biased method in the sense that particles are initially placed at the sites of a triangular lattice, and later suitable symmetrization methods are used.

As discussed, these biased methods have been tried mainly for potentials of Lennard-Jones type, motivated by problems in chemistry and crystallography. Since our aim is to use a good numerical algorithm for a wider range of potentials whose minimizers may behave very differently, an adaptation of these methods does not seem straightforward, especially for the cases which have a continuous limit such as those discussed in Section 6.4, where particles do not arrange as large-scale crystals. Instead, we use a technique known as *basin-hopping*, first reported for the Lennard-Jones potential in [131], and before used by [92] for a different problem in chemistry. This technique has been in particular quite successful for Lennard-Jones type potentials. It is an *unbiased* algorithm in the sense that it does not assume any particular structure of the minimizers, and it seems a more appropriate algorithm for the range of potentials we are interested in. It works as follows: first, the energy $E_N(X)$ is substituted by an energy $\widetilde{E}_N(X)$, obtained by performing a suitable descent algorithm starting from the configuration X (the Polak-Ribiere variant of the conjugate gradient algorithm is mentioned in [131]). That is: if we denote by $M(X)$ the result of running a descent algorithm from the starting configuration X, then

$$\widetilde{E}_N(X) := E_N(M(X)).$$

Hence the new *energy landscape* $\widetilde{E}_N$ is piecewise constant function, which is constant in a region where our chosen descent algorithm stops at the same local minimum Y, and whose value in this region is $E_N(Y)$. Now several algorithms are used:

1. A Monte Carlo exploration of the landscape $\widetilde{E}_N$ is carried out with a fixed temperature, chosen so that the acceptance rate of new points is about $1/2$ (as explained in our brief earlier discussion of simulated annealing).

2. During this exploration, we also observe the *individual energy* (or just energy) of each particle i, defined by
$$E_{N,i} = \sum_{j \neq i} V(x_i - x_j).$$
We consider the particle i_{max} which has a maximum energy among all N particles, and the one i_{min} which has minimum energy. If this maximum energy is larger than a certain multiple of the lowest energy, then an *angular move* is performed for the particle i_{max}: this particle is removed from the cluster, and placed at a random position close to the boundary of the cluster.

In addition to this, a further Monte Carlo exploration is carried out with the following special starting positions:

1. The best configuration found by the algorithm with $N-1$ particles, adding one particle at the best position found by a fixed number of angular moves.

2. The best configuration found by the algorithm with $N+1$ particles, removing the particle with highest energy.

We have applied this algorithm for different potentials, otherwise with no modifications. Some of the results are explored in the next sections, together with a short review of the expected behavior of minimizers. We would like to emphasize that while obtaining local minimizers is straightforward in almost all cases, obtaining good candidates for a *minimizer* is a hard numerical problem. As an example, the hexagonal-shaped minimizers for very singular potentials such as Lennard-Jones (see Fig 6.1) require some kind of global search algorithm as described above. Or consider for example a minimizer for the locally integrable potential (6.1.2) with $a = 2$ and $b = 0.5$ (figure 6.2). Asymptotically as $N \to +\infty$, this density is known to converge to the density of a minimizer of the continuous energy (6.1.5) (see Section 6.4), but the way this happens seems to show several interesting phenomena. One sees that locally particles still seem to be arranged in triangular patterns; but since the overall shape must be round (since the support of the minimizer is strongly suspected to be a ball), these local triangular arrangements must undergo some kind of dislocation patterns in order to fit the global shape. In figure 6.2 one can clearly appreciate dislocation curves along which triangular patterns with different orientations meet. These patterns are quite sensitive to the minimization algorithm used, and we do not know whether the plot in figure 6.2 actually represents a minimizer. But an understanding of these patterns is certainly an interesting problem, and even its numerical study requires powerful algorithms which can handle a large number of particles and yield good approximations to the minimizer. For particle numbers over a few thousand it is likely that this is still out of reach, even numerically.

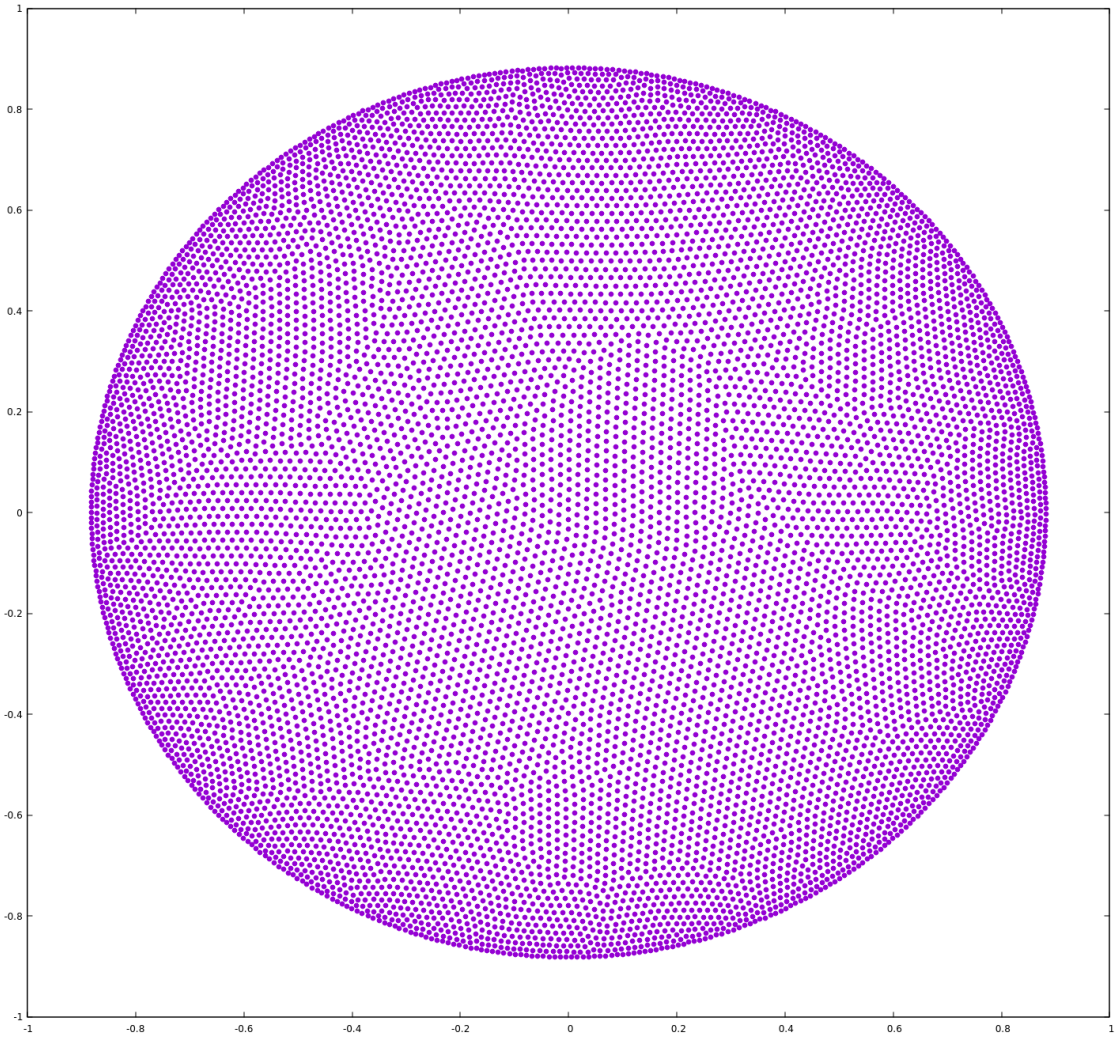

Figure 6.2: **Our best numerical candidate for a minimizer of the potential** (6.1.2) **with** $a = 2$**,** $b = 0.5$ **and** 10^4 **particles.** (We thank David Wales for providing this result)

6.3 Crystallization phenomena

The wider problem of understanding the reason why matter is often arranged in crystalline patterns is known as the problem of crystallization. The reviews by [111, 126] are a good introduction to this, giving a motivation and related mathematical problems. It happens that minimizers of E_N have a close relationship to the observed arrangement of atoms or molecules at low temperature, and hence an aspect of the crystallization problem which is particularly simple to state is: *prove rigorously that (or whether) minimizers of* E_N *approach a periodic arrangement as* $N \to +\infty$. For some potentials V which have a singularity stronger than $|x|^{-d}$ at $x = 0$, minimizers of E_N numerically seem to do exactly

this, but proofs are surprisingly difficult even in dimension 1! The review by [8] is a nice source of references on this problem, and we would like to give a short summary with our current understanding.

Let us first state the problem a bit more precisely, essentially following [8]. In the context of crystallization, we usually consider potentials $V = V(x)$ which are positive at $x = 0$ (or have a singularity where the potential diverges to $+\infty$ as $x \to 0$), have a strictly negative minimum value, and satisfy

$$\lim_{|x|\to+\infty} V(x) = 0. \tag{6.3.1}$$

Further conditions are needed for minimizers to show any kind of crystallization behavior; see more on this below. The canonical example of the potentials which exhibit this kind of phenomena is the Lennard-Jones potential from equation (6.1.3).

For a particle distribution $X = (x_1, \dots, x_N) \in \mathbb{R}^{Nd}$ we consider the associated *empirical measure* given by

$$\mu_X := \sum_{i=1}^{N} \delta_{x_i}. \tag{6.3.2}$$

Notice that we are *not* dividing by N, so this measure has total mass equal to N. In many cases we expect this measure to approach some periodic arrangement as $N \to +\infty$, and in order to define this precisely we recall that a *lattice* in $\mathbb{R}^d$ is a subgroup of $\mathbb{R}^d$ of the form

$$L = \{k_1 v_1 + k_2 v_2 + \cdots + k_d v_d \mid k_1, \dots, k_d \in \mathbb{Z}\}, \tag{6.3.3}$$

where $(v_1, \dots, v_d)$ form a vector space basis of $\mathbb{R}^d$. Lattices are a simple form of periodic structures, and are a basic concept in crystallography, where they are often referred to as *Bravais lattices*. The reason for this special naming is that in crystallography the name *lattice* is often broadened to include periodic structures which are not lattices in the sense of the above definition; notable examples are the honeycomb arrangement in 2D, or the hexagonal close packed arrangement in 3D. Here we will always use the word *lattice* in the mathematical sense stated in (6.3.3). Consistently with (6.3.2), for a lattice L we denote by μ_L the measure

$$\mu_L := \sum_{p\in L} \delta_p. \tag{6.3.4}$$

Notice that μ_L has infinite mass (is an unbounded measure), but it is finite in compact sets. Here is a very strong formulation of the problem of crystallization:

Q1 (lattice crystallization) Does there exist a lattice $L \subseteq \mathbb{R}^d$ and a sequence of minimizers $(X_N)_{N\geq 2}$ of E_N such that (possibly up to a subsequence)

$$\mu_{X_N} \overset{*}{\rightharpoonup} \mu_L \qquad \text{as } N \to +\infty?$$

The convergence here is the weak-$*$ convergence of measures (convergence when tested against continuous, compactly supported functions). Or even stronger: does this take place for *all* sequences of minimizers, up to rigid movements of these minimizers?

Crystalline structures may well be periodic structures which are not lattices. A very natural formalization of a periodic structure is a measure μ on $\mathbb{R}^d$ such that $\mu(\cdot + p) = \mu(\cdot)$ for all p in some lattice L (that is, a measure which is invariant by translations of vector p, for all p in a given lattice). If this happens, we say that μ is *invariant by the lattice* L. Following this, here is a weaker form of the above problem:

Q2 (periodic crystallization) Does there exist a lattice $L \subseteq \mathbb{R}^d$ and a sequence of minimizers $(X_N)_{N\geq 2}$ of E_N such that (possibly up to a subsequence)

$$\mu_{X_N} \overset{*}{\rightharpoonup} \mu \qquad \text{as } N \to +\infty,$$

where μ is a measure invariant by the lattice L? Or even stronger: does this take place for *all* sequences of minimizers, up to rigid movements of these minimizers?

If these questions are too hard, one may consider the large-N behavior of some macroscopic quantities like the energy per particle. Given a lattice L in $\mathbb{R}^d$ and a potential V we define its *energy per particle* by

$$e(L) := \sum_{p\in L\setminus\{0\}} V(p), \tag{6.3.5}$$

when this sum converges absolutely. Also, given a subset $X = (x_1, \ldots, x_N) \subseteq \mathbb{R}^d$ we define its energy per particle by

$$e_N(X) := \frac{1}{N} E_N(X).$$

Here is a related, usually weaker, statement of the problems **Q1** and **Q2**:

Q3 (energy crystallization) Does there exist a lattice $L \subseteq \mathbb{R}^d$ and a sequence of minimizers $(X_N)_{N\geq 2}$ of E_N such that (possibly up to a subsequence)

$$e_N(X_N) \to e(L) \qquad \text{as } N \to +\infty?$$

Or even stronger: does this take place for *all* sequences of minimizers?

In a related problem, one can try to give good estimates for the convergence of $e_N(X_N)$ to $e(L)$, for example giving bounds on its rate of convergence. The fact that $e_N(X_N)$ has *some* limit is known for a wide range of potentials.

In the context of crystallization phenomena one always assumes (6.3.1). As a consequence, a sequence of configurations with N particles such that the interparticle distances all diverge to $+\infty$ has energy as close to 0 as we wish. Hence for a minimizer X_N it must happen that $E_N(X_N) \leq 0$, so if **Q3** holds one must have $e(L) \leq 0$. In any case **Q3** in particular implies that for some $C > 0$

$$E_N(X_N) \geq -CN \tag{6.3.6}$$

for all $N \geq 2$. Potentials V satisfying (6.3.6) are called *H-stable*, or sometimes just *stable* in the literature; see for example [116, Section 3.2]. Often (6.3.6), though seemingly weaker, actually implies that $e_N(X_N)$ does have a limit as $N \to +\infty$. Since the terminology comes from statistical mechanics and thermodynamics, interest is placed on potentials for which thermodynamical quantities (such as the energy-per-particle) have a finite limit, which justifies the word *stable*. Minimizers for potentials which are *not* stable may still have different scaling limits which are also interesting, though their study has different motivations and is more recent; see Section 6.4 below.

Finally, there is the related question of the *formation of a macroscopic object*. The *diameter* of a minimizer is defined as the maximum distance between two of its points. If we rescale minimizers in order to fix their diameter, does the resulting measure converge to something? If we look at the regime where one expects that particles approach a periodic distribution, we would expect the diameter of a minimizer to be roughly proportional to $N^{1/d}$, and hence we pose the following question:

MO (formation of a macroscopic object) Does there exist a nontrivial measure μ on $\mathbb{R}^d$ and a sequence of minimizers $(X_N)_{N\geq 2}$ of E_N such that (possibly up to a subsequence)

$$\frac{1}{N}\mu_{X_N/N^{1/d}} \overset{*}{\rightharpoonup} \mu \qquad \text{as } N \to +\infty? \tag{6.3.7}$$

Or even stronger: does this take place for *all* sequences of minimizers, up to rigid movements of these minimizers?

The empirical measure $\mu_{X_N/N^{1/d}}$ corresponds to the scaled minimizer

$$\frac{1}{N^{1/d}}X_N := \left\{\frac{x_1}{N^{1/d}}, \ldots, \frac{x_N}{N^{1/d}}\right\},$$

and we divide the measure by N to ensure a total mass equal to 1. This question concerns behavior at a different scale from questions **Q1**–**Q3**.

An answer to **MO** seems to not give much information on any of **Q1**–**Q3**, and reciprocally.

We have focused on the above questions because we are interested in the behavior of N-particle minimizers. However, there are many related aspects of these problems which involve infinite distributions of particles. Among these we mention the following: ones:

1. Among all lattices in $\mathbb{R}^d$, which ones minimize the energy per particle (6.3.5)?

2. Given a countably infinite set of points in $\mathbb{R}^d$, it is possible to define their *mean energy per particle* in a reasonable way, so that it is consistent with the energy per particle of a lattice given in (6.3.3). Among all infinite particle distributions, which ones minimize the energy per particle?

We do not elaborate on different mathematical interpretations of the problem, namely: minimization problems with fixed density; modified models with a background energy; statistical mechanical or quantum mechanical models. We refer the reader to the reviews mentioned above for more on these matters [8, 111].

Minimizers for a specific case of potential V have links to sphere packing problems. If we consider the following *sticky hard sphere* potential

$$V(x) := \begin{cases} +\infty & \text{if } |x| < 1, \\ -1 & \text{if } |x| = 1, \\ 0 & \text{if } |x| > 1, \end{cases} \tag{6.3.8}$$

then minimizers cannot have any two particles at a distance closer than 1 (otherwise their energy would be $+\infty$), and there is a reward for spheres which are touching. Hence a minimizer of this potential is just a configuration of N hard spheres in d-dimensional space with the maximum total number of contact points among them. In dimension 2 this problem was solved by [78]; see also [94] for a more recent proof. But the problem is far from understood in dimensions 3 and higher, with open questions even for low values of N (above 11). A popular review of the problem can be found in [77], and see [85, 95] for some recent results. Attempts have been made to relate the structure of these minimizers to those for the Lennard-Jones potential [123], but a precise link remains unclear. It is also tempting to make a connection of the sticky hard sphere problem with that of *sphere packing*, which is the problem of finding a distribution of identical hard spheres in $\mathbb{R}^d$ with maximum possible density. This link has often been remarked, but as far as we know there are no rigorous results backing this up. There have been some surprising recent results in sphere packing by [42, 129], which give specific lattices in dimensions 8 and 24 which can be proved to be the densest possible sphere distributions in these dimensions.

The proof relies on the existence of specially symmetric lattices in these dimensions, which are natural candidates for this densest packing.

Now that we have made an effort to state rigorously the results we are interested in, we can try to summarize the available rigorous results:

One-dimensional results In dimension 1 there were several early results by [125, 127, 128]. These results concern mainly infinite particle distributions (as mentioned in points 1,2 above) but specifically [125] contains a proof of the strong version of **Q3** for a wide class of power-law potentials of the form (6.1.2) with $b < 1$ and a certain restriction on a: the energy per particle of any sequence of minimizers converges to the energy per particle of a given lattice; this lattice is the unique one with minimum energy per particle. This is a rather complete answer to **Q3** for some power-law potentials. However, as far as we know there are no satisfying general conditions on V which ensure a similar answer.

In contrast, the problem **Q1** is not so well understood even in dimension 1. The best available result seems to be the one by [72], which does show the strong version of **Q1** for some potentials including the Lennard-Jones one. The conditions for this to hold are more restrictive, and it seems a hard problem to generalize them to a wide class of potentials.

In dimension 1 the minimization problem for the sticky hard sphere potential (6.3.8) is trivial, and minimizers are distributions of N equally spaced particles at interparticle distance 1.

Two-dimensional results For the sticky hard sphere potential (6.3.8) in dimension 2 results are already interesting. A first proof that minimizers must be placed at the sites of a triangular lattice was given by [78], giving an answer to **Q1** (and hence **Q2**) and **Q3**. For a specific piecewise linear potential not too far from (6.3.8), a positive answer to **Q3** was also given by [110]. Then **MO** was answered by [2] for a family of short-range potentials with V compactly supported and close enough to the sticky sphere potential (6.3.8): the convergence (6.3.7) takes place up to a subsequence, and the measure μ is $\frac{2}{\sqrt{3}}\mathbb{1}_E$, where $\mathbb{1}_E$ is the characteristic of a finite-perimeter set E of area $\sqrt{3}/2$. In [121], **Q3** is answered positively for a certain family of potentials which allow similar growth conditions as the Lennard-Jones one. In addition, it is proved that with periodic boundary conditions, the triangular lattice is a minimizer. Adding a three-body potential (and hence for an energy not strictly of the form (6.1.1)), and still with periodic boundary conditions, [63] followed the ideas in [121] to show that minimizers must have particles placed at the sites of a *hexagonal* periodic arrangement (the vertices of a honeycomb, which are not a lattice in the sense we are using in this chapter). Hence in this case, a version of **Q2** holds, but not **Q1**.

Three-dimensional results From the point of view of rigorous results, the situation in three dimensions is almost completely open. As far as we know there are no results regarding any of **Q1**, **Q2**, **Q3** or **MO**, even for the sticky hard sphere potential (6.3.8). The problem of optimal packing, however, was solved by [76] with a non-conventional proof which requires several computer checks. One of the difficulties of the 3D problem is that there are many non-equivalent sphere distributions in $\mathbb{R}^3$ which maximize density, including non-periodic structures.

Higher dimensional results In higher dimensions there have been important breakthroughs on optimal sphere packing, for which the optimal lattices have been recently identified in dimension 8 [129] and 24 [42]. As a consequence of these ideas, in [43] it was proved that these optimal lattices are also *universally optimal*: they minimize the interaction energy among infinite configurations of points with fixed density 1, for any potentials V which are completely monotone functions of the squared distance. it is conjectured that the same holds in dimension 2 for the usual triangular lattice, but this is not proved as far as we know. In [109] it is shown that this universal optimality also implies a corresponding result for Riesz and Coulomb interaction energies, which require an appropriate renormalized definition for infinite particle distributions. Hence this latter result is known in dimensions 8 and 24, and is a conjecture in dimension 2.

All of these results concern infinite particle configurations. As far as we know, no results are known concerning any of **Q1**, **Q2**, **Q3** or **MO** in dimensions $d \geq 3$.

6.4 Continuous limits

Consider a sequence $(X_N)_{N\geq 2}$ of minimizers of E_N, and a locally integrable potential V (in the case of potentials of the form (6.1.2) this holds if and only if $b > -d$). Then it may happen that

$$\nu_{X_N} := \frac{1}{N}\mu_{X_N} = \frac{1}{N}\sum_{i=1}^{N} \delta_{x_i^N} \overset{*}{\rightharpoonup} \nu \qquad \text{as } N \to +\infty$$

for some measure ν, where $X_N = (x_1^N, \dots, x_N^N)$. This type of limit is of *mean-field* type due to the factor $1/N$, and notice that there is no rescaling as there was in (6.3.7). In this case the discrete interaction energy E_N is an approximation of the continuous one E,

$$\begin{aligned}\frac{1}{N^2}E_N(X) = \frac{1}{N^2}\sum_{i=1}^{N}\sum_{\substack{j=1\\ j\neq i}}^{N} V(x_i - x_j) &= \int_{\mathbb{R}^d}\int_{\mathbb{R}^d} V(x-y)\,\mathrm{d}\nu_{X_N}(x)\,\mathrm{d}\nu_{X_N}(y)\\ &\approx \int_{\mathbb{R}^d}\int_{\mathbb{R}^d} V(x-y)\,\mathrm{d}\nu(x)\,\mathrm{d}\nu(y) = E(\nu), \quad (6.4.1)\end{aligned}$$

when this can be rigorously justified. Then we expect the measure ν to be a minimizer of the continuous interaction energy (6.1.5). Proving this is another interesting question which we will state explicitly:

MF (Mean-field limit) Does there exist a nontrivial measure ν in $\mathbb{R}^d$ and a sequence of minimizers $(X_N)_{N\geq 2}$ of E_N such that (possibly up to a subsequence)

$$\frac{1}{N}\mu_{X_N} \overset{*}{\rightharpoonup} \nu \qquad \text{as } N \to +\infty?$$

Does this take place for *all* sequences of minimizers, up to rigid movements of these minimizers? In this case, is ν a minimizer of the continuous interaction energy (6.1.5)?

In analogy to **Q3**, one may also look for good asymptotics of the energy-per-particle $E_N(X_N)/N$ as $N \to +\infty$. For locally integrable potentials, if **MF** holds we expect (6.4.1) to hold and hence we also expect that

$$E_N(X_N) \sim N^2 E(\nu).$$

It is interesting to study this approximation independently, and improve it to more precise approximations. This problem was studied by [108] when the potential V is repulsive and there is an additional external confining potential. For the particular case $-d < b < a = 2$ in (6.1.2), and when continuous minimizers are regular enough, this gives quite precise asymptotics for $E_N(X_N)$.

The only answer we know to question **MF** was given in [26] for power-law potentials (6.1.2) with $b \geq 1$, and in [21] for general potentials which include the power-laws (6.1.2) with $b > 2 - d$. In this case, the answer to all questions in **MF** is positive for *strictly unstable* potentials V, that is, potentials V for which there exists a probability distribution ρ on $\mathbb{R}^d$ such that

$$E(\rho) < \lim_{|x|\to+\infty} V(x)$$

(assuming this limit exists or is $+\infty$). For a wide range of potentials, this concept is actually shown to imply that the classical H-stability condition (6.3.6) does *not* hold [21, 119]. We believe **MF** should also be true in the range $-d < b \leq 2 - d$, but as far as we know there is no available proof. For the strategy in [21] two ingredients are needed:

1. One needs to show that the sequence of discrete energies E_N Gamma-converges in a suitable sense to the continuum energy E.

2. One needs to show that the diameter of a minimizer X_N stays bounded as $N \to +\infty$. As a consequence, the empirical measures μ_{X_N}/N have a convergent subsequence,

in the weak-$*$ sense, to a certain probability measure μ. By using the previous Gamma-convergence result (and possibly some additional uniform estimates on other properties of the minimizers) one may then deduce that μ must be a minimizer of E.

In relation to these questions, a description of the minimizers of E is also an interesting problem. As remarked in the introduction, these minimizers are of interest for collective behavior models, and are also quite interesting from the point of view of calculus of variations. A general result on existence of these minimizers was given in [37, 119], but there remain many questions on their uniqueness, symmetry and regularity properties. There has been a lot of recent activity regarding these, and we will try to give here a short account of the literature on this.

An early discussion on the problem of minimizing E can be found in [5, Section X]. In [113], for very regular potentials it is proved that stationary states (and in particular minimizers, if any) must be sums of delta functions. A link between the repulsive singularity of the potential at $x = 0$ and the dimension of the support of minimizers was given by [3], essentially by noticing that for any minimizer ρ the convolution $\Delta V * \rho$ must be bounded. A consequence of this is that the support of a minimizer for V of the form (6.1.2) with $2 - d \leq b < 2$ must have dimension at least $2 - b$. This is not optimal since numerical simulations seem to indicate that, at least for "usual" potentials, the support always has integer dimension, and some effort has been devoted to understanding this effect. See however [34] for an example of fractal behavior for a specifically tailored potential V.

For "strongly repulsive" potentials with $-d < b < 2 - d$ (but still locally integrable), regularity of minimizers can be obtained via obstacle problems [28]. Explicit candidates for minimizers can be found for $-d < b < a$ with $b \leq 2$, when a or b are even integers [30]. This is in contrast with minimizers for *mildly repulsive* potentials (potentials which are $\mathcal{C}^2$ at 0), for which minimizers must be supported on a finite number of points under quite general conditions [24]. This result is true even for *local* minimizers in the topology of the ∞-Wasserstein transport distance. This applies to power-law potentials of the form (6.1.2) whenever $a > 2$.

For $b = 2$ and $a \in (2, 4)$, the unique minimizer (up to translations) is the uniform measure on an $n - 1$-dimensional sphere of appropriate radius [48]. For $a \geq 4$ and $b \geq 2$ (excluding the case $(a, b) = (4, 2)$) the minimizer is unique up to rigid movements, and it must be a sum of equal delta functions supported at the vertices of a regular d-simplex [49]. In this same reference, the case $(a, b) = (4, 2)$ is studied. It is a special limit case in which minimizers are not unique (even up to rigid movements): minimizers may be supported on a sphere, on a finite number of points, or may be convex combinations of these possibilities. In the 1D case explicit minimizers are known for some power-law potentials of the form (6.1.2) [70].

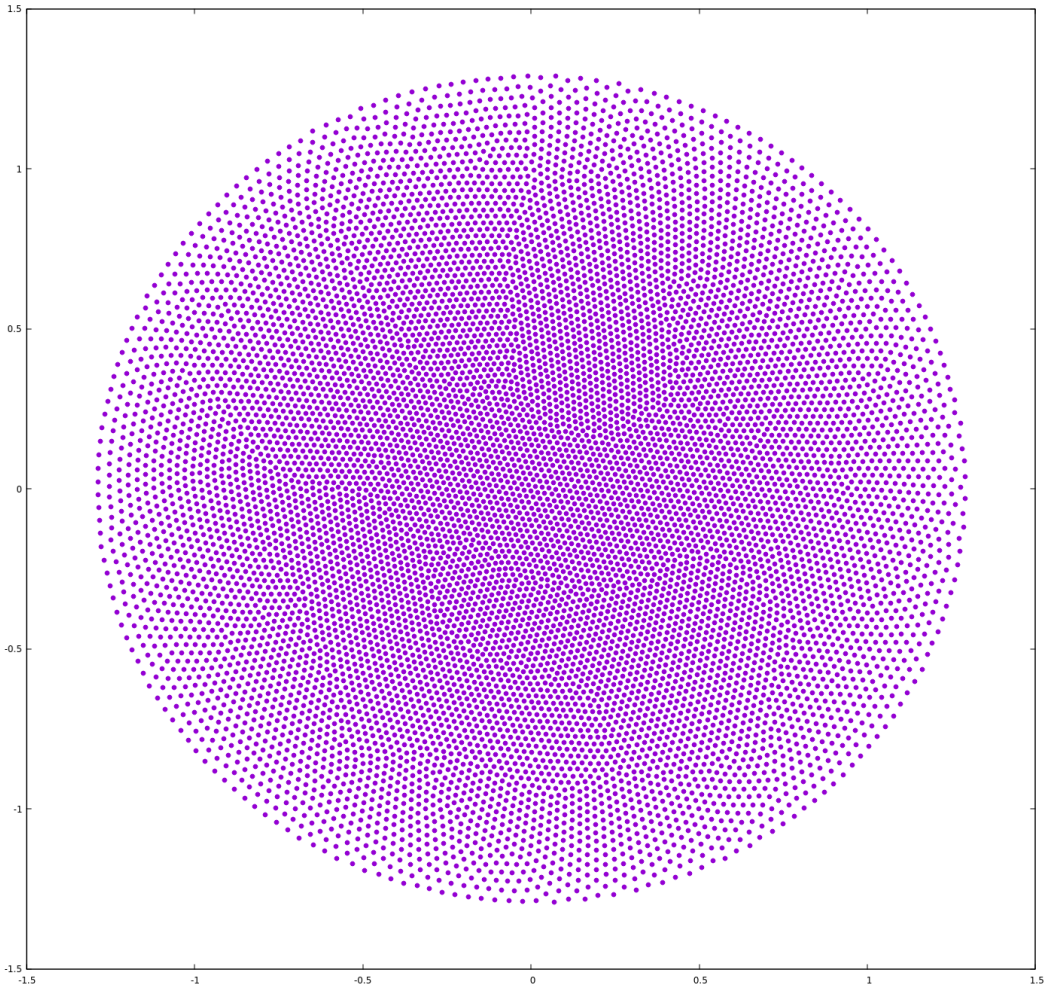

Figure 6.3: **Numerical candidate for minimizer of the potential** (6.1.2) **with** $a = 2$**,** $b = -1$ **and** 10^4 **particles.** (We thank David Wales for providing this result.) This corresponds to the "strongly repulsive" regime considered in [28]. In this regime it is conjectured that a sequence of minimizers $(X_N)_{N\geq 2}$ must converge to a measure ν which must have a smooth density with respect to Lebesgue measure. In fact, the most likely candidate measure is given in [30, eq. (38)] and is of the form

$$\nu(x) = C(R^2 - |x|^2)^{1-\frac{b+d}{2}},$$

with suitable constants $C, R > 0$ which ensure in particular that the total mass is 1. In the case corresponding to this figure we have $d = 2$, $b = -1$, so the density of ν vanishes at the boundary. By contrast, in the case of figure 6.2 the exponent $1-(b+d)/2$ becomes negative and the density of ν should diverge at the boundary.

In addition to this, the question of stability or instability of these minimizers for several dynamical models has been investigated in a few cases; see for example [67, 68] (for 1D stability of sums of Dirac masses for the aggregation equation (6.1.4)) or [4] (stability of spherical shells). We will also mention some results on non-isotropic potentials: see [31] and [35, 36].

There are also related minimization problems which would take us too far from the topic; we refer the reader to [8] and [71] for an introduction to similar problems and many references on them.

We will illustrate the above properties in 2D with a few numerical results for power-law potentials of the form (6.1.2). Let us first fix $a = 2$ and look at the appearance of numerical minimizers for several values of b. As the exponent b increases, the repulsion becomes progressively weaker. It is clearly seen in figure 6.4 that minimizers become more concentrated as b increases. Also, they become more concentrated on the boundary of a ball for higher b. For $b < 0$ we are in the regime studied in [28], so we know minimizers of E should be smooth, but it is not proved that N-particle minimizers approach minimizers of E. In contrast, for $b > 0$ we know from [21] that N-particle minimizers must approach minimizers of the continuous energy E, but we do not know the specific shape of these minimizers; for example, it is not proved in this range that minimizers must be regular functions on their support, or even L^P functions for some $p \geq 1$. Reasonable candidates for minimizers of E are given in [30], and they are all smooth functions on their support.

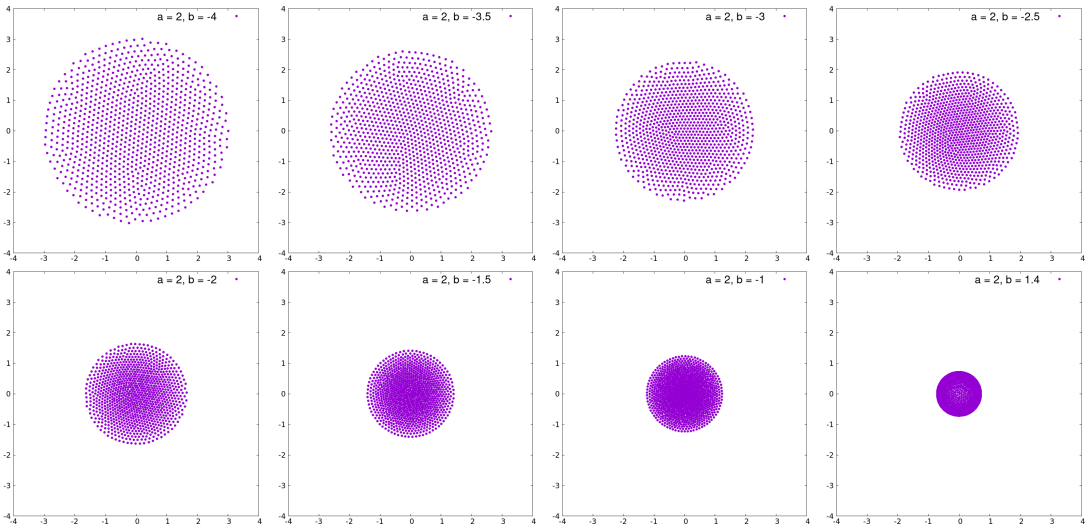

Figure 6.4: **Minimizer for the power-law potential (6.1.2) with $a = 2$ and several values of b, always with 10^3 particles.**

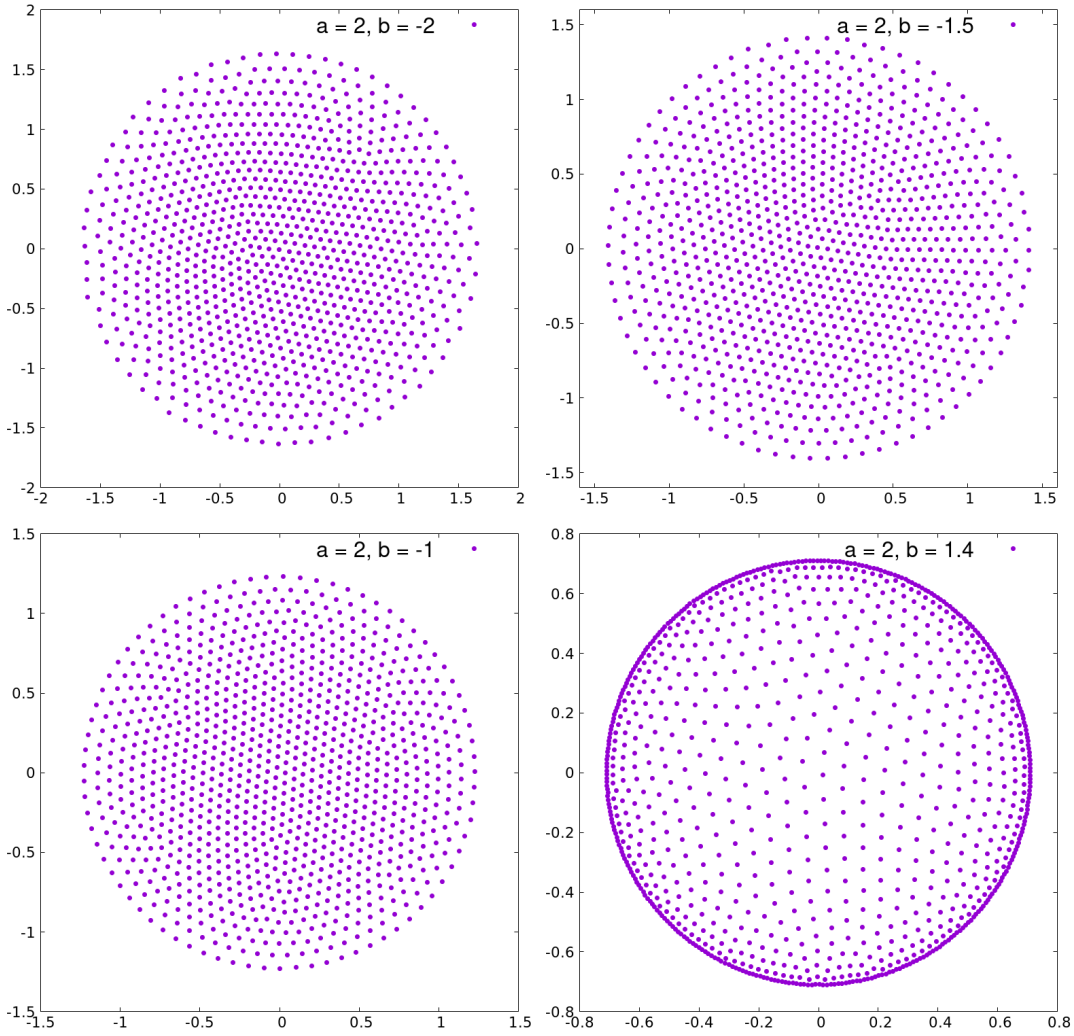

Figure 6.5: **Zoomed-in view of the last 4 minimizers in figure 6.4.**

For $a = 4$ the situation is similar, but now there is a range of exponents with $b \geq 2$ where the potential V is $\mathcal{C}^2$. This is the range studied in [48] and [24].

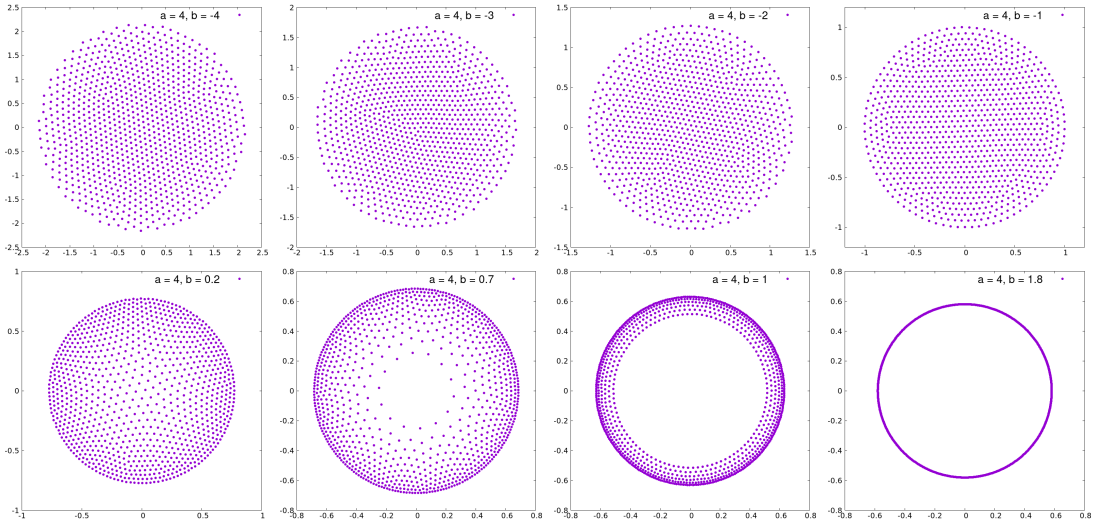

Figure 6.6: **Minimizer for the power-law potential** (6.1.2) **with** $a = 4$ **and several values of** b**, always with** 10^3 **particles.**

6.5 Between crystallization and continuous limits

We will also point out that there is a range of exponents for power-law potentials which has been left almost untouched in the literature. For potentials V which are not locally integrable (that is, with $b \leq -d$) there are ranges of a for which crystallization (in the sense of **Q1** to **Q3**) is not expected to take place, or has not been considered. The main unexplored range is $b \leq -d$, $a > 0$, since in the crystallization literature and in problems motivated by statistical mechanics it is always assumed that $V(x)$ decays to 0 as $|x| \to +\infty$. But there is also a range of exponents $b < a < 0$ for which crystallization does not seem to happen, and we are left with some kind of limiting behavior which is not yet understood. We conjecture that in this case there is still a scaling which leads to a well-defined limiting profile along the lines of **MO**:

MS (macroscopic scaling) Do there exist $s > d$, a nontrivial measure μ on $\mathbb{R}^d$ and a sequence of minimizers $(X_N)_{N\geq 2}$ of E_N such that (possibly up to a subsequence)

$$\frac{1}{N}\mu_{X_N/N^{1/s}} \overset{*}{\rightharpoonup} \mu \qquad \text{as } N \to +\infty? \tag{6.5.1}$$

Or even stronger: does this take place for *all* sequences of minimizers, up to rigid movements of these minimizers?

There are numerical results in 1D which seem to indicate that this is the case [26], but this has not been systematically explored, much less the subject of any rigorous proofs.

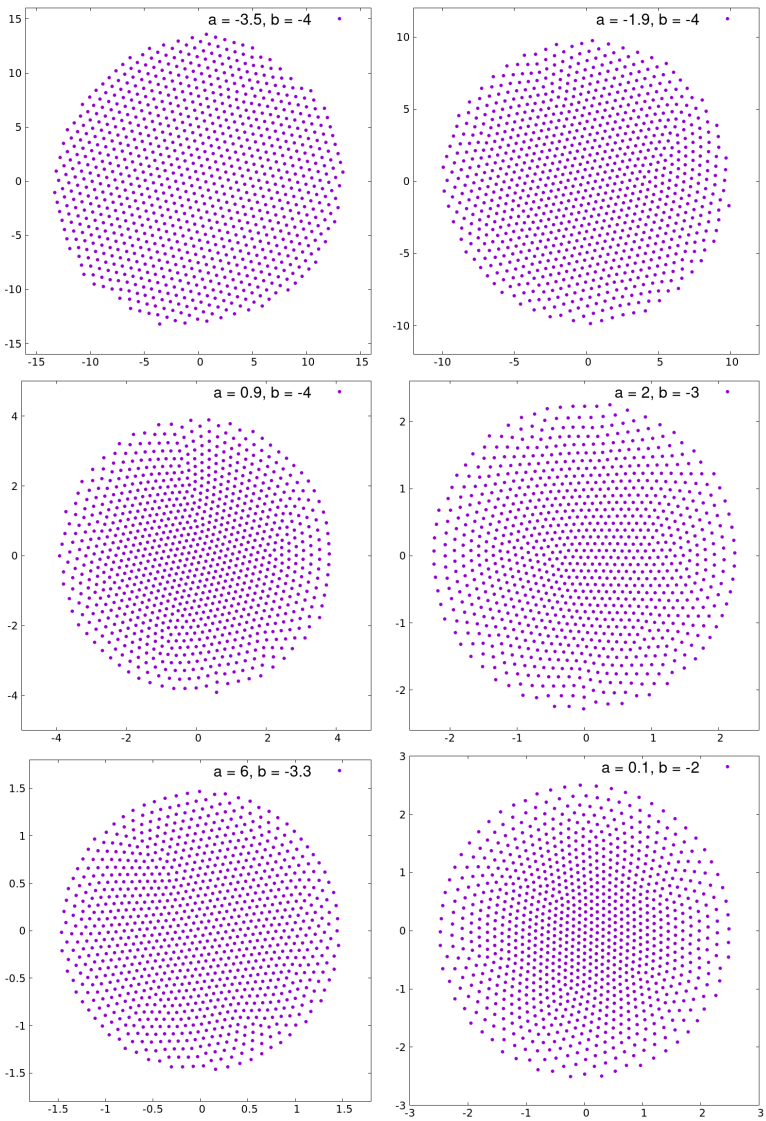

Figure 6.7: **Some minimizers with $b \leq -2$.**

Chapter 7

Conclusions

The starting point of this thesis was the numerical study of models from kinetic theory through computer simulation of their associated microscopic systems. Specifically, we focus on the case of the NNLIF model for neuron networks, for which we aimed to explain the question: What happens after the blow-up? The blow-up occurs for excitatory networks ($b > 0$) and it is understood as the moment at which the firing rate diverges [14], and therefore any of the numerical schemes used to simulate the mesoscopic system, defined by the Fokker-Planck equation (1.2.7), are unable to continue after the blow-up, or avoid it. When the firing rate becomes infinite, infinite mass is added to the reset potential, and thus the mass conservation principle is breached. However, some authors [52,53] have studied the microscopic system associated with the NNLIF model, offering new formulations of its solutions (physical solutions), such that they can avoid or surpass the blow-up phenomenon and show what happens afterwards. This, together with the well-known result that the implementation of transmission delay avoids blow-up [18], gave us the idea to implement such types of solutions and simulate the microscopic system [17] in order to find behaviors never observed in the mesoscopic system.

In chapter 2 we provide an extensive number of numerical simulations that give a fairly complete picture of the NNLIF model from the point of view of the microscopic system (1.2.6). These corroborate what was previously observed for the mesoscopic system, and extend the knowledge of the model through new observations. We show how the implementation of the physical solutions avoids the blow-up, for the cases where they make sense, when the excitation parameter is in the range $0 < b < V_F - V_R$. For more exciting cases, we implement delay and show how the system evolves through equilibrium-like states towards the plateau state, where the voltage distribution forms a uniform distribution between the reset and firing potentials. After this we realize that the establishment of a sufficiently large delay should lead to a process of passing through different pseudo-equilibria, that is, in each delay interval, the system behaves linearly and converges to the

equilibrium associated with it. During this process the nonlinear system converges to the corresponding equilibrium, or converges to the plateau state.

We then divided our work into two parallel branches. On the one hand [12] we improve the existing methods to study the stability of the equilibria of the mesoscopic system (1.2.7). On the other hand [13] we give theoretical and numerical evidence on the intuitive idea that, a sufficiently large delay should allow to study the global long-term behavior of the system, by means of its passage through a sequence of pseudo-equilibria.

The first line of research is included in chapter 3 where, in addition to improving the existing results [19,25] on the asymptotic behavior of the solutions of equation (1.2.7), we offer a new method to study the stability of its solutions, consisting in the linearization of the equation for its equilibria and the connection between the linearized and nonlinear stability. For this purpose, we perform a study of the existence and regularization properties of the linear equation associated with the system (1.2.7), where the drift coefficient does not depend on the firing rate. Along with this, we use spectral methods [38, 74, 96] to restrict the space in which the convergence to equilibrium of the linear equation occurs to one that includes part of the nonlinear term.

With respect to the second line of research, compiled in chapter 4, we carried out analytical and numerical work on the global behavior of the mesoscopic system. We define a discrete sequence called sequence of pseudo-equilibria, which is independent of the nonlinear system except for the system parameters (connectivity parameter and initial condition). We then give a proof on the monotonicity of this discrete sequence, for each region defined by the value of the excitation parameter and initial condition. We understand that it should be possible to prove that the nonlinear system, for a sufficiently large delay, follows this sequence and therefore the behavior of the sequence gives a global view of the behavior of the nonlinear system. However, for now we have only been able to prove it for small values of b, although improving on previously existing results [25] on convergence to equilibrium in the weakly exciting case. As an additional check, we implemented a well-known numerical scheme [118] to solve the Fokker-Planck equation (1.2.7) and we performed a test of each of the behaviors that we observed in the study of the pseudo-equilibrium sequence. In particular, the results observed for the very inhibitory case (b sufficiently negative) are very interesting, showing the break of equilibrium stability and consequent appearance of periodic solutions [87], when we consider a large delay. It is also important to corroborate, from the point of view of the mesoscopic system, the plateau states found for the microscopic system, when there is delay and the system is in a blow-up situation.

After the study carried out during these three chapters for the NNLIF model, we can give an up-to-date general summary of the expected behavior of the nonlinear system, derived from numerical and analytical results (for fully rigorous analytical results read chapter 3):

1. **Highly excitatory:** There is some $b_e > 0$ such that for $b > b_e$ no equilibria exist [14]. In this case, solutions without delay ($d = 0$) are expected to always blow-up [115]. Solutions with positive delay $d > 0$ (which cannot blow-up) are expected to converge as $t \to +\infty$ to the *plateau distribution* (the uniform distribution on $[V_R, V_F]$ [17]).

2. **Excitatory:** For $V_F - V_R < b < b_e$ two equilibria exist (in [14] it was proved that at least two exist). The higher equilibrium (the one with higher associated firing rate) is unstable for any delay $d \geq 0$ and the lower equilibrium (the one with lower firing rate) is asymptotically stable for any delay $d \geq 0$. Depending on the initial condition p_0, solutions either converge to the lower equilibrium, blow-up (only possible with $d = 0$), or converge to the plateau distribution (only possible when $d > 0$).

3. **Low excitatory:** For $0 < b < V_F - V_R$ the unique equilibrium is asymptotically stable regardless of delay. Solutions either converge to this unique equilibrium, or blow-up (only possible if $d = 0$ [14]).

4. **Inhibitory:** There is a critical value $b^* < 0$ such that for any $b^* < b < 0$, the unique equilibrium is asymptotically stable for all values of the delay. All solutions are expected to converge to this unique equilibrium, independently of the delay.

5. **Strongly inhibitory:** For $b < b^*$, there is also a unique equilibrium.

   (a) For small values of the delay, this equilibrium is stable. All solutions are expected to converge towards it.

   (b) For large values of the delay the equilibrium is unstable. All solutions are expected to approach a periodic solution.

As the last work carried out for the NNLIF model, in chapter 5 we have extended the analytical study of the discrete succession of pseudo-equilibria to the case of the model with refractory period [16], and jointly we have carried out numerical simulations in this case with both the microscopic scheme of chapter 2 and the mesoscopic scheme of chapter 4, making the corresponding adjustments to add the refractory state. The study of the succession of pseudo-equilibria and their associated simulations give us a general idea of how the model evolves with refractory period when we consider a large delay. In addition, the simulations of the microscopic system allow us to understand what happens after the blow-up for this model, observing in some cases periodic solutions without delay, which to

our knowledge had not been observed before. Finally, we show that the refractory state in the NNLIF model never leads to the trivial state observed for non-physical solutions in chapter 2, in which all neurons spike constantly. As the fundamental property of the physical solutions defined in chapter 2 is exactly that, it seems that solutions to NNLIF model with refractory period are indeed physical.

After discussing the main results obtained for the NNLIF model, it is also pertinent to mention the possible extensions, as well as the open problems that arise from it. With respect to the microscopic model, it would be desirable to expand the use of this model to more complex cases, considering separate excitatory and inhibitory populations of neurons, or extra variables such as conductance or age. Moreover, the analytical study of the microscopic system is not as advanced as that of the Fokker-Planck equation, and therefore advances in this field may be essential for a double boost to the understanding of the model. With respect to the stability criterion given in chapter 3 for equilibria to the nonlinear system, would be an appreciable improvement if we could translate it into a new criterion that does not require a numerical study of any function, but simply the establishment of parameter ranges where there is or is not stability of equilibria. On a side note, solving the technical problem we encountered in establishing that linearized stability implies nonlinear stability, when dealing with systems with delay, would complete our results from a technical point of view. In chapter 4, the problem that remains open and would be very interesting to deal with is the demonstration that the solution to the nonlinear Fokker-Planck equation behaves as the sequence of pseudo-equilibria, independently of the value of the connectivity parameter. Of course, the extension of this result to more special cases, such as convergence, in the appropriate sense, to plateau states, would be a very innovative and interesting work. Finally, with respect to the system with refractory period, a complete analysis of its local behavior, such as the one given in chapter 3 for the simplest model, is a work in progress for future publication. This would give us an idea of the stability of each equilibrium, for each value of the connectivity parameter, the delay and the refractory period.

Another work we are working on, together with Nicolas Torres, is to answer the question: How old are the neurons that fire? Understanding age as the time elapsed since the last firing. For this purpose, we want to relate the time elapsed type models [103, 104], whose long-time behavior has been widely studied in [122], to the NNLIF model, following the idea proposed in [62]. With this objective we will implement both the techniques that have emerged in this work, through the study of the NNLIF model, and those used specifically for the time elapsed model [23], in order to provide as much knowledge as possible about the joint model.

In conclusion, the work presented in this thesis represents a significant increase in the existing knowledge on the NNLIF model, especially on the long-time behavior and stability of its equilibria. In addition to this improvement, the thesis contains new methods that remained inapplied to this model, and original ideas for its study, which can be extrapolated to a multitude of alternative models, especially those modeled through differential equations with delay. On addition, the improvement of the knowledge available for the simpler neural models, and therefore those in which mathematical analysis is possible in a broad way, may help to enhance the understanding of more complex and realistic models and may have an interdisciplinary impact, helping other scientists to solve problems related to the brain, as those mentioned at the beginning of the thesis.

In parallel to the main work of the thesis, which has been the study of the NNLIF model, we decided to carry out a numerical study, from the microscopic point of view, of configurations of particles interacting with each other through attractive-repulsive potentials of the power-law type [22]. In particular, we became interested in finding and studying the properties of the minima of the interaction energy between these particles. In chapter 6 we show the numerical results we obtained with the help of the GMIN [130] program, which are accompanied by a review on the subject. These potentials have been extensively studied in the scientific literature, due to the wide variety of phenomena they model depending on the value of their parameters. They are associated with both crystal formation events in physics and collective behavior or swarming in biology. Finding an effective and efficient minimizer for the energy of particles interacting across this range of potentials can be of great use in dealing with a multitude of problems that remain open, such as the crystallization problem. Our future intention in this field is to use the numerical tools implemented in this chapter for the study of properties of the minima of these potentials, creating a connection between microscopic models and related PDEs by using a very high number of particles.

Conclusiones

El punto de partida de esta tesis fue el estudio numérico de modelos de la teoría cinética mediante la simulación por ordenador de sus sistemas microscópicos asociados. En concreto, nos centramos en el caso del modelo NNLIF para redes neuronales, para el que pretendíamos dar respuesta a la pregunta: ¿Qué ocurre después del blow-up? El blow-up se produce para redes excitatorias ($b > 0$) y se entiende como el momento en el que la tasa de disparo diverge [14], y por tanto cualquiera de los esquemas numéricos utilizados para simular el sistema mesoscópico, definido por la ecuación de Fokker-Planck (1.2.7), son incapaces de continuar tras el blow-up, o evitarlo. Cuando la tasa de disparo se hace infinita, se añade una masa infinita al potencial de reset y por tanto se incumple el principio de conservación de la masa. Sin embargo, algunos autores [52, 53] han estudiado el sistema microscópico asociado al modelo NNLIF, ofreciendo nuevas formulaciones de sus soluciones (soluciones físicas), de forma que pueden evitar o superar el fenómeno del blow-up y mostrar lo que ocurre después. Esto, unido al conocido resultado de que la implementación del retardo sináptico evita el blow-up [18], nos dio la idea de implementar este tipo de soluciones y simular el sistema microscópico [17] para encontrar comportamientos nunca observados en el sistema mesoscópico.

En el capítulo 2 proporcionamos un extenso repertorio de simulaciones numéricas que dan una imagen bastante completa del modelo NNLIF desde el punto de vista del sistema microscópico (1.2.6). Estas corroboran lo observado anteriormente para el sistema mesoscópico y amplían el conocimiento del modelo mediante nuevas observaciones. Mostramos como la implementación de las soluciones físicas evita el blow-up, para los casos en que tienen sentido, cuando el parámetro de excitación está en el rango $0 < b < V_F - V_R$. Para casos más excitadores, implementamos el retardo sináptico y mostramos cómo el sistema evoluciona a través de estados similares al equilibrio hacia el estado meseta, donde los voltajes forman una distribución uniforme entre los potenciales de reset y disparo. Entonces nos dimos cuenta de que el establecimiento de un retardo suficientemente grande debe conducir a un proceso de paso por diferentes pseudo-equilibrios, es decir, en cada intervalo de retardo, el sistema se comporta linealmente y converge al equilibrio asociado al mismo. Durante este proceso, el sistema no lineal converge al equilibrio correspondiente,

o converge al estado meseta.

A continuación, dividimos nuestro trabajo en dos ramas paralelas. Por un lado [12] mejoramos los métodos existentes para estudiar la estabilidad de los equilibrios del sistema mesoscópico (1.2.7). Por otro lado [13] damos evidencia teórica y numérica sobre la idea intuitiva de que, un retardo suficientemente grande debería permitir estudiar el comportamiento global a largo plazo del sistema, mediante su paso por una sucesión de pseudo-equilibrios.

La primera línea de investigación se incluye en el capítulo 3 y además de mejorar los resultados existentes [19,25] sobre el comportamiento asintótico de las soluciones de la ecuación (1.2.7), ofrecemos un nuevo método para estudiar la estabilidad de sus soluciones, que consiste en la linealización de la ecuación para sus equilibrios y la conexión entre la estabilidad linealizada y no lineal. Para ello, realizamos un estudio de las propiedades de existencia y regularización de la ecuación lineal asociada al sistema (1.2.7), donde el coeficiente de arrastre no depende de la tasa de disparo. Junto a esto, utilizamos métodos espectrales [38, 74, 96] para restringir el espacio en el que se produce la convergencia al equilibrio de la ecuación lineal, a uno que incluye parte del término no lineal.

Respecto a la segunda línea de investigación, recogida en el capítulo 4, realizamos trabajos analíticos y numéricos sobre el comportamiento global del sistema mesoscópico. Definimos una sucesión discreta denominada sucesión de pseudo-equilibrios, que es independiente del sistema no lineal excepto por los parámetros del sistema (parámetro de conectividad y condición inicial). A continuación, damos una prueba sobre la monotonía de esta sucesión discreta, para cada región definida por el valor del parámetro de excitación y la condición inicial. Entendemos que debería ser posible probar que el sistema no lineal, para un retardo suficientemente grande, sigue esta sucesión y, por tanto, el comportamiento de la sucesión da una visión global del comportamiento del sistema no lineal. Sin embargo, por ahora sólo hemos sido capaces de demostrarlo para valores pequeños de b, aunque mejorando resultados previamente existentes [25] sobre convergencia al equilibrio en el caso débilmente excitador. Como comprobación adicional, implementamos un conocido esquema numérico [118] para resolver la ecuación de Fokker-Planck (1.2.7) y realizamos una prueba de cada uno de los comportamientos que observamos en el estudio de la sucesión de pseudo-equilibrio. En particular, son muy interesantes los resultados observados para el caso muy inhibidor (b suficientemente negativo), mostrando la ruptura de la estabilidad del equilibrio y consecuente aparición de soluciones periódicas [87], cuando consideramos un retardo grande. También es importante corroborar, desde el punto de vista del sistema mesoscópico, los estados de meseta encontrados para el sistema microscópico, cuando existe retardo y el sistema se encuentra en situación de blow-up.

Tras el estudio realizado durante estos tres capítulos para el modelo NNLIF, podemos dar un resumen general actualizado del comportamiento esperado del sistema no lineal, derivado de resultados numéricos y analíticos (para resultados analíticos rigurosos leer el capítulo 3):

1. **Altamente excitador:** Existe algún $b_e > 0$ tal que para $b > b_e$ no existe ningún equilibrio [14]. En este caso, sin retardo ($d = 0$) se espera blow-up [115]. Las soluciones con retardo positivo $d > 0$ (donde no puede ocurrir blow-up) se espera que converjan para $t \to +\infty$ a la distribución meseta (la distribución uniforme en $[V_R, V_F]$ [17]).

2. **Excitador:** Para $V_F - V_R < b < b_e$ existen dos equilibrios (en [14] se demostró que existían al menos dos). El equilibrio alto (el que tiene asociada una mayor tasa de disparo) es inestable para cualquier retardo $d \geq 0$ y el equilibrio bajo (el que tiene una tasa de disparo más baja) es asintóticamente estable para cualquier retardo $d \geq 0$. Dependiendo de la condición inicial p_0, las soluciones convergen al equilibrio bajo, ocurre blow-up (sólo posible con $d = 0$), o convergen a la distribución meseta (sólo posible cuando $d > 0$).

3. **Poco excitador:** Para $0 < b < V_F - V_R$ el único equilibrio es asintóticamente estable independientemente del retardo. Las soluciones convergen a este, o alcanzan el blow-up (sólo posible si $d = 0$ [14]).

4. **Inhibidor:** Existe un valor crítico $b^* < 0$ tal que para cualquier $b^* < b < 0$, el único equilibrio es asintóticamente estable para cualquier valor del retardo. Se espera que todas las soluciones converjan a este equilibrio, independientemente del retardo.

5. **Fuertemente inhibidor:** Para $b < b^*$, también hay un único equilibrio.

   (a) Para valores pequeños del retardo, este equilibrio es estable. Se espera que todas las soluciones converjan hacia este.

   (b) Para grandes valores del retardo, el equilibrio es inestable. Se espera que todas las soluciones se aproximen a una solución periódica.

Como último trabajo realizado para el modelo NNLIF, hemos extendido el estudio analítico de la sucesión discreta de pseudo-equilibrios al caso del modelo con periodo refractario [16], y conjuntamente hemos realizado simulaciones numéricas en este caso tanto con el esquema microscópico del capítulo 2 como con el esquema mesoscópico del capítulo 4, realizando los ajustes correspondientes para añadir el estado refractario. El estudio de la sucesión de pseudo-equilibrios y sus simulaciones asociadas nos dan una idea general de cómo evoluciona el modelo con periodo refractario cuando consideramos un retardo grande. Además,

las simulaciones del sistema microscópico nos permiten comprender lo que ocurre después del blow-up para este modelo, observando en algunos casos soluciones periódicas sin retardo, que hasta donde sabemos no se habían observado antes. Por último, mostramos que el estado refractario en el modelo NNLIF nunca conduce al estado trivial observado para las soluciones no físicas en el capítulo 2, en el que todas las neuronas disparan constantemente. Como la propiedad fundamental de las soluciones físicas definidas en el capítulo 2 es exactamente esa, parece que las soluciones del modelo NNLIF con período refractario son efectivamente físicas.

Tras discutir los principales resultados obtenidos para el modelo NNLIF, también es pertinente mencionar las posibles extensiones, así como los problemas abiertos que se derivan del mismo. Con respecto al modelo microscópico, sería deseable ampliar el uso de este modelo a casos más complejos, considerando poblaciones de neuronas excitadoras e inhibidoras separadas, o variables extra como la conductancia o la edad. Además, el estudio analítico del sistema microscópico no está tan avanzado como el de la ecuación de Fokker-Planck, por lo que avances en este campo pueden ser esenciales para un doble impulso en la comprensión del modelo NNLIF. Respecto al criterio de estabilidad dado en el capítulo 3 para los equilibrios del sistema no lineal, sería una mejora apreciable si pudiéramos enunciar un nuevo criterio que no requiera el estudio numérico de ninguna función, sino simplemente el establecimiento de rangos de parámetros que determinen la estabilidad de los equilibrios. Como observación adicional, resolver el problema que encontramos al establecer que la estabilidad linealizada implica estabilidad no lineal, cuando se trata de sistemas con retardo, completaría nuestros resultados desde un punto de vista técnico. En el capítulo 4, el problema que queda abierto y que sería muy interesante tratar es la demostración de que la solución de la ecuación no lineal de Fokker-Planck se comporta como la sucesión de pseudo-equilibrios, independientemente del valor del parámetro de conectividad. Por supuesto, la extensión de este resultado a casos más especiales, como la convergencia, en el sentido apropiado, a estados de meseta, sería un trabajo muy innovador e interesante. Por último, con respecto al sistema con periodo refractario, un análisis completo de su comportamiento local, como el que se da en el capítulo 3 para el modelo más simple, es un trabajo en curso para una futura publicación. Esto nos daría una idea de la estabilidad de cada equilibrio, para cada valor del parámetro de conectividad, del retardo y del periodo refractario.

Otro trabajo en el que estamos inmersos, junto con Nicolas Torres, es el de responder a la pregunta: ¿Qué edad tienen las neuronas que disparan? Entendiendo la edad como el tiempo transcurrido desde el último disparo. Para ello, queremos relacionar los modelos de edad [103, 104], cuyo comportamiento a largo plazo ha sido ampliamente estudiado en [122], con el modelo NNLIF, siguiendo la idea propuesta en [62]. Con este objetivo implementaremos tanto las técnicas que han surgido de este trabajo, a través del estudio

del modelo NNLIF, como las utilizadas específicamente para el modelo de edad [23], con el fin de aportar el mayor conocimiento posible sobre el modelo conjunto.

En conclusión, el trabajo presentado en esta tesis supone una importante mejora del conocimiento existente sobre el modelo NNLIF, especialmente sobre el comportamiento a largo plazo y la estabilidad de sus equilibrios. Además de esta mejora, la tesis contiene nuevos métodos que permanecían inaplicados a este modelo, e ideas originales para su estudio, que pueden ser extrapoladas a multitud de modelos alternativos, especialmente aquellos modelados mediante ecuaciones diferenciales con retardo. Además, el avance en el conocimiento disponible para los modelos neuronales más simples, y por tanto aquellos en los que es posible el análisis matemático de forma amplia, puede ayudar a mejorar la comprensión de modelos más complejos y realistas y puede tener un impacto interdisciplinar, ayudando a otros científicos a resolver problemas relacionados con el cerebro, como los mencionados al principio de la tesis.

Paralelamente al trabajo principal de la tesis, que ha sido el estudio del modelo NNLIF, decidimos realizar un estudio numérico, desde el punto de vista microscópico, de configuraciones de partículas que interaccionan entre sí mediante potenciales atractivo-repulsivos del tipo leyes de potencias [22]. En particular, nos interesamos en encontrar y estudiar las propiedades de los mínimos de la energía de interacción entre estas partículas. En el capítulo 6 mostramos los resultados numéricos que obtuvimos con la ayuda del programa GMIN [130], que están acompañados de una revisión bibliográfica sobre el tema. Estos potenciales han sido ampliamente estudiados en la literatura científica, debido a la gran variedad de fenómenos que modelan en función del valor de sus parámetros. Están asociados tanto a eventos de formación de cristales en física como a fenómenos de comportamiento colectivo o swarming en biología. Encontrar un minimizador eficaz y eficiente para la energía de las partículas que interactúan en este rango de potenciales puede ser de gran utilidad para abordar multitud de problemas que permanecen abiertos, como el problema de la cristalización. Nuestra intención futura en este campo es utilizar las herramientas numéricas implementadas en este capítulo para el estudio de las propiedades de los mínimos de estos potenciales, conectando los modelos microscópicos con sus EDPs asociadas, mediante el uso de un número muy elevado de partículas.

Bibliography

[1] Acebrón, J., Bulsara, A., and Rappel, W. J. Noisy Fitzhugh-Nagumo model: From single elements to globally coupled networks. *Physical Review E 69*, 2 (2004), 026202.

[2] Au Yeung, Y., Friesecke, G., and Schmidt, B. Minimizing atomic configurations of short range pair potentials in two dimensions: crystallization in the Wulff shape. *Calculus of Variations and Partial Differential Equations 44*, 1–2 (July 2011), 81–100.

[3] Balagué, D., Carrillo, J. A., Laurent, T., and Raoul, G. Dimensionality of Local Minimizers of the Interaction Energy. *Archive for Rational Mechanics and Analysis 209*, 3 (Sept. 2013), 1055–1088.

[4] Balagué, D., Carrillo, J. A., Laurent, T., and Raoul, G. Nonlocal interactions by repulsive–attractive potentials: Radial ins/stability. *Physica D: Nonlinear Phenomena 260* (Oct. 2013), 5–25.

[5] Bavaud, F. Equilibrium properties of the Vlasov functional: The generalized Poisson-Boltzmann-Emden equation. *Reviews of Modern Physics 63*, 1 (Jan. 1991), 129+.

[6] Ben Haj Yedder, A., Blanc, X., and Le Bris, C. A numerical investigation of the 2-dimensional crystal problem. Preprint CERMICS, available at http://www.ann.jussieu.fr/publications/2003/R03003.html, 2003.

[7] Benita, J. M., Guillamon, A., Deco, G., and Sanchez-Vives, M. V. Synaptic depression and slow oscillatory activity in a biophysical network model of the cerebral cortex. *Frontiers in computational neuroscience 6* (2012), 64.

[8] Blanc, X., and Lewin, M. The crystallization conjecture: a review. *EMS Surveys in Mathematical Sciences 2*, 2 (2015), 225–306.

[9] Brette, R., and Gerstner, W. Adaptive exponential integrate-and-fire model as an effective description of neural activity. *Journal of neurophysiology 94* (2005), 3637–3642.

[10] Brunel, N. Dynamics of sparsely connected networks of excitatory and inhibitory spiking neurons. *Journal of computational neuroscience 8*, 3 (2000), 183–208.

[11] Brunel, N., and Hakim, V. Fast global oscillations in networks of integrate-and-fire neurons with low firing rates. *Neural computation 11*, 7 (1999), 1621–1671.

[12] Cáceres, M. J., Cañizo, J. A., and Ramos-Lora, A. On the asymptotic behavior of the NNLIF neuron model for general connectivity strength. *arXiv preprint arXiv:2401.13534* (2024).

[13] Cáceres, M. J., Cañizo, J. A., and Ramos-Lora, A. The sequence of pseudo-equilibria describes the long-time behaviour of the NNLIF model with large delay. *arXiv preprint arXiv:2403.00971* (2024).

[14] Cáceres, M. J., Carrillo, J. A., and Perthame, B. Analysis of nonlinear noisy integrate & fire neuron models: blow-up and steady states. *The Journal of Mathematical Neuroscience 1*, 1 (2011), 7.

[15] Cáceres, M. J., Carrillo, J. A., and Tao, L. A numerical solver for a nonlinear Fokker–Planck equation representation of neuronal network dynamics. *Journal of Computational Physics 230*, 4 (2011), 1084–1099.

[16] Cáceres, M. J., and Perthame, B. Beyond blow-up in excitatory integrate and fire neuronal networks: refractory period and spontaneous activity. *Journal of theoretical biology 350* (2014), 81–89.

[17] Cáceres, M. J., and Ramos-Lora, A. An understanding of the physical solutions and the blow-up phenomenon for nonlinear noisy leaky integrate and fire neuronal models. *Communications in Computational Physics 30*, 3 (2021), 820–850.

[18] Cáceres, M. J., Roux, P., Salort, D., and Schneider, R. Global-in-time solutions and qualitative properties for the NNLIF neuron model with synaptic delay. *Communications in Partial Differential Equations 44*, 12 (2019), 1358–1386.

[19] Cáceres, M. J., and Schneider, R. Blow-up, steady states and long time behaviour of excitatory-inhibitory nonlinear neuron models. *Kinetic & Related Models 10*, 3 (2017), 587.

[20] Cáceres, M. J., and Schneider, R. Analysis and numerical solver for excitatory-inhibitory networks with delay and refractory periods. *ESAIM: Mathematical Modelling and Numerical Analysis 52*, 5 (2018), 1733–1761.

[21] Cañizo, J. A., and Patacchini, F. S. Discrete minimisers are close to continuum minimisers for the interaction energy. *Calculus of Variations and Partial Differential Equations 57*, 1 (jan 2018).

[22] Cañizo, J. A., and Ramos-Lora, A. Discrete minimizers of the interaction energy in collective behavior: a brief numerical and analytic review. *arXiv preprint arXiv:2403.00594* (2024).

[23] Cañizo, J. A., and Yoldaş, H. Asymptotic behaviour of neuron population models structured by elapsed-time. *Nonlinearity 32*, 2 (2019), 464.

[24] Carrillo, J., Figalli, A., and Patacchini, F. Geometry of minimizers for the interaction energy with mildly repulsive potentials. *Annales de l'Institut Henri Poincaré C, Analyse non linéaire 34*, 5 (Oct. 2017), 1299–1308.

[25] Carrillo, J., Perthame, B., Salort, D., and Smets, D. Qualitative properties of solutions for the noisy integrate & fire model in computational neuroscience. *Nonlinearity 25* (2015), 3365–3388.

[26] Carrillo, J. A., Chipot, M., and Huang, Y. On global minimizers of repulsive–attractive power-law interaction energies. *Philosophical Transactions of the Royal Society A: Mathematical, Physical and Engineering Sciences 372*, 2028 (2014), 20130399.

[27] Carrillo, J. A., Clini, A., and Solem, S. The mean field limit of stochastic differential equation systems modeling grid cells. *SIAM Journal on Mathematical Analysis 55*, 4 (2023), 3602–3634.

[28] Carrillo, J. A., Delgadino, M. G., and Mellet, A. Regularity of local minimizers of the interaction energy via obstacle problems. *Communications in Mathematical Physics 343*, 3 (Mar. 2016), 747–781.

[29] Carrillo, J. A., González, M. d. M., Gualdani, M. P., and Schonbek, M. E. Classical solutions for a nonlinear Fokker-Planck equation arising in computational neuroscience. *Communications in Partial Differential Equations 38*, 3 (2013), 385–409.

[30] Carrillo, J. A., and Huang, Y. Explicit equilibrium solutions for the aggregation equation with power-law potentials. *Kinetic and Related Models 10*, 1 (2017), 171–192.

[31] Carrillo, J. A., Mateu, J., Mora, M. G., Rondi, L., Scardia, L., and Verdera, J. The equilibrium measure for an anisotropic nonlocal energy. *Calculus of Variations and Partial Differential Equations 60*, 3 (2021).

[32] Carrillo, J. A., Roux, P., and Solem, S. Noise-driven bifurcations in a nonlinear Fokker–Planck system describing stochastic neural fields. *Physica D: Nonlinear Phenomena 449* (2023), 133736.

[33] Carrillo, J. A., Roux, P., and Solem, S. Well-posedness and stability of a stochastic neural field in the form of a partial differential equation. *arXiv preprint arXiv:2307.08077* (2023).

[34] Carrillo, J. A., and Shu, R. From radial symmetry to fractal behavior of aggregation equilibria for repulsive–attractive potentials. *Calculus of Variations and Partial Differential Equations 62*, 1 (Nov. 2021).

[35] Carrillo, J. A., and Shu, R. Minimizers of 3D anisotropic interaction energies. *Advances in Calculus of Variations 0*, 0 (Nov. 2022).

[36] Carrillo, J. A., and Shu, R. Global minimizers of a large class of anisotropic attractive-repulsive interaction energies in 2D. *Communications on Pure and Applied Mathematics 77*, 2 (Sept. 2023), 1353–1404.

[37] Cañizo, J. A., Carrillo, J. A., and Patacchini, F. S. Existence of compactly supported global minimisers for the interaction energy. *Archive for Rational Mechanics and Analysis 217*, 3 (Mar. 2015), 1197–1217.

[38] Cañizo, J. A., Mischler, S., and Mouhot, C. Rate of convergence to self-similarity for Smoluchowski's coagulation equation with constant coefficients. *SIAM Journal on Mathematical Analysis 41*, 6 (2010), 2283–2314.

[39] Chevallier, J. Mean-field limit of generalized Hawkes processes. *Stochastic Processes and their Applications 127*, 12 (2017), 3870–3912.

[40] Chevallier, J., Cáceres, M. J., Doumic, M., and Reynaud-Bouret, P. Microscopic approach of a time elapsed neural model. *Mathematical Models and Methods in Applied Sciences 25*, 14 (2015), 2669–2719.

[41] Cockburn, B., Shu, C.-W., Johnson, C., Tadmor, E., and Shu, C.-W. *Essentially non-oscillatory and weighted essentially non-oscillatory schemes for hyperbolic conservation laws*. Springer, 1998.

[42] Cohn, H., Kumar, A., Miller, S., Radchenko, D., and Viazovska, M. The sphere packing problem in dimension 24. *Annals of Mathematics 185*, 3 (2017).

[43] Cohn, H., Kumar, A., Miller, S., Radchenko, D., and Viazovska, M. Universal optimality of the E_8 and Leech lattices and interpolation formulas. *Annals of Mathematics 196*, 3 (2022).

[44] Compte, A., Brunel, N., Goldman-Rakic, P. S., and Wang, X.-J. Synaptic mechanisms and network dynamics underlying spatial working memory in a cortical network model. *Cerebral cortex 10*, 9 (2000), 910–923.

[45] Compte, A., Sanchez-Vives, M. V., McCormick, D. A., and Wang, X.-J. Cellular and network mechanisms of slow oscillatory activity (¡ 1 hz) and wave propagations in a cortical network model. *Journal of neurophysiology 89*, 5 (2003), 2707–2725.

[46] Cormier, Q., Tanré, E., and Veltz, R. Long time behavior of a mean-field model of interacting neurons. *Stochastic Processes and their Applications 130*, 5 (2020), 2553–2595.

[47] Cormier, Q., Tanré, E., and Veltz, R. Hopf bifurcation in a mean-field model of spiking neurons. *Electronic Journal of Probability 26* (2021), 1–40.

[48] Davies, C., Lim, T., and McCann, R. J. Classifying minimum energy states for interacting particles: Spherical shells. *SIAM Journal on Applied Mathematics 82*, 4 (Aug. 2021), 1520–1536.

[49] Davies, C., Lim, T., and McCann, R. J. Classifying minimum energy states for interacting particles: Regular simplices. *Communications in Mathematical Physics 399*, 2 (Nov. 2022), 577–598.

[50] Dayan, P., Abbott, L. F., et al. Theoretical neuroscience: computational and mathematical modeling of neural systems. *Journal of Cognitive Neuroscience 15*, 1 (2003), 154–155.

[51] Deaven, D. M., Tit, N., Morris, J. R., and Ho, K. M. Structural optimization of Lennard-Jones clusters by a genetic algorithm. *Chemical Physics Letters 256*, 1-2 (1996), 195–200.

[52] Delarue, F., Inglis, J., Rubenthaler, S., and Tanré, E. Particle systems with a singular mean-field self-excitation. Application to neuronal networks. *Stochastic Processes and their Applications 125*, 6 (2015), 2451–2492.

[53] Delarue, F., Inglis, J., Rubenthaler, S., Tanré, E., et al. Global solvability of a networked integrate-and-fire model of McKean–Vlasov type. *The Annals of Applied Probability 25*, 4 (2015), 2096–2133.

[54] Diekmann, O., Gils, S. A., Lunel, S. M. V., and Walther, H.-O. *Delay Equations*. Applied Mathematical Sciences. Springer, 1995.

[55] Dittner, M., and Hartke, B. Conquering the hard cases of Lennard-Jones clusters with simple recipes. *Computational and Theoretical Chemistry 1107* (May 2017), 7–13.

[56] Doetsch, G. *Introduction to the Theory and Application of the Laplace Transformation*. Springer London, Limited, 1974.

[57] D'Orsogna, M. R., Chuang, Y. L., Bertozzi, A. L., and Chayes, L. S. Self-propelled particles with soft-core interactions: Patterns, stability, and collapse. *Physical Review Letters 96*, 10 (Mar. 2006), 104302+.

[58] Du, Z., Xie, Y., and Zhou, Z. A synchronization-capturing multi-scale solver to the noisy integrate-and-fire neuron networks. *arXiv preprint arXiv:2305.05915* (2023).

[59] Dumont, G., and Gabriel, P. The mean-field equation of a leaky integrate-and-fire neural network: measure solutions and steady states. *Nonlinearity 33*, 12 (2020), 6381.

[60] Dumont, G., and Henry, J. Population density models of integrate-and-fire neurons with jumps: well-posedness. *Journal of Mathematical Biology 67*, 3 (2013), 453–481.

[61] Dumont, G., and Henry, J. Synchronization of an excitatory integrate-and-fire neural network. *Bulletin of mathematical biology 75*, 4 (2013), 629–648.

[62] Dumont, G., Henry, J., and Tarniceriu, C. O. A theoretical connection between the noisy leaky integrate-and-fire and the escape rate models: the non-autonomous case. *Mathematical Modelling of Natural Phenomena 15* (2020), 59.

[63] E, W., and Li, D. On the crystallization of 2D hexagonal lattices. *Communications in Mathematical Physics 286*, 3 (July 2008), 1099–1140.

[64] Engel, K.-J., and Nagel, R. *One-Parameter Semigroups for Linear Evolution Equations (Graduate Texts in Mathematics)*. Springer.

[65] Erneux, T. *Applied Delay Differential Equations*, vol. 3 of *Surveys and Tutorials in the Applied Mathematical Sciences*. Springer-Verlag New York, New York, NY, 2009.

[66] Faugeras, O., Soret, E., and Tanré, E. Asymptotic behaviour of a network of neurons with random linear interactions. hal-01986927, 2020.

[67] Fellner, K., and Raoul, G. Stability of stationary states of non-local equations with singular interaction potentials. *Mathematical and Computer Modelling* (Mar. 2010).

[68] Fellner, K., and Raoul, G. Stable stationary states of non-local interaction equations. *Mathematical Models and Methods in Applied Sciences 20*, 12 (Dec. 2010), 2267–2291.

[69] Fitzhugh, R. Impulses and physiological states in theoretical models of nerve membrane. *Biophysical journal 1*, 6 (1961), 445–466.

[70] Frank, R. L. Minimizers for a one-dimensional interaction energy. *Nonlinear Analysis 216* (2022), 112691.

[71] Frank, R. L. *Some minimization problems for mean field models with competing forces*. EMS Press, July 2023, pp. 277–294.

[72] Gardner, C. S., and Radin, C. The infinite-volume ground state of the Lennard-Jones potential. *Journal of Statistical Physics 20*, 6 (June 1979), 719–724.

[73] Gerstner, W., and Kistler, W. M. *Spiking neuron models: Single neurons, populations, plasticity*. Cambridge university press, 2002.

[74] Gualdani, M. P., Mischler, S., and Mouhot, C. *Factorization of non-symmetric operators and exponential H-theorem*. No. 153 (nouvelle série) in Mémoires de la Société Mathematique de France. Société Mathématique de France, Paris, 2018.

[75] Guillamon, T. An introduction to the mathematics of neural activity. *Butl. Soc. Catalana Mat 19*, 2 (2004), 25–45.

[76] Hales, T. A proof of the Kepler conjecture. *Annals of Mathematics 162*, 3 (2005), 1065–1185.

[77] Hayes, B. The science of sticky spheres. *American Scientist 100*, 6 (2012), 442.

[78] Heitmann, R. C., and Radin, C. The ground state for sticky disks. *Journal of Statistical Physics 22*, 3 (1980), 281–287.

[79] Hoare, M. R. Structure and dynamics of simple microclusters. In *Advances in Chemical Physics*, I. Prigogine and S. A. Rice, Eds., vol. 40. John Wiley & Sons, 1979, pp. 49–135.

[80] Hoare, M. R., and Pal, P. Physical cluster mechanics: Statics and energy surfaces for monatomic systems. *Advances in Chemical Physics 20* (1971), 161–196.

[81] Hoare, M. R., and Pal, P. Statics and stability of small cluster nuclei. *Nature (Physical Sciences) 230* (1971), 5–8.

[82] Hoare, M. R., and Pal, P. Geometry and stability of "spherical" f.c.c. microcrystallites. *Nature (Physical Sciences) 236* (1972), 35–37.

[83] Hodgkin, A. L., and Huxley, A. F. The components of membrane conductance in the giant axon of loligo. *The Journal of physiology 116*, 4 (1952), 473.

[84] Hodgkin, A. L., and Huxley, A. F. A quantitative description of membrane current and its application to conduction and excitation in nerve. *The Journal of physiology 117*, 4 (1952), 500.

[85] Hoy, R. S., Harwayne-Gidansky, J., and O'Hern, C. S. Structure of finite sphere packings via exact enumeration: Implications for colloidal crystal nucleation. *Physical Review E 85*, 5 (2012), 051403.

[86] Hu, J., Liu, J.-G., Xie, Y., and Zhou, Z. A structure preserving numerical scheme for Fokker-Planck equations of neuron networks: Numerical analysis and exploration. *Journal of Computational Physics 433* (2021), 110195.

[87] Ikeda, K., Roux, P., Salort, D., and Smets, D. Theoretical study of the emergence of periodic solutions for the inhibitory NNLIF neuron model with synaptic delay. *Mathematical Neuroscience and Applications*, 4 (2022), 1–37.

[88] Kandel, E., and Siegelbaum, S. An introduction to synaptic transmission. *Essentials of Neural Science and Behavior. Appleton & Lange, Stanford* (1995), 183–195.

[89] Kandel, E. R., Schwartz, J. H., Jessell, T. M., Siegelbaum, S., Hudspeth, A. J., Mack, S., et al. *Principles of neural science*, vol. 4. McGraw-hill New York, 2000.

[90] Kirkpatrick, S., Gelatt, C. D., and Vecchi, M. P. Optimization by simulated annealing. *Science 220*, 4598 (1983), 671–680.

[91] Lapique, L. Researches quantatives sur l'excitation electrique des nerfs traitee comme une polarization. *Journal of Physiology, Pathology and Genetics 9* (1907), 620–635.

[92] Li, Z., and Scheraga, H. A. Monte Carlo-minimization approach to the multiple-minima problem in protein folding. *Proceedings of the National Academy of Sciences 84*, 19 (1987), 6611–6615.

[93] Liu, J.-G., Wang, Z., Zhang, Y., and Zhou, Z. Rigorous justification of the Fokker–Planck equations of neural networks based on an iteration perspective. *SIAM Journal on Mathematical Analysis 54*, 1 (2022), 1270–1312.

[94] Luca, L. D., and Friesecke, G. Crystallization in two dimensions and a discrete Gauss–Bonnet theorem. *Journal of Nonlinear Science 28*, 1 (2018), 69–90.

[95] Meng, G., Arkus, N., Brenner, M. P., and Manoharan, V. N. The free-energy landscape of clusters of attractive hard spheres. *Science 327*, 5965 (2010), 560–563.

[96] Mischler, S., and Mouhot, C. Exponential stability of slowly decaying solutions to the kinetic Fokker-Planck equation. *Archive for Rational Mechanics and Analysis 221*, 2 (Feb. 2016), 677–723.

[97] Mischler, S., Quininao, C., and Touboul, J. On a kinetic Fitzhugh–Nagumo model of neuronal network. *Communications in Mathematical Physics 342*, 3 (2016), 1001–1042.

[98] Newhall, K., Kovačič, G., Kramer, P., Rangan, A. V., and Cai, D. Cascade-induced synchrony in stochastically driven neuronal networks. *Physical Review E 82* (2010), 041903.

[99] Newhall, K., Kovačič, G., Kramer, P., Zhou, D., Rangan, A. V., and Cai, D. Dynamics of current-based, poisson driven, integrate-and-fire neuronal networks. *Communications in Mathematical Sciences 8* (2010), 541–600.

[100] Niesse, J. A., and Mayne, H. R. Minimization of small silicon clusters using the space-fixed modified genetic algorithm method. *Chemical Physics Letters 261*, 4-5 (1996), 576–582.

[101] Northby, J. A. Structure and binding of Lennard-Jones clusters: $13 \leq N \leq 147$. *Journal of Chemical Physics 87*, 10 (1987), 6166–6177.

[102] Omurtag, A., W., K. B., and Sirovich, L. On the simulation of large populations of neurons. *Journal of Computational Neuroscience 8* (2000), 51–63.

[103] Pakdaman, K., Perthame, B., and Salort, D. Dynamics of a structured neuron population. *Nonlinearity 23* (2010), 55–75.

[104] Pakdaman, K., Perthame, B., and Salort, D. Relaxation and self-sustained oscillations in the time elapsed neuron network model. *SIAM Journal on Applied Mathematics 73*, 3 (2013), 1260–1279.

[105] Pakdaman, K., Perthame, B., and Salort, D. Adaptation and fatigue model for neuron networks and large time asymptotics in a nonlinear fragmentation equation. *The Journal of Mathematical Neuroscience (JMN) 4*, 1 (2014), 1–26.

[106] Perthame, B., and Salort, D. On a voltage-conductance kinetic system for integrate and fire neural networks. *Kinetic and related models, AIMS 6*, 4 (2013), 841–864.

[107] Perthame, B., and Salort, D. Derivation of a voltage density equation from a voltage-conductance kinetic model for networks of integrate-and-fire neurons. *Communications in Mathematical Sciences 17*, 5 (2019).

[108] Petrache, M., and Serfaty, S. Next order asymptotics and renormalized energy for Riesz interactions. *Journal of the Institute of Mathematics of Jussieu 16*, 3 (2017), 501–569.

[109] Petrache, M., and Serfaty, S. Crystallization for Coulomb and Riesz interactions as a consequence of the Cohn-Kumar conjecture. *Proceedings of the American Mathematical Society 148*, 7 (2020), 3047–3057.

[110] Radin, C. The ground state for soft disks. *Journal of Statistical Physics 26*, 2 (Oct. 1981), 365–373.

[111] Radin, C. Low temperature and the origin of crystalline symmetry. *International Journal of Modern Physics B 1*, 5/6 (Oct. 1987), 1157–1191.

[112] Rangan, A. V., Kovačič, G., and Cai, D. Kinetic theory for neuronal networks with fast and slow excitatory conductances driven by the same spike train. *Physical Review E 77*, 041915 (2008), 1–13.

[113] Raoul, G. Nonlocal interaction equations: Stationary states and stability analysis. *Differential and Integral Equations 25*, 5/6 (2012).

[114] Renart, A., Brunel, N., and Wang, X.-J. Mean-field theory of irregularly spiking neuronal populations and working memory in recurrent cortical networks. *Computational neuroscience: A comprehensive approach* (2004), 431–490.

[115] Roux, P., and Salort, D. Towards a further understanding of the dynamics in the excitatory NNLIF neuron model: Blow-up and global existence. *Kinetic & Related Models 14*, 5 (2021).

[116] Ruelle, D. *Statistical mechanics: rigorous results*. W.A. Benjamin, 1969.

[117] Salort, D., and Smets, D. Convergence towards equilibrium for a model with partial diffusion. *hal-03845918* (2022).

[118] Schneider, R. *Analysis and numerical simulation of network of noisy leaky integrate and fire neuron models*. PhD thesis, University of Granada, 2018.

[119] Simione, R., Slepčev, D., and Topaloglu, I. Existence of Ground States of Nonlocal-Interaction Energies. *Journal of Statistical Physics 159*, 4 (Feb. 2015), 972–986.

[120] Sirovich, L., Omurtag, A., and K., L. Dynamics of neural populations: Stability and synchrony. *Network: Computation in Neural Systems 17* (2006), 3–29.

[121] Theil, F. A Proof of Crystallization in Two Dimensions. *Communications in Mathematical Physics 262*, 1 (Feb. 2006), 209–236.

[122] Torres, N. *Asymptotic behavior of solutions of the elapsed time model for neural assemblies*. PhD thesis, Sorbonne Université, 2022.

[123] Trombach, L., Hoy, R. S., Wales, D. J., and Schwerdtfeger, P. From sticky-hard-sphere to Lennard-Jones-type clusters. *Physical Review E 97*, 4 (2018), 043309.

[124] Tuckwell, H. *Introduction to Theoretical Neurobiology*. Cambridge Univ. Press, Cambridge, 1988.

[125] Ventevogel, W. J. On the configuration of a one-dimensional system of interacting particles with minimum potential energy per particle. *Physica A: Statistical Mechanics and its Applications 92*, 3-4 (1978), 343–361.

[126] Ventevogel, W. J. Why do crystals exist? *Physics Letters A 64*, 5 (1978), 463–464.

[127] Ventevogel, W. J., and Nijboer, B. R. A. On the configuration of systems of interacting particle with minimum potential energy per particle. *Physica A: Statistical Mechanics and its Applications 98*, 1-2 (1979), 274–288.

[128] Ventevogel, W. J., and Nijboer, B. R. A. On the configuration of systems of interacting particles with minimum potential energy per particle. *Physica A: Statistical Mechanics and its Applications 99*, 3 (1979), 569–580.

[129] Viazovska, M. The sphere packing problem in dimension 8. *Annals of Mathematics 185*, 3 (2017).

[130] Wales, D. J. GMIN optimisation software. Available at https://www-wales.ch.cam.ac.uk/GMIN/.

[131] Wales, D. J., and Doye, J. P. K. Global optimization by basin-hopping and the lowest energy structures of Lennard-Jones clusters containing up to 110 atoms. *The Journal of Physical Chemistry A 101*, 28 (1997), 5111–5116.

[132] Wales, D. J., Doye, J. P. K., Dullweber, A., Hodges, M. P., Naumkin, F. Y., Calvo, F., Hernández-Rojas, J., and Middleton, T. F. The Cambridge Cluster Database. Online. URL http://www-wales.ch.cam.ac.uk/CCD.html.

[133] Wille, L. T. Minimum-energy configurations of atomic clusters: new results obtained by simulated annealing. *Chemical Physics Letters 133*, 5 (Jan. 1987), 405–410.

[134] Wille, L. T. Searching potential energy surfaces by simulated annealing. *Nature 325* (1987), 374–374.

[135] Zhang, J. A brief review on results and computational algorithms for minimizing the Lennard-Jones potential.

[136] Zhang, P., Wang, Y., and Zhou, Z. A spectral method for a Fokker-Planck equation in neuroscience with applications in neural networks with learning rules. *arXiv preprint arXiv:2305.00275* (2023).